An Examination of the Effect of Diluent on Microbial Dynamics in Oil Sands Tailings and the Mechanistic Insight on Carbon Dioxide-mediated Turbidity Reduction in Oil Sands Surface Water

by

Ho Yin Poon

A thesis submitted in partial fulfillment of the requirements for the degree of

Doctor of Philosophy

In Environmental Science

Department of Civil and Environmental Engineering
University of Alberta

Abstract

Oil sands fluid fine tailings (FFT) are comprised of sand, silt, clay, residual organics, salt, trace metals and process-affected water (OSPW). In order to accommodate and remediate large amounts of FFT, a full-scale demonstration pit lake, where FFT was capped with a mixture of OSPW and fresh water, was constructed and named Base Mine Lake (BML). This strategy allows FFT to dewater and the water cap to gradually develop into a permanent wet-landscape with the expectation of an aquatic ecosystem development. However, high BML surface water turbidity has been observed, which hinders aquatic ecosystem development. The residual organics in the tailings have been shown to stimulate microbial activity thus generating CH_4 and H_2S in tailings. Ebullition of these biogenic gases could contribute to turbidity observed in BML, as well as transporting the residual organics to the surface water.

The impact of naphtha diluent (at 0.2, 0.8 and 1.5%) on microbial activity resulting in biogenic gases generation were investigated. In our anaerobic mesocosm study, H_2S production preceded CH_4 generation, and the amount gases producted increased linearly with increasing naphtha diluent concentration. The SRB communities were stimulated week 0-5, as an increase of relative abundance for Desulfobulbaceae (580%) and Desulfomicrobiaceae (505%) observed in MFT-PW-0.8% mesocosms. Consistent with the chemical data, an increase for Methanoregulaceae (380%) and Methanotrichaceae (360%) were observed in MFT-PW-0.8% mesocosms at week 11. Furthermore, Anaerolinealeaceae and Synergistaceae families were detected, suggesting competitive and syntrophic relationships. Organics from the naphtha diluent were fermented by members of Anaerolinealeaceae and Synergistaceae to generate fatty acids and H_2, which serve as substrates for SRB and methanogens.

The ebullition of these biogenic gases from the FFT could transport BTEX compounds, which are a component of naphtha diluent. Thus, the changes of benzene and toluene concentrations in the headspace was monitored in these mesocosms. The highest benzene release rate was 1.1 μg/mL MFT/d (week 4-6), coincided with the H_2S emission in week 6. The highest toluene release rate was 0.35 μg/mL MFT/d (week 11-15), corresponded with the CH_4 emission in week 11. These data suggest the correlation between biogenic gas emissions and the transport of benzene and toluene from tailings to the surface water. Therefore, removing the BTEX compounds from the surface water may reduce biogenic gases production. Expanded graphite (EG) has large surface area, strong adsorption and electrical properties. As a result, the adsorption capacity of each BTEX compound was tested on EG and BioLargo's advanced oxidation system (AOS). EG and AOS showed adsorption preference for BTEX compounds with higher hydrophobicity. In a batch experiment, ~37% of *p*-xylene and ~29% of ethylbenzene compared to 12% benzene and 17% were adsorbed using 500 mg EG. Electricity application further enhanced removal in AOS system for *p*-xylene (99%) and ethylbenzene (38%). These results showed that AOS system can only effectively removal *p*-xylene amongst BTEX compounds.

Several previous studies showed dissolved CO_2 improves FFT dewatering/densification and reduces surface water turbidity, but the mechanism is not well understood. The effect of CO_2-mediated carbonate dissolution on BML water turbidity reduction was examined. Greater than 98% turbidity reduction was observed in columns receiving CO_2-treatment and calcite compared to ~95% turbidity reduction with CO_2 treatment alone. Despite turbidity reduction, the Ca^{2+} concentration was (4X) below the theoretically equilibrium concentration. Since OSPW contains high sulfate concentration, the inhibitory effect on calcite dissolution was tested on synthetic

BML water. A 23% reduction on calcite dissolution rate was calculated for the 400 mg/L SO_4^{2-} column compared to the 50 mg/L SO_4^{2-} column. These results demonstrated the high SO_4^{2-} concentration reduce the calcite dissolution rate. Dolomite and siderite minerals were identified from previous oil sands tailings studies. As a result, CO_2-mediated dissolution of calcite and dolomite mixture (100%, 50%, 25%, 0% dolomite) was tested. A mathematical (DLVO) model was constructed to determine suspended FFT stability. A reduction in energy barrier below 20 kT was calculated for all columns received carbonate minerals (100% to 0% dolomite) and CO_2-treatment. Interestingly, an inverse correlation was observed between the amount of dolomite present and energy barrier values at day 42 of the experiment, with a difference of 3.2 kT for 100% dolomite and 100% calcite columns. These results suggest CO_2-mediated calcite dissolution provides an optimal condition for suspended FFT to settle.

Preface

Some of the research conducted for this thesis was a result of collaboration with either Kathleen Frances Mign-tze Day Gee (MSc student) or Jordan Brandon (MSc student) in Dr. Ulrich's lab (Environmental Engineering at University of Alberta).

Some of the research results from Chapter 3 of this thesis has been published as Gee, K. F., Poon, H. Y., Hashisho, Z., & Ulrich, A. C. ″Effect of naphtha diluent on greenhouse gases and reduced sulfur compounds emissions from oil sands tailings″ Science of the Total Environment Journal, Volume 598, 916-924. I shared the responsibility in experimental setup and manuscript preparation. In addition, I was responsible for MFT samples and BTEX data collections, and molecular biology analyses, functional gene assay, 16S rRNA Sequencing and molecular data analysis. I was also responsible for the editing of manuscript.

Some of the research results from Chapter 5a of this thesis has been published as Poon, H. Y., Brandon, J. T., Yu, X. X., & Ulrich, A. C. ″Turbidity Mitigation in an Oil Sands Pit Lake through pH Reduction and Fresh Water Addition″ Journal of Environmental Engineering, Volume 144, issue 12. I was responsible for the X-ray Powder Diffraction results that identify minerals from OSPW sediment and FFT samples and for the re-interpretation of water chemistry results obtained by Mr. Brandon. Finally, I was responsible for the composition and editing of the manuscript.

Acknowledgement

Firstly, I would like to express my sincere gratitude to my supervisor Dr. Ania C. Ulrich for the continuous support of my PhD study and related research, for her patience, motivation, and technical and personal guidance. I could not have imagined a better advisor and mentor for my PhD study.

I am grateful to my supervisory committee members Drs. Vinay Prasad and Yang Liu for their continuous support and immense knowledge.

Lastly, I would like to express my profound gratitude to my wife Maki Sakata for her unfailing support and continuous encouragement.

Table of Contents

Chapter 1 : Introduction *1*

1.1 Introduction **2**

1.1.1 Oil Sands Industry 2

1.1.2 Pit Lakes 3

1.2 Research Objectives **5**

1.3 Hypothesis **6**

1.4 Outline of Thesis **7**

1.5 References **8**

Chapter 2 : Theoretical Background and Literature Review *10*

2.1 Clay Behaviour in Suspension **11**

2.1.1 Water Clarity 11

2.1.2 Physical and Chemical Characteristics of Clay Minerals 12

2.2 DLVO Theory of Colloid Stability **16**

2.3 Mineral Phase Reaction and Adsorption Isotherm (Langmuir, 1997) **18**

2.3.1 Gibbs Free Energy 18

2.3.2 Saturation Indices 20

2.3.3 Thermodynamics of Calcite Dissolution and Precipitation 20

2.3.4 Thermodynamics of Biochemical Reactions 22

2.4 Chemical Partitioning **24**

2.5 Literature Review of Oil Sands Tailings Densification **27**

2.5.1 End Pit Lakes 27

2.5.2 Biogenic Gas Emission from the Oil Sands Tailings Ponds 29

2.5.3 Oil Sands Tailings Dewatering/Consolidation Through Carbon Dioxide Addition 32

2.6 References **36**

Chapter 3 : Effect of Naphtha Diluent on Organic Release and Microbial Dynamics in Oil Sands Tailings *41*

3.1 Introduction **42**

3.2 Materials and Methods **44**

3.2.1 Mesocosm Setup 44

3.2.2 BTEX Measurement 45

3.2.3 Microbial Community Analysis 46

3.3 Results and Discussion **48**

3.3.1 Sulfate reduction and methanogenesis 48

3.3.2 BTEX Release from MFT 58

3.4 Conclusion **66**

3.5 References **68**

Chapter 4 : Organic Removal with an Advanced Oxidation System ***72***

4.1 Introduction **73**

4.2 Materials and Methods **75**

4.2.1 Determination of EG Adsorptive Capacity for Organics with Batch Experiment 75

4.2.2 AOS Experiment 76

4.2.3 Chemical Analyses 77

4.2.4 Adsorption Isotherm Calculation 79

4.3 Results and Discussion **80**

4.3.1 Batch Experiment 80

4.3.2 AOS Experiment 85

4.4 Conclusion **91**

4.5 References **92**

Chapter 5 a: Turbidity Reduction Mechanisms ***94***

5.1 Introduction **95**

5.2 Materials and Methods **97**

5.2.1 Big Column Experiments 98

5.2.2 Secchi Depth and Light Intensity 99

5.2.3 Small Column Experiments 100

5.2.4 Turbidity 100

5.2.5 Water Characterization 101

5.2.6 Carbonate Minerals in the FFT Solid Phase 102

5.2.7 X-Ray Diffraction Analysis 102

5.2.9 Geochemical Modelling 103

5.2.10 DLVO theory 103

5.3 Results and Disscusions **104**

5.3.1 Analysis of Previous Preliminary Results 106

5.3.2 Big Column Study 109

5.3.3: Calcite Dissolution Experiment 115

5.4 Conclusion **128**

5.5 References **129**

Chapter 5 b: The effect of sulfate on calcite dissolution ***132***

5.6 Introduction **133**

5.7 Materials and Methods **136**

5.8 Results and Discussion **136**

5.9 Conclusion **141**

5.10 Reference **142**

Chapter 5 c: The effect of dolomite dissolution on CO_2-mediated turbidity reduction ***143***

5.11 Introduction **144**

5.12 Materials and Methods **144**

5.13 Results and Discussion **146**

5.14 Conclusion **160**

5.15 Reference **162**

Chapter 6 : Summary, Engineering Significance and Recommendations for Future Work . ***164***

6.1 Summary **165**

6.2 Conclusions and Engineering Significance **166**

6.2.1 Effect of Naphtha Diluent on Organic Transport and Microbial Dynamics in Oil Sands Tailings 166

6.2.2 Organic Removal with an Advanced Oxidation System 169

6.2.3 A Mechanistic Study for Carbon Dioxide-mediated Turbidity Reduction 170

6.3 Avenues for Future Research **172**

6.3.1 Future Research: Extension of the Present Work 172

6.4 References **175**

Bibliography **177**

Appendix: Additional Results ***A1***

LIST OF TABLES

TABLE 2-1 STOICHIOMETRIC EQUATIONS AND STANDARD FREE ENERGY CHANGES FOR BENZENE OXIDATION WITH VARIOUS ELECTRON ACCEPTORS. 24
TABLE 2-2 LINEAR FORMS OF FREUNDLICH AND LANGMUIR ISOTHERM MODELS 26
TABLE 2-3 SUMMARY OF EXPERIMENTAL DATA FOR MFT SETTLING EXPERIMENTS (ZHU ET AL., 2011). NOTE: CNRL= CANADIAN NATURAL RESOURCES LTD., SETTLING HEIGHT EXPERIMENT WAS PERFORMED IN AN AUTOCLAVE AT 100 KPA AND 25°C. THE SETTLING HEIGHT IS A NORMALIZED HEIGHT (SEDIMENT HEIGHT [H] ÷ SEDIMENT+SUPERNATANT [H]). THE SUPERNATANT TURBIDITY WAS MEASURED AS A FUNCTION OF CO2 PARTIAL PRESSURE. ONLY THE MAJOR OBSERVATIONS ARE PRESENTED IN THIS TABLE. COMPILED FROM ZHU ET AL. (2011). 33
TABLE 2-4 EXPERIMENTAL DATA SUMMARY FOR SIDDIQUE ET AL. 2014A. NOTE: A 50 L COLUMN CONTAINING MFT AND CAP WATER (FROM SYNCRUDE'S MILDRED LAKE SETTLING BASIN) WAS AMENDED WITH HYDROLYSED CANOLA MEAL, OR NOT AMENDED. UNLESS OTHERWISE INDICATED, ALL VALUES PRESENTED HERE ARE FOR DAY ~230 (THE END DAY OF THE EXPERIMENT). THE ABIOTIC CO2 EXPERIMENT WAS CONDUCTED IN A 2 L COLUMN CONTAINING MFT, AND CO2 GAS WAS SPARGED INTO THE COLUMN UNTIL PH REACHED 6.54–6.68. ALL EXPERIMENTS WERE CONDUCTED AT 20°C, AND ONLY THE MAJOR OBSERVATIONS ARE PRESENTED IN THIS TABLE. N/A = DATA NOT AVAILABLE. COMPILED FROM SIDDIQUE ET AL. (2014). 35
TABLE 3-1 EXPERIMENTAL TIMELINE AND MEASUREMENTS PERFORMED 45
TABLE 3-2 PARAMETERS USED IN THE FID METHOD USED TO MEASURE BTEX CONCENTRATIONS IN MESOCOSMS. 45
TABLE 3-3 LIST OF PRIMERS AND CONDITIONS USED FOR DSRAB AND MCR PCR AMPLIFICATION. 48
TABLE 4-1 PARAMETERS OF THE FLUORESCENCE METHOD USED TO MEASURE BTEX AQUEOUS SAMPLES IN THE AOS EXPERIMENT. 78
TABLE 4-2 TCD METHOD USED TO MEASURE CO_2 CONCENTRATION FROM AOS EXPERIMENT. 79
TABLE 4-3 LINEAR FORMS OF LANGMUIR AND FREUNDLICH ADSORPTION ISOTHERMS 79
TABLE 4-4 PHYSICAL CHARACTERISTICS RELATED TO SORPTION OF GAC AND EG. 80
TABLE 4-5 PERCENT REDUCTION FOR BTEX BATCH EXPERIMENT 81
TABLE 4-6 LANGMUIR AND FREUNDLICH ISOTHERM PARAMETERS FOR GAC AND EG. 85
TABLE 4-7 PERCENT REMOVAL OF BTEX COMPOUNDS AT 120 MIN IN THE AOS SYSTEM. 88
TABLE 4-8 SUMMARY OF CO_2 ADSORPTION VIA AOS EXPERIMENT 89
TABLE 5-1 SATURATION INDICES OF ARAGONITE, CALCITE AND DOLOMITE. 108
TABLE 5-2 INITIAL PHYSICAL AND CHEMICAL PARAMETERS FOR THE 80% BML-OSPW 20% BCR (80/20) COLUMN EXPERIMENT 111
TABLE 5-3 A SUMMARY OF TURBIDITY CHANGES IN THE 80/20 COLUMNS 121
TABLE 5-4 A SUMMARY OF TURBIDITY CHANGES IN THE 60/40 COLUMNS 124
TABLE 5-5 A COMPILATION OF PREVIOUSLY REPORTED CALCITE DISSOLUTION RATE VALUES. 127
TABLE 5-5 A COMPARISON OF CALCITE DISSOLUTION SIMULATION AND EXPERIMENTAL RESULTS. 134
TABLE 5-6 SUMMARY OF CALCITE DISSOLUTION EXPERIMENTAL SETUP IN SYNTHETIC BML WATER 136
TABLE 5-7 SUMMARY OF MIXED CARBONATE MINERAL (DOLOMITE-2 AND CALCITE) DISSOLUTION EXPERIMENTAL SETUP. 145
TABLE 5-8 SUMMARY OF TURBIDITY CHANGES IN THE DOLOMITE-1 DISSOLUTION EXPERIMENT 149
TABLE 5-9 SUMMARY OF TURBIDITY REDUCTION PERCENTAGES FOR THE MIXED CARBONATE MINERAL (DOLOMITE AND CALCITE) DISSOLUTION EXPERIMENT. 156

List of Figures

Figure 2-1 Simplified graphical representation of octahedron and tetrahedron structures of clay minerals. Figure excerpted from Appelo and Postma (2005). 13
Figure 2-2 A representation of the DDL surrounding a kaolinite clay particle (left) and the Stern models (right) of the interaction between the negatively charged clay surface with cations and anions in the bulk solution. Adopted and modified from Liu et al. (2013) and from Masliyah and Bhattacharjee (2006). 14
Figure 2-3 A schematic representation of the total DLVO interaction energy profile as a function of separation distance. This example plot uses the following parameters: A=8.3x10-21 J, a=5x10-7 m, k=3.2x107 m, ψ=−25 mV, in a 0.2 M electrolyte solution (adapted from Elimelech (1998)). EB=energy barrier. 17
Figure 2-4 Aerial view of BML. Modified from Dompierre et al. (2017). 29
Figure 3-1 Hydrogen sulfide measurement for the (a) PW and (b) SPW groups over the 14-week study period. Filled circles: PW or SPW +0.8% diluent; open diamonds: +MFT; open triangle: +MFT/+0.2% diluent, open square: +MFT/+0.8% diluent; x: +MFT/+1.5% diluent. (c) The dissimilatory sulfite reductase (Dsr) gene was amplified from each of the duplicate MFT samples. MFT obtained prior to experiment (week 0) was used as control for both week 5 and 11. Figure was modified from Gee et al. (2017). 51
Figure 3-2 Methane measurement for the (a) PW and (b) SPW groups over the 11-week study period. Filled circles: PW or SPW +0.8% diluent; open diamonds: +MFT; open triangle: +MFT/+0.2% diluent, open square: +MFT/+0.8% diluent; x: +MFT/+1.5% diluent. (c) The MCR gene was amplified from each of the duplicate MFT samples. MFT obtained prior to experiment (week 0) was used as control. Figure is excerpted from Gee et al. (2017). 54
Figure 3-3 16S rRNA gene microbial community analysis of mesocosm samples at week 5 and week 11. The relative abundance (%) of microbial communities within the mesocosms were plotted at family levels. Figure excerpt from Gee et al. (2017). 55
Figure 3-4 Benzene and toluene mass (mg) measured in mesocosm headspace. 60
Figure 3-5 Benzene and toluene release rate for PW and SPW groups over the 15 week study period. The change in benzene and toluene concentration (mg/mL MFT/d) between 1-0, 2-1, 4-2, 6-4, 11-6, and 15-11 weeks were plotted. Note that any negative values were set to be 0. 62
Figure 4-1 A Simplified Schematic of Advance Oxidation System. This schematic was generated with ChemDraw Prime 17.1. 76
Figure 4-2 BTEX adsorption batch experiment results. The graphs shown are average of n=3, and error bar represent one standard error. 81
Figure 4-3 EG adsorption preferences. Each BTEX compound is shown in the order of EG adsorption preference from high to low (left to right); EG shows similar preference to both benzene and toluene. Note: chemical structures are modified from chemspider.com. The log Kow values were obtained from Agteren et al. (1998). 83
Figure 4-4 Linear fit adsorption isotherm models for GAC and EG. Note: when calculating adsorption capacity (qe) for EG with benzene, the benzene concentration from the 8 mg/L GAC was used as initial concentration (Co) due to a low benzene concentration measured in the control. 84
Figure 4-5 Breakthrough curves of AOS experiment at 10 mL/min flowrate with or without electricity applied. 86
Figure 4-6 Breakthrough curves of AOS experiment at 4 mL/min flowrate with or without electricity applied. 87

FIGURE 5-1 A SCHEMATIC OF A TOWNSEND COLUMN AND ITS RELEVANT DIMENSIONS. ALL MEASUREMENTS ARE DENOTED IN METERS, AND THE COLUMN'S FIVE PORTS ARE INDICATED BY THE LINES ON EITHER SIDE OF THE OUTSIDE OF THE COLUMN. 99
FIGURE 5-2 CHEMICAL AND PHYSICAL PARAMETERS FOR THE 60/40+CO_2, 60/40-NOCO_2, AND 20/80+CO_2 COLUMNS OVER THE 113 DAY EXPERIMENTAL PERIOD. A) PH, B) SECCHI DISK DEPTH, C) TURBIDITY AND D) ALKALINITY * = $P < 0.05$ AND *** = $P < 0.001$. MODIFIED FROM POON ET AL. (2018). 105
FIGURE 5-3 PIPER DIAGRAMS FOR A) 60/40+CO_2, B) 60/40+NOCO_2, AND C) 20/80+CO_2 WATER COLUMNS. FIGURE EXCERPT FROM POON ET AL. (2018)....107
FIGURE 5-4 X--RAY POWDER DIFFRACTION RESULTS FOR A) BML SURFACE WATER AND B) FFT. FIGURE EXCERPT FROM POON ET AL. (2018). CALCITE MINERAL INDICATED BY A BLUE ARROW. 110
FIGURE 5-5 MEAN PH, CONDUCTIVITY, AND ALKALINITY OF CO_2 TREATED AND NOCO_2 COLUMNS OVER 191 DAYS. NOTE: ERROR BARS REPRESENT ONE STANDARD ERROR OF DUPLICATE SAMPLE MEASUREMENTS. 112
FIGURE 5-6 TURBIDITY, LIGHT INTENSITY, AND SECCHI DISK DEPTH OF CO_2 TREATED AND NOCO_2 COLUMNS OVER 191 DAYS. NOTE: ERROR BARS REPRESENT ONE STANDARD ERROR OF DUPLICATE SAMPLES....113
FIGURE 5-7 CHARACTERIZATION OF ICELAND SPAR (45–75 μM) BY A) XRD AND B-E) SEM-EDS. NOTE: AN ENLARGED VERSION OF ICELAND SPAR XRD RESULTS IS SHOWN IN THE APPENDIX (FIGURE A-4)....116
FIGURE 5-8 SMALL COLUMN CALCITE DISSOLUTION RESULTS FOR THE 80% OSPW 20%BCR WATER MIX WITH 0.5 G (A, C, E, G) OR 1 G (B, D, F, H) CALCITE ADDITION. NOTE: THE ZETA POTENTIAL VALUE WAS AN AVERAGE OF REPEATED MEASUREMENTS OF A SINGLE SAMPLE, AND THE ERROR BAR REPRESENTS ONE STANDARD ERROR..119
FIGURE 5-9 CATION AND ANION CONCENTRATION FOR THE A & C) 80/20+0.5G CALCITE, B & D) 80/20+1G CALCITE AND E & F) 80/20 COLUMN EXPERIMENTS. 120
FIGURE 5-10 PHYSICAL AND CHEMICAL RESULTS FOR THE CALCITE DISSOLUTION EXPERIMENT IN THE 60/40 WATER MIX. A) PH, B) ALKALINITY, C) TURBIDITY, D) ZETA POTENTIAL, AND CATION AND ANION RESULTS FOR THEE & F) 60/40+0.5G CALCITE AND G & H) 60/40 COLUMNS. NOTE: ALL DATA SHOWN ARE AN AVERAGE FROM DUPLICATE EXPERIMENTS AND THE ERROR BAR REPRESENTS ONE STANDARD ERROR OF THE AVERAGED VALUE. 123
FIGURE 5-11 CALCITE DISSOLUTION RATES IN DIFFERENT WATERS UNDER DIFFERENT CO_2 AND CALCITE TREATMENTS. NOTE: DISSOLUTION RATE WAS CALCULATED FROM DISSOLVED CALCIUM ION CONCENTRATION UNDER THE ASSUMPTION THAT THE MEASURED DISSOLVED CALCIUM MOLAR CONCENTRATION IS DIRECTLY CORRELATED TO THE CALCITE DISSOLUTION. 127
FIGURE 5-12 WATER CHEMISTRY RESULTS FOR 1 L COLUMN CALCITE DISSOLUTION EXPERIMENTS PERFORMED WITH SYNTHETIC BML WATER. 138
FIGURE 5-13 CALCULATED CALCITE DISSOLUTION RATE IN SYNTHETIC BML WATER USED FOR THE 1 L COLUMN EXPERIMENTS. NOTE: THE CALCITE DISSOLUTION RATE WAS CALCULATED FROM THE DISSOLVED CALCIUM CONCENTRATION RESULT UNDER THE ASSUMPTION THAT THE MEASURED CONCENTRATION REFLECTS THE DISSOLUTION EVENT. 140
FIGURE 5-14 CHARACTERIZATION OF CRUSHED DOLOMITE-1 CRYSTAL (45–75 μM) BASED ON A) XRD AND B-D) SEM-EDS RESULTS. NOTE: AN ENLARGED VERSION OF THE DOLOMITE-1 XRD RESULT IS PRESENTED IN THE APPENDIX (FIGURE A-6). 146
FIGURE 5-15 PHYSICAL AND CHEMICAL RESULTS FROM THE DOLOMITE-1 DISSOLUTION EXPERIMENT. NOTE: AVERAGED VALUES ARE PLOTTED AND THE ERROR BARS REPRESENT THE STANDARD ERROR. 148
FIGURE 5-16 CHARACTERIZATION OF CRUSHED DOLOMITE-2 (45–75 μM) BASED ON A) XRD AND B-D) SEM-EDS RESULTS. NOTE: AN ENLARGED VERSION OF THE DOLOMITE-2 XRD RESULT IS PRESENTED IN THE APPENDIX (FIGURE A-7). 150
FIGURE 5-17 PHYSICAL AND CHEMICAL MEASUREMENTS FOR THE MIXED CARBONATE MINERAL (DOLOMITE AND CALCITE) DISSOLUTION EXPERIMENT. NOTE: AVERAGED VALUES ARE PLOTTED AND THE ERROR BARS REPRESENT THE STANDARD ERROR. 155

FIGURE 5-18 DISSOLVED ION CONCENTRATIONS IN THE MIXED CARBONATE MINERAL (DOLOMITE AND CALCITE) DISSOLUTION EXPERIMENT.....157
FIGURE 5-19 TOTAL INTERACTION ENERGY AS A FUNCTION OF INTERPARTICLE DISTANCE FOR CO_2 TREATMENT COLUMNS. A) 60/40+CO_2+100%-DOLOMITE-2 COLUMN, B) 60/40+CO_2+50%-DOLOMITE-2 COLUMN, C) 60/40+CO_2+25%-DOLOMITE-2 COLUMN, D) 60/40+CO_2+0%-DOLOMITE-2 COLUMN AND INTERACTION ENERGY PROFILES ON DAY 42 FOR E) CO_2-TREATED COLUMNS AND F) NOCO_2 COLUMNS 158

List of Nomenclature, or Abbreviations

16S rRNA	16S ribosomal Ribonucleic acid
AOS	Advanced oxidation system
BET	Brunauer-Emmett-Teller
BTEX	Benzene, Toluene, Ethylbenzene, Xylene
BML	Base Mine Lake
BCR	Breaver Creek Reservoir
CEC	Cation exchange capacity
CH_4	Methane
CH_3	Methyl group
CNRL	Canadian Natural Resources Limited
CO_2	Carbon dioxide
COSIA	Canada's Oil Sands Innovation Alliance
DDL or EDL	Diffuse double layer or electrical double layer
DLVO	Derjaguin, Landau, Verwey, and Overbeek
DNA	Deoxyribonucleic Acid
Dsr	Dissimilatory sulfite reductase
EG	Expanded Graphite
FFT	Fluid Fine Tailings
GAC	Granular activated carbon
GC-FID	Gas chromatography with flame ionization detector
GC-TCD	Gas chromatography with thermal conductivity detector
GHG	Greenhouse gases
H_2	hydrogen
H_2S	Hydrogen Sulfide
ICP-OES	Inductively coupled plasma-optical emission spectroscopy
KI	Postassium iodide
K_{ow}	n-Octanol/water partition coefficient
MCR	methyl-coenzyme M reductase
MFT	Mature Fine Tailings
MLSB	Mildred Lake Settling Basin
NMDS	Non-matric multidimension scaling
NTU	Nephelometric turbidity units
OTU	Operational Taxonomic Unit
OSPW	Oil Sands Process affected Water
PCR	Polymerase Chain Reaction
PHREEQC	pH-REdox-EQuilibrium
PL	Pit Lake
PW	Pond Water (from Oil Sands Tailings Ponds)
RTR	Ready to reclaim
SBML water	Synthetic Base Mine Lake water
SO_4	sulfate
SPW	Synthetic Pond Water
SRB	Sulfate-Reducing Bacteria
TIC	Total inorganic carbon
XRD	X-ray diffraction
Vol	Volume

Chapter 1 : Introduction

1.1 Introduction

1.1.1 Oil Sands Industry

The Alberta oil sands are the third largest contributor to global oil reserves (Government of Alberta, 2016). Oil sands are composed of sand, clay, water and bitumen. In general, surface mining followed by Clark Hot Water Extraction, or *in situ* methods, are used to extract bitumen from the oil sands deposits (Humphries, 2008). The *in situ* method, where bitumen is extracted from a underground well after being liquified by steam, is suitable for recovering the bitumen that is too deep for surface mining (Alberta Energy Regulator, 2016b). In general, a greater understanding of the site geology is needed for the *in situ* method (Alberta Energy Regulator, 2016b). The surface mining method is suitable when there is less than 75 m of overburden (Humphries, 2008), and generates by-products such as fluid fine tailings (FFT) and oil sands process affected water (OSPW) during the bitumen extraction process (Humphries, 2008). Oil sands mining companies currently do not have regulatory approval to discharge OSPW, so these by-products are contained in tailings ponds (Government of Alberta 2015). Oil sands tailings contain a mixture of sand, clay, silt, residual organics, salts, trace metals and water (Government of Alberta, 2015). FFT is defined as fluids with greater than 5% wt/wt suspended solids content and less than 5 kPa undrained shear strength (Government of Alberta, 2015). It takes 2–4 years for tailings to consolidate by gravity from ~10 wt% (initial) to ~30 wt% solids contents (also known as mature fine tailings; Arkell et al., 2015; Fedorak et al., 2003; Jeeravipoolvarn et al., 2009), and will take an estimated 125 - 150 years for FFT to be completely consolidated (Eckert et al., 1996). The FFT in the tailings ponds is allowed to settle and release process water, which is recycled into the bitumen extraction process to reduce fresh water consumption. However, it will require decades for tailings to consolidate from ~30 wt% to 60 wt% solids through gravity

settling (Fedorak et al., 2003; Jeeravipoolvarn et al., 2009). As of 2013, approximately 976 million m^3 of FFT has been accumulated (Government of Alberta, 2016), and bitumen production is projected to increase from 2.5 million barrels per day to 4 million barrels per day by 2035 (Canadian Association of Petroleum Producers, 2018). This rapid expansion of oil sands operations has generated a greater need for reclamation treatment and storage strategy for FFT and OSPW.

1.1.2 Pit Lakes

In 2016, the Alberta Energy Regulator issued Directive 085 to provide a guideline for oil sands tailings management (Alberta Energy Regulator, 2016a). Directive 085 specifies that new fluid tailings treated and placed in the final landscape must be ready to reclaim (RTR) within ten years after the end of mine life (Alberta Energy Regulator, 2016a). In addition, all legacy tailings must be RTR by the end of mine life (Alberta Energy Regulator, 2016a). The main objective of tailings reclamation is to support the transformation of oil sands mining projects (including mined or disturbed lands) into "a self-sustaining boreal forest ecosystem" (Alberta Energy Regulator, 2016a) after mining is complete. Slow FFT settling and OSPW toxicity are the key challenges for mine reclamation (Allen, 2008). A significant amount of research has been conducted to improve the shear strength of tailings for reclamation and storage—one such technology is water capping.

Water capping of tailings in a pit lake is a reclamation strategy where water (OSPW or other water sources) is placed on top of a layer of FFT (Alberta Energy Regulator, 2016a). The FFT is allowed to dewater, and the water cap gradually develops into a self-sustaining aquatic ecosystem. Toxicity is reduced through natural attenuation (Alberta Energy Regulator, 2016a; Cumulative Environmental Management Association, 2012). Small experimental ponds were

constructed in the late 1980s and early 1990s by Syncrude Canada Ltd. to test the feasibility of the pit lake technology (Mackinnon & Boerger, 1991). Results from these studies showed that 1) FFT densification and dewatering occurred over time, 2) OSPW released during the dewatering process did not increase water toxicity, and 3) a diverse ecosystem developed in the water cap (Mackinnon & Boerger, 1991; Westcott & Watson, 2005). Based on these positive results, Base Mine Lake (BML), a full scale PL demonstration, was commissioned in 2012. By 2013, BML was filled with 186 million m^3 FFT (45 m depth) and capped with 90% OSPW and 10% fresh water from Beaver Creek Reservoir (BCR). The expectation is that BML will develop into a self-sustaining aquatic ecosystem, and will provide long-term storage and remediation of FFT and OSPW. Despite the encouraging results from Syncrude's experimental ponds, a full scale EPL has not yet been fully tested (Mackinnon & Boerger, 1991). As such, several environmental issues need to be addressed prior to the PL technology used by other oil sands operators such as: (1) emission of biogenic gases (Holowenko et al., 2000; Penner & Foght, 2010), (2) toxicity of organic compounds, including naphthenic acids (NAs; Scarlett et al., 2012), and (3) high surface water turbidity cause by fine suspended particles (OSTC, 2012).

While many studies focus on surface water toxicity in the oil sands tailings ponds and pit lakes, there is still not a comprehensive understanding of what contributes to turbidity in the water column.

High turbidity (maximum 290 – 630 NTU, 2013–2015; information obtained from unreleased BML monitoring program report provided by Syncrude) in the BML surface water could hinder the development of aquatic ecosystems, including macrophytes, phytoplankton, fish, bird, reptiles, and amphibians (Cumulative Environmental Management Association, 2012; Tundisi & Tundisi, 2012; Westcott & Watson, 2005). Ebullition of biogenic gases is one mechanism for

chemical flux and FFT resuspension (Lawrence et al., 2016). There have been limited studies on the 1) microbial activities and 2) chemical flux in the FFT related to the amount of residual naphtha diluent in the FFT, as well as 3) technology to remove organics from oil OSPW. FFT dewatering can be accelerated by adding carbon dioxide, but the exact mechanism of CO_2-mediated FFT dewatering is still poorly understood. Addressing these knowledge gaps is a critical step towards increasing the rate of FFT settlement and OSPW recycling from tailings ponds, and developing a healthy aquatic ecosystem in BML.

1.2 Research Objectives

The three research objectives of this study will focus on turbidity mitigation:

1) Assess the impact of residual naphtha diluent on microbially-produced gas emissions and BTEX release from the FFT under anaerobic conditions.
2) Investigate the capacity of BioLargo's advanced oxidation system to remove organics in water, which combines iodine electrochemistry and expanded graphite adsorption.
3) Investigate the effect of CO_2-mediated calcite and dolomite dissolution on turbidity reduction in relation to suspended FFT.

Despite many research advancements, FFT storage and reclamation still pose a significant challenge in the oil sands industry. The clay particles from the FFT are highly stable in aqueous suspension, which hinders water recycling from the tailings ponds and the development of a healthy aquatic ecosystem in BML. This research is anticipated to be of interest to the entire oil sands mining industry.

1.3 Hypothesis

The following hypotheses was established at the outset of the research project:

Residual organics promote biological activities in the FFT, generating methane and hydrogen sulfide (Arkell et al., 2015; Gee et al., 2017; Siddique et al., 2006; Siddique et al., 2007; Siddique et al., 2012; Siddique et al., 2011). The ebullition of these biogenic gases is one likely mechanism of FFT resuspension in tailings ponds and BML (Lawrence et al., 2016). The settling of suspended clay particles from FFT can be improved through carbon dioxide-induced carbonate mineral dissolution. Ebullition also contributes to the transport of organics from the FFT into the surface water (Hurley, 2017), which can be treated more quickly with advanced oxidation as opposed to biodegradation alone.

- The evolution of CH_4, CO_2 and reduced sulfur compounds (RSC; including H_2S) in tailings relates to: i) naphtha diluent concentration and ii) microbial activity, and influences the chemical flux from tailings.
- Advance oxidation systems may be used to remove organics commonly found in the naphtha diluent, such as BTEX (benzene, toluene, ethylbenzene, and xylenes) compounds.
- The pH changes induced by CO_2 addition allow calcium and dolomite dissolution, which could further enhance FFT dewatering.

1.4 Outline of Thesis

Chapter 2 provides an overview of the related research conducted to date, as well as necessary background information to understand the work presented in the later chapters. Chapter 3 explores objective 1 by examining the effect of the varying diluent concentrations on microbial community dynamics and benzene and toluene relases. Chapter 4 investigates objective 2 by characterizing the expanded graphite (EG) adsorption capacity for organic compounds and determining the capacity of the advance oxidation system to remove organic compounds. Chapter 5 explores objective 3 by examining the calcite and dolomite dissolution characteristics in CO_2-treated OSPW and synthetic OSPW.

1.5 References

Alberta Energy Regulator. (2016a). *Directive 085: Fluid Tailings Management for Oil Sands Mining Projects*. Retrieved from http://www.aer.ca/documents/directives/Directive085.pdf.

Alberta Energy Regulator. (2016b). *In Situ* Impacts. Retrieved from https://www.aer.ca/about-aer/spotlight-on/oil-sands/in-situ-impacts

Allen, E. W. (2008). Process water treatment in Canada's oil sands industry: I. Target pollutants and treatment objectives. *J Environ Eng and Sci, 7*(2), 123-138.

Arkell, N., Kuznetsov, P., Kuznetsova, A., Foght, J. M., & Siddique, T. (2015). Microbial metabolism alters pore water chemistry and increases consolidation of oil sands tailings. *J Environ Qual, 44*(1), 145-153.

Canadian Association of Petroleum Producers. (2018). *2018 CAPP Crude Oil Forecast, Markets & Transportation*. Retrieved from https://www.capp.ca/publications-and-statistics/publications/320294

Cumulative Environmental Management Association. (2012). *End pit lakes guidance document* (pp. 1 online resource (434 p.)). Retrieved from http://www.deslibris.ca/ID/234915

Eckert, W. F., Masliyah, J. H., Gray, M. R., & Fedorak, P. M. (1996). Prediction of sedimentation and consolidation of fine tails. *AIChE J, 42*(4), 960-972.

Fedorak, P. M., Coy, D. L., Dudas, M. J., Simpson, M. J., Renneberg, A. J., & MacKinnon, M. D. (2003). Microbially-mediated fugitive gas production from oil sands tailings and increased tailings densification rates. *J Environ Eng and Sci, 2*(3), 199-211.

Gee, K. F., Poon, H. Y., Hashisho, Z., & Ulrich, A. C. (2017). Effect of naphtha diluent on greenhouse gases and reduced sulfur compounds emissions from oil sands tailings. *Sci Total Environ, 598*, 916-924.

Government of Alberta. (2015). *Lower Athabasca Region : tailings management framework for the mineable Athabasca oil sands*.

Government of Alberta, (2016). Oil Sands: Facts and Statistics. Retrieved from https://open.alberta.ca/publications/oil-sands-facts-and-stats

Holowenko, F. M., MacKinnon, M. D., & Fedorak, P. M. (2000). Methanogens and sulfate-reducing bacteria in oil sands fine tailings waste. *Can J Microbiol, 46*(10), 927-937.

Humphries, M. (2008). *North American Oil Sands history of development, prospects for the future* (pp. 31 p.). Retrieved from http://fas.org/sgp/crs/misc/RL34258.pdf

Hurley, D. L. (2017). *Wind waves and internal waves in Base Mine Lake.* (Master's thesis) University of British Columbia. Retrieved from https://open.library.ubc.ca/collections/ubctheses/24/items/1.0351993

Jeeravipoolvarn, S., Scott, J. D., & Chalaturnyk, R. J. (2009). 10 m standpipe tests on oil sands tailings: long-term experimental results and prediction. *Can Geotech J, 46*(8), 875-888.

Lawrence, G. A., Tedford, E. W., & Pieters, R. (2016). Suspended solids in an end pit lake: potential mixing mechanisms. *Can J Civ Eng, 43*(3), 211-217.

Mackinnon, M., & Boerger, H. (1991). *Assessment Of A Wet Landscape Option For Disposal Of Fine Tails Sludge From Oil Sands Processing*. Annual Technical Meeting. Petroleum Society of Canada.

OSTC. (2012). *Technical Guide for Fluid Fine Tailings Management*. Retrieved from http://www.cosia.ca/uploads/documents/id7/TechGuideFluidTailingsMgmt_Aug2012.pdf

Penner, T. J., & Foght, J. M. (2010). Mature fine tailings from oil sands processing harbour diverse methanogenic communities. *Can J Microbiol, 56*(6), 459-470.

Scarlett, A. G., West, C. E., Jones, D., Galloway, T. S., & Rowland, S. J. (2012). Predicted toxicity of naphthenic acids present in oil sands process-affected waters to a range of environmental and human endpoints. *Sci Total Environ, 425*, 119-127.

Siddique, T., Fedorak, P. M., & Foght, J. M. (2006). Biodegradation of short-chain n-alkanes in oil sands tailings under methanogenic conditions. *Environ Sci Technol, 40*(17), 5459-5464.

Siddique, T., Fedorak, P. M., MacKinnon, M. D., & Foght, J. M. (2007). Metabolism of BTEX and naphtha compounds to methane in oil sands tailings. *Environ Sci Technol, 41*(7), 2350-2356.

Siddique, T., Penner, T., Klassen, J., Nesbo, C., & Foght, J. M. (2012). Microbial communities involved in methane production from hydrocarbons in oil sands tailings. *Environ Sci Technol, 46*(17), 9802-9810.

Siddique, T., Penner, T., Semple, K., & Foght, J. M. (2011). Anaerobic biodegradation of longer-chain n-alkanes coupled to methane production in oil sands tailings. *Environ Sci Technol, 45*(13), 5892-5899.

Tundisi, J. G., & Tundisi, T. M. (2012). *Limnology* (pp. 1 online resource (xxii, 864 p.)). Retrieved from http://search.ebscohost.com/login.aspx?direct=true&scope=site&db=nlebk&db=nlabk&AN=437330

Westcott, F., & Watson, L. (2005). End pit lakes technical guidance document: Report. Cumulative Environmental Management Association. 51p. Report. Cumulative Environmental Management Association. 51p.

Chapter 2 : Theoretical Background and Literature Review

This chapter provides the background information that will help the reader to better understand the concepts discussed in later chapters. Section 2.1 will provide a general introduction to water clarity and the physical and chemical characteristics of clay particles in solution. Section 2.2 will discuss the theory for a mathematical model (the Derjaguin-Landau-Verwey-Overbeek model or DLVO), which is an important concept for chapter 5b. Section 2.3 will include background on mineral phases and microbial energetics, which will help readers to understand chapters 3 and 5. Section 2.4 will discuss adsorption isotherms, which provides context for chapter 4. Section 2.5 presents a literature summary of past relevant research on oil sands tailings densification.

2.1 Clay Behaviour in Suspension

2.1.1 Water Clarity

Water clarity is often used to describe the optical properties of a water body (Davies-Colley & Smith, 2001). Suspended fine particles affect the inherent and apparent optical properties of the water (Davies-Colley & Smith, 2001; Morel & Loisel, 1998). The scattering and/or absorption of photons by suspended fine particles determines the inherent optical properties of a water body, as seen in nephelometric turbidity measurements (Morel & Loisel, 1998). The apparent optical properties of a water body depend on the directional structure of the ambient light source, as seen in the Secchi depth measurement (Davies-Colley & Smith, 2001; Morel & Loisel, 1998). In natural water, fine mineral particles 0.2–5 μm in size will remain in suspension and cause most of the light attenuation in natural water systems (Davies-Colley & Smith, 2001). According to Alberta surface water quality guidelines for protection of freshwater aquatic life, the turbidity must not increase more than 8 NTU if background turbidity is 8–80 NTU. If the background turbidity is >80 NTU, the turbidity may not increase more than 10% (Government of Alberta, 2018). Decreased water clarity also affects aquatic organisms by interfering with invertebrate

and vertebrate feeding, and can damage fish gill and tissue (Cumulative Environmental Management Association, 2012; Tundisi & Tundisi, 2012; Westcott & Watson, 2005). High turbidity (27–108 NTU) has a significant negative impact on fish predation (Gregory & Levings, 1998). Turbidity between 3 to 8 NTU has low impact on fish predation (Birtwell, 2008). Turbidity below 3 NTU has no apparent impact on fish (Birtwell, 2008).

2.1.2 Physical and Chemical Characteristics of Clay Minerals

This section will focus on the physical and chemical characteristics of clay minerals that are typically found in oil sands tailings. Clay minerals comprise a large and specific sub-group of hydrous aluminosilicate minerals (Hunter, 2001; J. G. Ibanez, 2007). These minerals consist of multiple repeats of two layers: an octahedral sheet and a tetrahedral sheet (Figure 2-1;Appelo & Postma, 2005; Hunter, 2001). Different clay minerals have different ratios of octahedral and tetrahedral sheets. For example, kaolinite is arranged in a 1:1 ratio of octahedral and tetrahedral sheets, and pyrophyllite is arranged in a 2:1 ratio of octahedral and tetrahedral sheets (Hunter, 2001). Oxygen atoms surrounding the centre cation join each sheet and layer, and this arrangement results in the highly negatively charged surface of the clay particle (Appelo & Postma, 2005; Hunter, 2001).

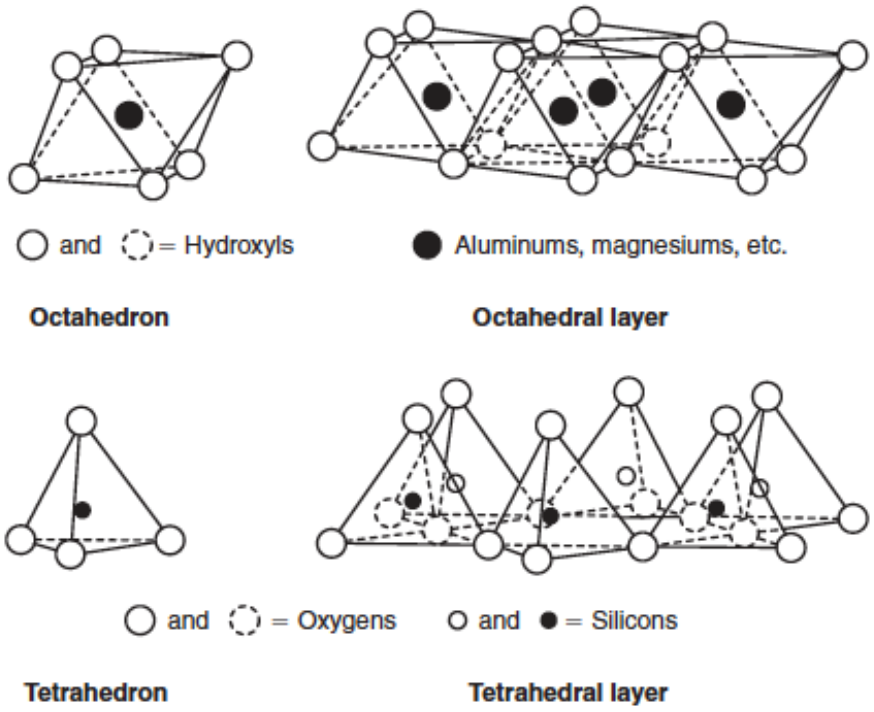

Figure 2-1 Simplified graphical representation of octahedron and tetrahedron structures of clay minerals. Figure excerpted from Appelo and Postma (2005).

A diffuse double layer (DDL) around the clay particle forms in aqueous solution, where the diffused distribution of the excess positively charged ions (counter-ions) and negatively charged ions (co-ions) surround a clay particle (Figure 2-2;Hunter, 2001; Liu et al., 2013). The shear plane serves as a boundary to separate the fixed (stern plane) and more mobile diffuse layers (Figure 2-2). This is also the region where the electrical potential (zeta potential) is measured (Masliyah & Bhattacharjee, 2006; Sawyer et al., 1994).

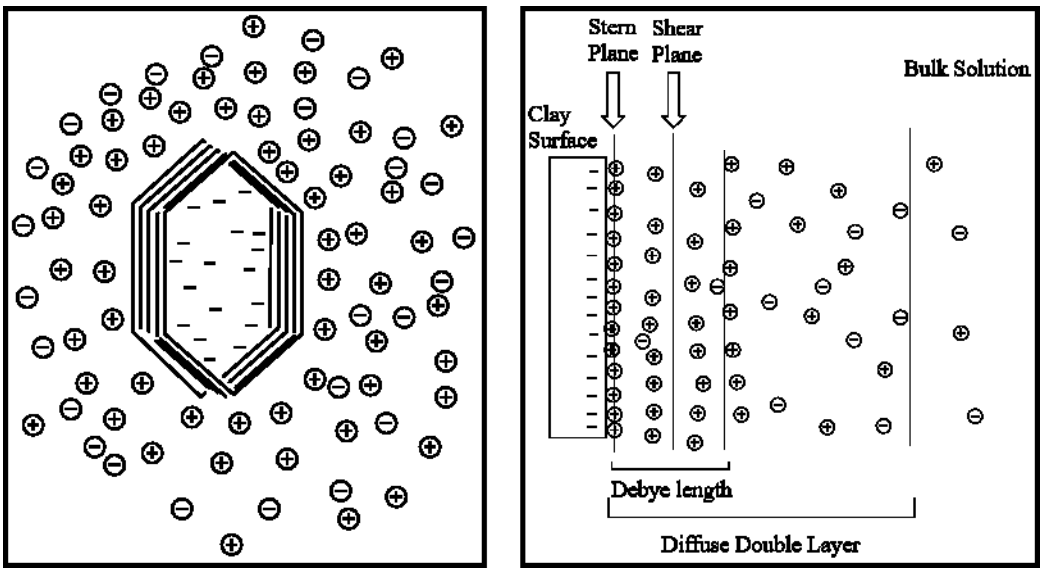

Figure 2-2 A representation of the DDL surrounding a kaolinite clay particle (left) and the Stern models (right) of the interaction between the negatively charged clay surface with cations and anions in the bulk solution. Adopted and modified from Liu et al. (2013) and from Masliyah and Bhattacharjee (2006).

The zeta potential is an electrokinetic parameter used to evaluate the stability of colloids (in this case clay) in aqueous media using the mathematical model DLVO model by balancing the attractive force (van der Waals) and repulsive force (electrostatic;Benitez et al., 2007; Grasso et al., 2002; Missana & Adell, 2000).

Several parameters that affect the stability of clay in aqueous suspension are solution pH, cation exchange capacity and ionic strength. The surface charge of a clay particle is both pH-independent and -dependent, and the pH of the solution can influence the surface charge of clay particles (Bolland et al., 1980; Liu et al., 2013; Zhu et al., 2011). For example, in kaolinite the tetrahedral sheet surface charge is permanently negative while the surface charges along the edges (of the clay particle) and octahedral sheet changes with the solution pH (Liu et al., 2013). Under acidic pH more oxygen atoms in the clay particle are bound to hydrogen atoms, which reduces the surface charge (Appelo & Postma, 2005).

Cation exchange capacity (CEC) affects clay stability in solution. The interlayer region of clay particles can adsorb and exchange cations from the solution due to the unbalanced charge within the clay crystal structures (Hunter, 2001). Typically, Al^{3+}, Mg^{2+}, Fe^{2+}, Mn^{2+}, Ca^{2+}, Na^{+}, or K^{+} ions occupy the centre of the octahedral sheet, and either Si^{4+} or Al^{3+} metal ions occupy the centre of the tetrahedral sheet (Appelo & Postma, 2005). Different clay minerals have different CEC, for example kaolinite has a CEC of 30–150 meq/kg and montmorillonite has a CEC of 800–1200 meq/kg (Appelo & Postma, 2005; Liu et al., 2013).

Ionic strength is a measure of the total ion concentration in a solution and is an important parameter for the thickness of the DDL in clay (Benitez et al., 2007). The DDL thickness or Debye length (Figure 2-2) depends on the temperature and ionic strength (Equation 2-1;Appelo & Postma, 2005; Benitez et al., 2007; Grasso et al., 2002).

$$\kappa^{-1} = \sqrt{\frac{\varepsilon k_B T}{2IeF'}} \qquad \text{(Equation 2-1)}$$

Where, κ^{-1} is DDL thickness (Debye length) surrounding the particle (nm), ε is permittivity of the medium ($C^2/J{\cdot}m$), k_B is Boltzmann constant (1.381×10^{-23} J/K), T is temperature (K), I is ionic strength of medium (mol/L), e is electron charge (1.602×10^{-19} C), and F' is Faraday's constant (96485.332 C/mol)

According to Equation 2-1, the DDL thickness decreases (double layer compression) as the ionic strength increases, and this compression improves the coagulation/flocculation process (Hunter, 2001; Siddique et al., 2014). Ibanez et al. (2014) observed that the electrophoretic mobility (zeta potential) measurements are incrementally less negative when commercial kaolinite samples are placed in various media: no salt (≈ −40 mV), potassium chloride (≈ −30 mV), and magnesium

chloride (≈ −20 mV). These observations suggest that the instability of suspended clay particles can be induced by increasing the divalent cation concentration.

2.2 DLVO Theory of Colloid Stability

As mentioned in section 2.1.2, the DLVO theory is a mathematical model that describes the surface interactions of two colloidal particles in solution by the balance of the attractive and repulsive forces between the particles (Derjaguin & Landau, 1993; Grasso et al., 2002; Verwey, 1947). The DLVO theory can be used to predict the stability of colloid systems and microbial adhesion. A stable colloid is one where agglomeration and settling are not favoured so the colloid remains in suspension (Langmuir, 1997; Ohshima, 2012). The classical DLVO theory assumes that the net interaction potential (Φ_{net}) in a colloid system is the sum of the van der Waals attractive (Φ_A) and electrical double layer (EDL) repulsive (Φ_R) forces as a function of distance between colloids (Derjaguin & Landau, 1993; Grasso et al., 2002; Verwey, 1947).

$$\Phi_{net} = \Phi_A + \Phi_R \qquad \text{(Equation 2-2)}$$

The Φ_A can be calculated using the following equation (Berg, 2010; Hogg et al., 1966):

$$\Phi_A = -\frac{Aa}{12S_0} \qquad \text{(Equation 2-3)}$$

where A is Hamaker constant (J), a is the radius of colloid particle (m), and S_0 is the distance between particles (nm).

The Φ_R can be calculated using the following equation (Hogg et al., 1966):

$$\Phi_R = \frac{\varepsilon a \psi^2}{2} ln[1 + \exp(-kS_0)] \qquad \text{(Equation 2-4)}$$

where ε is the permittivity of the medium (F/m), a is the radius of colloid particle (m), ψ is the zeta potential (V), k is the Debye length (Equation 2-1), and S_0 is the distance between particles (nm). (Note: Equations 2-3 and 2-4 assume the interaction is between two spherical particles with equal diameter.)

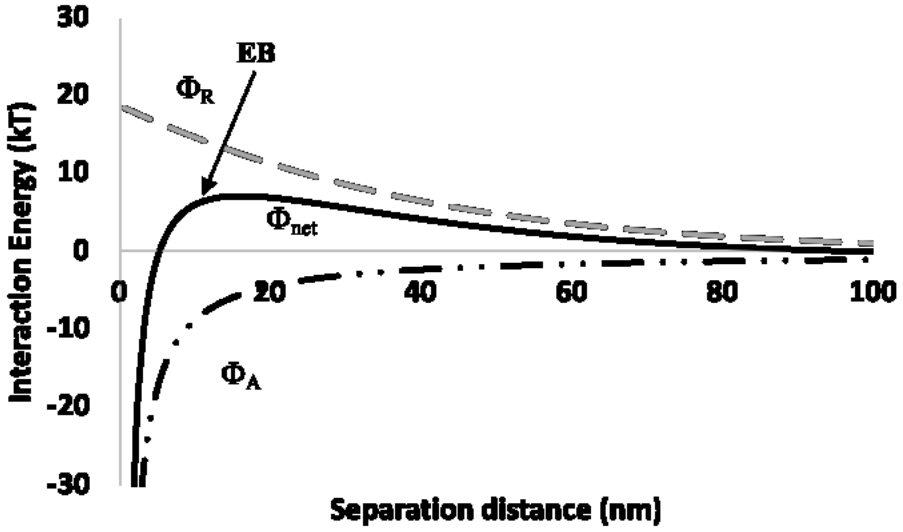

Figure 2-3 A schematic representation of the total DLVO interaction energy profile as a function of separation distance. This example plot uses the following parameters: A=8.3x10-21 J, a=5x10-7 m, k=3.2x107 m, ψ=−25 mV, in a 0.2 M electrolyte solution (adapted from Elimelech (1998)). EB=energy barrier.

Based on Equations 2-3 and 2-4, the ionic strength of the solution and the zeta potential of the particle can influence the interplay of attractive and repulsive forces. The EDL repulsive force can overpower the van der Waals force when highly charged particles encounter each other in a medium with low ionic strength (Berg, 2010; Elimelech, 1998; Li et al., 2008). Under these conditions, the colloidal particles are highly stable and remain in suspension (Li et al., 2008). On the other hand, the EDL repulsive force is not as strong when weakly-charged or neutral particles are present, or a solution has high ionic strength (Li et al., 2008). Under these conditions, the van de Waals attractive force dominates, and the particles aggregate (Li et al., 2008) when the

Brownian motion of the colloid particles provides sufficient energy to overcome the energy barrier needed for aggregation (Elimelech, 1998). Typically, the Brownian motion rarely contributes more than a few units of thermal energy (kT, the unit of interaction energy shown in Figure 2-3), so a system with more than 20 kT total interaction energy indicates a highly stable condition with little aggregation (Elimelech, 1998).

2.3 Mineral Phase Reaction and Adsorption Isotherm (Langmuir, 1997)

Chemical equilibrium and kinetics determine the progress of chemical reactions, which govern the composition and the fate of chemicals in an aqueous system. If these two concepts are understood for given system, it is possible to predict the direction and stable state of a chemical reaction. Two other important concepts for understanding and predicting chemical reactions are Gibbs free energy and saturation indices. These concepts provide information on the chemical equilibrium and kinetics for specific chemical and biological reactions, such as mineral dissolution or precipitation, and biodegradation of organics in the environment.

2.3.1 Gibbs Free Energy

Gibbs free energy can indicate if a chemical reaction will proceed spontaneously. The absolute value for the Gibbs free energy cannot be measured directly in a given system, instead a maximum energy change as work is calculated. Consider a general chemical reaction as shown in Equation 2-5, where lower case letters represent the stoichiometric coefficients of the reaction species (in upper case letters).

$$aA + bB = cC + dD \qquad \text{(Equation 2-5)}$$

The Gibbs free energy of one mole of the reactant "A" (G_A) at a constant temperature and pressure, is:

$$G_A = \Delta G_A^\circ + RTln[A] \quad \text{(Equation 2-6)}$$

where R is the gas constant (8.314 J/mol K), [A] is the activity of reactant A (the fraction of the total concentration of reactant A that is participating in the given reaction; unitless), T is the reaction temperature (K), and ΔG_A° is the standard Gibbs free energy of A when the activity of A is 1 (kJ/mol).

As a result, Gibbs free energy for the overall reaction (ΔG_r; kJ/mol) can be calculated by subtracting the sum of values for the products with the sum of values for the reactants (Equation 2-7).

$$\Delta G_r = (cG_C + dG_{D)} - (aG_A + bG_B) \quad \text{(Equation 2-7)}$$

The resulting equation can be expressed as:

$$\Delta G_r = \Delta G_r^\circ + RTln\frac{[C]^c[D]^d}{[A]^a[B]^b} \; or \; \Delta G_r = \Delta G_r^\circ + RTlnQ \quad \text{(Equation 2-8)}$$

Equilibrium is defined as the lowest Gibbs free energy state for a given reaction, which is $\Delta G_r = 0$. The ratio of reactants over products is known as reaction quotient (Q), and when the reaction is at equilibrium the reaction quotient is equal to equilibrium constant (K_{eq}; i.e. $Q = K_{eq}$). The Gibbs free energy for the given reaction at equilibrium can therefore be expressed as:

$$\Delta G_r^\circ = -RTlnK_{eq} \quad \text{(Equation 2-9)}$$

Combining Equations 2-8 and 2-9 leads to:

$$\Delta G_r = \Delta G_r^\circ + RTlnQ = -RTlnK_{eq} + RTlnQ = RTln\left(\frac{Q}{K_{eq}}\right) \quad \text{(Equation 2-10)}$$

Based on Equation 2-10, the direction of a given chemical reaction can be predicted. At equilibrium, Q is equal to K_{eq} and ΔG_r is equal to 0. When Q is less than K_{eq} ($G_r<0$), the chemical reaction (as written in Equation 2-5) tends to proceed forward (from left to right). When Q is greater than K_{eq} ($G_r>0$), the chemical reaction (as written in Equation 2-5) tends to proceed in the opposite direction (from right to left).

2.3.2 Saturation Indices

The saturation state of minerals in an aqueous system is called the saturation index (SI), which is related to the ΔG_r expression.

$$SI = log_{10}(Q/K_{eq}) \; or \; SI = {}^{\Delta G_r}/_{(2.3026\,RT)} \qquad \text{(Equation 2-11)}$$

Following the same principle, whether a mineral will be dissolved or precipitated can be deduced from the SI value. At equilibrium the SI value is equal to 0. When the SI value is less than 0, a mineral is subsaturated in an aqueous system, meaning that dissolution could occur. When the SI value is greater than 0, a mineral is supersaturated in an aqueous system, meaning that precipitation could occur.

Chemical kinetics provides information on the chemical pathways and the time required to reach equilibrium. As described above, a chemical reaction can proceed either forward (left to right) or reverse (right to left). The overall rate of a given reaction is the difference between the forward reaction rate (k+) and the reverse reaction rate (k-).

2.3.3 Thermodynamics of Calcite Dissolution and Precipitation

Calcite ($CaCO_3$) dissolution and precipitation processes can be used as relevant examples here and in later chapters. Consider the following reactions:

$$CaCO_3 + H^+ = Ca^{2+} + HCO_3^- \quad \text{k1} \quad \text{(Equation 2-12)}$$

$$CaCO_3 + H_2CO_3^\circ = Ca^{2+} + HCO_3^- \quad \text{k2} \quad \text{(Equation 2-13)}$$

$$CaCO_3 + H_2O = Ca^{2+} + HCO_3^- + OH^- \quad \text{k3} \quad \text{(Equation 2-14)}$$

where $H_2CO_3°$ is a mixture of dissolved carbon dioxide and carbonic acid, and k1, k2, and k3 are the rate constants for the reactions depicted.

The rate for the calcite dissolution and precipitation can be expressed as:

$$R = k_1[H^+] + k_2\left[H_2CO_3^\circ\right] + k_3[H_2O] - k_4[Ca^{2+}][HCO_3^-] \quad \text{(Equation 2-15)}$$

where R is the overall rate, $k_{1\text{-}3}$ are the rate constants for the elementary reactions (Equations 2-12 to 2-14), k_4 is the rate constant for reverse reaction, and the activities of the reaction components are denoted in brackets.

Plummer et al. (1978) have systematically identified the parameters that influence calcite dissolution kinetics, including pH, CO_2 pressure (pCO_2), and temperature. Under acidic conditions (up to pH 4.5–5.5) and at low pCO_2, the calcite dissolution rate is influenced by the activity of H^+ (Equation 2-12), so the k_1 term governs the overall dissolution rate (Langmuir, 1997; Plummer et al., 1978). At high pCO_2 (>0.1 bar) and moderate pH, a linear relationship exists between the activity of $H_2CO_3°$ and the overall calcite dissolution rate, and the k_2 term dominates (Langmuir, 1997; Plummer et al., 1978). At higher pH (above pH 5.5) and low pCO_2, the overall calcite dissolution rate is constant and not dependant on other chemicals present in the solution (Chou et al., 1989), so the k_3 term strongly influences the reaction (Langmuir, 1997; Plummer et al., 1978). Finally, the reverse reaction (k_4) is governed by the adsorption reaction between the bulk dissolved species (Ca^{2+} and HCO_3^-) and the mineral surface (Chou et al., 1989;

Plummer et al., 1978). The overall calcite dissolution/precipitation rate (Equation 2-15) assumes the reaction proceeds in the absence of catalytic or inhibitory effects. Several aqueous species have inhibitory effect on calcite dissolution, including phosphate, scandium, copper, and sulfate (Gledhill & Morse, 2006; Morse et al., 2007; Sjöberg, 1978).

2.3.4 Thermodynamics of Biochemical Reactions

Thermodynamics also provides insights into biochemical reactions. Hydrocarbons (e.g. benzene, toluene, ethylbenzene and xylenes) can be metabolized by organisms in the environment through enzymatic activities. Since enzymes can only affect the chemical reaction rate by reducing the reaction energy barrier, the chemical reaction equilibrium is still defined by the Gibbs free energy state (discussed above;Alberts, 2002).

Organisms obtain energy from metabolizing organic compounds through a series of oxidation/reduction reactions. Briefly, during oxidation an electron is removed from a substance, and during reduction an electron is added to a substance (Brown, 2006). In other words, a redox reaction involves a transfer of electrons from an electron donor (reductant) to an electron acceptor (oxidant;Appelo & Postma, 2005; Brown, 2006).

Consider a general redox reaction as shown in Equation 2-16, where lower case letters represent the stoichiometric coefficients of the reaction species (in upper case letters).

$$bB_{\text{red}} + cC_{\text{ox}} \rightarrow dD_{\text{ox}} + gG_{\text{red}} \qquad \text{(Equation 2-16)}$$

where red is reductant and ox is oxidant.

By convention, the redox reaction is expressed as half-reactions; as a result, Equation 2-16 can be re-written as:

$$bB_{\text{red}} \rightarrow dD_{\text{ox}} + ne^{-}$$ (Equation 2-17)

where e^- are electrons and n is the number of electrons.

However, the electrons do not exist in a free state in solution (Appelo & Postma, 2005). As a result, a reduction reaction must occur with any oxidation reaction, represented by the other half-reaction shown in Equation 2-18.

$$gG_{\text{red}} \rightarrow cC_{\text{ox}} + ne^{-}$$ (Equation 2-18)

The standard Gibbs free energy of a given redox reaction can be expressed as

$$\Delta G_r^0 = nFE^0$$ (Equation 2-19)

where n is the number of electrons transferred, F is the Faraday's constant, and E^0 is the standard reduction potential. The standard reduction potential (E^0) can be calculated using Equation 2-20.

$$E = E^0 + \frac{RT}{nF} ln \frac{[D_{\text{ox}}]^d [G_{\text{red}}]^g}{[B_{\text{red}}]^b [C_{\text{ox}}]^c}$$ (Equation 2-20)

where n is the number of electrons transferred and F is the Faraday's constant.

The standard Gibbs free energy for biodegradation of environmental organics can be calculated. Benzene, toluene, ethylbenzene and xylene (BTEX) compounds are thought to be highly favourable electron donors for cell growth under certain oxidation/reduction conditions. For example, Gibbs free energy change for benzene utilization has been calculated under various conditions (Table 2-1;Burland & Edwards, 1999; Kleinsteuber et al., 2008; Weelink et al., 2010). Benzene biodegradation is extremely favourable under aerobic, nitrate-reducing, and iron-reducing conditions (Table 2-1). However, due to relatively low ΔG^0 values, benzene is considered highly recalcitrant under sulfate-reducing and methanogenic conditions (Weelink et

al., 2010). Three biochemical pathways have been hypothesized for anaerobic benzene degradation, one of which involves the activation of benzene to toluene through methylation (Weelink et al., 2010). The toluene is then metabolized through the benzylsuccinate synthase pathway (Weelink et al., 2010). The benzene activation pathway may support the observations that it is more difficult to degrade benzene under anaerobic conditions compared to other aromatic compounds, such as toluene (Weelink et al., 2010).

Table 2-1 Stoichiometric equations and standard free energy changes for benzene oxidation with various electron acceptors.

Electron Acceptor (ox/red)	Overall Stoichiometric Equation	$\triangle G^{\circ}$ (kJ/mol)
O_2/H_2O	$C_6H_6+7.5O_2+3H_2O \rightarrow 6HCO_3^-+6H^+$	-3173[a]
NO_3^-/N_2	$C_6H_6+6NO_3^- \rightarrow 6HCO_3^-+3N_2$	-2978[a]
Fe^{3+}/Fe^{2+}	$C_6H_6+90Fe(OH)_{3(s)} \rightarrow 6HCO_3^-+132H_2O+30Fe_3O_{4(s)}+6H^+$	-3070[b]
NO_3^-/NO_2^-	$C_6H_6+15NO_3^-+3H_2O \rightarrow 6HCO_3^-+15NO_2^-+6H^+$	-2061[a]
SO_4^{2-}/H_2S	$C_6H_6+3.75SO_4^{2-}+3H_2O \rightarrow 6HCO_3^-+1.88HS^-+0.38H^+$	-185[c]
CO_2/CH_4	$C_6H_6+3.75CO_2+10.5H_2O \rightarrow 6HCO_3^-+3.75CH_4+6H^+$	-116[b]

Values obtained from a) Weelink et al. (2010), b) Burland and Edwards (1999), c) Kleinsteuber et al. (2008).

2.4 Chemical Partitioning

Many hydrocarbons are hydrophobic, and tend to partition with solid phases such as clay particles by a process called adsorption.

Adsorption describes the retention of gas or liquid substances (adsorbate) onto the surface of a solid substance (adsorbent;Bansal & Goyal, 2005). Adsorption can be either a physical or

chemical process (Çeçen & Aktaş, 2012; Sawyer et al., 2003). Physical adsorption relies on van der Waals force, while chemical adsorption relies on chemical (covalent or ionic) bonds generated between the adsorbate and adsorbent (Bandosz, 2006; Bansal & Goyal, 2005; Çeçen & Aktaş, 2012; Sawyer et al., 2003). At equilibrium, the interaction between adsorbent and adsorbate can be described using adsorption isotherm models (Hsieh & Teng, 2000). Adsorption isotherm modeling is a graphical representation of the equilibrium distribution of a chemical between the solution and adsorbent at a given temperature (Boethling & Mackay, 2000). The resulting plot can be used to evaluate, compare and optimize the performance of an adsorbent (Chen, 2015; Suthersan, 1997). Two adsorption isotherm models are commonly used; Langmuir and Freundlich (Hemond & Fechner-Levy, 2015). Langmuir isotherm model is derived from the law of mass action and uses a kinetic approach to generate an empirical model (Appelo & Postma, 2005; Chen, 2015). The mathematical expression can be represented as:

$$q_e = q_m K_L \frac{C_e}{1+K_L C_e} \qquad \text{(Equation 2-21)}$$

where q_e is the adsorption capacity, q_m is the maximum adsorption capacity at equilibrium, K_L is adsorption capacity related constant, C_e is the substrate concentration at equilibrium.

Equation 2-21 illustrates that linear adsorption occurs as the solute concentration increases when $C_e << K_L$, and the surface becomes saturated when solute concentration is greater than K_L ($C_e >> K_L$;Appelo & Postma, 2005). The Langmuir isotherm model assumes that adsorption 1) is through monolayer interaction, 2) occurs at a finite number of identical sites within a given adsorbent, and 3) is homogeneous (Arasteh et al., 2010; Chen, 2015; Septhum et al., 2007).

The Freundlich isotherm model describes a multilayer, non-ideal and reversible adsorption process (Appelo & Postma, 2005; Chen, 2015). The mathematical expression can be represented as:

$$q_e = K_F C_e^{1/n} \quad \text{(Equation 2-22)}$$

where q_e is the adsorption capacity, K_F is the adsorption capacity related constant, C_e is the substrate concentration at equilibrium, and n is the adsorption intensity constant.

The Freundlich isotherm model assumes that adsorption is heterogenous.

Experimental data can be analyzed using linearized form of the Langmuir or Freundlich equations (Table 2-2). The Langmuir model can be expressed by four different equations in linearized form (Langmuir I-IV; Table 2-2), and different parameters can be calculated for each equation. For example, the maximum adsorption capacity (q_m) and adsorption capacity related constant (K_L) can be calculated from the slope and intercept of experimental data plotted with C_e/q_e and C_e based on Langmuir type I (Chen, 2015; Kumar & Sivanesan, 2005).

Table 2-2 Linear forms of Freundlich and Langmuir isotherm models.

Isotherm	Linear form	Plot
Freundlich	$\ln(q_e)=\ln K_F+(1/n)*\ln(C_e)$	$\ln(q_e)$ vs $\ln(C_e)$
Langmuir-I	$C_e/q_e=(C_e/q_m)+(1/K_L*q_m)$	C_e/q_e vs C_e
Langmuir-II	$1/q_e=[1/q_mK_L]1/C_e+1/q_m$	$1/q_e$ vs $1/C_e$
Langmuir-III	$q_e=q_m-(1/K_L)*(1/C_e)+(1/q_m)$	q_e vs q_e/C_e
Langmuir-IV	$q_e/C_e=K_Lq_m-K_Lq_e$	q_e/C_e vs q_e

2.5 Literature Review of Oil Sands Tailings Densification

2.5.1 End Pit Lakes

In 2016, the Alberta Energy Regulator issued Directive 085 to provide a guideline for managing tailings generated from the oil sands mining process (Alberta Energy Regulator, 2016). Directive 085 specifies that new fluid tailings must be ready to reclaim within ten years after the end of mine life (Alberta Energy Regulator, 2016). In addition, all legacy tailings must be ready to reclaim by the end of mine life (Alberta Energy Regulator, 2016). The main objective of tailings reclamation is to support the transformation of oil sands mining projects (including mined or disturbed lands) into "a self-sustaining boreal forest ecosystem" (Alberta Energy Regulator, 2016) upon completion of mining. Slow settling of fluid find tailings (FFT) and the toxicity of OSPW are key challenges for the reclamation effort (Allen, 2008b). A significant amount of research has been conducted to improve the FFT and OSPW inventories management. Water capping to create a pit lake (PL) is a reclamation and storage strategy where water (e.g., OSPW or other water sources) is placed on top of a layer of FFT (Cumulative Environmental Management Association, 2012). The water capping strategy allows FFT to dewater and the water cap to gradually develop into a self-sustaining aquatic ecosystem. Toxicity is reduced through natural attenuation processes (Alberta Energy Regulator, 2016; Cumulative Environmental Management Association, 2012). Small experimental ponds were constructed in the late 1980s and early 1990s by Syncrude Canada Ltd. to test the feasibility of the PL technology (Mackinnon & Boerger, 1991). Results from these studies showed that 1) FFT densification and dewatering occurred over time, 2) OSPW released during the dewatering process could contribute to the chronic toxicity but did not increase the acute toxicity of the water, and 3) a diverse ecosystem developed in the cap water layer (Mackinnon & Boerger,

1991; Westcott & Watson, 2005). Based on these positive results, a large scale PL project was developed by Syncrude Canada Ltd. to further demonstrate that PL technology can be used as a remediation and storage strategy before full-scale implementation (Alberta Energy Regulator, 2016; Cumulative Environmental Management Association, 2012; Westcott & Watson, 2005). In 2012, Base Mine Lake (BML), a full scale pit lake demonstration, was commissioned. BML was filled with 186 million m^3 FFT (45 m depth) and capped with 90% OSPW and 10% fresh water from BCR (Figure 2-4;Dompierre et al., 2016).

As the data obtained from the small-scale experimental ponds may not reflect the full-scale implementation of PL technology, the experimental and field data which is collected on BML will allow a comprehensive assessment of PL technology as a remediation and FFT storage strategy for the oil sands industry. Typical FFT samples contain 30–40% w/w solids with the following size distributions: >44 μm (10%), 1–44 μm (57%) and <1 μm (33%;Dompierre et al., 2016; Voordouw, 2013). Approximately 34% of the clay in oil sands tailings is kaolinite, and 26% is illite, and is 0.2–2 μm in size (Kaminsky et al., 2009). The clay particles in the oil sands fine tailings are highly stable in suspension and slow to settle (Siddique et al., 2014; Zhu et al., 2011). Indeed, high turbidity is observed in the BML surface water and slows the development of an aquatic ecosystem.

Figure 2-4 Aerial view of BML. Modified from Dompierre et al. (2017).

2.5.2 Biogenic Gas Emission from the Oil Sands Tailings Ponds

Three major mechanisms have been hypothesized for the cause of persistent turbidity in the BML surface water: wind-driven resuspension (e.g. oscillating motions under wind-waves), FFT-driven resuspension (e.g. gas bubbles emerging from the FFT), and processes occurring under the ice (e.g. solar induced under-ice convection; Lawrence et al., 2016). Ebullition of gas bubbles from the FFT into the water column is one of the FFT-driven processes, and has been documented in BML in winter (Lawrence et al., 2016).

The release of biogenic gases from oil sands tailings ponds has been widely reported (Bordenave et al., 2010; Fedorak et al., 2003; Fedorak et al., 2002; Holowenko et al., 2000; Salloum et al.,

2002; Siddique et al., 2006; Siddique et al., 2007; Stasik et al., 2014). Tailings ponds are used to contain the FFT generated from oil sands extraction, and to allow the FFT to settle and release OSPW which can be recycled back into the extraction process, and are a significant source of methane (CH_4) and carbon dioxide (CO_2), both greenhouse gases (GHG; Siddique et al., 2012; Small et al., 2015). Tailings ponds that receive froth treatment tailings, which contain hydrocarbons and diluent, were reported to have higher GHG emissions and were more prone to intensive bubbling compared to those containing composite tailings and thickened tailings (Burkus et al., 2014). Diluents are added to improve recovery rates of bitumen (Small et al., 2015). The *n*-alkanes and BTEX compounds found in naphtha diluent stimulate the biological production of greenhouse gases (Siddique et al., 2006; Siddique et al., 2007). Several key methanogenic microorganisms were identified from the oil sands tailings samples. Ramos-Padron et al. (2011) reported that members of the Methanoregulaceae (between ~4% and ~6% abundance) and Methanotrichaceae (~7% abundance) were identified from a microcosm study with gypsum-treated FFT using 16S rRNA pyrosequencing. Siddique et al. (2012) also identified members of the Methanosaetaceae in high abundance from FFT enrichment cultures supplemented with *n*-alkanes, BTEX and naphtha. Recent research has also revealed the presence of black, sulfidic zones beneath the tailings-water interface (M. Chen et al., 2013; Chi Fru et al., 2013; Ramos-Padron et al., 2011; Stasik & Wendt-Potthoff, 2014) that contain abundant sulfate-reducing bacteria (SRB;Stasik & Wendt-Potthoff, 2014), and several key SRB families were identified from oil sands tailings samples. Ramos-Padron et al. (2011) identified Desulfobulbaceae (~10% abundance) and Desulfovibrionaceae (~5% abundance). Penner and Foght (2010) reported about 4% and 17% abundance of Deltaproteobacteria in tailings samples obtained from Mildred Lake Settling Basin and West In-Pit respectively. Siddique et al. (2011)

detected Desulfobacterales and Desulfuromonadales orders in FFT that was incubated with longer-chain *n*-alkanes: *n*-tetradecane, *n*-hexadecane, and *n*-octadecane. Potentially, the SRB in these zones are consuming sulfate and producing hydrogen sulfide (H_2S) gas (Stasik & Wendt-Potthoff, 2014). The biogenic H_2S produced was hypothesized to have precipitated or dissolved in the form of HS^- (Stasik & Wendt-Potthoff, 2014). Adding gypsum to increase FFT densification increases the sulfate concentration in tailings, which in the presence of organics such as naphtha diluent, provides SRB with substrates for H_2S production.

As discussed above, residual organics can stimulate microbial activity to produce GHGs and possibly H_2S. Ebullition of these biogenic gases could generate a flux of chemicals (e.g. salts and organics) from FFT to surface water. Removing key constituents like residual organics from OSPW could minimize fugitive gas (e.g. benzene, toluene, ethylbenzene and xylenes) emissions and improve the OSPW inventory management. Allen (2008a & b) has compiled comprehensive reviews on emerging OSPW treatment technologies, so only activated carbon adsorption will be reviewed in this section. Activated carbon adsorption is particularly relevant to chapter 4 in this thesis.

Typical OSPW from tailings ponds contains 0.01–6 mg/L of aromatic hydrocarbons (benzene, toluene, and PAHs), which exceeds the Canadian environmental guideline for surface water quality and may cause chronic toxicity in the reclaimed environment (Allen, 2008a). The removal of aromatic hydrocarbons from OSPW is one focus of the research to help manage the large inventory of OSPW generated from the rapid expansion of the oil sands operations. Several research studies tested activated carbon as an adsorbent material for organics in oil and gas produced water, including naphthalenes, aliphatics, benzene, toluene, and xylene (BTX;Allen, 2008a). However, mixed results were observed from these studies. For example, Hansen and

Davies (1994) estimated that the removal efficiency of BTX with granular activated carbon was 95%, while Gallup et al. (1996) reported that granular activated carbon (GAC) showed poor removal of benzene (~35%) and toluene (~20%) in a field column study. Several technical issues made GAC a less than ideal candidate for the OSPW treatment, such as fouling by oil and grease from the oil field produced water (Gallup et al., 1996) and a large operational footprint (Hansen & Davies, 1994).

2.5.3 Oil Sands Tailings Dewatering/Consolidation Through Carbon Dioxide Addition

As mentioned in sections 2.1 and 2.2 that clay colloidal particles are highly stable in suspension, which is likely contribute to the surface water turbidity observed in the BML (described in section 2.5.1). Suspended colloidal destabilization has been well studied, and many of these principles have been used as wastewater treatment technology, including particle charge neutralization, electrolytes addition, and flocculant/coagulant addition (Metcalf & Eddy et al., 2014). Indeed, charge neutralization and electrolytes addition promotes colloidal instability by reducing the DDL (Metcalf & Eddy et al., 2014; Zbik et al., 2008). In addition, polymers and alum are routinely as coagulant/flocculant in wastewater treatment plants (Metcalf & Eddy et al., 2014).

There is limited literature on how FFT settles in a pit lake such as BML. However, BML was filled with FFT from an active tailings pond, so the research on FFT or mature fine tailings (MFT) densification will be described here. It is well established that coagulant or flocculant addition, pH reduction, or cation addition can enhance the settling rate of clay particles in water (M. Ibanez et al., 2014; Zbik et al., 2008; Zhu et al., 2011). Several studies have explored the effect of dissolved carbon dioxide (CO_2) on the settling of oil sands tailings (M. Ibanez et al., 2014; Siddique et al., 2014; Zhu et al., 2011).

Zhu et al. (2011) examined the densification of MFT (from Syncrude Canada Ltd. and Canadian Natural Resources Ltd.; CNRL) by abiotic CO_2 addition, and found that the treatment significantly improved the MFT settling and turbidity reduction for the Syncrude MFT (Table 2-3). A moderate improvement was observed for the treated CNRL MFT (Table 2-3; Zhu et al., 2011). These authors noted an increase in the concentration of calcium ions (from 7.3 to 19.1 mg/L) and magnesium ions (from 5.6 to 12 mg/L) in the diluent Syncrude MFT sample after the CO_2 treatment (Zhu et al., 2011). These authors suggested that MFT densification was achieved by the exchange of hydrogen ions from carbonic acid with the calcium, magnesium and sodium ions on the clay particles (Zhu et al., 2011). These authors also argued that the calcium or magnesium ions did not contribute to CO_2 mineral carbonation sequestration because calcium- or magnesium-carbonate precipitates were not observed on the tailings solids with X-ray diffraction (Zhu et al., 2011).

Table 2-3 Summary of experimental data for MFT settling experiments (Zhu et al., 2011). Note: CNRL= Canadian Natural Resources Ltd., Settling height experiment was performed in an autoclave at 100 kPa and 25°C. The settling height is a normalized height (sediment height [h] ÷ sediment+supernatant [H]). The supernatant turbidity was measured as a function of CO_2 partial pressure. Only the major observations are presented in this table. Compiled from Zhu et al. (2011).

	pH		Settling height (h/H)		Turbidity (NTU)	
MFT source	Initial (t = 0)	Final (t = 25 h)	Initial (t = 0)	Final (t = 25 h)	Initial (t = 0)	Final (t = 25 h)
Syncrude	8.4	6.2	0.95	0.55	846	200 (at 100 kPa)
CNRL	8.2	5.8	0.98	0.75	753	513 (at 1000 kPa)

Ibanez et al. (2014) examined the effect of monovalent and divalent electrolytes and pH on the stability of oil sands fine tailings. These authors observed that the zeta potential became less negative as the MFT (at pH 4, 6, or 8) was subjected to increasing divalent salt concentrations ($MgCl_2$;M. Ibanez et al., 2014). Despite having different initial zeta potential values with different sample pH (~−34 mV at pH 8, ~−23 mV at pH 6, and ~−24 mV at pH 4), the final zeta potential measurements converged at ~−9 mV for all sample pHs (M. Ibanez et al., 2014). The overall improvement in zeta potential measurements was not observed when the MFT was subjected to an increasing concentration of the monovalent electrolyte solution (NaCl;M. Ibanez et al., 2014). Based on these results, these authors concluded that rapid flocculation can be achieved with 5 mM of divalent salt at all pH values.

Siddique et al. (2014) examined the effect of dissolved biogenic gases (CO_2 and CH_4) on MFT consolidation and pore water recovery in a column study (Table 2-4). These authors showed that anaerobic microbial activity was promoted by hydrolysed canola meal amendment, increasing the production of CO_2 and CH_4 (Siddique et al., 2014). These authors demonstrated that dissolved biogenic CO_2, but not the dissolved abiotic CO_2, improved the porewater recovery and MFT consolidation (Siddique et al., 2014). These authors also noticed that a higher concentration of divalent cations (Ca^{2+} and Mg^{2+}) was observed in the pore and cap water recovered from the amended column which had biogenic gas production (Siddique et al., 2014). Based on these results, these authors concluded that pH reduction by biogenic CO_2 caused an increase in the calcium and magnesium concentrations in the pore water (Siddique et al., 2014). These authors further reasoned that this pH change dissolved carbonates in the FFT, which along with microbial iron reduction, played a role in FFT densification. In contrast, the addition of abiotic CO_2 had no effect on FFT densification (Siddique et al., 2014).

Table 2-4 Experimental Data Summary for Siddique et al. 2014a. Note: A 50 L column containing MFT and cap water (from Syncrude's Mildred Lake Settling Basin) was amended with hydrolysed canola meal, or not amended. Unless otherwise indicated, all values presented here are for day ~230 (the end day of the experiment). The abiotic CO_2 experiment was conducted in a 2 L column containing MFT, and CO_2 gas was sparged into the column until pH reached 6.54–6.68. All experiments were conducted at 20°C, and only the major observations are presented in this table. n/a = data not available. Compiled from Siddique et al. (2014).

	pH		Porewater recovery (vol %)	Consloidation (vol %)	Porewater cation (mg/L)	
	Initial	Final			Ca^{2+}	Mg^{2+}
Amended	7.7	~6.4 (day147)	34	~33	32	19
Unamend	7.5	~7.5 (day 200)	24	~19	17	10
Abiotic CO_2	n/a	n/a	8.2	9.5	n/a	n/a
Control	n/a	n/a	8.2	9.8	n/a	n/a

These studies demonstrated that dissolved CO_2-induced pH reduction can improve MFT settling, MFT densification, pore water recovery, and water clarity (M. Ibanez et al., 2014; Siddique et al., 2014; Zhu et al., 2011).

The work presented in this thesis focuses on BML specifically and materials from BML are used in work described in chapters 3 and 5.

2.6 References

Alberta Energy Regulator. (2016). *Directive 085: Fluid Tailings Management for Oil Sands Mining Projects*. Retrieved from http://www.aer.ca/documents/directives/Directive085.pdf.

Alberts, B. (2002). *Molecular biology of the cell* (4th ed.). New York: Garland Science.

Allen, E. W. (2008a). Process water treatment in Canada's oil sands industry: II. A review of emerging technologies. *J Environ Eng and Sci, 7*(5), 499-524.

Allen, E. W. (2008b). Process water treatment in Canada's oil sands industry: I. Target pollutants and treatment objectives. *J Environ Eng and Sci, 7*(2), 123-138.

Appelo, C. A. J., & Postma, D. (2005). *Geochemistry, groundwater and pollution* (2nd ed.). Leiden ; New York: Balkema.

Arasteh, R., Masoumi, M., Rashidi, A. M., Moradi, L., Samimi, V., & Mostafavi, S. T. (2010). Adsorption of 2-nitrophenol by multi-wall carbon nanotubes from aqueous solutions. *Appl Surf Sci, 256*(14), 4447-4455.

Bandosz, T. J. (2006). *Activated carbon surfaces in environmental remediation Interface science and technology v. 7* (pp. 1 online resource.). Retrieved from http://www.sciencedirect.com/science/bookseries/15734285/7

Bansal, R. C., & Goyal, M. (2005). *Activated carbon adsorption* (pp. 1 online resource.). Retrieved from https://www.taylorfrancis.com/books/9781420028812

Benitez, E. I., Genovese, D. B., & Lozano, J. E. (2007). Effect of pH and ionic strength on apple juice turbidity: Application of the extended DLVO theory. *Food Hydrocoll, 21*(1), 100-109.

Berg, J. C. (2010). *An introduction to interfaces & colloids : the bridge to nanoscience*. World Scientific. 785p

Birtwell, I. K. (2008). The validity of including turbidity criteria for aquatic resource protection in land development guidelines (Pacific and Yukon Region). In M. A. Farrell & A. Jonsson (Eds.). [Ottawa] :: Fisheries and Oceans Canada.

Boethling, R. S., & Mackay, D. (2000). *Handbook of property estimation methods for environmental chemicals environmental and health sciences* (pp. 1 online resource.). Retrieved from https://www.taylorfrancis.com/books/9781420026283

Bolland, M. D. A., Posner, A. M., & Quirk, J. P. (1980). Ph-Independent and Ph-Dependent Surface-Charges on Kaolinite. *Clays and Clay Minerals, 28*(6), 412-418.

Bordenave, S., Kostenko, V., Dutkoski, M., Grigoryan, A., Martinuzzi, R. J., & Voordouw, G. (2010). Relation between the activity of anaerobic microbial populations in oil sands tailings ponds and the sedimentation of tailings. *Chemosphere, 81*(5), 663-668.

Brown, T. L. (2006). *Chemistry : the central science* (10th ed.). Upper Saddle River, NJ: Pearson Prentice Hall.

Burkus, Z., Wheler, J., & Pletcher, S. (2014). *GHG Emissions from Oil Sands Tailings Ponds: Overview and Modelling Based on Fermentable Substrates*. Retrieved from Edmonton:

Burland, S. M., & Edwards, E. A. (1999). Anaerobic benzene biodegradation linked to nitrate reduction. *Appl Environ Microbiol, 65*(2), 529-533.

Çeçen, F., & Aktaş, Ö. (2012). *Activated carbon for water and wastewater treatment integration of adsorption and biological treatment* (pp. 1 online resource (xxviii, 388 p.)). Retrieved from https://ebookcentral.proquest.com/lib/ualberta/detail.action?docID=822729

Chen. (2015). Modeling of Experimental Adsorption Isotherm Data. *Information, 6*(1), 14-22.

Chen, M., Walshe, G., Fru, E. C., Ciborowski, J. J. H., & Weisener, C. G. (2013). Microcosm assessment of the biogeochemical development of sulfur and oxygen in oil sands fluid fine tailings. *Appl Geochem, 37*, 1-11.

Chi Fru, E., Chen, M., Walshe, G., Penner, T., & Weisener, C. (2013). Bioreactor studies predict whole microbial population dynamics in oil sands tailings ponds. *Appl Microbiol Biotechnol, 97*(7), 3215-3224.

Chou, L., Garrels, R. M., & Wollast, R. (1989). Comparative-Study of the Kinetics and Mechanisms of Dissolution of Carbonate Minerals. *Chem Geol, 78*(3-4), 269-282.

Cumulative Environmental Management Association. (2012). *End pit lakes guidance document* (pp. 1 online resource (434 p.)). Retrieved from http://www.deslibris.ca/ID/234915

Davies-Colley, R. J., & Smith, D. G. (2001). Turbidity, suspended sediment, and water clarity: A review. *J Am Water Resour Assoc, 37*(5), 1085-1101.

Derjaguin, B., & Landau, L. (1993). Theory of the Stability of Strongly Charged Lyophobic Sols and of the Adhesion of Strongly Charged-Particles in Solutions of Electrolytes. *Prog Mater Sci, 43*(1-4), 30-59.

Dompierre, K. A., Barbour, S. L., North, R. L., Carey, S. K., & Lindsay, M. B. J. (2017). Chemical mass transport between fluid fine tailings and the overlying water cover of an oil sands end pit lake. *Water Resour Res, 53*(6), 4725-4740.

Dompierre, K. A., Lindsay, M. B. J., Cruz-Hernandez, P., & Halferdahl, G. M. (2016). Initial geochemical characteristics of fluid fine tailings in an oil sands end pit lake. *Sci Total Environ, 556*, 196-206.

Elimelech, M. (1998). *Particle deposition and aggregation : measurement, modelling, and simulation* (Pbk. ed.). [Oxford, [England] ; Boston]: Butterworth-Heinemann.

Fedorak, P. M., Coy, D. L., Dudas, M. J., Simpson, M. J., Renneberg, A. J., & MacKinnon, M. D. (2003). Microbially-mediated fugitive gas production from oil sands tailings and increased tailings densification rates. *J Environ Eng and Sci, 2*(3), 199-211.

Fedorak, P. M., Coy, D. L., Salloum, M. J., & Dudas, M. J. (2002). Methanogenic potential of tailings samples from oil sands extraction plants. *Can J Microbiol, 48*(1), 21-33.

Gallup, D. L., Isacoff, E. G., & Smith, D. N. (1996). Use of Ambersorb(R) carbonaceous adsorbent for removal of BTEX compounds from oil-field produced water. *Environmental Progress, 15*(3), 197-203.

Gledhill, D. K., & Morse, J. W. (2006). Calcite dissolution kinetics in Na-Ca-Mg-Cl brines. *Geochim Cosmochim Acta, 70*(23), 5802-5813.

Government of Alberta. (2018). *Environmental Quality Guidelines for Alberta Surface Waters*. Edmonton, Alberta Retrieved from https://open.alberta.ca/dataset/5298aadb-f5cc-4160-8620-ad139bb985d8/resource/38ed9bb1-233f-4e28-b344-808670b20dae/download/environmentalqualitysurfacewaters-mar28-2018.pdf.

Grasso, D., Subramaniam, K., Butkus, M., Strevett, K., & Bergendahl, J. (2002). A review of non-DLVO interactions in environmental colloidal systems. *Rev Environ Sci Bio, 1*(1), 17-38.

Gregory, R. S., & Levings, C. D. (1998). Turbidity reduces predation on migrating juvenile Pacific salmon. *Transactions of the American Fisheries Society, 127*(2), 275-285.

Hansen, B. R., & Davies, S. R. H. (1994). Review of Potential Technologies for the Removal of Dissolved Components from Produced Water. *Chem Eng Res Des, 72*(A2), 176-188.

Hemond, H. F., & Fechner-Levy, E. J. (2015). *Chemical fate and transport in the environment* (Third edition. ed.).

Hogg, R., Healy, T. W., & Fuerstenau, D. W. (1966). Mutual Coagulation of Colloidal Dispersions. *Trans Faraday Soc, 62*(522p), 1638.
Holowenko, F. M., MacKinnon, M. D., & Fedorak, P. M. (2000). Methanogens and sulfate-reducing bacteria in oil sands fine tailings waste. *Can J Microbiol, 46*(10), 927-937.
Hsieh, C. T., & Teng, H. S. (2000). Influence of mesopore volume and adsorbate size on adsorption capacities of activated carbons in aqueous solutions. *Carbon, 38*(6), 863-869.
Hunter, R. J. (2001). *Foundations of colloid science* (2nd ed.). Oxford ; New York: Oxford University Press.
Ibanez, J. G. (2007). *Environmental chemistry : fundamentals*. 1st Ed. New York: Springer. 334p
Ibanez, M., Wijdeveld, A., & Chassagne, C. (2014). The Role of Mono- and Divalent Ions in the Stability of Kaolinite Suspensions and Fine Tailings. *Clays and Clay Minerals, 62*(5-6), 374-385.
Kaminsky, H. A. W., Etsell, T. H., Ivey, D. G., & Omotoso, O. (2009). Distribution of Clay Minerals in the Process Streams Produced by the Extraction of Bitumen from Athabasca Oil Sands. *Can J Chem Eng, 87*(1), 85-93.
Kleinsteuber, S., Schleinitz, K. M., Breitfeld, J., Harms, H., Richnow, H. H., & Vogt, C. (2008). Molecular characterization of bacterial communities mineralizing benzene under sulfate-reducing conditions. *FEMS Microbiol Ecol, 66*(1), 143-157.
Kumar, K. V., & Sivanesan, S. (2005). Comparison of linear and non-linear method in estimating the sorption isotherm parameters for safranin onto activated carbon. *J Hazard Mater, 123*(1-3), 288-292.
Langmuir, D. (1997). *Aqueous environmental geochemistry*. Upper Saddle River, N.J.: Prentice Hall.
Lawrence, G. A., Tedford, E. W., & Pieters, R. (2016). Suspended solids in an end pit lake: potential mixing mechanisms. *Can J Civ Eng, 43*(3), 211-217.
Li, Q., Jonas, U., Zhao, X. S., & Kapp, M. (2008). The forces at work in collodial self-assembly: a review on fundamental interactions between collodial particels. *Asia-Pac J Chem Eng, 3*(3), 255-268.
Liu, L. Y., Hu, Y., Min, F. F., Zhang, M. X., & Song, S. X. (2013). Characterizations and Stability of Colloidal Coal-Measure Kaolinite in Aqueous Suspensions: A Review. *Surf Rev Lett, 20*(1).
Mackinnon, M., & Boerger, H. (1991). *Assessment Of A Wet Landscape Option For Disposal Of Fine Tails Sludge From Oil Sands Processing*. Annual Technical Meeting. Banff.
Masliyah, J. H., & Bhattacharjee, S. (2006). *Electrokinetic and colloid transport phenomena*. Hoboken, N.J.: Wiley-Interscience.
Metcalf & Eddy, Tchobanoglous, G., Stensel, H. D., Tsuchihashi, R., Burton, F. L., Abu-Orf, M., Bowden, G., & Pfrang, W. (2014). *Wastewater engineering : treatment and resource recovery* (Fifth edition / ed.).
Missana, T., & Adell, A. (2000). On the applicability of DLVO theory to the prediction of clay colloids stability. *J Colloid Interface Sci, 230*(1), 150-156.
Morel, A., & Loisel, H. (1998). Apparent optical properties of oceanic water: dependence on the molecular scattering contribution. *Applied Optics, 37*(21), 4765-4776.
Morse, J. W., Arvidson, R. S., & Luttge, A. (2007). Calcium carbonate formation and dissolution. *Chemical Reviews, 107*(2), 342-381.
Ohshima, H. (2012). *Electrical phenomena at interfaces and biointerfaces fundamentals and applications in nano-, bio-, and environmental sciences* (pp. 1 online resource (xviii, 850

p.)). Retrieved from https://ebookcentral.proquest.com/lib/ualberta/detail.action?docID=818455
Penner, T. J., & Foght, J. M. (2010). Mature fine tailings from oil sands processing harbour diverse methanogenic communities. *Can J Microbiol, 56*(6), 459-470.
Plummer, L. N., Wigley, T. M. L., & Parkhurst, D. L. (1978). The kinetics of calcite dissolution in CO 2 -water systems at 5 degrees to 60 degrees C and 0.0 to 1.0 atm CO 2. *278*(2), 179-216.
Ramos-Padron, E., Bordenave, S., Lin, S., Bhaskar, I. M., Dong, X., Sensen, C. W., Fournier, J., Voordouw, G., Gieg, L. M. (2011). Carbon and sulfur cycling by microbial communities in a gypsum-treated oil sands tailings pond. *Environ Sci Technol, 45*(2), 439-446.
Salloum, M. J., Dudas, M. J., & Fedorak, P. M. (2002). Microbial reduction of amended sulfate in anaerobic mature fine tailings from oil sand. *Waste Manag Res, 20*(2), 162-171.
Sawyer, C. N., McCarty, P. L., & Parkin, G. F. (2003). *Chemistry for environmental engineering and science* (5th ed.). Boston: McGraw-Hill.
Sawyer, C. N., McCarty, P. L., Parkin, G. F., & Sawyer, C. N. (1994). *Chemistry for environmental engineering* (4th ed.). New York: McGraw-Hill.
Septhum, C., Rattanaphani, S., Bremner, J. B., & Rattanaphani, V. (2007). An adsorption study of A1(III) ions onto chitosan. *J Hazard Mater, 148*(1-2), 185-191.
Siddique, T., Fedorak, P. M., & Foght, J. M. (2006). Biodegradation of short-chain n-alkanes in oil sands tailings under methanogenic conditions. *Environ Sci Technol, 40*(17), 5459-5464.
Siddique, T., Fedorak, P. M., MacKinnon, M. D., & Foght, J. M. (2007). Metabolism of BTEX and naphtha compounds to methane in oil sands tailings. *Environ Sci Technol, 41*(7), 2350-2356.
Siddique, T., Kuznetsov, P., Kuznetsova, A., Arkell, N., Young, R., Li, C., Guigard, S., Underwood, E., Foght, J. M. (2014). Microbially-accelerated consolidation of oil sands tailings. Pathway I: changes in porewater chemistry. *Front Microbiol, 5*, 106.
Siddique, T., Penner, T., Klassen, J., Nesbo, C., & Foght, J. M. (2012). Microbial communities involved in methane production from hydrocarbons in oil sands tailings. *Environ Sci Technol, 46*(17), 9802-9810.
Siddique, T., Penner, T., Semple, K., & Foght, J. M. (2011). Anaerobic biodegradation of longer-chain n-alkanes coupled to methane production in oil sands tailings. *Environ Sci Technol, 45*(13), 5892-5899.
Sjöberg, E. L. (1978). *Kinetics and mechanism of calcite dissolution in aqueous solutions at low temperatures.* Almqvist & Wiksell.
Small, C. C., Cho, S., Hashisho, Z., & Ulrich, A. C. (2015). Emissions from oil sands tailings ponds: Review of tailings pond parameters and emission estimates. *J Petrol Sci Eng, 127*, 490-501.
Stasik, S., Loick, N., Knoller, K., Weisener, C., & Wendt-Potthoff, K. (2014). Understanding biogeochemical gradients of sulfur, iron and carbon in an oil sands tailings pond. *Chem Geol, 382*, 44-53.
Stasik, S., & Wendt-Potthoff, K. (2014). Interaction of microbial sulphate reduction and methanogenesis in oil sands tailings ponds. *Chemosphere, 103*, 59-66.
Suthersan, S. S. (1997). *Remediation engineering : design concepts*. Boca Raton, Fl.: CRC-Lewis Publishers.

Tundisi, J. G., & Tundisi, T. M. (2012). *Limnology* (pp. 1 online resource (xxii, 864 p.)). Retrieved from http://search.ebscohost.com/login.aspx?direct=true&scope=site&db=nlebk&db=nlabk&AN=437330

Verwey, E. J. W. (1947). Theory of the Stability of Lyophobic Colloids. *J Phys Colloid Chem, 51*(3), 631-636.

Voordouw, G. (2013). Interaction of oil sands tailings particles with polymers and microbial cells: First steps toward reclamation to soil. *Biopolymers, 99*(4), 257-262.

Weelink, S. A. B., van Eekert, M. H. A., & Stams, A. J. M. (2010). Degradation of BTEX by anaerobic bacteria: physiology and application. *Rev Environ Sci Bio, 9*(4), 359-385.

Westcott, F., & Watson, L. (2005). End pit lakes technical guidance document: Report. Cumulative Environmental Management Association. 51p. Report.

Zbik, M. S., Smart, R. S. C., & Morris, G. E. (2008). Kaolinite flocculation structure. *J Colloid Interface Sci, 328*(1), 73-80.

Zhu, R., Liu, Q. X., Xu, Z. H., Masliyah, J. H., & Khan, A. (2011). Role of Dissolving Carbon Dioxide in Densification of Oil Sands Tailings. *Energy & Fuels, 25*(5), 2049-2057.

Chapter 3 : Effect of Naphtha Diluent on Organic Release and Microbial Dynamics in Oil Sands Tailings

3.1 Introduction

Substantial greenhouse gases (namely methane and carbon dioxide) were detected in most of the tailings ponds (Siddique et al., 2012; Small et al., 2015). Naphtha diluent, a complex mixture containing more than 280 aliphatic and aromatic hydrocarbons including *n*-alkanes and BTEX (benzene, toluene, ethylbenzene, and xylenes), is added to improve the bitumen recovery from the oil sands ores (Siddique et al., 2006; Siddique et al., 2007; Small et al., 2015). The majority of the diluent used in this process is recovered, and less than 1% of diluent is lost to the tailings (Foght et al., 2017).

In 2016, the Alberta Energy Regulator issued Directive 085 to provide a guideline for oil sands tailings reclamation (Alberta Energy Regulator, 2016). Water capping of tailings (pit lakes) is one technology currently undergoing research. Pit lakes reclaim mine pits and can be used to store fluid or treated tailings (Cumulative Environmental Management Association, 2012). A full-scale demonstration pit lake, Base Mine Lake (BML), was commissioned in 2012. However, little is known about the effect of long-term storage of tailings on the generation of greenhouse gases and chemical flux from the tailings. Lawrence et al. (2016) reported rising gas bubbles at BML field monitoring sites in the winter of 2014. In the summer of 2015, ~40 μM aqueous methane and ~0.7 μM aqueous hydrogen sulfide were measured in the BML hypolimnion (Risacher et al., 2018). The long-term performance of water capped tailings can be predicted from the short term studies and experiment conducted using materials from older tailings ponds. Based on the emission flux chamber measurements in 2011, methane (CH_4) emission was calculated to be ~6000 tons/year (t/y), ~2600 t/y and ~320 t/y from Suncor, Syncrude and Shell tailings ponds respectively (Burkus et al., 2014). The carbon dioxide (CO_2) emissions were calculated to be ~165000 t/y, ~225000 t/y and ~33000 t/y from Suncor, Syncrude and Shell

tailings ponds respectively (Burkus et al., 2014). Furthermore, the total measured greenhouse gas emission per diluent volume was 4.5 kg CO_2 eq/L diluent, 11 kg CO_2 eq/L diluent and 1 kg CO_2 eq/L diluent from Suncor, Syncrude and Shell tailings ponds respectively (Burkus et al., 2014). Due to complex geochemical and microbial processes, limited data was available for the H_2S or sulfur related emissions from tailings ponds. Emission flux chamber data compiled by Small et al. (2015) showed that less than 0.5 tons/hectare/year of sulfur emissions were measured from oil sands tailings ponds.

Several studies demonstrated that methane is generated from oil sands tailings samples under anaerobic conditions with organic amendments, and this methane production is attributed to microbial activities in the tailings (Fedorak et al., 2002; Holowenko et al., 2000; Siddique et al., 2007).

Dissolved oxygen is a key factor in the development of healthy aquatic ecosystems, which is one of the goals for BML. Dissolved oxygen concentrations in the BML water cap can be reduced by high concentrations of oxygen consuming constituents, such as aqueous CH_4 and H_2S (Risacher et al., 2018). In addition, ebullition of these biogenic gases could contribute to the transport and the subsequent release of volatile organics, such as BTEX compounds, into the atmosphere, resulting in environmental and health hazards (Allouch et al., 2013; Anderson et al., 1974; Durmusoglu et al., 2010; Headley et al., 2001). As a result, the overall objective of the study presented in this chapter is to understand the evolution of CH_4 and H_2S in tailings as it relates to i) diluent concentration and ii) microbial activity, and to understand the relationship between gas generation and organic release. This chapter serves as a foundation for optimizing current and future pit lake conditions, and to mitigate potential environmental and health risks for the oil sands operations and reclamation.

3.2 Materials and Methods

The research presented in this chapter is from a collaboration with Kathleen Frances Mign-tze Day Gee in Dr. Ulrich's lab (MSc Environmental Engineering at University of Alberta). Information pertaining to materials, experimental methods and results was published in a co-authored article (Gee et al., 2017), and my research contribution to this project will be the focus of this chapter. The hydrogen sulfide and methane gas production and water chemistry data, collected by Kathleen Gee, are shown in this chapter with permission from Ms. Gee (Figure 3-1a, b and 3-2a, b). This data aids in understanding the microbial community changes within the mesocosms and relationships to BTEX evolution (data obtained by me).

Mature fine tailings (MFT) and oil sands tailings pond water (PW) were obtained from Canada's Oil Sands Innovation Alliance (COSIA) in 2012. In this thesis MFT is defined as fluids with greater than 30%wt/wt suspended solids content (Siddique et al., 2014a). Surrogate pond water (SPW) was prepared and for the experiments presented here, and a detailed recipe can be found in Mahdavi (2014).

3.2.1 Mesocosm Setup

The mesocosm experiment was constructed using 400 mL of MFT and 400 mL of either PW or SPW in a 1 L Pyrex® glass bottle fitted with a butyl septa. In addition, the MFT was amended with naphtha diluent: 0.8% w/v for PW mesocosm and 0.2%, 0.8%, and 1.5% w/v for SPW mesocosms. Prior to the experiment, MFT and pond water (either PW and SPW) were sparged with argon gas (Praxair) to maintain anaerobic conditions. The constructed mesocosms were then assembled and incubated in an anaerobic chamber (5% CO_2, 5% H_2, balance N_2) at 24°C, covered with a black cloth. The mesocosms were incubated for a total of 15 weeks, and chemical and molecular analyses were conduct (Table 3-1).

Table 3-1 Experimental timeline and measurements performed

Analyses	Conducted in week
H_2S (g)	0, 4, 6, and 14
CH_4 (g)	0, 1, 2, 5, 7, and 11
BTEX (headspace)	0, 1, 2, 4, 6, 11, and 15
Molecular	0, 5, and 11

3.2.2 BTEX Measurement

Concentrations of BTEX compounds were measured using gas chromatography with flame ionization detector (GC-FID) equipped with HP-5 column (30 m x 320 µm x 0.25 µm; Agilent). Helium 5.0 (Praxair) was used as the carrier gas. The parameters for the FID method used in BTEX measurement are listed in Table 3-2.

Table 3-2 Parameters used in the FID method used to measure BTEX concentrations in mesocosms.

Component	Parameter	Values
Inlet	Temperature	250°C
	Total Flow	47.5 mL/min
	Septum purge flow	3 mL/min
Detector	Temperature	250°C
	Make-up flow	25 mL/min
Oven	Temperature	50°C

Headspace samples (200 µL) were taken with a VICI Pressure Lok glass syringe (A-2 series, 050032, Valco Instruments Co. Inc.), and subjected to the GC-FID for BTEX measurement. In

order to gain further insight, the benzene and toluene release rate was calculated from the GC data. The following sample calculation for MFT-PW-0.8% is provided to assist reader to understand the benzene and toluene release rate results:

To calculate the benzene release rate for MFT-PW-0.8% between weeks 4-6:

$\Delta 6-4=(1.8mg-0.9mg)/14day=0.06mg/d$ benzene

$0.06mg/d$ benzene $/400mL$ MFT $=0.00015\,mg/mL$ MFT$/d*1000\,ug/mg=$

$0.15\,ug/mL$ MFT$/d$

In addition, standard error (±0.01 mg) was calculated from 3 benzene standard curves obtained from a different GC with similar column and similar method parameters.

3.2.3 Microbial Community Analysis

A slurry of MFT/PW (~1.5 mL) was collected with continuous flow of argon gas (Praxair, ultra-high purity 5.0) during week 5 and 11. MFT was also collected prior to the experiment to serve as the week 0 sample. Prior to DNA extraction, MFT/PW slurry samples were centrifuged for 30 seconds at 10000g, and the supernatant was discarded. Genomic DNA was extracted from ~0.25 g MFT samples using PowerSoil DNA Extraction Kit (Cat # 12888-100, MoBio Laboratories, USA), according to manufacture recommended procedures. The extracted DNA (~0.5 μL) was subjected to PCR amplification for dissimilatory sulfite reductase (*dsr*AB) and methyl-coenzyme M reductase (*mcr*) genes. PCR was performed with Phusion High-fidelity DNA polymerase (Thermo scientific, USA) with the initial denaturation 98°C for 2 min and final extension 72°C for 2 min. The amplification conditions and sequences of the primers *dsr* (Wagner et al., 1998) and *mcr*A (Springer et al., 1995) are listed in Table 3-2. The resulting PCR products were analysed on 2% agarose gels. Microbial communities were characterized by 16S

rRNA gene with the Illumina MiSeq sequencing platform. Total metagenomic DNA was subjected to PCR amplification of the V4 hypervariable regions of prokaryotic 16S rRNA genes, using the primers 515F and 806R (Table 3-3). Both forward and reverse primers were tagged with adapter, pad and linker sequences. Each barcode sequence (12-mer) was added to the reverse primer for pooling multiple samples in one run of MiSeq sequencing. The PCR conditions were 95°C for 3 min, 30 cycles of 94°C for 30 s, 50°C for 30 s and 72°C for 1 min of extension, followed by 72°C for 5 min. PCR products were purified and combined in equimolar ratios with the quantitative DNA binding method to create a DNA pool that was then sequenced from the adaptor. The 16S rRNA gene fragments were sequenced using the Illumina MiSeq platform following the manufacturer's procedure. The sequences were deposited in SRA within the study with accession number starting with PRJ. Sequences were sorted according to their barcode tags and trimmed to remove sequencing adaptors and primers. After removing the low-quality sequences, operational taxonomic units (OTUs) were defined and assigned to taxa using UPARSE pipeline. The community matrix was normalized with the DESeq package. The bacterial communities were ordinated with non-matric multidimensional scaling (NMDS) based on the Bray-Curtis distance matrix using phyloseq.

Table 3-3 List of primers and conditions used for *dsr*AB and *mcr*A PCR amplification.

	Primers	Condition
*dsr*AB	DSR1F:5'-ACS CAC TGG AAG CAC G-3' DSR4R: 5'-GTG TAG CAG TTA CCG CA-3'	28 cycles (98°C-10s, 55°C-10s, 72°C-1min)
*mcr*A	F:5'-TAY GAY CAR ATH TGG YT-3' R:5'-ACR TTC ATN GCR TAR TT-3'	38 cycles (98°C-10s, 50°C-30s, 72°C-30s)
16S rRNA	515F:5'-GTG CCA GCM GCC GCG GTA A-3' 806R:5'-GGA CTA CVS GGG TAT CTA AT-3'	30 cycles (95°C-30s, 50°C-30s, 72°C-1min)

3.3 Results and Discussion

3.3.1 Sulfate reduction and methanogenesis

To understand the effect of naphtha diluent on microbial dynamics and organic release from the tailings, anaerobic mesocosms were set up and monitored for 14 weeks under nitrogen and phosphorus limiting conditions. Typically, less than 1% diluent is lost to the tailings, so three different diluent concentrations were tested in this study to represent a typical (0.8%), low (0.2%) and high (1.5%) diluent concentrations. During the 14 week incubation period, a reduction of aqueous sulfate concentrations and an increase of H_2S gas concentration in the headspace was observed in both the MFT-PW and -SPW mesocosms, with or without diluent amendment (Figure 3-1a, b;Gee et al., 2017). An increase in H_2S was observed in mesocosms containing MFT-PW and MFT-SPW between week 4 and week 14 (Figure 3-1a, b). In the week 14 sample from the MFT-SPW-1.5% mesocosm, H_2S concentrations declined to a similar level observed in MFT-SPW-0.2% mesocosm (Figure 3-1b). An earlier and more pronounced increase in H_2S levels was observed in the mesocosms that received diluent amendment (Figure 3-1a, b). Given the decrease in sulfate concentration combined with the increase in H_2S concentration, the

sulfate-reducing bacteria (SRB) community is likely active in the diluent-amended mesocosms, specifically through the dissimilatory pathway (Schiffer et al., 2008; K. Tang et al., 2009). Dissimilatory sulfate reduction utilizes inorganic sulfate (e.g. SO_4^{2-}) to generate sulfite, and the final reduction of sulfite to H_2S is catalysed by the dissimilatory (bi)sulfite reductase (Dsr) enzyme (Grein et al., 2013; Santillano et al., 2010; Schiffer et al., 2008; K. Tang et al., 2009). The Dsr enzyme exists in either heterotetrameric (α and β subunits) or multisubunit (α & β + small γ & δ subunits) complexes depending on the organism (Grein et al., 2013; Schiffer et al., 2008). As a result, the *dsr*AB genes encoding the α and β subunits are often used as a target for molecular analysis the SRB community (Grein et al., 2013; Muller et al., 2015; Steger et al., 2011; Straalen & Roelofs, 2012; Wagner et al., 1998).

To investigate the microbial dynamics in the MFT-containing mesocosms, the *dsr*AB gene was amplified from the MFT samples (week 5) indicating that SRB were present (Figure 3-1c). In general, a higher PCR band intensity was observed in samples with higher diluent concentrations, for example MFT-SPW-1.5% samples had a higher band intensity than MFT-SPW-0.8% or -0.2% samples (Figure 3-1c). At week 11, a lower PCR band intensity was observed in MFT-SPW-1.5% samples, which corresponded to lower H_2S measured in this mesocosm (Figure 3-1c). Anaerobic sulfate reduction is a very energy demanding process, where adenosine triphosphate (ATP; a form of energy source used in various cellular processes) must be spent to catalyse the sulfate reduction process (Grein et al., 2013; Schiffer et al., 2008; K. Tang et al., 2009). A faint *dsr*AB band was observed for the week 0 MFT sample, which suggests that an endogenous SRB community exists in the MFT and the observed effects are likely due to the stimulation of the endogenous community. Numerous species of SRBs have been reported to metabolize oil and gas related hydrocarbons, including alkanes (C_{6-16}), *o*- & *m*-

xylene, *n*-decane, toluene, ethylbenzene, naphthalene, and benzene (Abu Laban et al., 2015a, 2015b; K. Tang et al., 2009). All of the hydrocarbon substrates mentioned above are components of the naphtha diluent (Siddique et al., 2006; Siddique et al., 2007; Small et al., 2015).

Several SRB families were identified through the 16S rRNA gene amplicon sequencing, including Desulfobulbaceae, Desulfobacteraceae, Desulfuromonadceae, and Desulfomicrobiaceae (Figure 3-3). The relative abundance of the Desulfobulbaceae family (*Desulfocapsa*) showed a similar pattern to the PCR results and 16S rRNA sequencing results (Figures 3-1c, 3-3 and A1).

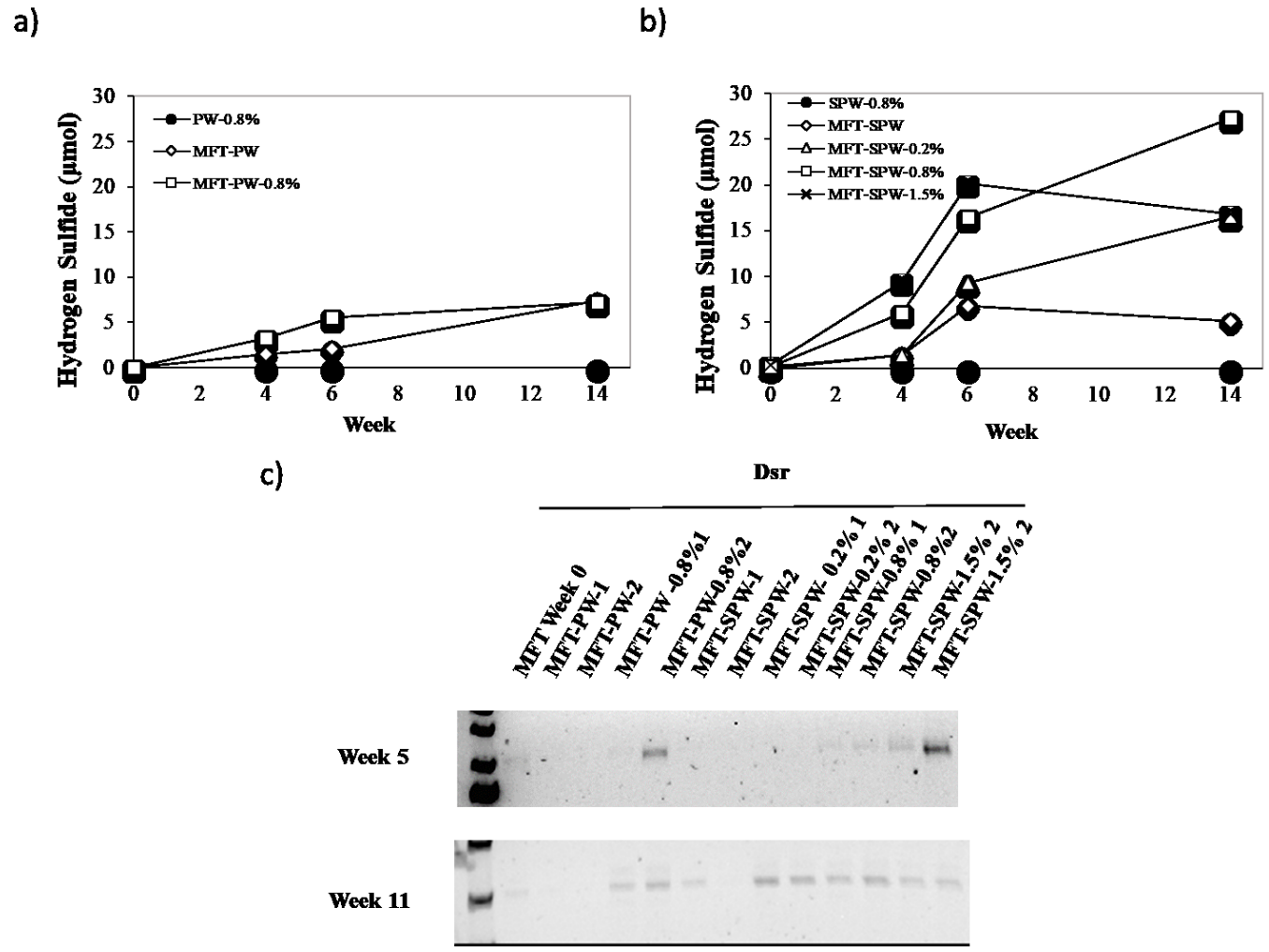

Figure 3-1 Hydrogen sulfide measurement for the (a) PW and (b) SPW groups over the 14-week study period. Filled circles: PW or SPW +0.8% diluent; open diamonds: +MFT; open triangle: +MFT/+0.2% diluent, open square: +MFT/+0.8% diluent; x: +MFT/+1.5% diluent. (c) The dissimilatory sulfite reductase (*dsr*) gene was amplified from each of the duplicate MFT samples. MFT obtained prior to experiment (week 0) was used as control for both week 5 and 11. Figure was modified from Gee et al. (2017).

The three SRB families identified in this study have also been previously identified in oil sands tailings (Penner & Foght, 2010; Ramos-Padron et al., 2011; Siddique et al., 2014b; Siddique et al., 2012; Siddique et al., 2011). All of the above mentioned SRB families are Gram negative bacteria and belong to the phylum Proteobacteria and class of delta-Proteobacteria (Rosenberg et al., 2014). Genes for a completely functional sulfate-reduction pathway, including *dsr*AB, were

identified from species from each of the families detected in this study (Rosenberg et al., 2014). Interestingly, only the family Desulfobulbaceae showed a noticeable increase in relative abundance with diluent concentration (Table A1). Desulfobulbaceae are strictly anaerobic microorganisms such as the genera *Desulfobulbus*, *Desulfocapsa*, and *Desulfofustis* (Rosenberg et al., 2014). A higher percentage of the family Desulfobulbaceae is often found in industrial samples compared to Desulfobacteraceae and Desulfomicrobiaceae (Muller et al., 2015). Siddique et al. (2011) detected Desulfobulbaceae in MFT incubated with longer-chain *n*-alkanes: *n*-tetradecane, *n*-hexadecane, and *n*-octadecane. Furthermore, two Desulfobubaceae strains (Tol-SR and Tol-M) capable of degrading toluene have been isolated from oil sands tailings (Abu Laban et al., 2015a, 2015b). These findings further support the hypothesis that biogenic H_2S production in this study was performed by SRBs, which were stimulated by hydrocarbons from naphtha diluent.

With regards to the mesocosm study, the methane (CH_4) concentration increased with the amount of diluent, starting in week 5 and continuing to week 11 (Figure 3-2a & b). Several studies demonstrated that methanogens are often found closely associated with SRB communities as they share a syntrophic relationship (Siddique et al., 2014b; Straalen & Roelofs, 2012). Methanogenesis is a complex biochemical process, and three pathways have been proposed depending on the initial substrates; acetoclastic, hydrogenotrophic, and methylotrophic pathways (Guo et al., 2015; Zavarzin, 2010). Regardless of the pathway, the last step of methanogenesis is to convert methyl-CoM to methane, and is catalysed by the methyl-coenzyme M reductase enzyme (Ermler et al., 1997; Guo et al., 2015). Methyl-coenzyme M reductase consists of three different subunits forming heterohexamer protein ($\alpha_2\beta_2\gamma_2$; Ermler et al., 1997).

No lateral transfer of the *mcr* gene been reported, and the three subunits (α, β, γ) are highly conserved across the phylogeny (Dhillon et al., 2005; Springer et al., 1995). The methyl-coenzyme M reductase A (*mcrA*) gene, which encodes for the α subunit, is often used as a genetic marker for methanogens (Dhillon et al., 2005; Springer et al., 1995). The *mcrA* was undetectable in week 5 except for in the MFT-SPW-1.5% sample (Figure 3-2c). At week 11, *mcrA* was detected in the diluent-containing samples (MFT-PW-0.8%, MFT-SPW-0.8%, and MFT-SPW-1.5%), and the band intensity in the SPW samples increased with diluent concentration (MFT-SPW-0.8% and -1.5%; Figure 3-2c).

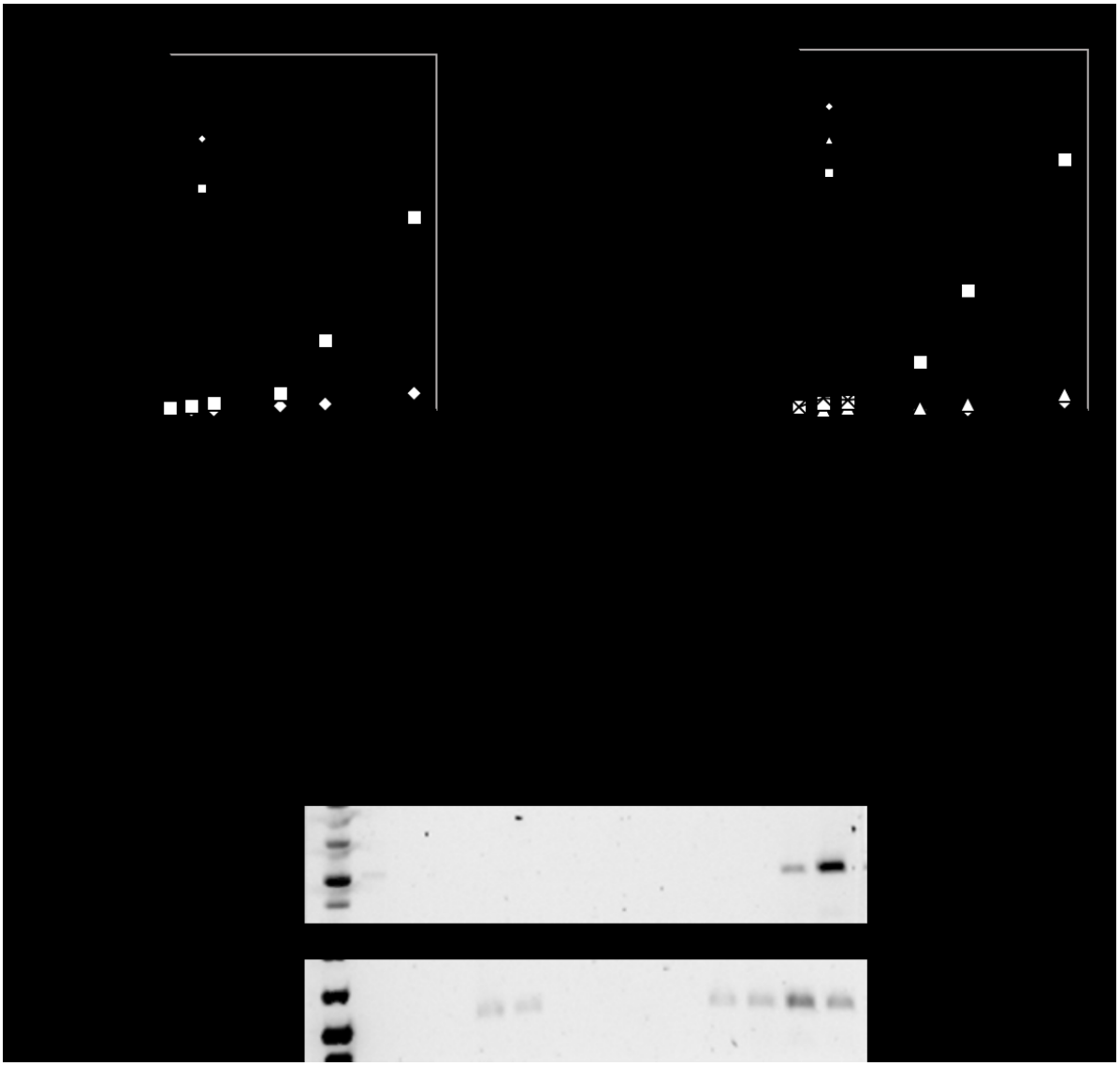

Figure 3-2 Methane measurement for the (a) PW and (b) SPW groups over the 11-week study period. Filled circles: PW or SPW +0.8% diluent; open diamonds: +MFT; open triangle: +MFT/+0.2% diluent, open square: +MFT/+0.8% diluent; x: +MFT/+1.5% diluent. (c) The *mcr* gene was amplified from each of the duplicate MFT samples. MFT obtained prior to experiment (week 0) was used as control. Figure is excerpted from Gee et al. (2017).

Two of the methanogen families were identified from the 16S rRNA sequencing, Methanoregulaceae (*Methanoregula*) and Methanotrichaceae (*Methanothrix;* Figures 3-3 and A1). Overall, the pattern of the relative abundance observed in the two methanogen families was similar to the PCR results (Figures 3-2, 3-3, A1 and Table A1). Interestingly, an increase in the

relative abundance of *Methanothrix* in the SPW week 11 sample was observed with a slight increase in relative abundance for a few other organisms, including *Leptolinea*, *Longilinea*, *Bellilinea* and *Syntrophus* (Figure A1), perhaps indicating a syntrophic relationship between these organisms.

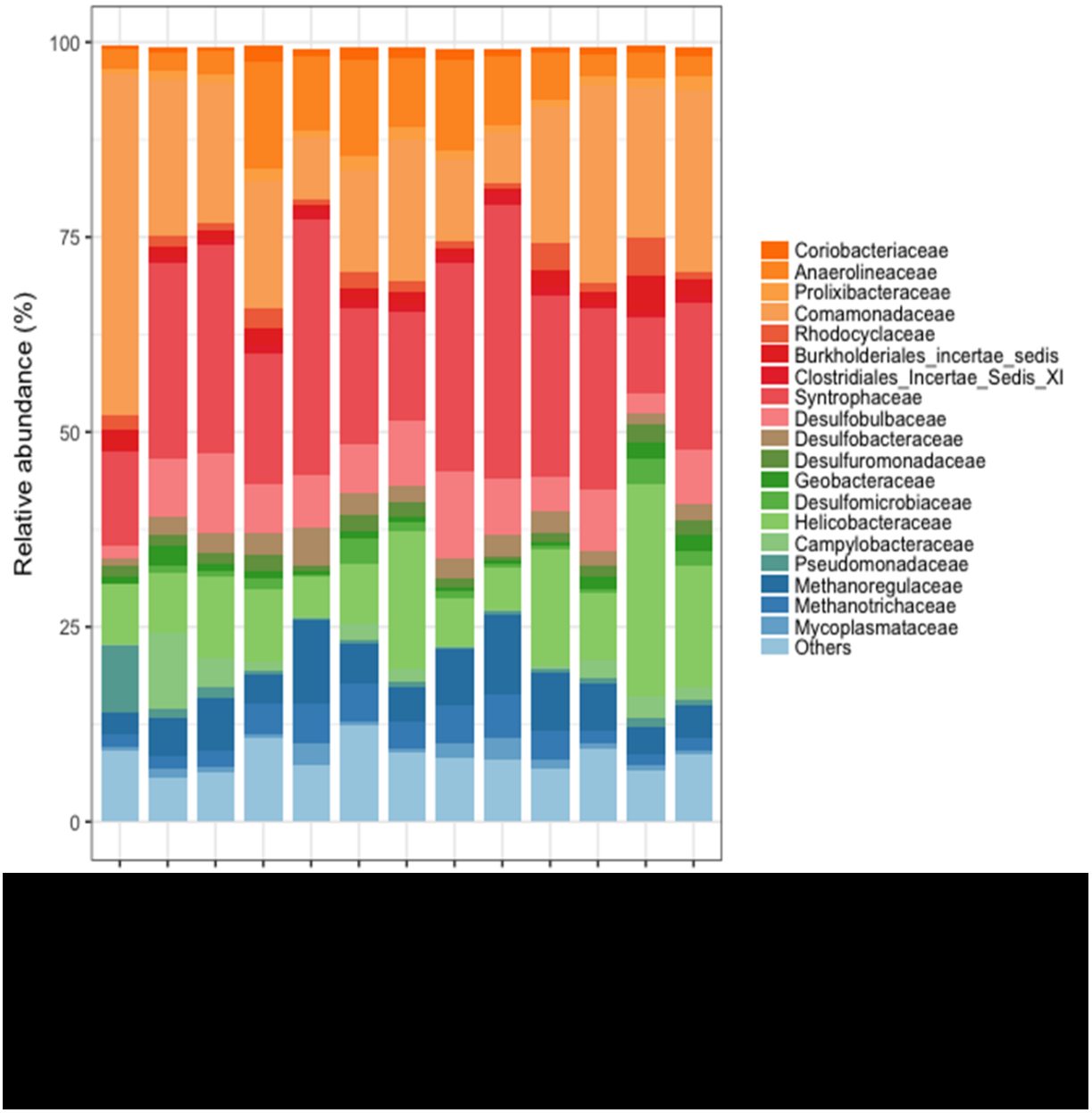

Figure 3-3 16S rRNA gene microbial community analysis of mesocosm samples at week 5 and week 11. The relative abundance (%) of microbial communities within the mesocosms were plotted at family levels. Figure excerpt from Gee et al. (2017).

Both Methanoregulaceae and Methanotrichaceae families are nonmotile and strictly anaerobic methanogens (Rosenberg et al., 2014). However, they utilize different metabolic pathways; namely acetoclastic (Methanotrichaceae) and hydrogenotrophic (Methanoregulaceae) pathways (Rosenberg et al., 2014). The Methanotrichaceae family uses only acetate as a substrate (Rosenberg et al., 2014). While acetate serves as growth factor, the Methanoregulaceae family uses mainly H_2/CO_2 as substrate (Rosenberg et al., 2014). The Methanoregulaceae family is often identified in oil fields, oil production water and oil waste treatment sites (Folarin et al., 2013; Lan et al., 2011; Li et al., 2012; Y. Q. Tang et al., 2012). Members of the Methanoregulaceae were identified in oil sands field samples by the partial 16S rRNA gene sequencing analysis (Hubert et al., 2012). Members of the Methanoregulaceae and Methanotrichaceae were also identified in primary cultures from MFT and in a microcosm study with gypsum-treated MFT by 16S rRNA pyrosequencing (Ramos-Padron et al., 2011; Siddique et al., 2012). The amount of H_2S and CH_4 generated in the mesocosms is linearly correlated with the amount of the diluent present (Figure 3-1 & -2). This result further supports the hypothesis that H_2S and CH_4 gas production in the mesocosms reflects the biodegradation of organic compounds, in this case naphtha diluent. In addition, H_2S production preceded CH_4 generation (Figure 3-1 & -2). Taken together, these observations may suggest a complex relationship between SRB, methanogens, and other microbial communities.

Interestingly, since SRB use hydrogen during the sulfate reduction process, the identification of hydrogenotrophic methanogens (Methanoregulaceae) from the mesocosms may suggest a competitive relationship between SRB and methanogens. It has long been known that SRB compete with methanogens for the same electron donors, namely acetate or hydrogen (Achtnich et al., 1995; Salloum et al., 2002). Several studies reported that high sulfate concentrations in

MFT (1.7–4.0 g/L) prevent methanogenesis (Salloum et al., 2002; Stasik & Wendt-Potthoff, 2014). SRB can out-compete methanogens at high sulfate concentrations because more energy can be generated through sulfate reduction (based on free energy calculation;Salloum et al., 2002; Zinder, 1993). A competitive relationship is further supported by our observation that H_2S production preceded CH_4 production, and that SRBs were identified at a higher relative abundance in week 5 MFT samples, even when the sulfate concentration was around eight times less (224–376 mg/L) than in the studies mentioned above.

In addition to SRB and methanogens, both the families Anaerolinealeaceae (*Leptolinea*, *Longilinea*, and *Bellilinea*) and Synergistaceae (*Syntrophus* and *Smithella*) were identified from the MFT samples (Figures 3-3 and A1), suggesting a syntrophic relationship among these anaerobes. A synergistic relationship in MFT was also proposed by Siddique et al. (2014b). Briefly, organic substrates are fermented by Clostridiales and Synergistaceae to generate fatty acids, alcohols, CO_2 and H_2 (Siddique et al., 2014b). Subsequently, these products are used by the SRB and methanogens (Siddique et al., 2014b). The microbial community in the MFT-PW-0.8% mesocosm seems to agree with the complex relationship proposed by Siddique et al. (2014b). Despite an increase in relative abundance for the family Desulfobulbaceae (*Desulfocapsa*) in MFT-PW-0.8% mesocosm in week 5, Syntrophaceae (*Smithella*), Anaerolineaceae (*Leptolinea*, *Longilinea* and *Bellilinea*) and methanogens (*Methanothrix* and *Methanoregula*) also increased in relative abundance in the week 5 samples compared to the MFT-PW control. The increase in syntrophic and methanogenic organisms signified the switch from sulfate-reducing to methanogenic conditions. Indeed, a significant increase in CH_4 production between weeks 4 and 6 (from 940 to 3925 μmol) was observed in the MFT-PW-0.8%

mesocosm, while a slight increase in H_2S (from 3.3 to 5.5 μmol) was observed between weeks 4 and 6 (Figures 3-1a and 3-2a).

Taken together, the mesocosm results indicate highly complex and dynamic microbial interactions. Interestingly, there is no apparent toxicity of naphtha diluent to the microbiota in the MFT even at the highest diluent concentration (1.5%) tested, which is consistent with a study conducted by Saeed et al. (1998). These authors reported that the EC_{50} for naphtha was 14%, measured by Microtox analysis after 24 hours incubation at 25°C (Saeed et al., 1998). However, Salanitro et al. (1997) showed that Microtox analysis was less sensitive compared to the earthworm bioassay when examining the toxicity of soil exposed to heavy, medium or light crude oil (at 5% w/w concentration).

3.3.2 BTEX Release from MFT

In previous section, the effect of naphtha diluent on the production of biogenic gas was demonstrated. However, several studies have hypothesized that chemical and biological processes could reduce the accumulation and subsequent release of these biogenic gases. For example, H_2S was hypothesized to remain within the tailings ponds (~pH 8) as dissolved HS^- (Ramos-Padron et al., 2011), and sulfide oxidation (Ramos-Padron et al., 2011) and methanotrophy (Saidi-Mehrabad et al., 2013) could oxidize H_2S and CH_4 respectively within the oxic zone of the water cap. Despite these processes, intensive bubbling and emission of CH_4 gas has been observed in oil sands tailings ponds (Burkus et al., 2014; Fedorak et al., 2003; Holowenko et al., 2000). This evolution of CH_4 gas from the MFT to the surface of tailings ponds could resuspend fine particles from the tailings, reduce oxygen levels in the surface water (Fedorak et al., 2002), and transport toxic chemicals to the surface water (Fedorak et al., 2002;

Ramos-Padron et al., 2011). These impacts could slow reclamation efforts of water capped-tailings such as in BML (further discussion can be found in chapter 5).

As mentioned above, *n*-alkanes and BTEX are the major components of naphtha diluent (Table A2), and because of their carcinogenicity, the release of these volatile organic compounds could increase public health risk and aquatic toxicity (Allouch et al., 2013; Anderson et al., 1974; Canadian Centre for Occupational Health and Safety.; Durmusoglu et al., 2010; Headley et al., 2001). As a result, the chemical transport of these hydrocarbons from the FFT via biogenic gas production was studied by measuring BTEX compounds in the mesocosm headspace. Of all the BTEX compounds, only benzene and toluene were detected during the 15 week incubation period (Figure 3-4). In general, higher benzene and toluene levels were observed in the mesocosms that received higher diluent amendments (Figure 3-4). Approximately six times more benzene was observed in the headspace of the MFT-PW-0.8% mesocosm (from 0.5 to 2.9 mg), while only a minor increase was observed in headspace of the MFT-PW mesocosm (from 0 to 0.27 mg; Figure 3-4a). A similar trend was observed for the toluene levels in the headspace of the MFT-PW-0.8% mesocosms (from 0 to 0.76 mg), and the toluene level remained at 0 mg throughout the entire experiment in the headspace of the MFT-PW mesocosm (Figure 3-4b). The SPW-containing mesocosms showed similar pattern to the MFT-PW mesocosms, with an increase in benzene and toluene with increasing diluent concentration (Figure 3-4 c & d). However, the MFT-SPW-1.5% mesocosm had lower benzene and toluene in week 11 and 15 compared to the MFT-SPW-0.8% (Figure 3-4 b &d).

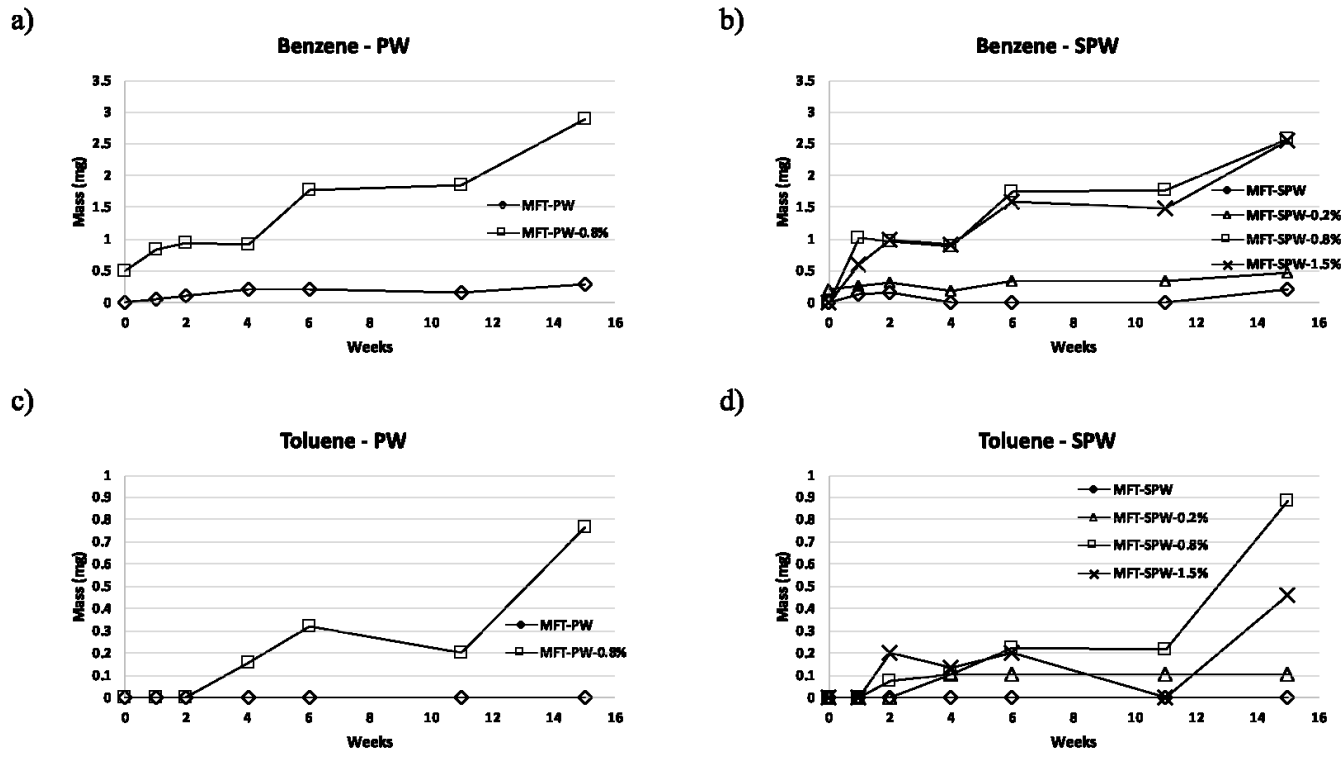

Figure 3-4 Benzene and toluene mass (mg) measured in mesocosm headspace. Note: standard error was estimated as ±0.01 mg.

A distinct pattern of benzene and toluene release rate was observed based on the chemical data, and the observed trends correlated with the increase in H_2S and CH_4 gases in the headspace (Figure 3-1a,b, Figure 3-2a,b, Figure 3-4, and Figure 3-5). The overall benzene release rate was highest between week 4 and 6, and dropped to its lowest between week 11 and 15 (Figure 3-5a,b). For the 0.8% diluent mesocosms (PW & SPW), the release rate was about 0.15 µg/mL MFT/d respectively (Figure 3-5a,b). For the MFT-SPW-1.5% mesocosms, the benzene release rate was about 0.12 and 0.1 µg/mL MFT/d for weeks 4–6 and 11–15 respectively (Figure 3-5b). For the MFT-SPW-0.2% mesocosms, the benzene release rate between week 4 to 6 was 0.02 µg/mL MFT/d, which was about twice as much as observed between week 11 to 15 (0.01 µg/mL

MFT/d; Figure 3-5b). The benzene release pattern seemed to coincide with H_2S evolution (Figure 3-5a,b and Figure 3-1a,b).

Interestingly, a more complex pattern and an earlier toluene release rate was observed compared to the benzene release (Figure 3-5c,d). For the MFT-PW-0.8% mesocosm, the earliest toluene release was ~0.03 μg/mL MFT/d during week 2–6 and a further 0.05 μg/mL MFT/d increase during week 11–15 was observed (Figure 3-5c). The SPW group showed that the concentration of diluent influences the timing and frequency of the toluene release. For the MFT-SPW-0.2% mesocosm, the only toluene release was observed at a rate of 0.02 μg/mL MFT/d between week 2 and 4 (Δw4-2; Figure 3-5d). Both MFT-SPW-0.8% and -1.5% mesocosms showed 3 distinct toluene releases between week 1 and 2, 4 and 6, and 11 and 15 (Figure 3-5d). The toluene release pattern seemed to coincide with the CH_4 evolution (Figure 3-5c,d and Figure 3-2a,b).

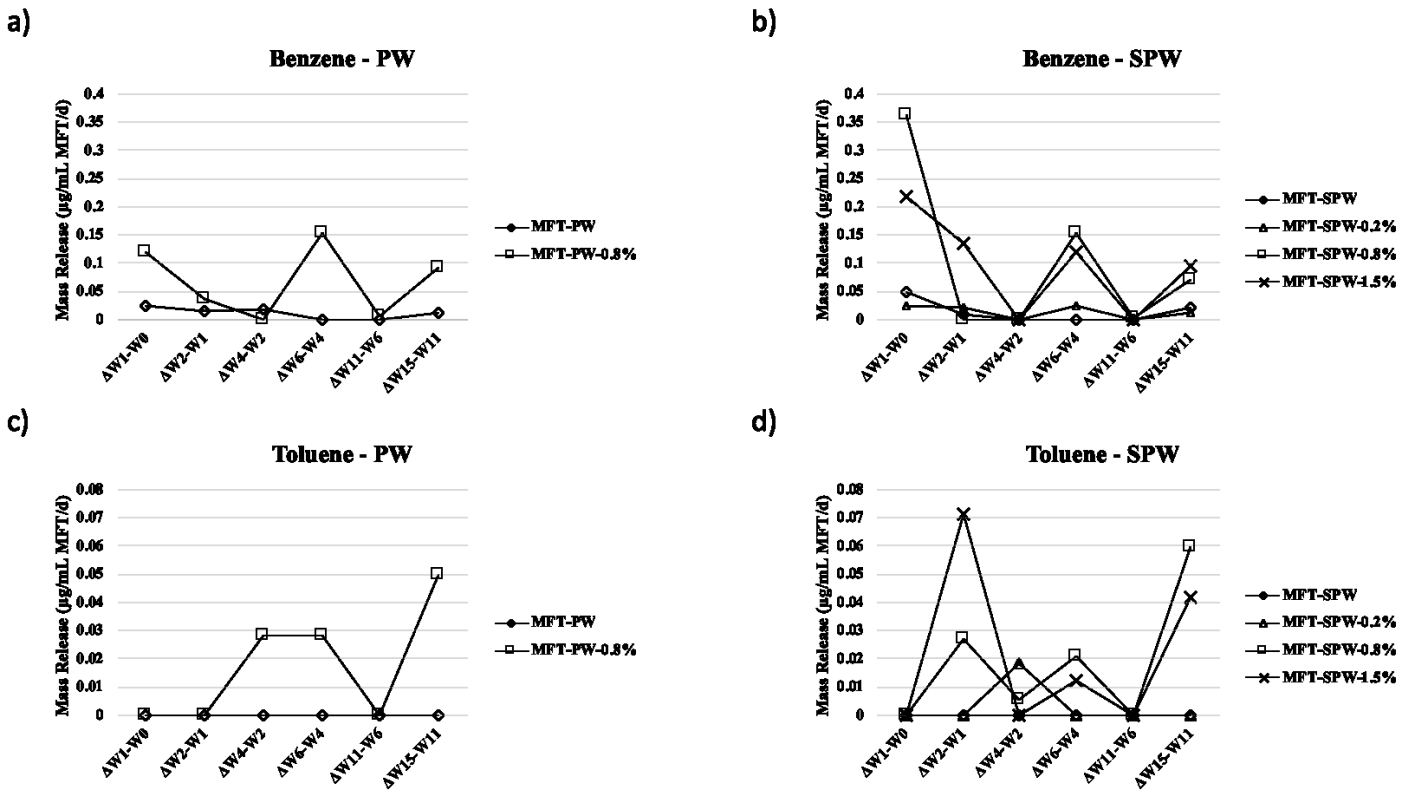

Figure 3-5 Benzene and toluene release rate for PW and SPW groups over the 15 week study period. The change in benzene and toluene concentration (mg/mL MFT/d) between 1-0, 2-1, 4-2, 6-4, 11-6, and 15-11 weeks were plotted. Note that any negative values were set to be 0.

Short-term inhalation of benzene and toluene could affect the central nervous system, and thus the threshold limit value time-weighted average (TLV-TWA) permissible exposure concentration is 10 ppm for benzene and 200 ppm for toluene (Canadian Centre for Occupational Health and Safety, 2017). In addition, according to the Alberta ambient air quality guidelines, the emissions from industrial facilities should be below 30 µg/m^3 for benzene and 1880 µg/m^3 for toluene in one hour period. The benzene and toluene concentrations were calculated using the headspace volume of mesocosms (~310 mL or 3.65x10^{-4} m^3). The highest rate of release of benzene in the headspace was 7000 µg/m^3/hr for the 0.8% diluent mesocosms (PW & SPW) between week 4 and 6. Between week 4 and 6, the lowest benzene rate of release was 1100

μg/m^3/hr for the MFT-SPW-0.2% mesocosm. A slightly lower benzene rate of release (5400 μg/m^3/hr) was observed for the MFT-SPW-1.5% mesocosms between week 4 and 6.

Similar rates of toluene release (1900 to 2700 μg/m^3/hr) were observed for the 0.8% diluent mesocosms (PW & SPW) and MFT-SPW-1.5% mesocosms between week 11 and 15. For the MFT-SPW-0.2% mesocosms, the toluene release during week 11 and 15 was 0 μg/m^3/hr.

The mesocosm results showed that benzene headspace concentration during the peak release periods (week 4-6) exceeded the Alberta ambient air quality guideline for all three diluent concentrations (0.2%, 0.8% and 1.5%) tested. All mesocosms that received 0.8% and 1.5% diluent had toluene release rates that exceeded the Alberta ambient air quality guideline. The three diluent concentrations (0.2%, 0.8%, and 1.5%) were selected to represent low, typical, and high diluent concentration respectively. These results suggested that further effort might be needed to focus on BTEX removal instead on diluent recovery, as experimental results from this section showed that benzene emission is likely exceed the environmental guideline even at the lowest diluent concentration (0.2%). BTEX can be removed by biotic and abiotic processes, and abiotic BTEX removal will be discuss in Chapter 4.

BTEX degradation has been reported under anaerobic methanogenic and/or sulfate-reducing conditions (Siddique et al., 2007; Weelink et al., 2010). Anaerobic BTEX degradation was demonstrated by several members of the Pseudomonadaceae, Geobacteraceae, Desulfobacteraceae, Desulfobulbaceae, Rhodocyclaceae and Clostridiales (Chakraborty et al., 2005; Ulrich & Edwards, 2003; Weelink et al., 2010). In a microcosm study, Siddique et al. (2007) showed BTEX degradation preferences under methanogenic conditions: toluene > *o*-xylene > *m*- & *p*-xylene > ethylbenzene > benzene. Only a minor change in benzene

concentration (from 97–82 mg/L) occurred even after 36 weeks of incubation (Siddique et al., 2007). Based on this and other studies, benzene is considered recalcitrant compared to other BTEX compounds, because anaerobic benzene degradation is more energy demanding and is often limited by electron acceptor availability (Siddique et al., 2007; Weelink et al., 2010). Furthermore, under methanogenic conditions, more labile hydrocarbons such as *n*-alkanes were consumed prior to the BTEX degradation (Shahimin & Siddique, 2017; Siddique et al., 2007).

These observations could explain the benzene and toluene accumulations and release from MFT. In this study, several BTEX-degrading microbial communities were identified from MFT samples, including Clostridiales, Geobacteraceae, Desulfobulbaceae, Rhodocyclaceae and Pseudomonadaceae (Figures 3-3 and 3-4). Several previous studies suggest a complex and syntrophic relationship in the anaerobic BTEX degradation processes. Firstly, Desulfobulbaceae was found to dominate in methanogenic benzene-degrading enrichment cultures (Ulrich & Edwards, 2003). Secondly, members of the Clostridiales (Peptococcaceae) and Geobacteraceae have been implicated in anaerobic benzene degradation (Kunapuli et al., 2007; Rooney-Varga et al., 1999). Thus, Clostridiales and Geobacteraceae were hypothesized to be capable of anaerobic benzene degradation and share a syntrophic relationship with Desulfobulbaceae (Kunapuli et al., 2007; Siddique et al., 2014b).

With respect to toluene degradation and accumulation in our mesocosm study, members of the Pseudomonadaceae, Geobacteraceae, and Desulfobulbaceae have previously been documented by others for capable of degrading toluene under anaerobic conditions (Abu Laban et al., 2015a, 2015b; Lovley et al., 2004; Ulrich & Edwards, 2003). Even though toluene was preferentially degraded under methanogenic conditions in previous studies, in this study toluene was detected in the mesocosms but not ethylbenzene and xylene. Three possible explanations may exist for

this observation; 1) a higher toluene concentration in naphtha diluent, 2) BTEX partitioning properties, and 3) the presence of more labile hydrocarbon.

Firstly, Siddique et al. (2007) performed a full chemical analysis of the naphtha diluent, and the proportions of BTEX compounds in naphtha were as follows: toluene = 7.5%, ethylbenzene = 3.1%, *m*-xylene = 4%, *p*-xylene = 1.7%, and *o*-xylene = 2.2%. Secondly, ethylbenzene and xylenes have higher partitioning coefficient value (Log K_{ow} ≈3.2) than toluene (Log K_{ow} = 2.65) and benzene (Log K_{ow} = 2.13;Agteren et al., 1998). The higher partitioning coefficient value suggests that ethylbenzene and xylenes can be adsorbed more strongly to the MFT solids in the mesocosms, and a stronger ebullition force may be needed to transport these compounds from MFT to the headspace. Finally, *n*-alkanes were shown to be preferentially degraded prior to BTEX degradation under methanogenic conditions in previous microcosms studies (Shahimin & Siddique, 2017; Siddique et al., 2007). These observations support the benzene and toluene release patterns from our mesocosm study.

An active methane bubble zone has been observed in the Mildred Lake Settling Basin (MLSB) tailings pond (Holowenko et al., 2000). The ebullition of biogenic gases could be one mechanism of chemical transport between the tailings and surface water in tailings ponds and pit lakes. In fact, an oil film was observed covering parts of the BML, which impacted the formation of surface wind waves (Hurley, 2017). The increase of hydrocarbons such as BTEX can increase surface water toxicity to aquatic organisms (Headley et al., 2001). Ebullition of biogenic gases could also serve as a mechanism to resuspend the FFT, resulting in the high turbidity observed in BML (Lawrence et al., 2016). Indeed, it is hypothesized that the liquid hydrocarbons from the FFT attach to the gas bubbles thereby the hydrocarbons accumulate in the surface water (Hurley, 2017; Lawrence et al., 2016).

3.4 Conclusion

This study demonstrated that 1) sulfate reduction and H_2S production occurs between week 0 and 6 (with 5.5 and 16 μmol H_2S increase in week 6 for 0.8% diluent-PW & SPW respectively); 2) methanogenesis occurs between week 5 and 11 (with 10700 and 13900 μmol CH_4 increase in week 11 for 0.8% diluent-PW & SPW respectively), 3) an increase in relative abundance of sequences associated with SRB (with maximum 580% increase in week 5 for Desulfobulbaceae) and key methanogens (with maximum 380% and 360% increase in week 11 for Methanoregulaceae and Methanotrichaceae respectively) were identified from MFT samples in week 5 and 11 respectively , and 4) benzene release between week 4 and 6 (with the highest rate 1.1 μg/mL MFT/d for 0.8% diluent with SPW & PW) correlated with the H_2S production, and toluene release between weeks 11 and 15 (with the highest rate 0.35 and 0.4 μg/mL MFT/d for 0.8% diluent with SPW & PW) correlated with CH_4 emission patterns. The overall gas production increased as the diluent amendment concentration increases.

Methanogens (Methanoregulaceae and Methanotrichaceae) and SRB (Desulfobulbaceae, Desulfobacteraceae, Desulfuromonadaceae, and Desulfomicrobiaceae) were detected and implicated in the observed gas generation. The H_2S production (with maximum increase observed between week 0 and 5) preceded CH_4 production (with maximum increase observed between week 5 and 11), which confirms competition between SRB and methanogens. In addition, several key microorganisms were identified from the MFT samples, including Clostridiales, Synergistaceae, Geobacteraceae, and Pseudomonadaceae. Detection of these organisms further suggests that biogenic gases are produced through a complex competitive and syntrophic microbiological ecosystem.

The potential for anaerobic BTEX degradation were previously studied in the above-mentioned microbial groups, including Clostridiales, Geobacteraceae, Desulfobulbaceae, Rhodocyclaceae and Pseudomonadaceae. In spite of these potential BTEX-degrading anaerobic groups identified from mesocosms amended with naphtha diluent, benzene and toluene were detected in the mesocosms headspace. This suggests that an abiotic process is transporting H_2S and CH_4 to the surface. The benzene release pattern (with the highest rate of release at 1.1 μg/mL MFT/d between week 4 and 6) correlated with the highest rate of H_2S release (5.5 μmol) between week 0 and 6 in the MFT-PW-0.8% mesocosm. The toluene release pattern (with the highest rate at 0.35 μg/mL MFT/d between week 11 and 15) coincided with the highest increase in CH_4 release rate (10870 μmol) in week 11.

The benzene and toluene release rates show that 1) the ebullition of biogenic gases could be a transport mechanism for the residual organics that are adsorbed on the MFT particles and 2) the anaerobic microbial communities identified in the mesocosms did not play a significant role in benzene and toluene degradation in the 15 weeks of this experiment. These results also suggested a potential strategy to reduce the biogenic gas production in the oil sands tailings ponds as well as in pit lakes by reducing the amount of unrecovered diluent released with the tailings. One such technology will be examined in chapter 4.

3.5 References

Abu Laban, N., Tan, B., Dao, A., & Foght, J. (2015a). Draft Genome Sequence of Uncultivated *Desulfosporosinus sp*. Strain Tol-M, Obtained by Stable Isotope Probing Using [13C6]Toluene. *Genome Announc, 3*(1).

Abu Laban, N., Tan, B., Dao, A., & Foght, J. (2015b). Draft Genome Sequence of Uncultivated Toluene-Degrading *Desulfobulbaceae* Bacterium Tol-SR, Obtained by Stable Isotope Probing Using [13C6]Toluene. *Genome Announc, 3*(1).

Achtnich, C., Bak, F., & Conrad, R. (1995). Competition for Electron-Donors among Nitrate Reducers, Ferric Iron Reducers, Sulfate Reducers, and Methanogens in Anoxic Paddy Soil. *Biology and Fertility of Soils, 19*(1), 65-72.

Agteren, M. H., Keuning, S., & Janssen, D. B. (1998). *Handbook on Biodegradation and Biological Treatment of Hazardous Organic Compounds*. Dordrecht: Springer Netherlands.

Alberta Energy Regulator. (2016). *Directive 085: Fluid Tailings Management for Oil Sands Mining Projects*. Retrieved from http://www.aer.ca/documents/directives/Directive085.pdf.

Allouch, A., Le Calve, S., & Serra, C. A. (2013). Portable, miniature, fast and high sensitive real-time analyzers: BTEX detection. *Sensor Actuat B Chem, 182*, 446-452.

Anderson, J. W., Neff, J. M., Cox, B. A., Tatem, H. E., & Hightower, G. M. (1974). Characteristics of Dispersions and Water-Soluble Extracts of Crude and Refined Oils and Their Toxicity to Estuarine Crustaceans and Fish. *Mar Biol, 27*(1), 75-88.

Burkus, Z., Wheler, J., & Pletcher, S. (2014). *GHG Emissions from Oil Sands Tailings Ponds: Overview and Modelling Based on Fermentable Substrates*. Retrieved from Edmonton:

Canadian Centre for Occupational Health and Safety. Chemical Profiles - Benzene. Retrieved January 9, 2019, from Canadian Centre for Occupational Health and Safety https://www.ccohs.ca/oshanswers/chemicals/chem_profiles/benzene.html

Chakraborty, R., O'Connor, S. M., Chan, E., & Coates, J. D. (2005). Anaerobic degradation of benzene, toluene, ethylbenzene, and xylene compounds by *Dechloromonas* strain RCB. *Appl Environ Microbiol, 71*(12), 8649-8655.

Cumulative Environmental Management Association. (2012). *End pit lakes guidance document* (pp. 1 online resource (434 p.)). Retrieved from http://www.deslibris.ca/ID/234915

Dhillon, A., Lever, M., Lloyd, K. G., Albert, D. B., Sogin, M. L., & Teske, A. (2005). Methanogen diversity evidenced by molecular characterization of methyl coenzyme M reductase A (*mcr*A) genes in hydrothermal sediments of the Guaymas Basin. *Appl Environ Microbiol, 71*(8), 4592-4601.

Durmusoglu, E., Taspinar, F., & Karademir, A. (2010). Health risk assessment of BTEX emissions in the landfill environment. *J Hazard Mater, 176*(1-3), 870-877.

Ermler, U., Grabarse, W., Shima, S., Goubeaud, M., & Thauer, R. K. (1997). Crystal structure of methyl coenzyme M reductase: The key enzyme of biological methane formation. *Science, 278*(5342), 1457-1462.

Fedorak, P. M., Coy, D. L., Dudas, M. J., Simpson, M. J., Renneberg, A. J., & MacKinnon, M. D. (2003). Microbially-mediated fugitive gas production from oil sands tailings and increased tailings densification rates. *J Environ Eng and Sci, 2*(3), 199-211.

Fedorak, P. M., Coy, D. L., Salloum, M. J., & Dudas, M. J. (2002). Methanogenic potential of tailings samples from oil sands extraction plants. *Can J Microbiol, 48*(1), 21-33.

Foght, J. M., Gieg, L. M., & Siddique, T. (2017). The microbiology of oil sands tailings: past, present, future. *FEMS Microbiol Ecol, 93*(5).

Folarin, Y., An, D., Caffrey, S., Soh, J., Sensen, C. W., Voordouw, J.,Jack, T., Voordouw, G. (2013). Contribution of make-up water to the microbial community in an oilfield from which oil is produced by produced water re-injection. *Int Biodeter Biodegr, 81*, 44-50.

Gee, K. F., Poon, H. Y., Hashisho, Z., & Ulrich, A. C. (2017). Effect of naphtha diluent on greenhouse gases and reduced sulfur compounds emissions from oil sands tailings. *Sci Total Environ, 598*, 916-924.

Grein, F., Ramos, A. R., Venceslau, S. S., & Pereira, I. A. C. (2013). Unifying concepts in anaerobic respiration: Insights from dissimilatory sulfur metabolism. *BBA Bioenergetics, 1827*(2), 145-160.

Guo, J. H., Peng, Y. Z., Ni, B. J., Han, X. Y., Fan, L., & Yuan, Z. G. (2015). Dissecting microbial community structure and methane-producing pathways of a full-scale anaerobic reactor digesting activated sludge from wastewater treatment by metagenomic sequencing. *Microb Cell Fact, 14*.

Headley, J. V., Goudey, S., Birkholz, D., Linton, L. R., & Dickson, L. C. (2001). Toxicity Screening of Benzene, Toluene, Ethylbenzene and Xylene (BTEX) Hydrocarbons in Groundwater at Sour-Gas Plants. *Can Water Resour J, 26*(3), 345-358.

Holowenko, F. M., MacKinnon, M. D., & Fedorak, P. M. (2000). Methanogens and sulfate-reducing bacteria in oil sands fine tailings waste. *Can J Microbiol, 46*(10), 927-937.

Hubert, C. R. J., Oldenburg, T. B. P., Fustic, M., Gray, N. D., Larter, S. R., Penn, K., Rowan, A.K., Seshadri, R., Sherry, A., Swainsbury, R., Voordouw, G., Voordouw, J.K., Head, I. M. (2012). Massive dominance of *Epsilonproteobacteria* in formation waters from a Canadian oil sands reservoir containing severely biodegraded oil. *Environ Microbiol, 14*(2), 387-404.

Hurley, D. L. (2017). *Wind waves and internal waves in Base Mine Lake.* (Master's thesis) University of British Columbia. Retrieved from https://open.library.ubc.ca/collections/ubctheses/24/items/1.0351993

Kunapuli, U., Lueders, T., & Meckenstock, R. U. (2007). The use of stable isotope probing to identify key iron-reducing microorganisms involved in anaerobic benzene degradation. *Isme Journal, 1*(7), 643-653.

Lan, G. H., Li, Z. T., Zhang, H., Zou, C. J., Qiao, D. R., & Cao, Y. (2011). Relationship of microbial diversity from recycled injection water and high-temperature petroleum reservoirs analyzed by polymerase chain reaction denaturing gradient gel electrophoresis (PCR-DGGE). *Afr J Biotechnol, 10*(53), 11004-11010.

Lawrence, G. A., Tedford, E. W., & Pieters, R. (2016). Suspended solids in an end pit lake: potential mixing mechanisms. *Can J Civ Eng, 43*(3), 211-217.

Li, H., Ai, M. Q., Han, S. Q., Guo, Y. L., Li, N. N., Shi, R. J., Zeng, X., Leng, S., Zhao, J., Liu, X., Zhang, Y. (2012). Microbial diversity and functionally distinct groups in produced water from the Daqing Oilfield, China. *Petrol Sci, 9*(4), 469-484.

Lovley, D. R., Holmes, D. E., & Nevin, K. P. (2004). Dissimilatory Fe(III) and Mn(IV) reduction. *Adv microb Physiol, Vol. 49, 49*, 219-286.

Mahdavi, H. (2014). *The application of algae for the removal of metals and naphthenic acids from oil sands tailings pond water.* (Doctoral thesis), University of Alberta. Retrieved from http://hdl.handle.net/10402/era.39068

Muller, A. L., Kjeldsen, K. U., Rattei, T., Pester, M., & Loy, A. (2015). Phylogenetic and environmental diversity of DsrAB-type dissimilatory (bi)sulfite reductases. *ISME J, 9*(5), 1152-1165.

Penner, T. J., & Foght, J. M. (2010). Mature fine tailings from oil sands processing harbour diverse methanogenic communities. *Can J Microbiol, 56*(6), 459-470.

Ramos-Padron, E., Bordenave, S., Lin, S., Bhaskar, I. M., Dong, X., Sensen, C. W., Fournier, J., Voordouw, G., Gieg, L. M. (2011). Carbon and sulfur cycling by microbial communities in a gypsum-treated oil sands tailings pond. *Environ Sci Technol, 45*(2), 439-446.

Risacher, F. F., Morris, P. K., Arriaga, D., Goad, C., Nelson, T. C., Slater, G. F., & Warren, L. A. (2018). The interplay of methane and ammonia as key oxygen consuming constituents in early stage development of Base Mine Lake, the first demonstration oil sands pit lake. *Appl Geochem, 93*, 49-59.

Rooney-Varga, J. N., Anderson, R. T., Fraga, J. L., Ringelberg, D., & Lovley, D. R. (1999). Microbial communities associated with anaerobic benzene degradation in a petroleum-contaminated aquifer. *Appl Environ Microbiol, 65*(7), 3056-3063.

Rosenberg, E., DeLong, E. F., Lory, S., Stackebrandt, E., & Thompson, F. L. (2014). *The prokaryotes : Other major lineages of bacteria and the archaea* (pp. 1 online resource). Retrieved from http://link.springer.com/10.1007/978-3-642-38954-2

Saeed, T., Al-mutairi, M., Ali, L. N., Al-obaid, T., & Beg, M. U. (1998). The Effect of Temperature on the Composition and Relative Toxicity of the Water-Soluble Fraction of Kuwait Crude Oil (Export) in the Seawater. *Int J Environ An Chem, 72*(4), 275-287.

Saidi-Mehrabad, A., He, Z., Tamas, I., Sharp, C. E., Brady, A. L., Rochman, F. F., Bodrossy, L., Abell, G.C.J., Penner, T., Dong, X., Dunfield, P. F. (2013). Methanotrophic bacteria in oilsands tailings ponds of northern Alberta. *ISME J, 7*(5), 908-921.

Salanitro, J. P., Dorn, P. B., Huesemann, M. H., Moore, K. O., Rhodes, I. A., Jackson, L. M. R., Vipond, T.E., Western, M.M., Wisniewski, H. L. (1997). Crude oil hydrocarbon bioremediation and soil ecotoxicity assessment. *Environ Sci Technol, 31*(6), 1769-1776.

Salloum, M. J., Dudas, M. J., & Fedorak, P. M. (2002). Microbial reduction of amended sulfate in anaerobic mature fine tailings from oil sand. *Waste Manag Res, 20*(2), 162-171.

Santillano, D., Boetius, A., & Ramette, A. (2010). Improved dsrA-Based Terminal Restriction Fragment Length Polymorphism Analysis of Sulfate-Reducing Bacteria. *Appl Environ Microbiol, 76*(15), 5308-5311.

Schiffer, A., Parey, K., Warkentin, E., Diederichs, K., Huber, H., Stetter, K. O., Kroneck, P.M., Ermler, U. (2008). Structure of the dissimilatory sulfite reductase from the hyperthermophilic archaeon *Archaeoglobus fulgidus*. *J Mol Biol, 379*(5), 1063-1074.

Shahimin, M. F. M., & Siddique, T. (2017). Sequential biodegradation of complex naphtha hydrocarbons under methanogenic conditions in two different oil sands tailings. *Environ Pollut, 221*, 398-406.

Siddique, T., Fedorak, P. M., & Foght, J. M. (2006). Biodegradation of short-chain *n*-alkanes in oil sands tailings under methanogenic conditions. *Environ Sci Technol, 40*(17), 5459-5464.

Siddique, T., Fedorak, P. M., MacKinnon, M. D., & Foght, J. M. (2007). Metabolism of BTEX and naphtha compounds to methane in oil sands tailings. *Environ Sci Technol, 41*(7), 2350-2356.

Siddique, T., Kuznetsov, P., Kuznetsova, A., Arkell, N., Young, R., Li, C., Guigard, S., Underwood, E., Foght, J. M. (2014a). Microbially-accelerated consolidation of oil sands tailings. Pathway I: changes in porewater chemistry. *Front Microbiol, 5*, 106.

Siddique, T., Kuznetsov, P., Kuznetsova, A., Li, C., Young, R., Arocena, J. M., & Foght, J. M. (2014b). Microbially-accelerated consolidation of oil sands tailings. Pathway II: solid phase biogeochemistry. *Front Microbiol, 5*, 107.

Siddique, T., Penner, T., Klassen, J., Nesbo, C., & Foght, J. M. (2012). Microbial communities involved in methane production from hydrocarbons in oil sands tailings. *Environ Sci Technol, 46*(17), 9802-9810.

Siddique, T., Penner, T., Semple, K., & Foght, J. M. (2011). Anaerobic biodegradation of longer-chain *n*-alkanes coupled to methane production in oil sands tailings. *Environ Sci Technol, 45*(13), 5892-5899.

Small, C. C., Cho, S., Hashisho, Z., & Ulrich, A. C. (2015). Emissions from oil sands tailings ponds: Review of tailings pond parameters and emission estimates. *J Petrol Sci Eng, 127*, 490-501.

Springer, E., Sachs, M. S., Woese, C. R., & Boone, D. R. (1995). Partial gene sequences for the A subunit of methyl-coenzyme M reductase (*mcr*I) as a phylogenetic tool for the family *Methanosarcinaceae*. *Int J Syst Bacteriol, 45*(3), 554-559.

Stasik, S., & Wendt-Potthoff, K. (2014). Interaction of microbial sulphate reduction and methanogenesis in oil sands tailings ponds. *Chemosphere, 103*, 59-66.

Steger, D., Wentrup, C., Braunegger, C., Deevong, P., Hofer, M., Richter, A., Baranyi, C., Pester, M., Wagner, M., Loy, A. (2011). Microorganisms with Novel Dissimilatory (Bi)Sulfite Reductase Genes Are Widespread and Part of the Core Microbiota in Low-Sulfate Peatlands. *Appl Environ Microbiol, 77*(4), 1231-1242.

Straalen, N. M. v., & Roelofs, D. (2012). *An introduction to ecological genomics* (2nd ed.). Oxford ; New York: Oxford University Press.

Tang, K., Baskaran, V., & Nemati, M. (2009). Bacteria of the sulphur cycle: An overview of microbiology, biokinetics and their role in petroleum and mining industries. *Biochem Eng J, 44*(1), 73-94.

Tang, Y. Q., Li, Y., Zhao, J. Y., Chi, C. Q., Huang, L. X., Dong, H. P., & Wu, X. L. (2012). Microbial communities in long-term, water-flooded petroleum reservoirs with different *in situ* temperatures in the Huabei Oilfield, China. *PLoS One, 7*(3), e33535.

Ulrich, A. C., & Edwards, E. A. (2003). Physiological and molecular characterization of anaerobic benzene-degrading mixed cultures. *Environ Microbiol, 5*(2), 92-102.

Wagner, M., Roger, A. J., Flax, J. L., Brusseau, G. A., & Stahl, D. A. (1998). Phylogeny of dissimilatory sulfite reductases supports an early origin of sulfate respiration. *J Bacteriol, 180*(11), 2975-2982.

Weelink, S. A. B., van Eekert, M. H. A., & Stams, A. J. M. (2010). Degradation of BTEX by anaerobic bacteria: physiology and application. *Rev Environ Sci Bio, 9*(4), 359-385.

Zavarzin, G. A. (2010). *Microbial cycles* (Vol. 1): Academic Press. Encyclopedia of Ecology. pp. 2335-2341.

Zinder, S. H. (1993). Physiological Ecology of Methanogens. In J. G. Ferry (Ed.), *Methanogenesis: Ecology, Physiology, Biochemistry & Genetics* (pp. 128-206). Boston, MA: Springer US.

Chapter 4 : Organic Removal with an Advanced Oxidation System

4.1 Introduction

Tailings ponds are currently used to contain FFT and OSPW until a suitable technology is developed to remove the residual organics in OSPW, such as unrecovered bitumen and diluent. Naphtha diluent, which is used to improve the bitumen recovery, contains many low molecular weight aliphatic and monoaromatic hydrocarbons, such as n-alkanes and BTEX (benzene, toluene, ethylbenzene and xylenes;Siddique et al., 2006; Siddique et al., 2007; Small et al., 2015). These compounds stimulate microbial activity in fluid tailings under anaerobic conditions, producing greenhouse gases (carbon dioxide and methane) and reduced sulfide compounds (e.g. hydrogen sulfide; Gee et al., 2017; Siddique et al., 2006; Siddique et al., 2007). Based on the findings in Chapter 3, the amount of diluent present showed a linear correlation to hydrogen sulfide and methane generation by microbial activity in the tailings. These biogenic gases drive the flux of benzene and toluene from FFT to the surface water. Therefore, removing residual organics from the tailings could reduce the generation of biogenic gases and chemical flux, allowing FFT to dewater under more stable conditions.

Carbonaceous materials, such as charcoal and granular activated carbon (GAC), are commonly used in drinking water purification, wastewater treatment, and air pollution control (Bansal & Goyal, 2005; Çeçen & Aktaş, 2012). High surface area and porous characteristics allow activated carbon to be an effective adsorbent material (Bansal & Goyal, 2005; Çeçen & Aktaş, 2012). In addition, the presence of a heteroatom surface group, such as oxygen and hydrogen, enable the adsorption of polar and polarizable compounds, and increase the activated carbon wettability (Bandosz, 2006; Bansal & Goyal, 2005; Çeçen & Aktaş, 2012; Siriwardane et al., 2001). Once adsorbed, chemicals remain bound to the activated carbon, and if enough chemical compounds are encountered, the surface of the carbon material is eventually saturated and will not bind

further. In general, adsorption can be classified into two types: physical and chemical (Çeçen & Aktaş, 2012; Sawyer et al., 2003). Physical adsorption relies on van der Waals force, while chemical adsorption relies on chemical (covalent or ionic) bonds generated between the adsorbate and adsorbent (Bandosz, 2006; Bansal & Goyal, 2005; Çeçen & Aktaş, 2012; Sawyer et al., 2003).

In addition to GAC, expanded graphite (EG) has a high sorption capacity for spilled heavy oil, naphthenic acids, polycyclic aromatic hydrocarbons, and biological fluids (Inagaki et al., 2002; Inagaki et al., 2001; Kang et al., 2003; Moustafa et al., 2014; Qin et al., 2015; Shen et al., 1999; Toyoda & Inagaki, 2000). In one study, 1 g of EG was shown to sorb more than 80 g of heavy oil (Toyoda & Inagaki, 2000). Prior to the exfoliation, graphite is usually intercalated with various chemical species that alter the physical and chemical characteristics of the porous structures formed during the exfoliation treatment (Akuzawa et al., 2004; Bandosz, 2006; Dresselhaus & Dresselhaus, 2002). BioLargo Water, Inc., uses a proprietary EG to manipulate iodine chemistry under an electric field in an advanced oxidation system (AOS) reactor. A previous study has shown that application of electricity can enhance EG adsorption of phenanthrene (Qin et al., 2015). In addition, several studies showed that under high temperature, the iodine free radical can interact with hydrocarbons through dehydrogenation, aromatization, and aliphatic free radical rearrangements (Mullineaux & Raley, 1963; Raley et al., 1963; Slaugh et al., 1963). It is hypothesized that EG could accelerate chemical reactions and facilitate the rapid breakdown of chemicals with the application of electrical current. This chapter focus on determining the EG adsorption capacity of oil and gas-related organic compounds (BTEX) and the AOS organic removal capacity with or without the application of electrical current.

4.2 Materials and Methods

An Advanced Oxidation System (AOS) reactor, power supply, EG and a 10 mm pathlength quartz cell (6610000900, Agilent) were supplied by BioLargo Water Canada. To prepare the EG, sulfuric acid intercalated graphite (CAS# 12777-87-6) were heat shocked for 1 minutes at 1000 °C (Moustafa et al., 2014). Benzene (319953-1L) was purchased from Sigma-Aldrich, and toluene (T324-4), ethylbenzene (02751-1) and *p*-xylene (05082-500) were purchased from Fisher Scientific. GAC (12–40 mesh, 395710010) was purchased from Acros Organics. Tubing used to pump BTEX to the AOS (Masterflex L/S Viton precision pump tubing; HV-96412-17) was purchased from Cole-Parmer.

4.2.1 Determination of EG Adsorptive Capacity for Organics with Batch Experiment

Historical maximum concentration of benzene and toluene in the tailings ponds was 6.3 and 3 mg/L respectively (Allen, 2008). Therefore, we chose to test the EG adsorption capacity with 10 mg/L of each BTEX compound separately, as 10 mg/L represent the maximum possible BTEX concentrations in the OSPW.

To determine the EG adsorptive characteristic for the BTEX organic compounds, a batch adsorption experiment was performed in triplicate according to ASTM D4646. Approximately 10 mg/L stock of either benzene, toluene, ethylbenzene, or *p*-xylene compound was dissolved in ultra-pure water (Milli-Q) overnight prior to starting the experiment. The EG (8, 16, 325, and 500 mg) was exposed to either 10 mg/L of benzene, toluene, ethylbenzene, or *p*-xylene in triplicate. A 10 mg/L of either benzene, toluene, ethylbenzene, or *p*-xylene stock solution was made prior to each experiment in a 250 mL Boston round brown bottle sealed with a Mininert valve (24 mm, Supelco). These bottles were mixed with a single speed (385 rpm) wrist action shaker (Model 75, Burrell) at 10° shaking angle for 24 hours. The resulting water phase was

analysed for BTEX concentration using purge and trap gas chromatography (detailed information is given in section 4.2.3). A positive control was set up with GAC (8, 16, 325, 650 mg) under identical conditions. A bottle containing 10 ppm of each of the BTEX compounds (without the addition of either EG or GAC) was included as a negative control.

4.2.2 AOS Experiment

To determine whether the compounds were completely mineralized to carbon dioxide and water within the AOS, each BTEX compound (at approximately 10 mg/L) was fed through an EG--packed AOS column with either no electricity or 12 V of electricity applied (Figure 4-1).

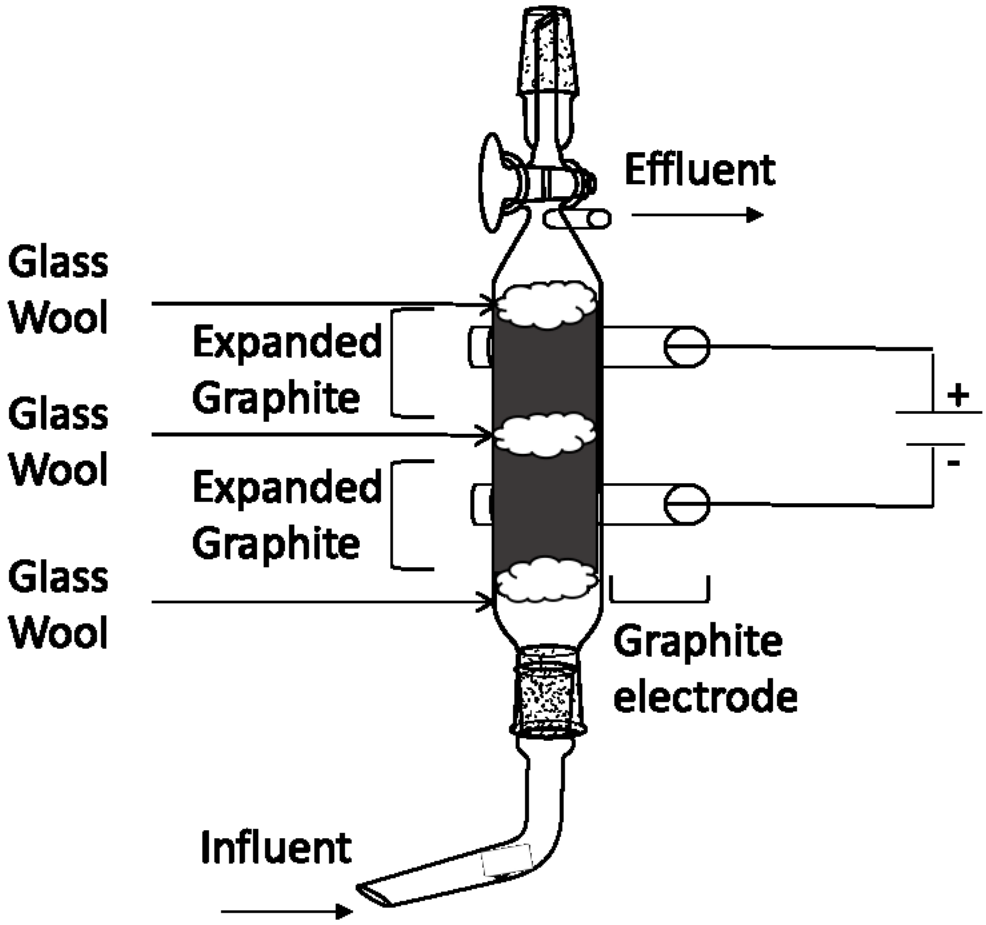

Figure 4-1 A Simplified Schematic of Advance Oxidation System. This schematic was generated with ChemDraw Prime 17.1.

The top spigot was sealed with 3M vinyl tape (471; COY-1600320, Mandel Scientific), and 200 µL of gas sample was withdrawn for CO_2 measurements. A flowrate of 4 mL/min was determined to be optimal in preliminary experiments conducted by BioLargo; an additional experiment at 10 mL/min flow rate was conducted to determine if breakthrough occurs. The packed AOS column was primed with 50 mg/L potassium iodide (KI) for 30 min prior to each experiment. In addition, 50 mg/L KI was dissolved in the 10 mg/L each of the BTEX stock solution before the start of all experiment. Influent and effluent liquid samples were taken at 15-minute intervals, and the BTEX concentration was measured with a fluorescence spectrophotometer (Cary Eclipse, Agilent; detailed information is given in section 4.2.3). Every 30 minutes, the gaseous (headspace) samples was collected and analysed by gas chromatography thermal conductivity detector (GC-TCD), and the effluent liquid samples was collected and analysed for total inorganic carbon (TIC). (detailed information is given in section 4.2.3).

4.2.3 Chemical Analyses

Aqueous samples from the batch experiment were prepared for BTEX analysis by adding 40 mL of Milli-Q ultra-pure water to a 2 mL of sample in a 40 mL clear EPA vial (02-912-376, Fisher Scientific) fitted with PTFE/Silicon septa cap (B7995-24, Thermo Scientific). The diluted samples were analysed with a Hewlett-Packard purge and trap concentrator (G1900-60500) coupled with a gas chromatography (HP6890).

Aqueous samples from the AOS experiment were analysed for BTEX concentrations using a Cary Eclipse fluoresce spectrophotometer (Agilent) and a 10 mm pathlength quartz cell (6610000900, Agilent; parameters listed on Table 4-1).

Table 4-1 Parameters of the fluorescence method used to measure BTEX aqueous samples in the AOS experiment.

Parameters	Settings
Scan type	Fluorescence Synchronous
Excitation Wavelength	200 nm
Emission Wavelength	217.96 nm
Excitation Filter	Auto
Emission Filter	Open
Excitation Slit Width	5 nm
Emission Slit Width	5 nm

TIC was measured using Shimadzu DOC analyser (TOC-LCPH). Samples were diluted 1:10 with Milli-Q water prior to analysis.

Carbon dioxide (CO_2) was collected from the AOS top spigot with a VICI precision sampling syringe, and was measured using a thermal conductivity detector (TCD) attached to a 7890A GC. Helium (Praxair) was used as the carrier gas. The column used was a Supelco 80/100 Hayesep Q column, 10' x 1/8" SS (detailed parameters are listed Table 4-2).

Table 4-2 TCD method used to measure CO_2 concentration from AOS experiment.

Component	Parameter	Values
Inlet	Temperature	200℃
	Total Flow	15 mL/min
	Septum purge flow	3 mL/min
Detector	Temperature	200℃
	Reference flow	30 mL/min
	Make-up flow	2 mL/min
Oven	Temperature	25℃
	Ramp 1	50℃/min to 110℃ (hold for 2 mins)
Signal	Frequency/min	5 Hz/0.04 min

4.2.4 Adsorption Isotherm Calculation

The Langmuir and Freundlich model isotherms were used to fit the batch adsorption experiment data. Linear regression was used to estimate the adsorption parameters (Table 4-3). Both Langmuir-I and -III were tested to better describe adsorption experimental data (Table 4-3).

Table 4-3 Linear forms of Langmuir and Freundlich adsorption isotherms

Isotherm	Linear form
Freundlich	$\ln(q_e)=\ln K_F+(1/n)*\ln(C_e)$
Langmuir-I	$C_e/q_e=(C_e/q_m)+(1/K_L*q_m)$
Langmuir-III	$q_e=q_m-(1/K_L)*(1/C_e)+(1/q_m)$

Adopted from Chen (2015). Where q_e=adsorption capacity, K_F=adsorption capacity related constant, n=adsorption strength related constant, C_e=substrate concentration at equilibrium, q_m=maximum adsorption capacity at equilibrium.

4.3 Results and Discussion

4.3.1 Batch Experiment

The physical characteristics of EG and GAC were previously described (Table 4-4). The EG is composed of 96% carbon and 4% oxygen, with a density of 4.8 g/L (Moustafa et al., 2014). The Brunauer-Emmett-Teller (BET) surface area of EG is 76.9±1.4 m^2/g, and contains only mesopores (Moustafa et al., 2014). Mesopores promote faster adsorption kinetics with liquid phase adsorbates (Moustafa et al., 2014; Small et al., 2012). The BET surface area of GAC is 1030 m^2/g, ~13 times greater than EG (Table 4-4), and both mesopores and micropores are present (Small et al. 2012). GAC with 12 – 40 mesh size was chosen for this experiment as it is the most commonly used mesh size for the "liquid phase adsorption" (Çeçen & Aktaş, 2012).

Table 4-4 Physical characteristics related to sorption of GAC and EG.

Sample	BET (m^2/g)	Size (μm)	Reference
GAC	1030	420 - 1680	Small et al. 2012
EG	76.9	16 - 46	Moustafa et al. 2014

The BTEX adsorptive capacity of EG was determined using a batch method with 24 hour mixing. As the density of EG is 4.8 g/L, 500 mg was used in this experiment because 650 mg of EG was shown to hinder mixing in a 250 mL bottle. This volume of EG removed 12% benzene, 17% toluene, 29% ethylbenzene and 37% *p*-xylene from the water system (Figure 4-2; Table 4-5). EG displayed lower adsorptive capacity than GAC, because of EG had ~13 times lower specific area than GAC (Figure 4-2; Table 4-5).

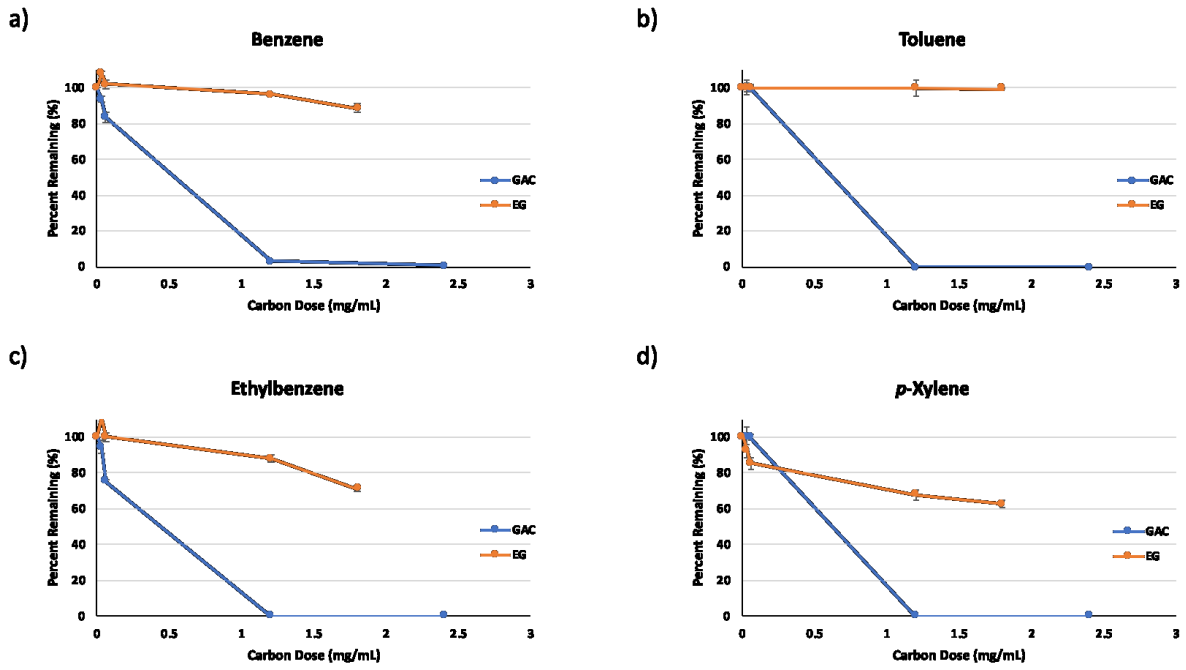

Figure 4-2 BTEX adsorption batch experiment results. The graphs shown are average of n=3, and error bar represent one standard error.

Table 4-5 Percent reduction for BTEX batch experiment

GAC (mg)	0	8	16	325	650
Benzene (%)	0	6.6	16.4	96.7	100
Toluene (%)	0	7	23.5	100	100
Ethylbenzene (%)	0	5.4	24.6	100	100
p-Xylene (%)	0	15.7	27.7	100	100
EG (mg)	0	8	16	325	500
Benzene (%)	0	0	0	3.6	11.5
Toluene (%)	0	1.4	6.8	15.2	16.5
Ethylbenzene (%)	0	0	0.4	12.4	29.1
p-Xylene (%)	0	7.6	14.6	32.2	37.4

The presence of mesopores may also play an important role in accelerating adsorbate diffusion into micropores in an aqueous phase (Hsieh & Teng, 2000). Since EG consists of only mesopores, the BTEX adsorption to EG is likely limited by available adsorption sites. The batch experiment results showed that GAC has similar adsorptive capacity for each of the BTEX compounds, and that GAC can completely remove BTEX compounds (96–100% removal) at the higher carbon doses (325-650 mg). EG, on the other hand, showed higher adsorptive capacity towards *p*-xylene and ethylbenzene as compared to benzene and toluene when using 500 mg of EG (Figure 4-2). This observation suggests that EG adsorption is influenced by functional groups on the aromatic hydrocarbons. For example, *p*-xylene contains two methyl (CH_3) functional groups and 37% was removed with 500 mg EG, compared to benzene (no functional group) where 12% was removed with 500 mg EG. Indeed, the interactions between hydrophobic organic and water molecules increase the heat capacity, and it is thermodynamically unfavourable for interaction (Gutmann, 1991). It is thought that a CH_3 group can contribute to a -2000 calories per mole per CH_3 group in free energy difference when a hydrocarbon molecule dissolve in a hydrocarbon liquid versus in water (Tanford, 1979). Interestingly, EG was also shown to display a higher affinity to more highly-branched naphthenic acids (trans-4-isopropyl cyclohexanoic acid > trans-4-propyl cyclohexanoic acid > cyclohexanoic acid; Moustafa et al., 2014). Hydrophobicity and hydrogen bonds of the weak acids also play a role in the EG adsorption capacity (Moustafa et al., 2014). The contribution of hydrogen bonds to EG adsorption of BTEX compounds is likely to be minimal, and hydrophobicity impacted by molecular structure and nonspecific attraction force (e.g. van der Waals forces) likely play a more important role in EG adsorption of BTEX compounds. Indeed, the EG batch experiments showed that the EG preferentially adsorbs BTEX compounds with log K_{ow} values in descending

order (Figure 4-3), which suggests adsorption via hydrophobicity. Furthermore, it is hypothesized that BTEX adsorption on activated carbons may not depend on surface groups including total acid, carboxylic, and basic groups (Daifullah & Girgis, 2003).

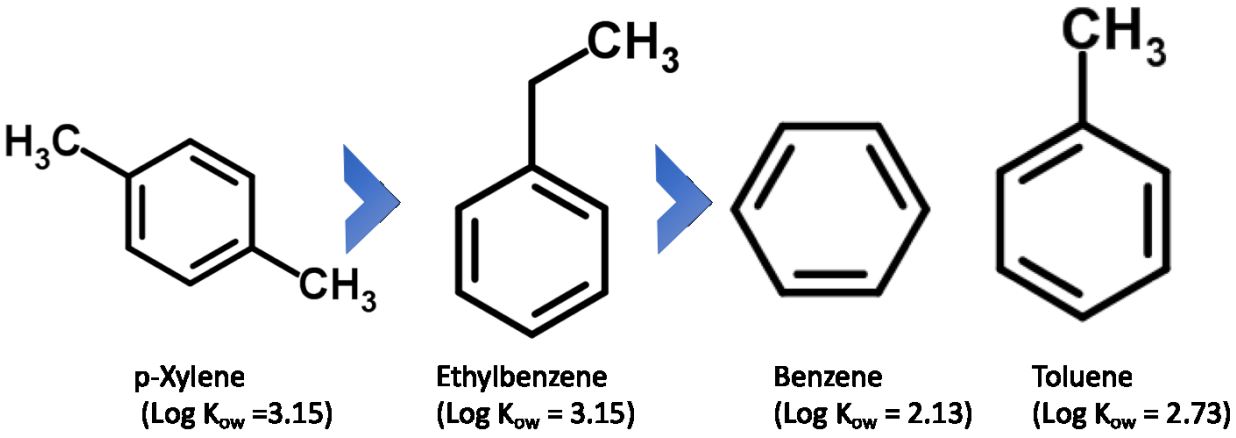

Figure 4-3 EG adsorption preferences. Each BTEX compound is shown in the order of EG adsorption preference from high to low (left to right); EG shows similar preference to both benzene and toluene. Note: chemical structures are modified from chemspider.com. The log Kow values were obtained from Agteren et al. (1998).

To gain further insight for the mechanism of BTEX adsorption to EG, Langmuir and Freundlich adsorption isotherm models were constructed using batch experiment data. Figure 4-4 shows that the Langmuir adsorption isotherm model provided overall best fit to the experimental data, and Table 4-6 summarizes the Langmuir and Freundlich isotherm parameters and correlation coefficients (R^2). As the batch experimental data was better described with the Langmuir isotherm model, several adsorption characteristics can be derived from the assumptions of the Langmuir isotherm model. The BTEX adsorption on EG likely occurs 1) through a monolayer adsorption, 2) at a finite number of identical sites throughout the EG surface, and 3) at uniform adsorption energies (Arasteh et al., 2010; Chen, 2015; Septhum et al., 2007).

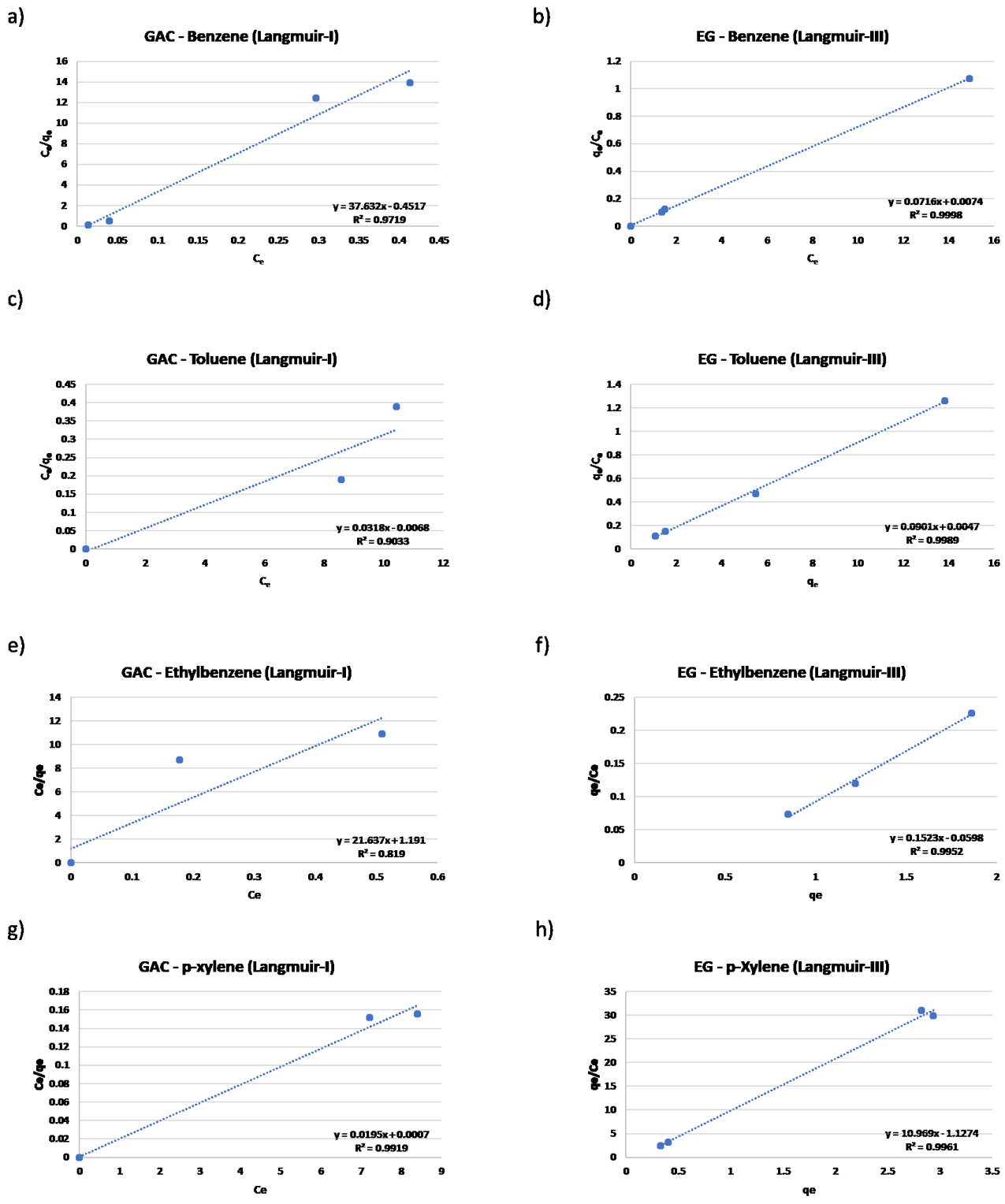

Figure 4-4 Linear fit adsorption isotherm models for GAC and EG. Note: when calculating adsorption capacity (qe) for EG with benzene, the benzene concentration from the 8 mg/L GAC was used as initial concentration (Co) due to a low benzene concentration measured in the control.

Table 4-6 Langmuir and Freundlich isotherm parameters for GAC and EG.

Langmuir Isotherm	GAC			EG		
	q_m	K_L	R^2	q_m	K_L	R^2
Benzene	0.03	-0.07	0.9719	-0.07	-0.1	0.9998
Toluene	31.44	4623	0.9033	-0.09	-0.05	0.9989
Ethylbenzene	0.05	0.04	0.819	-0.15	0.5	0.9952
p-Xylene	51.3	73260	0.9919	-11	0.1	0.9961
Freundlich Isotherm	GAC			EG		
	n	K_F	R^2	n	K_F	R^2
Benzene	2.8	1	0.9853	24.5	0.9	0.615
Toluene	0.6	-0.7	1*	18.4	0.8	0.6573
Ethylbenzene	0.4	-1.4	1*	-0.4	1.7	0.9906
p-Xylene	1	1.7	1*	7.6	0.7	0.9645

Note: * = Due to limited data points are compatible with Freundlich isotherm, only 2 data points were used in the Freundlich isotherm model. Where K_L&K_F=adsorption capacity related constant, n=adsorption strength related constant, q_m=maximum adsorption capacity at equilibrium.

4.3.2 AOS Experiment

Mineralization of BTEX compounds was tested in the AOS in a flow through setting. At 10 mL/min flowrate, no significant removal of any of the four compounds was observed regardless of electricity application (Figure 4-5). At 4 mL/min flowrate and with the application of electricity, significant removal of ethylbenzene and *p*-xylene was observed (37.6% and 98.9% respectively after 120 min; Figure 4-6, Table 4-7 and Figure A-3).

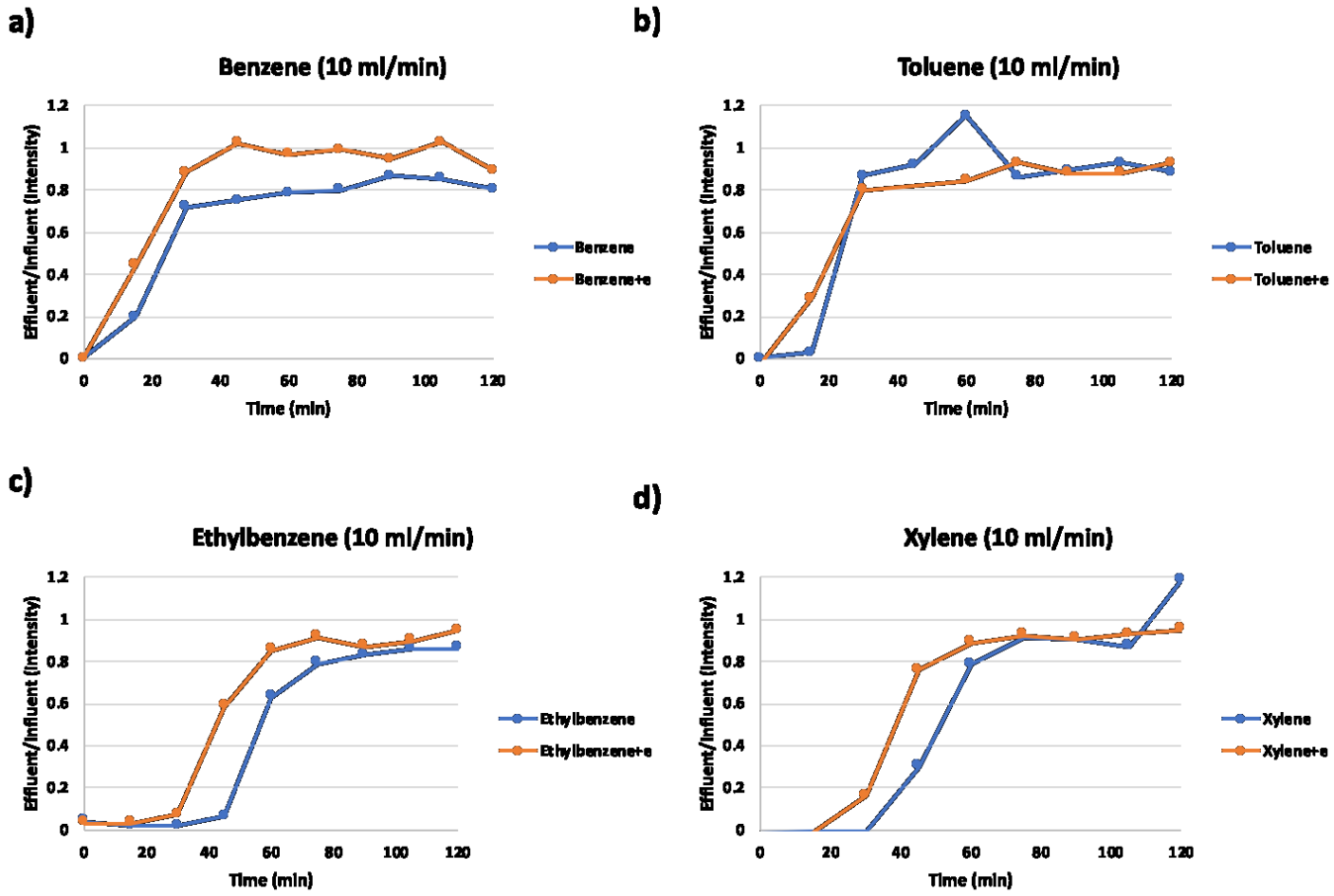

Figure 4-5 Breakthrough curves of AOS experiment at 10 mL/min flowrate with or without electricity applied. Data obtained from 1 experimental trial.

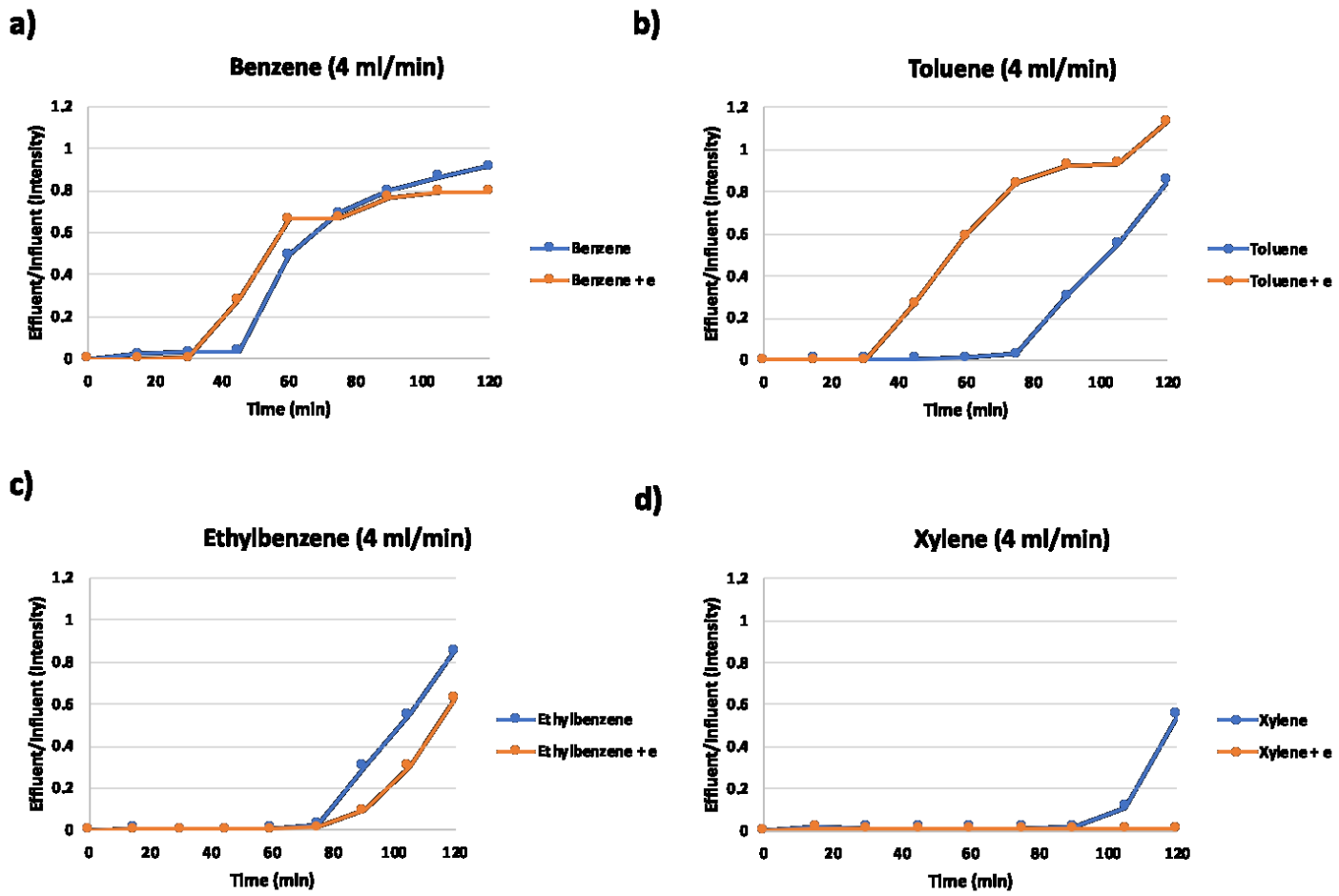

Figure 4-6 Breakthrough curves of AOS experiment at 4 mL/min flowrate with or without electricity applied. Data obtained from 1 experimental trial.

Table 4-7 Percent removal of BTEX compounds at 120 min in the AOS system.

4 mL/min Flow Rate	Percent Removal (%)
Benzene+KI	8.5
Benzene+KI +electricity	20.4
Toluene+KI	28.8
Toluene+KI +electricity	6.7*
Ethylbenzene+KI	14.6
Ethylbenzene+KI +electricity	37.6
p-Xylene+KI	45.0
p-Xylene+KI +electricity	98.9

Note: *= For toluene, the 105-minute time point was used for the percent removal calculation.

Qin et al. (2015) showed that electricity application increased the adsorption of phenanthrene, however these authors did not use KI in their experiment (Qin et al., 2015). Oxidation of cyclohexanol to cyclohexanone was demonstrated through electrochemistry method in the presence of KI (Ogumi et al., 1985), therefore simpler compounds such as BTEX could be completely oxidized, which was verified by measuring carbon dioxide (CO_2) during this AOS experiment at 4 mL/min flowrate. The CO_2 gas was collected from the AOS top spigot (Figure 4-1) and measured using gas chromatography (GC-TCD). The effluent was collected and the dissolved CO_2 was measured with TIC analysis. Gaseous CO_2 concentrations in the AOS headspace was the same as in laboratory air (0.06%). Dissolved CO_2 concentrations were stable throughout the experiment (0.16–0.36 mg/L at 4 mL/min depending on the compound; Table

A3). Taken together, these results show non-significant amount of CO_2 is measured in the effluent samples, suggesting either 1) complete oxidation may not have occurred, or 2) the CO_2 produced was adsorbed in the AOS system.

To test if the CO_2 was adsorbed into the AOS system, the EG adsorptive capacity for CO_2 was measured. A preliminary experiment was performed using ultra-pure water saturated with carbon dioxide gas (20% CO_2, 80% N_2) in the AOS column with 4 mL/min flowrate, with or without applying electricity. The mass of CO_2 measured in the influent, effluent, and headspace were calculated based on the measured CO_2 concentration of the liquid and gaseous samples. The amount of CO_2 adsorbed onto the EG was determined for the duration of the experiment (120 minutes). In the absence of electricity, 1.2 mg of CO_2 was adsorbed onto the EG in 120 min, which corresponds to 3.4% removal (Table 4-8). With the addition of electricity, 15.1 mg of CO_2 was adsorbed onto the EG in 120 min, which corresponds to 61% removal (Table 4-8).

Table 4-8 Summary of CO_2 adsorption via AOS experiment

	Total Mass Influent (mg)	Total Mass Effluent (mg)	Total Mass Headspace (mg)	Mass Adsorbed (mg)	Percent Removal (%)
CO_2+KI	34.9	20.5	13.2	1.2	3.4
CO_2+KI+electricity	25.6	9.9	0.003	15.7	59.0

Theoretically, 15.9 mg of CO_2 would be produced during complete oxidation of 10 mg/L *p*-xylene, therefore, it is possible that the CO_2 produced from *p*-xylene oxidation (if occurred) could be adsorbed to the EG within the AOS system. These results also suggest that electricity application increases the amount of carbon dioxide sorption, assuming that the total aqueous inorganic carbon reflects only the dissolved CO_2. However, an exact mechanism contributes to

the *p*-xylene removal in the AOS system was not determined in this study. As such, oxidation and/or adsorption of *p*-xylene within the AOS system cannot be ruled out.

The use of EG has some potential in medical and environmental applications (Inagaki et al., 2002; Inagaki et al., 2001; Kang et al., 2003; Moustafa et al., 2014; Qin et al., 2015; Shen et al., 1999; Toyoda & Inagaki, 2000), and the AOS system has the potential to disinfect water (personal communication with BioLargo Water). However, based on experimental results from this chapter, EG or EG-based systems might have limited application for BTEX removal. In fact, the results are consistent with previous findings that activated carbon did not effectively remove benzene and toluene from oil field water (Allen, 2008; Gallup et al., 1996). Adsorbent fouling, a condition where the adsorbent surface is coated with residual crude oil and grease, was attributed to the low removal of BTEX (Allen, 2008; Gallup et al., 1996), and more research is needed to achieve similar or higher removal than GAC using the AOS reactor.

4.4 Conclusion

Activated carbon has been widely used to remove organic contaminants through adsorption. However, it is not cost effective to use GAC to treat a large volume of water in the oil & gas industry such as OSPW. BioLargo Water Inc. Canada is developing an AOS which combines adsorption using EG and iodine electro-oxidation chemistry. This technology may be used to remove organics from OSPW, which is commonly found in oil sands tailings ponds and pit lakes (including Base Mine Lake). The adsorptive and removal capacity of BTEX compounds using activated carbon were tested in a series of laboratory experiments.

EG shows the highest adsorptive capacity to *p*-xylene among all four BTEX compounds in both batch and AOS experiments. EG has a moderate adsorptive preference to xylene and ethylbenzene and has low preference to benzene and toluene. However, based on the both headspace and aqueous phase analyses, carbon dioxide may not be the end product of the AOS treatment. These results suggest that hydrophobicity is likely one of the adsorption mechanisms for *p*-xylene and ethylbenzene as both of these compounds have a higher log K_{ow} value than that of benzene and toluene.

Further research is required to optimize the AOS configuration, flowrate and voltage for the removal of benzene, toluene, ethylbenzene, and *p*-xylene. More time points should be included to 1) establish adsorption kinetics and mechanism in the batch experiment and 2) determine if breakthrough could occur for *p*-xylene with the use of AOS and electricity. Finally, the degradation product(s), if any, should be identified. Further research could also be directed to the EG exfoliation process (including intercalation), and to reactor configuration for enhancing the BTEX adsorption capacity.

4.5 References

Agteren, M. H., Keuning, S., & Janssen, D. B. (1998). *Handbook on Biodegradation and Biological Treatment of Hazardous Organic Compounds*. Dordrecht: Springer Netherlands.

Akuzawa, N., Hane, Y., Toyama, E., & Abe, T. (2004). Electrical conductivity change of AM-GICs by ternarization with ammonia. *J Phys Chem Solids, 65*(2-3), 191-194.

Allen, E. W. (2008). Process water treatment in Canada's oil sands industry: I. Target pollutants and treatment objectives. *J Environ Eng and Sci, 7*(2), 123-138.

Arasteh, R., Masoumi, M., Rashidi, A. M., Moradi, L., Samimi, V., & Mostafavi, S. T. (2010). Adsorption of 2-nitrophenol by multi-wall carbon nanotubes from aqueous solutions. *Appl Surf Sci, 256*(14), 4447-4455.

Bandosz, T. J. (2006). *Activated carbon surfaces in environmental remediation Interface science and technology v. 7* (pp. 1 online resource.). Retrieved from http://www.sciencedirect.com/science/bookseries/15734285/7

Bansal, R. C., & Goyal, M. (2005). *Activated carbon adsorption* (pp. 1 online resource.). Retrieved from https://www.taylorfrancis.com/books/9781420028812

Çeçen, F., & Aktaş, Ö. (2012). *Activated carbon for water and wastewater treatment integration of adsorption and biological treatment* (pp. 1 online resource (xxviii, 388 p.)).

Chen, X. J. (2015). Modeling of Experimental Adsorption Isotherm Data. *Information, 6*(1), 14-22.

Daifullah, A. A. M., & Girgis, B. S. (2003). Impact of surface characteristics of activated carbon on adsorption of BTEX. *Colloid Surface A, 214*(1-3), 181-193.

Dresselhaus, M. S., & Dresselhaus, G. (2002). Intercalation compounds of graphite. *Adv Phys, 51*(1), 1-186.

Gallup, D. L., Isacoff, E. G., & Smith, D. N. (1996). Use of Ambersorb(R) carbonaceous adsorbent for removal of BTEX compounds from oil-field produced water. *Environ Prog, 15*(3), 197-203.

Gee, K. F., Poon, H. Y., Hashisho, Z., & Ulrich, A. C. (2017). Effect of naphtha diluent on greenhouse gases and reduced sulfur compounds emissions from oil sands tailings. *Sci Total Environ, 598*, 916-924.

Gutmann, V. (1991). Fundamental Considerations About Liquid Water. *Pure Appl Chem, 63*(12), 1715-1724.

Hsieh, C. T., & Teng, H. S. (2000). Influence of mesopore volume and adsorbate size on adsorption capacities of activated carbons in aqueous solutions. *Carbon, 38*(6), 863-869.

Inagaki, M., Toyoda, M., Iwashita, N., Nishi, Y., Konno, H., Fujita, A., & Kihara, T. J. T. (2002). Sorption, recovery and recycle of spilled heavy oils using carbon materials. Spill Sci Technol Bull. *2002*(201), 16-25.

Inagaki, M., Toyoda, M., Iwashita, N., Nishi, Y., & Konno, H. J. C. l. (2001). Exfoliated graphite for spilled heavy oil recovery. Carbon Letters *2*(1), 1-8.

Kang, F. Y., Zheng, Y. P., Zhao, H., Wang, H. N., Wang, L. N., Shen, W. C., & Inagaki, M. (2003). Sorption of heavy oils and biomedical liquids into exfoliated graphite - Research in China. *New Carbon Mater, 18*(3), 161-173.

Moustafa, A. M., McPhedran, K. N., Moreira, J., & Gamal El-Din, M. (2014). Investigation of mono/competitive adsorption of environmentally relevant ionized weak acids on

graphite: impact of molecular properties and thermodynamics. *Environ Sci Technol, 48*(24), 14472-14480.
Mullineaux, R. D., & Raley, J. H. (1963). High Temperature Reactions of Iodine with Hydrocarbons .2. Aromatization. *J Am Chem Soc, 85*(20), 3178-&.
Ogumi, Z., Ohashi, S., & Takehara, Z. (1985). Application of the Spe Method to Organic Electrochemistry .6. Oxidation of Cyclohexanol to Cyclohexanone on Pt-Spe in the Presence of Iodine and Iodide. *Electrochimica Acta, 30*(1), 121-124.
Qin, J. Y., Moustafa, A., Harms, H., El-Din, M. G., & Wick, L. Y. (2015). The power of power: Electrokinetic control of PAH interactions with exfoliated graphite. *J Hazard Mater, 288*, 25-33.
Raley, J. H., Bittner, C. W., & Mullineaux, R. D. (1963). High Temperature Reactions of Iodine with Hydrocarbons .1. Dehydrogenation. *J Am Chem Soc, 85*(20), 3174.
Sawyer, C. N., McCarty, P. L., & Parkin, G. F. (2003). *Chemistry for environmental engineering and science* (5th ed.). Boston: McGraw-Hill.
Septhum, C., Rattanaphani, S., Bremner, J. B., & Rattanaphani, V. (2007). An adsorption study of A1(III) ions onto chitosan. *J Hazard Mater, 148*(1-2), 185-191.
Shen, W. C., Wen, S. Z., Cao, N. Z., Zheng, L., Zhou, W., Liu, Y. J., & Gu, J. L. (1999). Expanded graphite - A new kind of biomedical material. *Carbon, 37*(2), 356-358.
Siddique, T., Fedorak, P. M., & Foght, J. M. (2006). Biodegradation of short-chain n-alkanes in oil sands tailings under methanogenic conditions. *Environ Sci Technol, 40*(17), 5459-5464.
Siddique, T., Fedorak, P. M., MacKinnon, M. D., & Foght, J. M. (2007). Metabolism of BTEX and naphtha compounds to methane in oil sands tailings. *Environ Sci Technol, 41*(7), 2350-2356.
Siriwardane, R. V., Shen, M.-S., Fisher, E. P., & Poston, J. A. (2001). Adsorption of CO_2 on Molecular Sieves and Activated Carbon. *Energy & Fuels, 15*(2), 279-284.
Slaugh, L. H., Raley, J. H., & Mullineaux, R. D. (1963). High Temperature Reactions of Iodine with Hydrocarbons .3. Rearrangement of Aliphatic Free Radicals. *J Am Chem Soc, 85*(20), 3180-&.
Small, C. C., Cho, S., Hashisho, Z., & Ulrich, A. C. (2015). Emissions from oil sands tailings ponds: Review of tailings pond parameters and emission estimates. *J Petrol Sci Eng, 127*, 490-501.
Small, C. C., Ulrich, A. C., & Hashisho, Z. (2012). Adsorption of Acid Extractable Oil Sands Tailings Organics onto Raw and Activated Oil Sands Coke. *J Environ Eng, 138*(8), 833-840.
Tanford, C. (1979). Interfacial Free-Energy and the Hydrophobic Effect. *Proceedings of the National Academy of Sciences of the United States of America, 76*(9), 4175-4176.
Toyoda, M., & Inagaki, M. (2000). Heavy oil sorption using exfoliated graphite - New application of exfoliated graphite to protect heavy oil pollution. *Carbon, 38*(2), 199-210.

Chapter 5 a: Turbidity Reduction Mechanisms

5.1 Introduction

In 2016, operations at the Athabasca oil sands produced 2.5 million barrels per day of crude bitumen, and further growth in production is forecasted (Canadian Association of Petroleum Producers, 2018; Government of Alberta, 2016). The rapid expansion of oil sands exploration has resulted in increased effort being expended on storing and remediating the slurry by-products of the surface mining, such as fluid fine tailings (FFT) and oil sands process-affected water (OSPW; Humphries & Library of Congress. Congressional Research Service, 2008).

The Alberta Energy Regulator issued Directive 085 as a guideline for managing tailings inventory (Alberta Energy Regulator, 2016). Under Directive 085, new FFT must be ready to reclaim (RTR) by ten years after the end of the mine's life, and all legacy FFT must be RTR by the end of the mine's life (Alberta Energy Regulator, 2016). Water capping technology (i.e., a pit lake, PL) research is currently underway to reduce FFT and OSPW inventories and to support the aquatic ecosystem (Cumulative Environmental Management Association, 2012). In 2012, Base Mine Lake (BML) was commissioned as a full-scale demonstration PL and was filled with 186 million m^3 of FFT (depth 45 m) and capped with ~ 37 million m^3 of OSPW. In 2013, the BML received additional 3.2 million m^3 of OSPW and 11 million m^3 of fresh water from Beaver Creek Reservoir (BCR), which resulted in a 90% OSPW and 10% fresh water mixture. However, high turbidity (≈71–231 NTU) has been observed in the BML surface water.

Oil sands tailings contain a mixture of sand, clay, silt, residual organics, salts, trace metals and water (Government of Alberta, 2015). Resuspension of clay particles from FFT is a likely contributor to the turbidity observed in BML surface water (Dompierre et al., 2016; Lawrence et al., 2016). The high turbidity (≈71–231 NTU) in the BML surface water hinders the development of aquatic and adjacent terrestrial ecosystems, such as macrophyte, phytoplankton, and vertebrate

systems (Cumulative Environmental Management Association, 2012; Tundisi & Tundisi, 2012; Westcott & Watson, 2005).

Typical FFT samples contain 30%–40% w/w solids, and the size distribution of the solids is >44 μm (10%), 1–44 μm (57%) and <1 μm (33%; Dompierre et al., 2016; Voordouw, 2013). Approximately 34% and 26% of the clay in oil sands tailings are kaolinite and illite, respectively, with size ranges of 0.2–2 μm (Kaminsky et al., 2009). Several mechanisms contributing to FFT resuspension have been proposed, including ebullition of biogenic gases, seasonal turnover, and wind-driven mixing (Lawrence et al., 2016). Due to its small particle size and negative surface charge, FFT clay particles are highly stable and will remain in aqueous suspension for a long period. Indeed, it has been estimated that approximately 125–150 years are required for FFT to be completely consolidated (Eckert et al., 1996). In general, solution pH and ionic strength can affect the stability of suspended clay particles (Siddique et al., 2014a; Zbik et al., 2008). Clay particle surfaces, in general, are highly negatively charged, and thus, these particles repel each other, which contributes to the stability of a clay suspension (Chorom & Rengasamy, 1995; Missana & Adell, 2000).

Under an acidic pH, the clay surface charge is reduced due to the interaction between hydrogen atoms and the clay particle surface (Appelo & Postma, 2005; Chorom & Rengasamy, 1995; Missana & Adell, 2000). The stability behaviour of clay particles is also influenced by the diffuse double layer (DDL), which is a diffuse layer of counter- and co-ions surrounding a clay particle (Hunter, 2001; Liu et al., 2013). The ionic strength of a solution is one of the key parameters affecting DDL thickness, and ionic strength is especially affected by the presence of di- and tri-valent ions (Hunter, 2001; Siddique et al., 2014a). The DDL of a clay particle collapses in a solution with high di-/tri-valent cation concentrations, resulting in a favourable

condition for coagulation/flocculation processes (Hunter, 2001; Siddique et al., 2014a). Several studies have reported that dissolved carbon dioxide (CO_2) can aid in the consolidation/dewatering of oil sands tailings (Ibanez et al., 2014; Siddique et al., 2014a; Zhu et al., 2011). In addition, CO_2-mediated carbonate mineral dissolution is hypothesized to be a mechanism involved in DDL thickness reduction, thereby promoting oil sands tailings consolidation and dewatering (Dompierre et al., 2016; Siddique et al., 2014a). However, there are few reports on FFT settling processes within within a BML context, and direct evidence for the CO_2-mediated carbonate mineral dissolution hypothesis is limited. To examine three different aspects associated with a pH change triggered by CO_2 addition as it relates to water turbidity reduction in BML, this chapter is divided into three sub-chapters. Chapter 5a will examine the effect of CO_2 addition on FFT settling and the effect of CO_2-mediated calcite dissolution on FFT settling. Chapter 5b will examine the effect of different sulphate concentrations on CO_2-mediated calcite dissolution. Chapter 5c will examine the effect of dolomite/calcite dissolution on BML water turbidity reduction.

5.2 Materials and Methods

This section contains information regarding the materials and methods for sub-chapters 5a–5c. Some of the research presented in this chapter is from a collaboration with M.Sc. student Jordan Brandon in Dr. Ulrich's laboratory (M.Sc. Environmental Engineering at the University of Alberta). The work conducted by Jordan Brandon and my analysis of his results were published in a co-authored article (Poon et al., 2018). In addition, data pertaining to the chemical and physical parameters for the 60/40+CO_2, 60/40-noCO_2 and 20/80+CO_2 columns are presented in this chapter (Figure 5-2) with the permission of Mr. Brandon. These data are needed to describe water chemistry changes and explain the subsequent experimental design.

The OSPW from BML (BML-OSPW) and fresh water from the BCR were collected and provided by Syncrude Canada Ltd. in 2014 and 2015, respectively. The BML-OSPW was collected from the surface water layer of BML at the southwest (SW) BML platform in September 2014. The BML-OSPW represents an 80% OSPW and 20% BCR (80/20) fresh water mix. All samples were stored at 4°C until use.

The following carbonate materials were obtained for use in the experiments: Iceland spar crystal (470014-650, Ward's Scientific Inc.), dolomite crystal (a kind gift from Marilyn Huff, Geology undergraduate laboratory coordinator, University of Alberta) and bulk dolomite (dolomite-2; a kind gift from Dr. Matthew Lindsay, University of Saskatchewan).

5.2.1 Big Column Experiments

Two Townsend acrylic columns were used in the big column experiments (Figure 5-1); a detailed description of the columns was included in J. Brandon's thesis (Brandon, 2016). One of the columns was treated with CO_2 (at 4 L/min) in a Seair microbubbling diffusion system (Seair Inc., Canada) for 1215 min, and 4862 L of CO_2 was used. The BML-OSPW in the control column was mixed using the Seair system without any gas addition for 1253 min. During the CO_2 application and control column mixing, the inlet pressure of the Seair system was 12 psi, while the pressures for the three vessels within the Seair system were 10 psi.

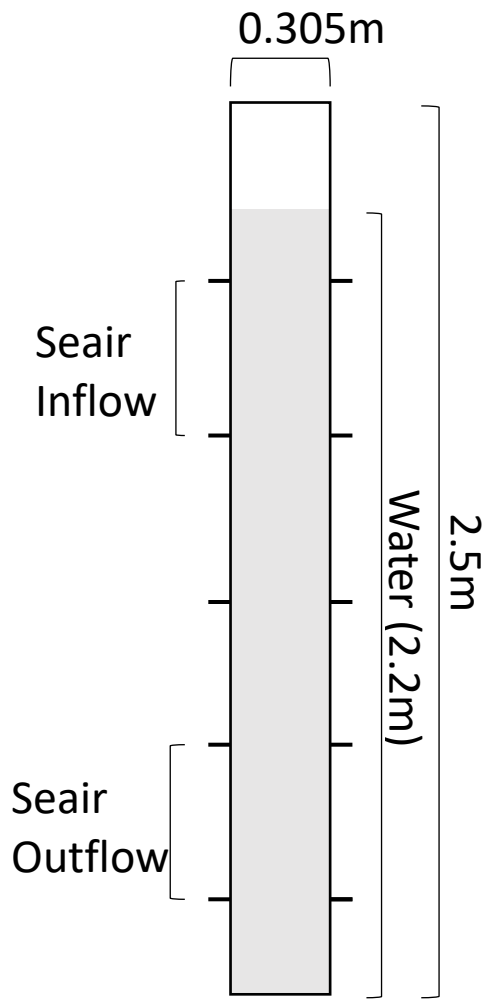

Figure 5-1 A schematic of a Townsend column and its relevant dimensions. All measurements are denoted in meters, and the column's five ports are indicated by the lines on either side of the outside of the column.

5.2.2 Secchi Depth and Light Intensity

Prior to Secchi depth and light intensity measurement, the outside of the column was covered with an opaque curtain to minimize interference from lateral light sources, and a globe-shaped halogen work light (250 Watts, Globe electric, model # 60568) was placed (28.5 cm) above the column.

A 20 cm diameter Secchi disk (78-010 Fieldmaster, Science First) with black and white patterning was lowered into the column. Briefly, the estimated Secchi depth is the average of the

depths at which the disk's white pattern first disappears and that when the disk's white pattern first reappears (Davies-Colley & Smith, 2001; Tundisi & Tundisi, 2012).

Upwelling photosynthetically active radiation (PAR; 400–700 nm) within the column was measured by using an LI-192SA underwater quantum sensor and LI-1400 data logger (LI-COR Inc.).

5.2.3 Small Column Experiments

Carbonate (calcite and dolomite) dissolution experiments were conducted in a 1 L glass graduated cylinder column (Pyrex C30221L, Fisher Scientific) covered with parafilm (PM-996) to minimize evaporation. CO_2 was added using a 20 µm pore-size stainless steel pump head (GA-36410649, Mandel) at a rate of ~0.5 L/min.

Synthetic BML water was created according to the method described in the 2016 Base Mine Lake Monitoring Program Surface Water Quality Report (provided by Syncrude Canada Ltd.), and the recipe for creation of synthetic BML is provided in the appendix (Table A3).

5.2.4 Turbidity

Aqueous samples were obtained from each of the five ports of the big (2.5 m) columns and were subjected to turbidity measurement with an Orbecco-Hellige Digital Direct-Reading Turbidimeter (model 965). Turbidimeter calibration was performed prior to each measurement.

Aqueous samples withdrawn from the small (1 L) columns were also subjected to turbidity measurement with a portable turbidimeter (2100Q01, Hach). Turbidimeter calibration was performed prior to each measurement.

5.2.5 Water Characterization

Throughout the experiments, chemical parameters were monitored in water samples collected from big and small columns. Parameters measured include pH, alkalinity, cations and anions and total organic carbon. The pH was measured by using an Accumet AR50 Dual Channel pH/Ion/Conductivity meter. Conductivity was measured by using an ExStikII (EC500, EXTECH). Alkalinity was measured using a Mettler Toledo titrator (DL 53, Mettler Toledo) with H_2SO_4 (0.02 N) as the titrant.

Water samples were filtered through a 0.2 μm nylon syringe filter (F2500-2) prior to ion analyses. Cation (Ca^{2+}, Cu^{2+}, Fe^{2+}, K^{+}, Mg^{2+}, Mn^{2+}, Zn^{2+}, Na^{+}) were assessed by inductively coupled plasma-optical emission spectroscopy (ICP-OES) performed by the natural resources analytical laboratory (NRAL) at the University of Alberta. Anions (Cl^{-} and SO_4^{2-}) were analyzed by performing Dionex ion chromatography (ICS-2100).

In order to gain further insight, the calcite dissolution rate was calculated from the ICP-OES data (Ca^{2+} concentration). The following sample calculation for 60/40-CO_2+0.5g calcite is provided to assist reader to understand the calcite and dolomite dissolution rate results:

To calculate calcite dissolution rate for the 60/40-CO_2+0.5g calcite column between day 49 and 56:

$$\Delta 56 - 49 = (0.0017 - 0.0014\, mol/L)/7\ day = 4.7 \times 10^{-5}\, mol/L/d$$

The water samples were subjected to zeta potential measurement using a Zetasizer Nano ZSP (Malvern Instruments Ltd.) conducted in Dr. Hongbo Zeng's laboratory in the University of Alberta Department of Chemical and Materials Engineering. For zeta potential testing,

approximately 1 mL of aqueous sample was transferred to a capillary cell (DTS1070, Malvern Instruments Ltd.).

5.2.6 Carbonate Minerals in the FFT Solid Phase

Determination of the level of carbonate minerals in the FFT solid phase was performed using a modification of the method presented by Siddique et al. (2015). Briefly, liquid samples containing FFT and suspended solids are filtered through a 0.22 µm PVDF membrane filter, and the resulting filter dried overnight in an oven. Once the filter membrane has dried and cooled, it is placed in a 10 mL serum vial (15 mL total capacity), sealed with a butyl septum and crimp seal and the sealed vial then purged with nitrogen for 5 min. The dried membrane filter containing the FFT and suspended solids is then incubated with 10 mL of 1 N nitric acid overnight at room temperature with shaking at 150 rpm. The level of CO_2 generated in the headspace was measured by performing gas chromatography with a thermal conductivity detector (GC/TCD; Agilent 7890A GC System). To determine the calcium and magnesium ion levels, the supernatant was analyzed using an ICP-OES at the NRAL of the University of Alberta.

5.2.7 X-Ray Diffraction Analysis

X-Ray Diffraction (XRD) analyses of the powdered FFT, sediments from BML-OSPW, crushed Iceland spar, crushed dolomite crystal and crushed bulk dolomite samples were performed by using a Geigerflex powder X-ray diffractometer equipped with a D/Tex detector (performed at the laboratory of the Department of Earth & Atmospheric Sciences, University of Alberta). XRD data were analyzed by using JADE 9.1 (Materials Data, Inc.) software, with peak locations being referenced against the International Centre for Diffraction Data (ICDD 2016) and the Inorganic Crystal Structure Database (ICSD 2016).

5.2.8 Scanning Electron Microscopy and Energy-dispersive X-ray Spectroscopy Analysis

The overall sizes and elemental analyses of the crushed carbonate powders (calcite, dolomite crystals and bulk dolomite samples) were determined by using a scanning electron microscope (Zeiss Sigma 300 VP-FESEM located at the Department of Earth & Atmospheric Sciences, University of Alberta). The crushed samples were coated with carbon conductive coating prior to analysis.

5.2.9 Geochemical Modelling

The water chemistry profile within a column (big or small) was estimated with the graphical user interface PHREEQCi (version 3.3.11.12535; Parkhurst and Appelo 2013). The mineral saturation indices (SIs) were calculated by using the provisions within the WATEQ4F (Ball et al. 1991) thermodynamic database. Piper diagrams were constructed using AqQA software (Version 1.5.0, RockWare Inc.). The water chemistry profile and SI for the carbonate minerals dissolution experiment were calculated using PHREEQCi (version 3.4.0.12927) and the WATEQ4F database (Ball et al., 1991; Parkhurst & Appelo, 2013).

5.2.10 DLVO theory

The total interparticle interaction energy was estimated from the electrostatic repulsion force and Van der Waals attraction force calculations. A list of relevant parameters used in this calculation is included in the appendix (Table A4). In addition, a sample calculation is provided in the appendix (page A13) to assist reader to understand the DLVO results.

5.3 Results and Discussions

Several studies have shown that dissolved CO_2 improves the coagulation/flocculation of clay and thereby improves the densification of FFT and water clarity. To date, it has been shown that a reduction of the DDL is needed for MFT coagulation/flocculation and densification (Brandon, 2016; Ibanez et al., 2014; Siddique et al., 2014a; Siddique et al., 2014b; Zhu et al., 2011). However, the mechanistic pathway by which the dissolved CO_2 contributes to the destabilization of suspended FFT is not fully described. However, a water column based study conducted by Brandon (2016) showed that water clarity improved after the addition of CO_2. The author noticed a significant lag time prior to water clarity improvement and observed that the water column that contained higher ionic strength water (i.e., 60%-OSPW and 40% BCR water) showed greater improvement following CO_2 addition than that observed in the water column containing lower ionic strength water (i.e., 20%-OSPW and 80% BCR water) (Figure 5-2; Poon et al., 2018).

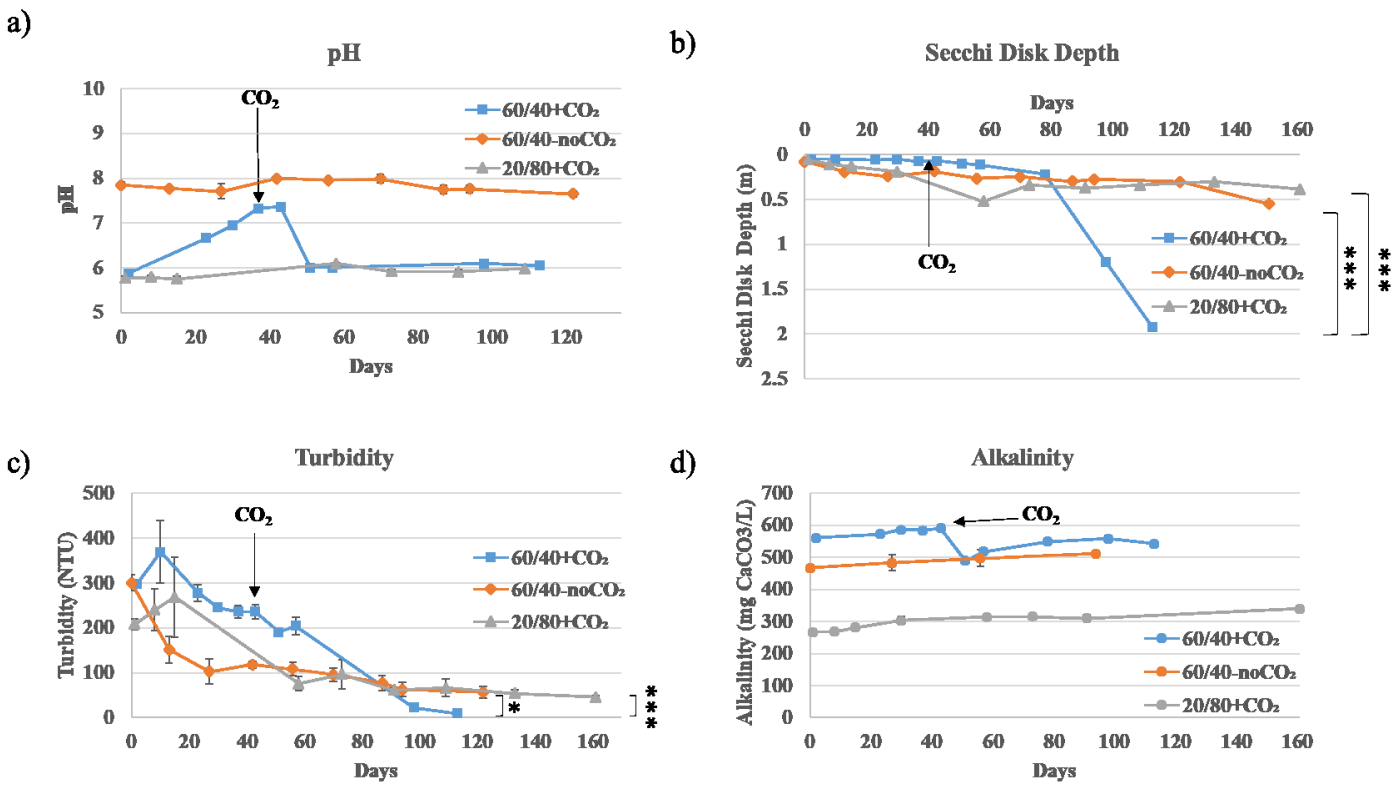

Figure 5-2 Chemical and physical parameters for the 60/40+CO_2, 60/40-noCO_2, and 20/80+CO_2 columns over the 113 day experimental period. a) pH, b) Secchi disk depth, c) turbidity and d) alkalinity * = $p < 0.05$ and *** = $p < 0.001$. Modified from Poon et al. (2018).

The results obtained from Brandon's 2016 study indicated that 1) CO_2 addition triggers a slow chemical process that can aid in turbidity reduction, and 2) a higher ionic strength solution is required for increased turbidity reduction.

5.3.1 Analysis of Previous Preliminary Results

To gain further insight, the Brandon (2016) water chemistry data for the 60/40+CO_2, 60/40+noCO_2 and 20/80+CO_2 columns were analyzed by examining piper diagrams and using PHREEQCi simulation. The piper diagrams showed a temporal shift from the "no dominant type" to the "bicarbonate type" in the anion zone of the 60/40+CO_2 and 20/80+CO_2 columns (Figure 5-3a & c). Moreover, the overall water type for the 60/40+CO_2 and 20/80+CO_2 columns changed over time from the "sodium chloride type" to a "mixed type" (Figure 5-3a & c). By contrast, the 60/40+noCO_2 column retained its "sodium chloride type" status over time (Figure 5-3b).

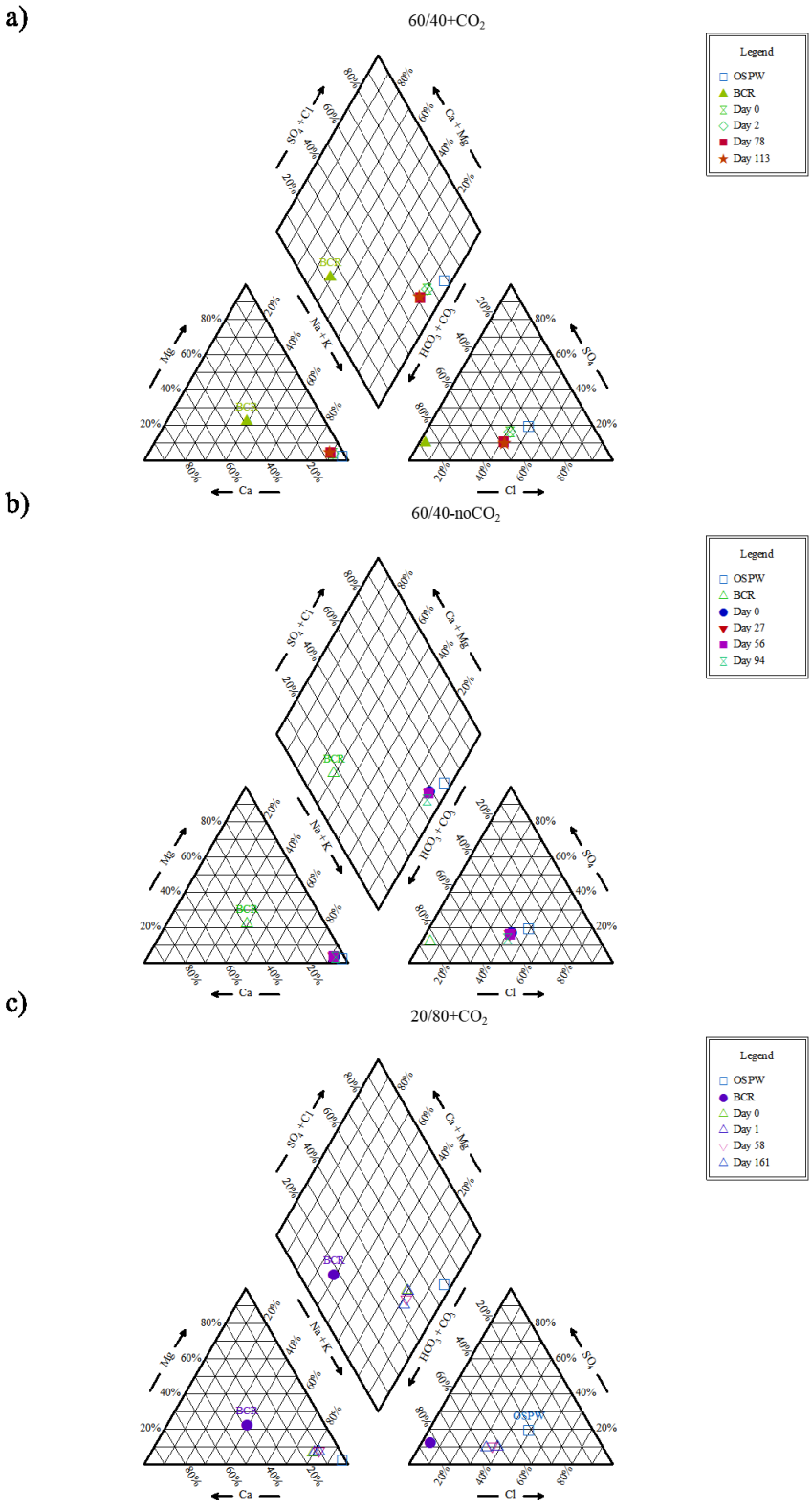

Figure 5-3 Piper diagrams for a) 60/40+CO_2, b) 60/40+noCO_2, and c) 20/80+CO_2 water columns. Figure excerpt from Poon et al. (2018).

The water chemistry data from these three columns were also used in a PHREEQCi computer simulation calculation. The SI calculation results showed that three carbonate minerals (aragonite, calcite, and dolomite) were undersaturated in the 60/40+CO_2 and 20/80+CO_2 columns on days 113 and 116, respectively (Table 5-1). However, the same carbonate minerals remained oversaturated in the 60/40+noCO_2 column for the 94 day duration of the experiment.

Table 5-1 Saturation indices of aragonite, calcite and dolomite.

	60/40+CO_2		60/40-noCO_2		20/80+CO_2	
	Initial	**Final (Day 113)**	**Initial**	**Final (Day 94)**	**Initial**	**Final (Day 116)**
Aragonite	0.67	−1.42	0.15	0.09	0.35	−1.24
Calcite	0.82	−1.27	0.3	0.23	0.49	−1.1
Dolomite	1.64	−2.59	0.55	0.43	0.76	−2.2

Note: Saturation indices values indicate degree of saturation 0 = equilibrium, >0 = oversaturation, and <0 = undersaturation. Table excerpt from Poon et al. (2018).

Taken together, the piper diagram and saturation index calculation results indicate that carbonate minerals, if present, are likely dissolved in the 60/40+CO_2 and 20/80+CO_2 columns. These results seemed to suggest the possibility that carbonate mineral dissolution may contribute to the observed turbidity reduction when the solution's pH is reduced by CO_2 addition, and that the ionic strength of the solution may play a role in turbidity reduction.

5.3.2 Big Column Study

The results of the water chemistry analysis in section 5.3.1 suggested that carbonate mineral dissolution could occur when a solution's pH reduction is triggered by the addition of CO_2. To determine the presence of carbonate minerals in water samples, powdered FFT and sediments from BML-OSPW were analyzed by applying an XRD method. The XRD results identified calcite as one of the constituents present in the FFT and the BML-OSPW sediments (Figure 5-4). The FFT was estimated to contain calcite as 4.5 wt% (dry weight) of the total carbonate. Indeed, calcite has also been identified in BML field samples (Dompierre et al., 2016).

a)

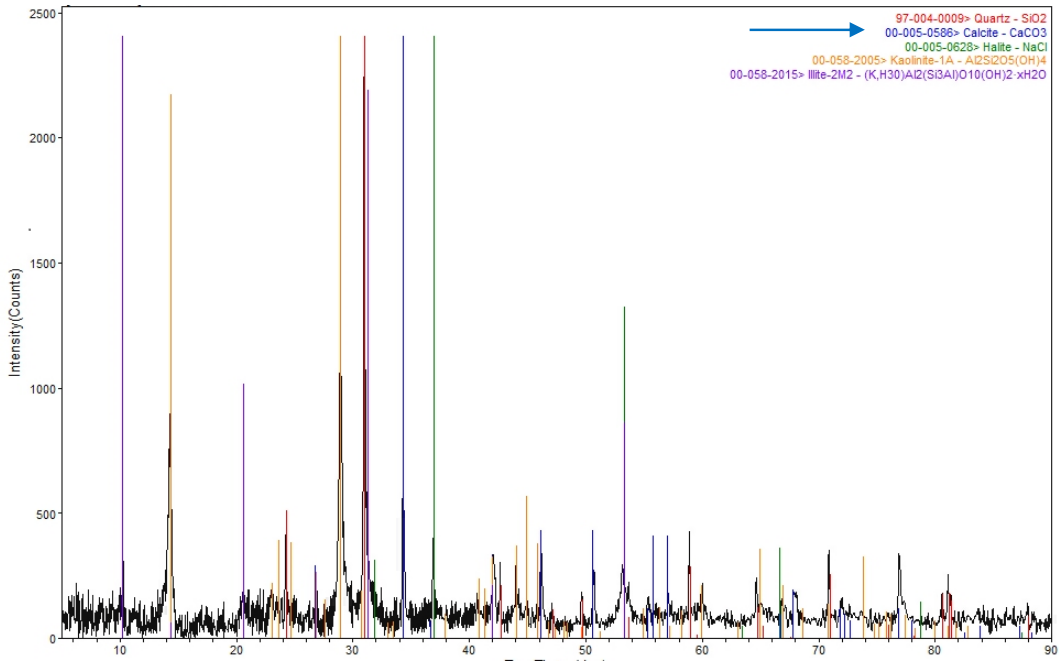

b)

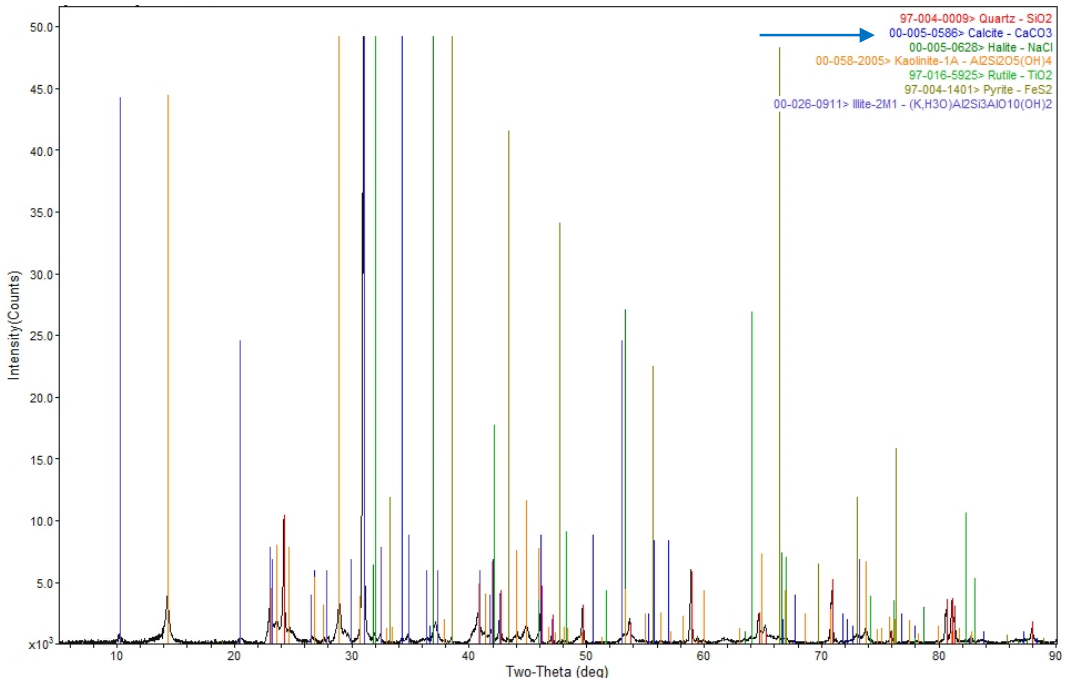

Figure 5-4 X--ray powder diffraction results for a) BML surface water and b) FFT. Figure excerpt from Poon et al. (2018). Calcite mineral indicated by a blue arrow.

Following the identification of calcite in the BML surface water and in the FFT, a series of experiments were designed to determine the effect of calcite dissolution triggered by the addition of CO_2 on the BML surface water turbidity reduction. First, the effect of CO_2 on water clarity in the absence of FFT is examined in order to establish a turbidity baseline for later experiments presented in this chapter and its sub-chapters.

Two big columns (2.5 m tall, ~148 L final volume; Figure 5-1) containing 80% BML-OSPW and 20% BCR water (80/20) were constructed. The initial parameters for the two columns were comparable prior to CO_2 treatment (Table 5-2).

Table 5-2 Initial physical and chemical parameters for the 80% BML-OSPW 20% BCR (80/20) column experiment

Column	Conditions	pH	Turbidity (NTU)	Conductivity (mS/cm)	Alkalinity (mg/L as $CaCO_3$)
1	**Before CO_2 addition**	8.0	350 ± 150	3.1	561 ± 4
2	**noCO_2 Before Mixing**	8.1	229 ± 88	3.1	582 ± 9

Note: pH, turbidity, conductivity and alkalinity values are averages for samples obtained from each of the five ports in each column.

A decrease from the initial pH was observed in the 80/20 columns immediately after CO_2 addition (Figure 5-5 and Table 5-2). A reduction in pH for the noCO_2 column was also noted but was recovered at day 81 (Figure 5-5 and Table 5-2). Both columns (CO_2 and control) showed comparable conductivity, alkalinity, and concentrations of Ca^{2+}, Mg^{2+}, Na^{+}, Cl^{-}, and SO_4^{2-} results (Figure 5-5 and -6).

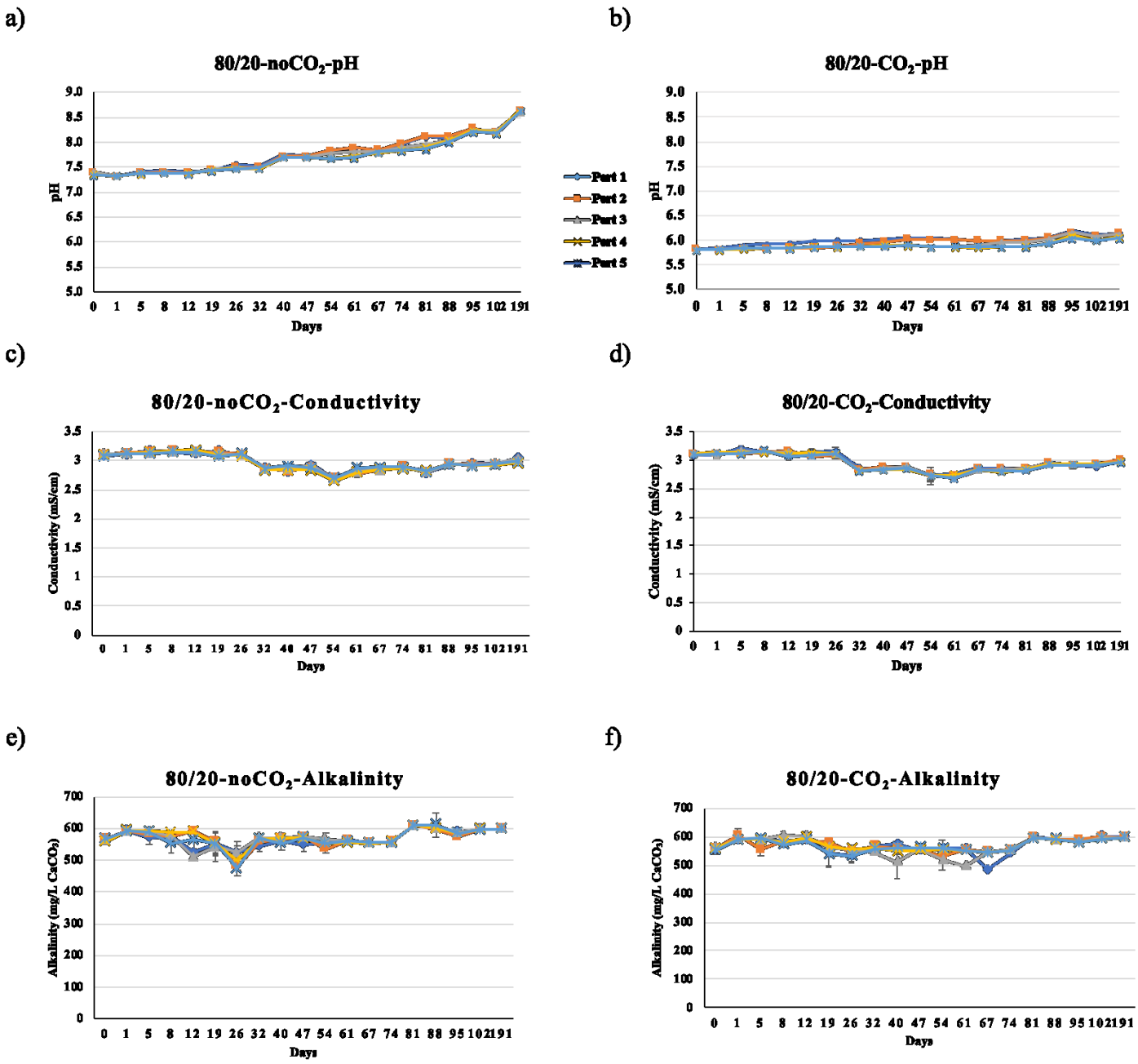

Figure 5-5 Mean pH, conductivity, and alkalinity of CO_2 treated and noCO_2 columns over 191 days. Note: error bars represent one standard error of duplicate sample measurements.

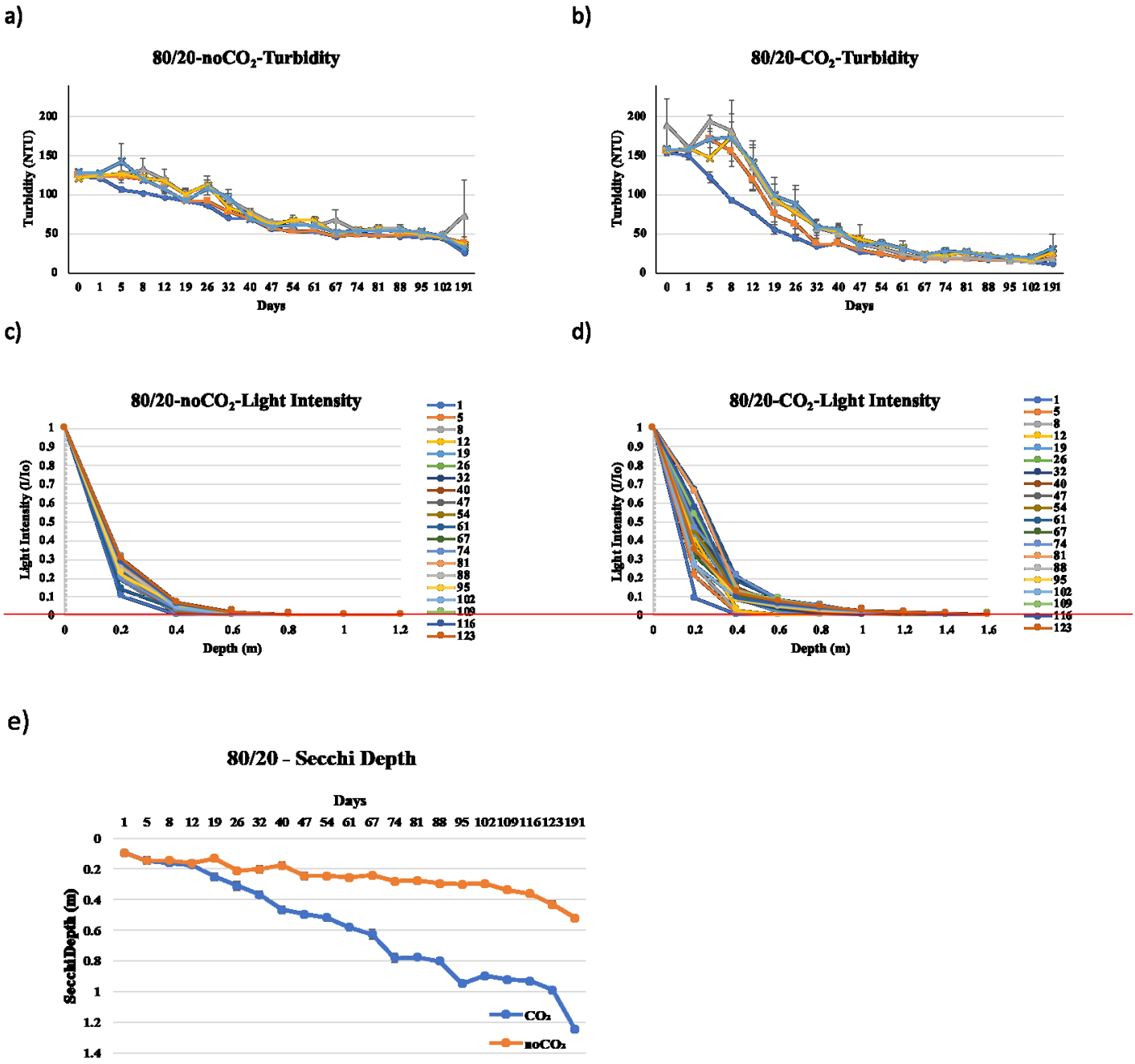

Figure 5-6 Turbidity, light intensity, and Secchi disk depth of CO_2 treated and noCO_2 columns over 191 days. Note: error bars represent one standard error of duplicate samples

The column with CO_2 added showed a 90.3% (average of data from 5 ports) turbidity reduction, whereas the control column showed a 63.1% (average of data from 5 ports) reduction in turbidity. A similar pattern was observed for the PAR light intensity and Secchi depth

measurements (Figure 5-6c, d, & e). The CO_2 treatment resulted in a greater turbidity reduction (90%, 10.7 NTU from column port 1 on day191) in the treated column than the maximum reduction of ~76.9% reported by Zhu et al. (2011). It is possible that the difference from the Zhu et al. (2011) study may be due to differences in the manner CO_2 was introduced (Zhu et al. introduced CO_2 using an autoclave, whereas CO_2 was introduced via Seair system in this study). These authors also noted that gas bubbles generated by high pressure ($pCO_2 \approx 100$ kPa) could resuspend newly settled particles (Zhu et al., 2011).

It is generally thought that the fine clay particles from FFT are highly stable in suspension and slow to settle in OSPW (pH ~8; Dompierre et al., 2016; Poon et al., 2018; Siddique et al., 2014a; Zhu et al., 2011). Despite this belief, an approximately 60% turbidity reduction was achieved in the noCO_2 column. This result could be attributed to: 1) clay aggregate formation may still occur at pH 8; and 2) the experiment was performed under a quiescent condition (i.e., lack of wind, wave, and/or thermal disturbances). Indeed, edge-to-face interparticle arrangements have been observed in suspended MFT and kaolinite at pH 8 (Mikula et al., 1993; Zbik et al., 2008), and such interparticle arrangements are loose and easily disrupted (Zbik et al., 2008). As a result, some FFT settlement can be observed under quiescent conditions, such as in this column study in which minimal settling was observed in the BML (Dompierre et al., 2016). On the other hand, CO_2 addition (pH ~5.8) resulted in water clarity improvement, and this was likely achieved by a reduction of the clay particles in suspension through coagulation/flocculation. Indeed, Chorom and Rengasamy (1995) showed that the amount of dispersible clay was greatly decreased in a NaCl solution at a reducing pH; 93% of kaolinite was dispersed at pH 8.4 compared to 33% kaolinite dispersal at pH 5.6.

Taken together, these results indicate that pH reduction through CO_2 addition can improve FFT settling and water clarity; moreover, a lag phase was not observed. The low amount of FFT in the experiment may have contributed to the apparent absence of mineral precipitation/dissolution processes in the current experiment. Indeed, Siddique et al. (2014a) and Dompierre et al. (2016) speculated that carbonate mineral dissolution is likely due to the presence of calcite and dolomite, whereas Siddique et al. (2014a) observed carbonate minerals reduction during examination of MFT solids from a column with canola meal hydrolysate but not from the control column.

5.3.3 Calcite Dissolution Experiment

In order to evaluate the contribution of carbonate dissolution (Equation 5-1) to turbidity reduction, a small (1 L) column experiment was conducted using Iceland spar crystal ($CaCO_3$). Due to the large water volume requirement of the Seair system, a 20 µm pore-size stainless steel pump head was used instead to deliver CO_2 for the calcite dissolution experiment. Microbubbles (<50 µm diameter) have a higher surface tension than bubbles generated from a regular sparger, and thus, the generated microbubbles remain in the aqueous phase for a longer period, which is suitable when performing a carbonate dissolution/precipitation experiment (Bang et al., 2011). The Iceland spar was crushed to a 45–75 µm particle size to mimic the typical particle size found within the FFT (Dompierre et al., 2016; Voordouw, 2013). The physical and chemical properties of crushed Iceland spar were characterized by using XRD and scanning electron microscopy with energy-dispersive spectroscopy (SEM-EDS). Both XRD and SEM-EDS results showed that the crushed Iceland spar ($CaCO_3$) was of high purity (Figure 5-7a & e). A carbon peak was detected in the SEM-EDS analysis because the sample was coated with a carbon conductive

material prior to the analysis (Figure 5-7e). The SEM analysis showed the Iceland spar was roughly uniform in size (45–75 µm diameter; Figure 5-7b &c).

$$CaCO_3 + CO_2 + H_2O \leftrightarrow Ca^{2+} + 2HCO_3 \quad \text{(Equation 5-1)}$$

Note: Equation 1 was adapted from work published by Gledhill and Morse (2006).

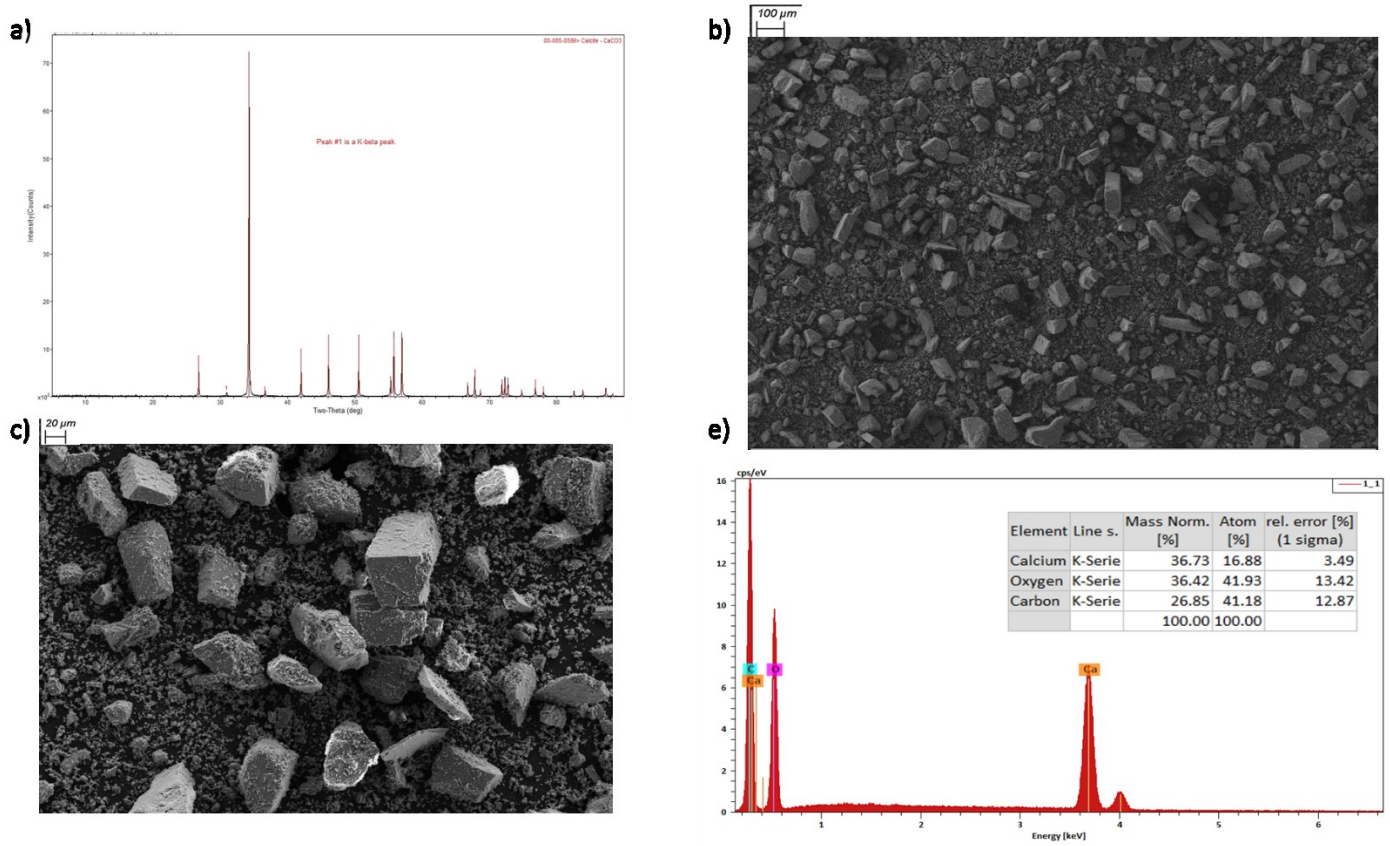

Figure 5-7 Characterization of Iceland spar (45–75 µm) by a) XRD and b-e) SEM-EDS. *Note: An enlarged version of Iceland spar XRD results is shown in the appendix (Figure A-4).*

Brandon (2016) observed that water clarity improvement only occurred in the high ionic strength water column treated with CO_2; as a result, the small-scale calcite dissolution experiment in this study was conducted using 80%- or 60%-OSPW water. In addition, it is estimated that a total of

7.5 mol of carbonate minerals (calculated using the molecular weight of $CaCO_3$) were present in a 0.2 m thick slice of FFT, which was used in the 2.5 m tall column study conducted by Brandon (2016). Since surface-reaction kinetics is a major control mechanism for calcite dissolution (Rickard & Sjoberg, 1983; Sjoberg, 1976), 5×10^{-3} mol/L of calcite, equivalent to the 2 cm of FFT surface (0.75 mol calcite / 130 L) in the Brandon (2016) study, was chosen as the concentration used in the present study to examine the effect of CO_2-mediated calcite dissolution on turbidity reduction.

The examination of pH-induced calcite dissolution was performed in 1 L columns with 0.5 g or 1 g of calcite placed at the bottom of the column prior to filling with 80%-OSPW 20% BCR (80/20) water. A pH reduction (pH 5.9–6.1) was observed in the CO_2 treated columns (Figure 5-8a & b). An initial reduction in alkalinity was observed in the 80/20+CO_2 column, while an increase in alkalinity was observed in 80/20+CO_2+0.5g- and 80/20+CO_2+1g-calcite columns throughout the experiment (Figure 5-8c & d). There were 98.2% and 98.9% decreases in turbidity observed in 80/20+CO_2+0.5g- and 80/20+CO_2+1g-calcite columns, respectively, compared to the 85.5% and 88.2% turbidity reductions in 80/20-noCO_2+0.5g- and 80/20-noCO_2+1g-calcite columns, respectively (Figure 5-8e, f and Table 5-3). A 95.9% reduction in turbidity was observed in the 80/20+CO_2 column compared to the 87.8% turbidity reduction in the 80/20-noCO_2 column (Figure 5-8e & f and Table 5-3). Substantial changes in zeta potential were observed but only in the 80/20+CO_2+0.5g- and 80/20+CO_2+1g-calcite columns; from −38.5mV to −28.1 mV and −26.7 mV, respectively (Figure 5-8g & h). Furthermore, increases in calcium ion levels were observed in the 80/20+CO_2+0.5g- and 80/20+CO_2+1g-calcite columns (263.6% and 247.6% increases, respectively; Figure 5-9a & b), whereas the levels of all other major ions (i.e., Na^+, Cl^-, K^+, Mg^{2+}, and SO_4^{2-}) remained unchanged during the course of

experiment (Figure 5-9a–f). The 98% turbidity reduction (to approximately 4 and 2 final NTU values, respectively) combined with the increases in Ca^{2+} ion concentration and alkalinity suggest that calcite dissolution occurred and clay settling was promoted in the 80/20+CO_2+0.5g- and 80/20+CO_2+1g-calcite columns. Slight decreases in Ca^{2+} concentrations were observed in the 80/20-noCO_2+0.5g- and 80/20+noCO_2+1g-calcite columns; i.e., 22.3% and 28.2% reductions, respectively (Figure 5-9a & b). A decrease in alkalinity was observed in both the 80/20-noCO_2+0.5g- and 80/20+noCO_2+1g-calcite columns (Figure 5-8c &d). These results suggest that $CaCO_3$ precipitation likely occurred in both the 80/20-noCO_2+0.5g- and 80/20+noCO_2+1g-calcite columns.

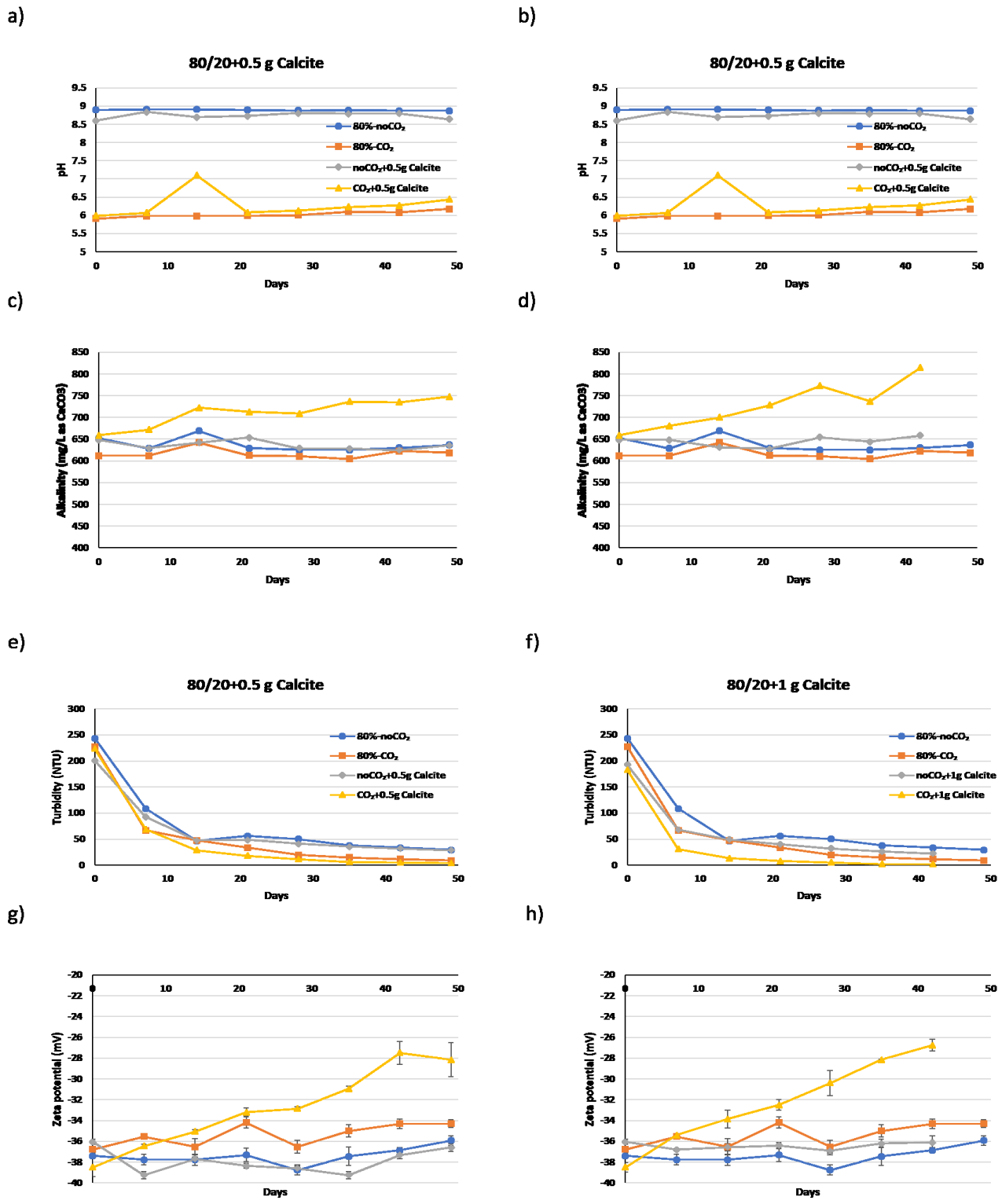

Figure 5-8 Small column calcite dissolution results for the 80% OSPW 20%BCR water mix with 0.5 g (a, c, e, g) or 1 g (b, d, f, h) calcite addition. Note: The zeta potential value was an average of repeated measurements of a single sample, and the error bar represents one standard error.

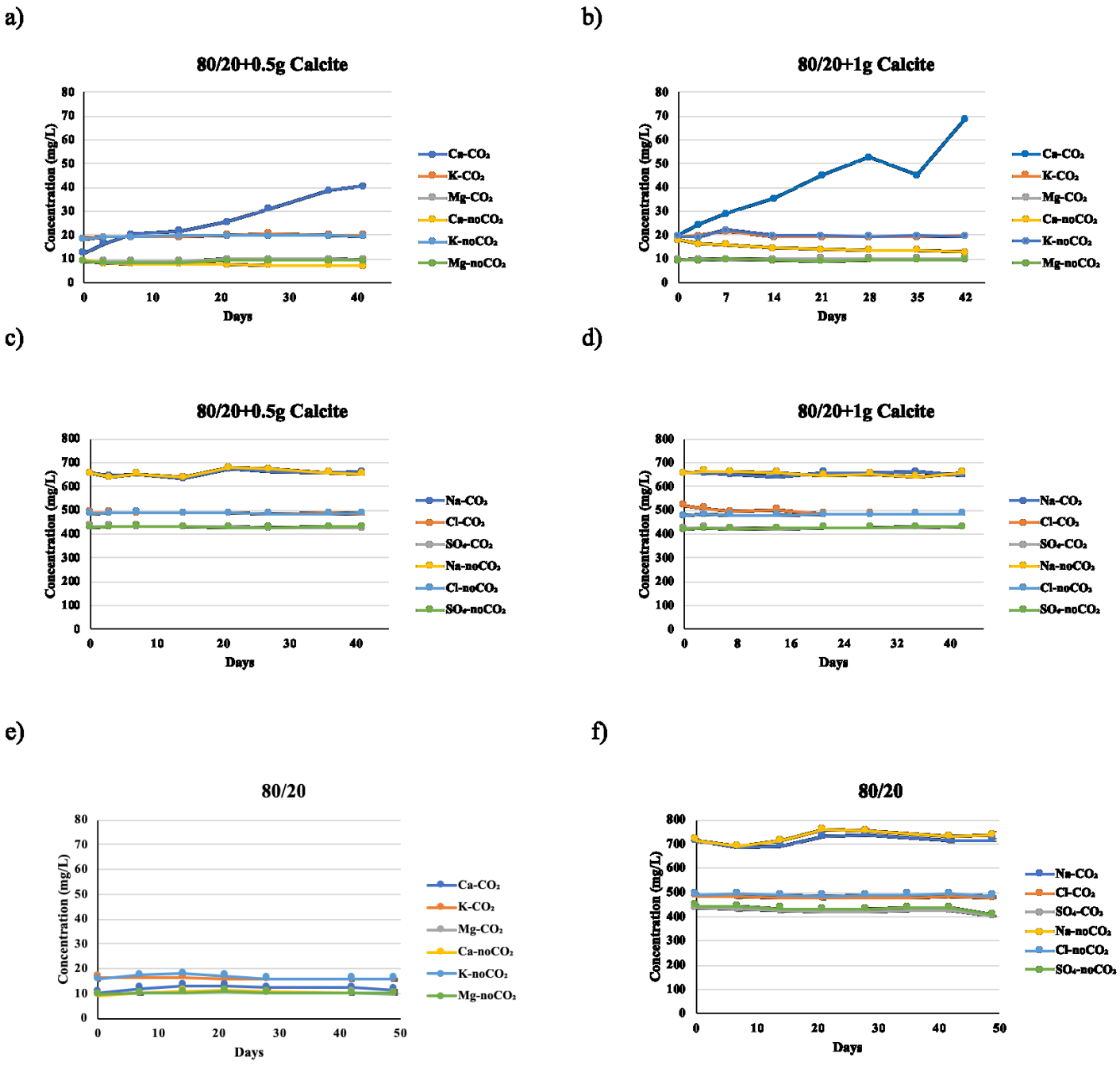

Figure 5-9 Cation and anion concentration for the a & c) 80/20+0.5g calcite, b & d) 80/20+1g calcite and e & f) 80/20 column experiments.

Table 5-3 A summary of turbidity changes in the 80/20 columns

Column Conditions	Initial (NTU)	Final (day 49) (NTU)	Percent change (%)
80/20-noCO_2	243.5	29.6	87.8
80/20+CO_2	227.5	9.3	95.9
80/20-noCO_2+0.5 g Calcite-	201.0	29.2	85.5
80/20+CO_2+0.5 g Calcite	224.0	4.1	98.2
	Initial (NTU)	Final (day 42) (NTU)	Percent change (%)
80/20-noCO_2+1 g Calcite	193.0	22.8	88.2
80/20+CO_2+1 g Calcite	183.0	2.0	98.9

Calcite dissolution was also tested in water containing 60%-OSPW, and similar change patterns were observed in the 60/40+CO_2+0.5g-calcite column. A 98.6% turbidity reduction was observed in the 60/40+CO_2+0.5g-calcite column, while a 95.4% turbidity reduction was observed in the 60/40+CO_2 column (p=0.48; Figure 5-10 and Table 5-4). There were 88.1% and 87.8% turbidity reductions observed in the 60/40-noCO_2 and 60/40-noCO_2+0.5g-calcite columns, respectively. These results suggest that calcite addition would not interfere with the settlement of FFT in OSPW (Figure 5-10 and Table 5-4), which is consistent with the results presented in Figure 5-9. Within the same time frame (49 days), similar increases in alkalinity, zeta potential and Ca^{2+} ion concentration were observed in the 60/40+CO_2+0.5g-calcite column compared to the levels in the 80/20+CO_2+0.5g-calcite column. These results further support the suggestion that FFT dewatering can be enhanced by the release of divalent cations (Ca^{2+}) through pH-mediated calcite dissolution and subsequent reduction of the DDL thickness (Siddique et al., 2014a), which was evidenced by the zeta potential result. However, only an ~30% increase in Ca^{2+} ion concentration was observed over the 49 day experiment; as a result,

the Ca^{2+} ion concentration was monitored for up to 91 days. A final 209.5% increase in Ca^{2+} concentration was observed in the 60/40+CO_2+0.5g-calcite column by day 91 (Figure 5-10). A statistical test (T-test) was performed on turbidity data between 60/40-CO_2 and +calcite columns; however, a significant difference was not observed (at 95% confidence level), and it is likely due to insufficient sample size.

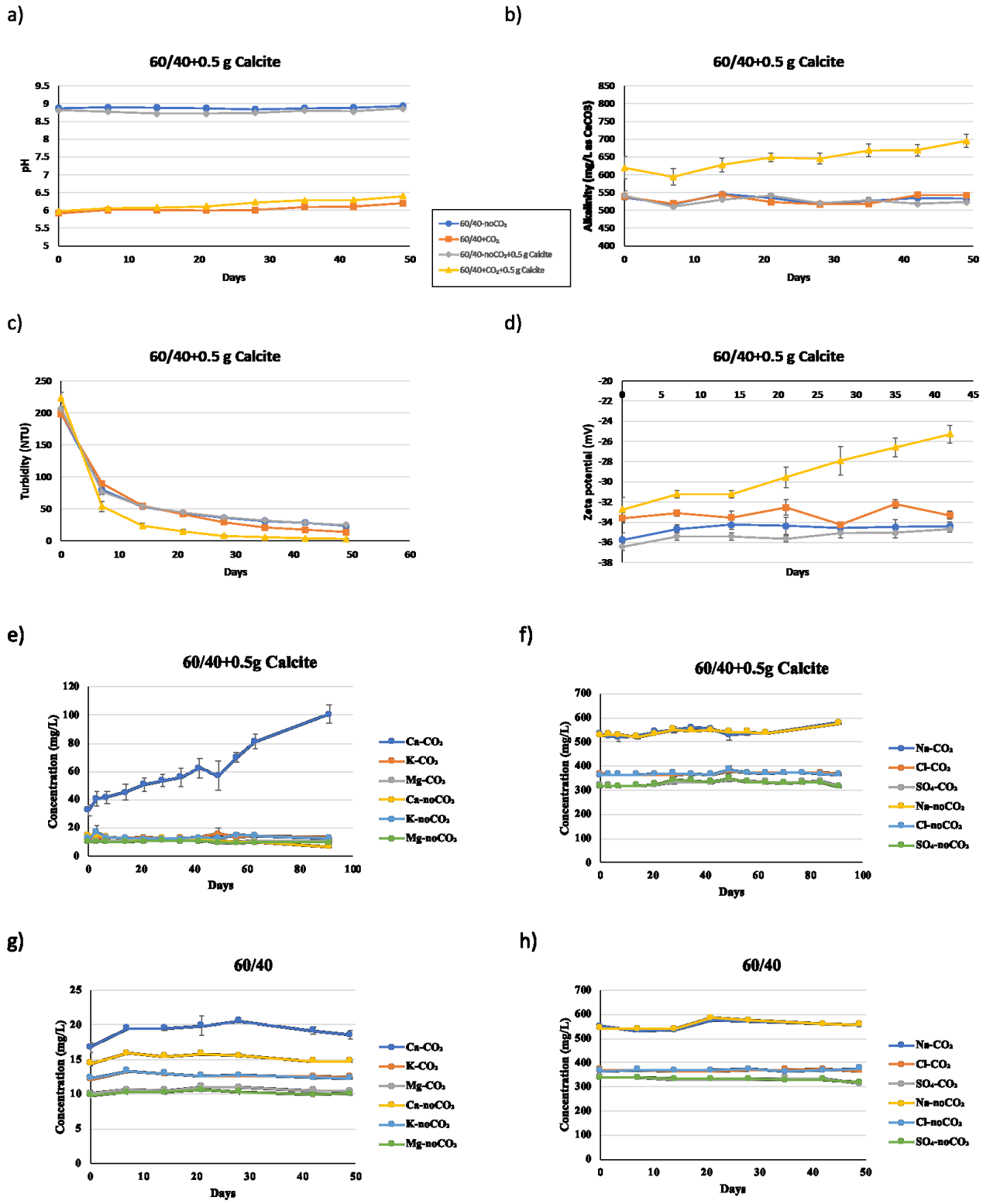

Figure 5-10 Physical and chemical results for the calcite dissolution experiment in the 60/40 water mix. a) pH, b) alkalinity, c) turbidity, d) zeta potential, and cation and anion results for thee & f) 60/40+0.5g calcite and g & h) 60/40 columns. Note: All data shown are an average from duplicate experiments and the error bar represents one standard error of the averaged value.

Table 5-4 A summary of turbidity changes in the 60/40 columns

	Initial (NTU)	Final (day 49) (NTU)	Percent change (%)
60/40-noCO_2	199.5	23.7	88.1
60/40+CO_2	198.5	9.1	95.4
60/40-noCO_2+0.5 g Calcite	206.5	25.1	87.8
60/40+CO_2+0.5 g Calcite	223.5	3.1	98.6

Calcite dissolution was tested in two water mixes (80% or 60% OSPW), and slight enhancement of turbidity reduction was observed in the columns that contained calcite and were treated with CO_2. The results from section 5.3.3 demonstrate that FFT settling can be influenced by CO_2-mediated 1) pH reduction and 2) calcite dissolution. These two mechanisms interact to achieve more favourable conditions for the suspended FFT particles to interact and subsequently settle. Since the zeta potential value is indicative of particle stability in a suspension, the following discussion will focus on this parameter.

Despite CO_2 addition, the initial zeta potential values (approximately −37 mV for 80/20 water and −33 mV for 60/40 water) suggested higher FFT stability in columns without calcite than that in columns with calcite and CO_2 treatment. However, Zhu et al. (2011) reported a zeta potential value of approximately −28 mV (pH 6) for tailings fines from Syncrude Canada Ltd. after treatment with CO_2. Comparisons of these values imply more destabilized conditions exist for FFT particles in suspension than for the tailings fines examined by Zhu et al. (2011). The apparent discrepancy may be attributed to differences in the temperatures at measurement and to the heterogeneity of the FFT samples. It is assumed that zeta potential measurement was performed at room temperature (20°C) in the Zhu et al. (2011) study as they reported a Z3110

Zetaphoremeter was used, whereas, in the current study, a temperature of 25°C was used with a Zetazier nano ZSP meter with a temperature incubation function. Several studies showed that an elevated temperature could result in an under-estimation of electro-osmotic flow velocities, as well as influencing the silanol equilibrium, adsorption equilibrium and DDL thickness (Revil et al., 1999; Venditti et al., 2006). Revil et al. (2002) showed the effect of temperature on zeta potential measurement using zeolites containing volcanic samples and reported an approximately −5 mV difference in zeta potential value for samples measured at 20°C and 25°C.

In the presence of calcite, a substantial change in zeta potential (with a maximum of −10 mV reduction) was observed in the CO_2 treated columns. In these columns, a linear increase in dissolved calcium ion concentration with time was observed, strongly suggesting that calcite dissolution had occurred. Divalent cations, such as calcium ion, have a strong influence on DDL thickness thereby promoting particle aggregation. A linear inverse relationship between calcium chloride ($CaCl_2$) concentration and zeta potential was observed in a study performed with a commercially available kaolinite sample at pH 5 (adjusted by either CO_2 or HCl; Ibanez et al., 2014). A zeta potential change of approximately −7 mV was observed between 0.5 and 1.5 mM $CaCl_2$ concentrations, which was similar to the change observed in the 80/20+CO_2+1 g Calcite column in the current study (~ −10 mV change from a 0.5 to 1.7 mM Ca^{2+} concentration increase). The lowest measured zeta potential values were −27.5, −26.8 and −25.3 mV for 80/20+CO_2+0.5 g calcite, 80/20+CO_2+1 g calcite and 60/40+CO_2+0.5 g calcite columns, respectively (at day 42). These values suggest that the applied conditions are favourable for FFT aggregation to occur. Significantly more kaolinite aggregates have been observed in a 0.25 mM $CaCl_2$ solution at pH 6 than in a 10 mM NaCl solution at pH 6 (Zbik et al., 2008). In addition, these authors observed the kaolinite aggregates mainly comprise particles connected in the form

of a butterfly shape with both edge-to-edge and edge-to-face orientations under 0.25 mM $CaCl_2$ and pH 6 conditions (Zbik et al., 2008). These observations were consistent with the general notion that an approximate 1×10^{-4} mol/L of divalent cation concentration is needed to induce DDL compression, thereby destabilizing the particles in suspension (Hogg, 2000).

Taken altogether, faster turbidity reduction was observed when the higher amount of calcite was present (80/20-CO_2+1 g calcite). A higher calculated calcite dissolution rate was observed in the 80/20-CO_2+1g calcite column with a maximum rate of 8.5×10^{-5} mol/L/d (ΔD42-D35; Figure 5-11). This result is in agreement with the observation that calcite dissolution is controlled by a surface-reaction mechanism (Appelo & Postma, 2005; Arvidson et al., 2003; Morse et al., 2007; Plummer et al., 1978). Interestingly, a lower calculated dissolution rate was observed in the 80/20-CO_2+0.5 g calcite column than in the 60/40-CO_2+0.5 g calcite column; maximum rates of 3.2×10^{-6} (ΔD21-D14) and 4.7×10^{-5} (ΔD56-D49) mol/L/d, respectively (Figure 5-11). A wide range of calcite dissolution rates have been reported (Table 5-5), and the calculated calcite dissolution rates obtained from the experiments presented in this chapter are about one order of magnitude lower than previously reported values. The observed discrepancies in calcite dissolution rates can be attributed to differences in experimental parameters, including pH, pCO_2, flow cells or free drift runs approaches, powders, rotating disks, grain sizes, and impurities, as well as vessel shape and interior designs (Arvidson et al., 2003; Sjoberg & Rickard, 1983).

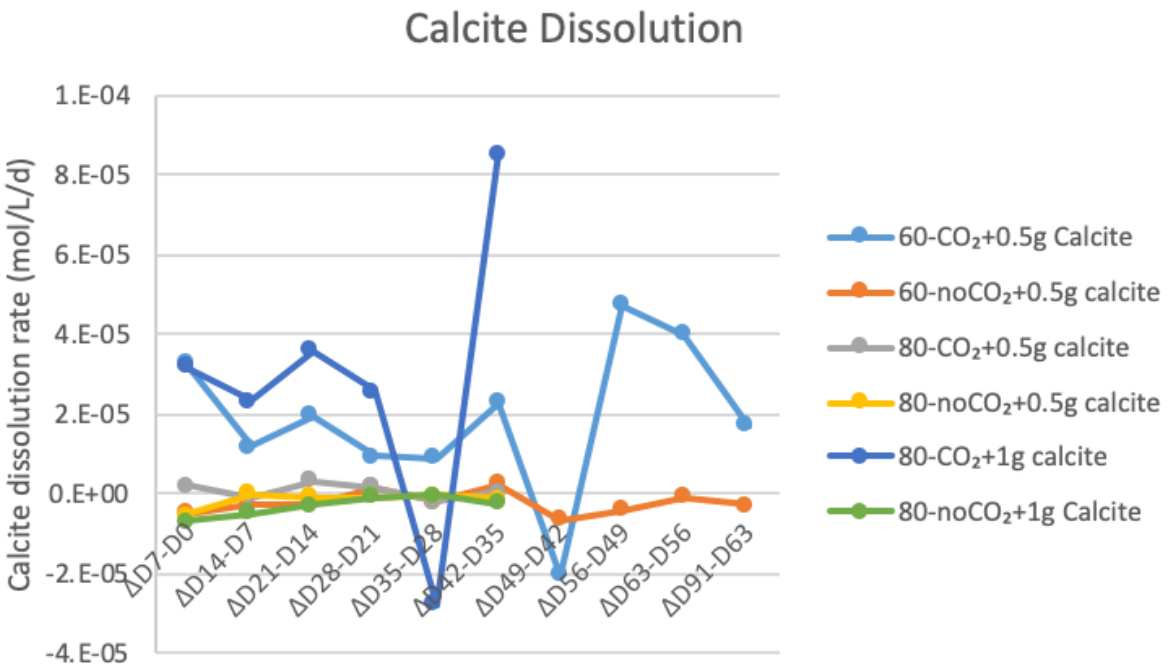

Figure 5-11 Calcite dissolution rates in different waters under different CO_2 and calcite treatments. Note: dissolution rate was calculated from dissolved calcium ion concentration under the assumption that the measured dissolved calcium molar concentration is directly correlated to the calcite dissolution.

Table 5-5 A compilation of previously reported calcite dissolution rate values.

Rate	pH	Temp (°C)	Conditions	Reference
0.04 mole/d	8.4	25	0.7 mol/L KCl, 1.5×10^{-5} M CO_2 (aq), 500 rpm	Sjoberg and Rickard (1983)
2.34 mole/d	3	25	0.1 mol/kg $MgCl_2$, 340 rpm	Alkattan et al. (2002)
1.6×10^{-4} mole/d	5.7	25	100–200 µm grain calcite, 0.001 M NaCl, $pCO_2 = 10^{-3.5}$, 370 cm^2/g Brunauer-Emmett-Teller (BET) surface area	Pokrovsky et al. (2005)
3.2×10^{-4} mole/d	8	25		

5.4 Conclusion

Several studies have demonstrated that dissolved CO_2 has a role in the settling and densification of oil sands FFT (Ibanez et al., 2014; Poon et al., 2018; Siddique et al., 2014a; Zhu et al., 2011). In addition, carbonate mineral dissolution has been hypothesized as one of the mechanisms active in CO_2-mediated oil sands tailings settlement or densification (Siddique et al., 2014a; Siddique et al., 2014b). In addition, calcite ($CaCO_3$) has been observed within FFT and sediments from BML-OSPW samples (Poon et al., 2018). The objective of chapter 5a was to examine the effect of calcite dissolution through CO_2 addition on BML surface water turbidity. Approximately 98% turbidity reductions (final turbidity 2 and 4 NTU) were observed in CO_2-treated columns containing calcite (80/20 and 60/40, respectively), whereas there was an approximately 95% turbidity reduction (final turbidity ~9 NTU) with CO_2 treatment alone. The results indicate a possible benefit of calcite dissolution on BML water turbidity reduction because no reported effect on fish predation has been observed below 3 NTU (Birtwell, 2008). Future research should increase the sample size to elucidate the statistical significance on turbidity reduction between CO_2+calcite and CO_2 alone treatments. A calcite dissolution rate approximately one order of magnitude slower than reported rates was calculated for the present study's results; i.e., 4.7×10^{-5} mole/L/d for the 60/40-CO_2+0.5g calcite column compared to 1.6×10^{-4} mole/d reported by Pokrovsky et al. (2005). One of the potential inhibitory mechanisms will be examined in the next sub-chapter (chapter 5b).

These results present in this sub-chapter demonstrate that calcite dissolution through CO_2 addition can improve water clarity. These results showed calcite dissolution mediated by pH reduction triggered by CO_2 addition can enhance BML water turbidity reduction under quiescent conditions.

5.5 References

Alberta Energy Regulator. (2016). *Directive 085: Fluid Tailings Management for Oil Sands Mining Projects*. Retrieved from http://www.aer.ca/documents/directives/Directive085.pdf.

Alkattan, M., Oelkers, E. H., Dandurand, J. L., & Schott, J. (2002). An experimental study of calcite dissolution rates at acidic conditions and 25 degrees C in the presence of NaPO3 and MgCl2. *Chem Geol, 190*(1-4), 291-302.

Appelo, C. A. J., & Postma, D. (2005). *Geochemistry, groundwater and pollution* (2nd ed.). Leiden ; New York: Balkema.

Arkell, N., Kuznetsov, P., Kuznetsova, A., Foght, J. M., & Siddique, T. (2015). Microbial metabolism alters pore water chemistry and increases consolidation of oil sands tailings. *J Environ Qual, 44*(1), 145-153.

Arvidson, R. S., Ertan, I. E., Amonette, J. E., & Luttge, A. (2003). Variation in calcite dissolution rates: A fundamental problem? *Geochim Cosmochim Acta, 67*(9), 1623-1634.

Ball, J. W., Nordstrom, D. K., & Geological Survey (U.S.). (1991). *User's manual for WATEQ4F, with revised thermodynamic data base and test cases for calculating speciation of major, trace, and redox elements in natural waters / by James W. Ball and Kirk Nordstrom*. Menlow Park, Calif.: U. S. Geological Survey.

Bang, J. H., Jang, Y. N., Kim, W., Song, K. S., Jeon, C. W., Chae, S. C., Lee, S-W, Park, S-J. Lee, M. G. (2011). Precipitation of calcium carbonate by carbon dioxide microbubbles. *Chem Eng J, 174*(1), 413-420.

Birtwell, I. K. (2008). The validity of including turbidity criteria for aquatic resource protection in land development guidelines (Pacific and Yukon Region). In M. A. Farrell & A. Jonsson (Eds.). [Ottawa] :: Fisheries and Oceans Canada.

Brandon, J. T. (2016). *Turbidity Mitigation in an Oil Sands End Pit Lake through pH Reduction and Fresh Water Addition.* (Master's thesis), University of Alberta. (130p)

Canadian Association of Petroleum Producers. (2018). *2018 CAPP Crude Oil Forecast, Markets & Transportation*. Retrieved from https://www.capp.ca/publications-and-statistics/publications/320294

Chorom, M., & Rengasamy, P. (1995). Dispersion and zeta potential of pure clays as related to net particle charge under varying pH, electrolyte concentration and cation type. *European J Soil Sci, 46*(4), 657-665.

Cumulative Environmental Management Association. (2012). *End pit lakes guidance document* (pp. 1 online resource (434 p.)). Retrieved from http://www.deslibris.ca/ID/234915

Davies-Colley, R. J., & Smith, D. G. (2001). Turbidity, suspended sediment, and water clarity: A review. *J Am Water Resour Assoc, 37*(5), 1085-1101.

Dompierre, K. A., Lindsay, M. B. J., Cruz-Hernandez, P., & Halferdahl, G. M. (2016). Initial geochemical characteristics of fluid fine tailings in an oil sands end pit lake. *Sci Total Environ, 556*, 196-206.

Eckert, W. F., Masliyah, J. H., Gray, M. R., & Fedorak, P. M. (1996). Prediction of sedimentation and consolidation of fine tails. *AIChE J, 42*(4), 960-972.

Gledhill, D. K., & Morse, J. W. (2006). Calcite dissolution kinetics in Na-Ca-Mg-Cl brines. *Geochim Cosmochim Acta, 70*(23), 5802-5813.

Government of Alberta. (2015). *Lower Athabasca Region : tailings management framework for the mineable Athabasca oil sands*.

Government of Alberta. (2016). Oil Sands: Facts and Statistics. Retrieved from https://open.alberta.ca/publications/oil-sands-facts-and-stats

Hogg, R. (2000). Flocculation and dewatering. *Int J Miner Process, 58*(1-4), 223-236.

Humphries, M., & Library of Congress. Congressional Research Service. (2008). *North American Oil Sands history of development, prospects for the future* (pp. 31 p.). Retrieved from http://fas.org/sgp/crs/misc/RL34258.pdf

http://www.scribd.com/doc/2402059/CRS-Report-for-US-Congress-NA-Oil-Sands-Jan-2008

Hunter, R. J. (2001). *Foundations of colloid science* (2nd ed.). Oxford ; New York: Oxford University Press.

Ibanez, M., Wijdeveld, A., & Chassagne, C. (2014). The Role of Mono- and Divalent Ions in the Stability of Kaolinite Suspensions and Fine Tailings. *Clays and Clay Minerals, 62*(5-6), 374-385.

Kaminsky, H. A. W., Etsell, T. H., Ivey, D. G., & Omotoso, O. (2009). Distribution of Clay Minerals in the Process Streams Produced by the Extraction of Bitumen from Athabasca Oil Sands. *Can J Chem Eng, 87*(1), 85-93.

Lawrence, G. A., Tedford, E. W., & Pieters, R. (2016). Suspended solids in an end pit lake: potential mixing mechanisms. *Can J Civ Eng, 43*(3), 211-217.

Liu, L. Y., Hu, Y., Min, F. F., Zhang, M. X., & Song, S. X. (2013). Characterizations and Stability of Colloidal Coal-Measure Kaolinite in Aqueous Suspensions: A Review. *Surf Rev Lett, 20*(1).

Mikula, R., Munoz, V., Lam, W., & Payette, C. (1993). *Structure in oil sands fine tailings.* Paper presented at the Proceedings of the Fine Tailings Fundamentals Symposium, Oil Sands our Petroleum Future, Edmonton, AB.

Missana, T., & Adell, A. (2000). On the applicability of DLVO theory to the prediction of clay colloids stability. *J Colloid Interface Sci, 230*(1), 150-156.

Morse, J. W., Arvidson, R. S., & Luttge, A. (2007). Calcium carbonate formation and dissolution. *Chem Rev, 107*(2), 342-381.

Parkhurst, D. L., & Appelo, C. A. J. (2013). *Description of input and examples for PHREEQC version 3—A Computer Program for Speciation, Batch-reaction, One-dimensional Transport, and Inverse Geochemical Calculations.* Denver, Colo.: U.S. Department of the Interior, U.S. Geological Survey.

Plummer, L. N., Wigley, T. M. L., & Parkhurst, D. L. (1978). The kinetics of calcite dissolution in CO 2 -water systems at 5 degrees to 60 degrees C and 0.0 to 1.0 atm CO 2. *Am J Sci. 278*(2), 179-216.

Pokrovsky, O. S., Golubev, S. V., & Schott, J. (2005). Dissolution kinetics of calcite, dolomite and magnesite at 25 degrees C and 0 to 50 atm pCO(2). *Chem Geol, 217*(3-4), 239-255.

Poon, H. Y., Brandon, J. T., Yu, X. X., & Ulrich, A. C. (2018). Turbidity Mitigation in an Oil Sands Pit Lake through pH Reduction and Fresh Water Addition. *J Environ Eng, 144*(12). 10.1061/(Asce)Ee.1943-7870.0001472

Revil, A., Hermitte, D., Spangenberg, E., & Cocheme, J. J. (2002). Electrical properties of zeolitized volcaniclastic materials. *J Geophys Res - Solid Earth, 107*(B8).

Revil, A., Pezard, P. A., & Glover, P. W. J. (1999). Streaming potential in porous media 1. Theory of the zeta potential. *J Geophys Res - Solid Earth, 104*(B9), 20021-20031.

Rickard, D., & Sjoberg, E. L. (1983). Mixed Kinetic Control of Calcite Dissolution Rates. *Am J Sci, 283*(8), 815-830.

Siddique, T., Kuznetsov, P., Kuznetsova, A., Arkell, N., Young, R., Li, C., Guigard, S., Underwood, E., Foght, J. M. (2014a). Microbially-accelerated consolidation of oil sands tailings. Pathway I: changes in porewater chemistry. *Front Microbiol, 5*, 106.

Siddique, T., Kuznetsov, P., Kuznetsova, A., Li, C., Young, R., Arocena, J. M., & Foght, J. M. (2014b). Microbially-accelerated consolidation of oil sands tailings. Pathway II: solid phase biogeochemistry. *Front Microbiol, 5*, 107.

Sjoberg, E. L. (1976). Fundamental Equation for Calcite Dissolution Kinetics. *Geochim Cosmochim Acta, 40*(4), 441-447.

Sjoberg, E. L., & Rickard, D. (1983). The Influence of Experimental-Design on the Rate of Calcite Dissolution. *Geochim Cosmochim Acta, 47*(12), 2281-2285.

Tundisi, J. G., & Tundisi, T. M. (2012). *Limnology* (pp. 1 online resource (xxii, 864 p.)). Retrieved from http://search.ebscohost.com/login.aspx?direct=true&scope=site&db=nlebk&db=nlabk&AN=437330

Venditti, R., Xuan, X. C., & Li, D. Q. (2006). Experimental characterization of the temperature dependence of zeta potential and its effect on electroosmotic flow velocity in microchannels. *Microfluid Nanofluid, 2*(6), 493-499.

Voordouw, G. (2013). Interaction of oil sands tailings particles with polymers and microbial cells: First steps toward reclamation to soil. *Biopolymers, 99*(4), 257-262.

Westcott, F., & Watson, L. (2005). End pit lakes technical guidance document: Report. Cumulative Environmental Management Association. 51p. Report.

Zbik, M. S., Smart, R. S. C., & Morris, G. E. (2008). Kaolinite flocculation structure. *J Colloid Interface Sci, 328*(1), 73-80.

Zhu, R., Liu, Q. X., Xu, Z. H., Masliyah, J. H., & Khan, A. (2011). Role of Dissolving Carbon Dioxide in Densification of Oil Sands Tailings. *Energy & Fuels, 25*(5), 2049-2057.

Chapter 5 b: The effect of sulfate on calcite dissolution

5.6 Introduction

An improvement in surface-water (BML-BCR mixture) turbidity reduction was observed when calcite was added (chapter 5a, section 5.3.3). As reported in section 5.3.3 (chapter 5a), increases in pH and calcium concentration were observed over time in the CO_2-treated columns implying that calcite dissolution was occurring. The water chemistry profile and solution pH at equilibrium of the calcite-containing columns were calculated using PHREEQCi program. In most tested columns, the solution pH matched the predicted values (Table 5-6); however, the measured pH values were substantially lower than expected for three of the columns. The pH values for the other columns were all higher than, or similar to, the pH that was expected (Table 5-6). The measured calcium concentration was approximately 10 times lower than the predicted concentration in the 80/20+CO_2+0.5g calcite column on day 42 of the experimental period. Even after extending the experimental period to 91 days, the calcium concentration was 4 times lower than the predicted value in the 60/40+CO_2+0.5g calcite column (Table 5-6).

Table 5-6 A comparison of calcite dissolution simulation and experimental results.

	Calcite (simulation parameters)			Solution parameters				
	Initial ($x10^{-3}$ mole)	Final ($x10^{-3}$ mole)	Saturation Index	Simulated final pH	Measured pH	Ca^{2+} ($x10^{-5}$ mole)	Simulated Ca^{2+} (mg)	Measured Ca^{2+} (mg/L)
80/20-noCO_2+0.5g calcite	5	5.2	0	8.5	8.6 (Day 42)	5.6	5.6	7.3 (Day 42)
80/20+CO_2+0.5g calcite	5	0	−0.05	6.3	6.4 (Day 42)	420	420.4	40.6 (Day 42)
80/20-noCO_2+1g calcite	10	10	0	8.3	8.5 (Day 42)	8.8	8.8	12.9 (Day 42)
80/20+CO_2+1g calcite	10	5.6	0	6.4	6.4 (Day 42)	380	380.3	69.0 (Day 42)
60/40-noCO_2+0.5g calcite	5	5.3	0	8.6	9.4 (Day 91)	5	5.1	6.6 (Day 91)
60/40+CO_2+0.5g calcite	5x10-3	4.5 x10-03	0	6.3	7.3 (Day 91)	4.6 x10-03	460.4	100.8 (Day 91)

These results suggest that neither solution nor calcite equilibria had been reached. One of the possible reasons for the apparent delay in reaching equilibria could be due to some parameters not being considered in the thermodynamic calculation performed by the PHREEQCi program. The calcite dissolution rate can be limited by 1) the slow conversion of CO_2 to $H_2CO_3°$, 2) the accumulation of dissolved species (i.e., Ca^{2+} and HCO_3^-) around the calcite surface and 3) a reduction in the surface reaction kinetics of calcite (Buhmann & Dreybrodt, 1987). The effect of the slow conversion of CO_2 to $H_2CO_3°$ was minimized through 1) an increase in CO_2 residency time in a solution with microbubbles (section 5.3.3), 2) allowing CO_2 to be equilibrated (~16 hours) within the water mixture prior to the experiment and 3) the addition of CO_2 equilibrated water to the calcite-containing experimental columns. A transport parameter was not used during the PHREEQCi calculation; therefore, accumulations of dissolved Ca^{2+} and HCO_3^- were assumed. Several studies have reported on the inhibitory effects on the calcite dissolution with

high magnesium (Mg^{2+}) and sulfate (SO_4^{2-}) concentrations (Alkattan et al., 2002; Buhmann & Dreybrodt, 1987; Compton & Brown, 1994; Gledhill & Morse, 2006; Pokrovsky et al., 2005; Sjöberg, 1978).

A reduction in surface reaction kinetics has been considered a contributor to the inhibitory effects on calcite dissolution (Gledhill & Morse, 2006; Song et al., 2017). Several studies have reported that an ionic strength below 1 M (NaCl was used) had a minor effect on the calcite dissolution rate (Buhmann & Dreybrodt, 1987; Pokrovsky et al., 2005). Contrasting results have been reported for the effect of magnesium ions on calcite dissolution (Alkattan et al., 2002; Buhmann & Dreybrodt, 1987; Compton & Brown, 1994; Gutjahr et al., 1996; Sjöberg, 1978). Finally, a high SO_4^{2-} (1–2.7 g/L) concentration has been observed to negatively affect calcite dissolution (Compton & Brown, 1994; Gledhill & Morse, 2006; Sjöberg, 1978).

Yearly addition of BCR water to the BML has been undertaken to simulate freshwater input from neighbouring reclaimed landforms (Dompierre et al., 2016). Typically, the BCR water has low salt (NaCl) and SO_4^{2-} concentrations, while its Mg^{2+} and Ca^{2+} concentrations are similar to those of OSPW (Poon et al., 2018). Thus, the BCR water added to the BML is likely to have relatively low NaCl and SO_4^{2-} concentrations. Since only minor effects of NaCl on calcite dissolution have been reported, the objective in this chapter is to examine the effect of SO_4^{2-} on calcite dissolution.

5.7 Materials and Methods

A detailed description of the materials and methods used in this experiment was presented in chapter 5a section 5.2. Thus, only the experimental setup is described in this section.

To investigate the impact of sulfate on calcite dissolution, synthetic BML (SBML) water with either a 400 mg/L or 50 mg/L SO_4^{2-} concentration was used in a 1 L column-based experiment (Table 5-7). To test the effects on calcite dissolution, two different calcite amounts (0.05 & 0.5 g) were used in the small-column experiment (Table 5-7).

Table 5-7 Summary of calcite dissolution experimental setup in synthetic BML water

	400 mg/L SO_4^{2-}	50 mg/L SO_4^{2-}	CO_2	Calcite	Duplicate
400SBML-noCO_2	✓				
400SBML+CO_2	✓		✓		
400SBML-noCO_2+0.5g calcite	✓			0.5 g	✓
400SBML-CO_2+0.5g calcite	✓		✓	0.5 g	✓
400SBML-noCO_2+0.05g calcite	✓			0.05 g	✓
400SBML-CO_2+0.05g calcite	✓		✓	0.05 g	✓
50SBML-noCO_2		✓			
50SBML+CO_2		✓	✓		
50SBML-noCO_2+0.5g calcite		✓		0.5 g	✓
50SBML-CO_2+0.5g calcite		✓	✓	0.5 g	✓
50SBML-noCO_2+0.05g calcite		✓		0.05 g	✓
50SBML-CO_2+0.05g calcite		✓	✓	0.05 g	✓

5.8 Results and Discussion

Similar to the observations described in chapter 5a, section 5.3.3, in the current experiment, the CO_2 treatment initially lowered the solution pH, which, subsequently, gradually increased over the 126 day experimental period (Figure 5-12a & b). Elevated alkalinity was observed in the CO_2+calcite columns (0.5 g and 0.05 g calcite; Figure 5-12c & d). Despite similar initial alkalinity levels, generally higher alkalinity concentrations were observed in the 400 mg/L SO_4^{2-} concentration columns than in the 50 mg/L SO_4^{2-} columns (Figure 5-12c & d). While no

significant changes in sulfate and other ion concentrations were observed in the 400SBML and 50SBML columns (Figure 5-12g & h, and Figure A-5), the dissolved calcium ion concentrations displayed an interesting pattern (Figure 5-12e & f); an approximately 80% reduction in Ca^{2+} ion concentration was observed in the 50SBML-noCO_2+0.5g calcite and 400SBML-noCO_2+0.5g calcite columns (Figure 5-12f). These results suggest that calcite precipitation may occur under the conditions present in these columns. With respect to the CO_2-treated columns, there were 152% and 163% increases in Ca^{2+}concentration in the 50SBML-CO_2+0.5g calcite (days 0–63) and 400SBML-CO_2+0.5g calcite (days 0–84) columns, respectively (Figure 5-12e).

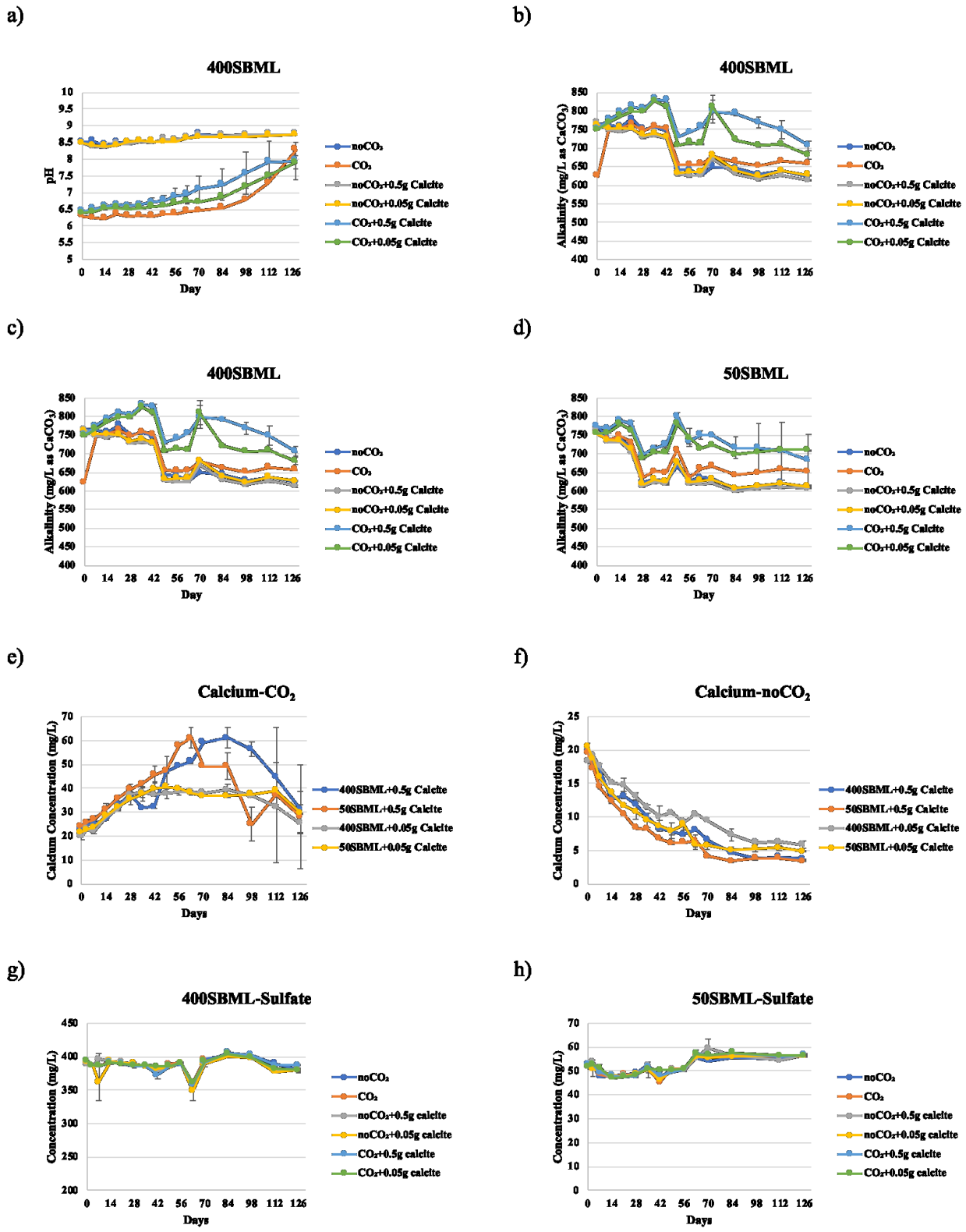

Figure 5-12 Water chemistry results for 1 L column calcite dissolution experiments performed with synthetic BML water.

There were no significant differences (p = 0.4) in the increases in Ca^{2+} concentration between the 400SBML-CO_2+0.5g calcite and 50SBML-CO_2+0.5g calcite columns. However, to reach the maximum Ca^{2+} concentration took two weeks longer in the 400SBML-CO_2+0.5g calcite column than in the 50SBML-CO_2+0.5g calcite column (Table A6). Indeed, statistical analysis from Figure 5-12e showed that a significant difference in day 63 peak was observed compared to Day 36 and 91 peaks for 40SBML+0.5g calcite CO_2 treated column (Table A6). A higher statistical significance was observed for Day 84 peak compared to the Day 42 and 126 peaks (Table A6). These analyses suggested that a significant increase in Ca^{2+} concentration in day 63 for 50-SBML-CO_2+0.5g calcite column, and that day 84 for 400SBML-CO_2+0.5g calcite column. This result suggests the possibility that a high SO_4^{2-} concentration could affect calcite dissolution kinetics. On that basis, calcite dissolution rates were calculated based on the obtained Ca^{2+} concentration.

With respect to the 400SBML-CO_2+0.5g calcite column, the calculated calcite dissolution rate between days 42 and 49 (Δ49-42; 5.2×10^{-5} mol/L/d) was discarded due a significant rate reduction between days 28 and 35 (Δ35-28; -2×10^{-5} mol/L/d; Figure 5-13). As a result, the 2.9×10^{-5} mol/L/d calcite dissolution rate between days 63 and 70 (Δ70-63) for the 400SBML-CO_2+0.5g calcite column was chosen for the comparison of dissolution rates among the columns. For the 50SBML-CO_2+0.5g calcite column, a 3.8×10^{-5} mol/L/d calcite dissolution rate was observed between days 49 and56 (Δ56-49; Figure 5-13). A 0.3-fold (23.6%) higher dissolution rate was observed for the 50SBML-CO_2+0.5g calcite column (days 49-56) than for the 400SBML-CO_2+0.5g calcite column (days 63-70). This result is consistent with previous observations made by Gledhill and Morse (2006), who reported a 20% reduction in the calcite dissolution rate in a solution that contained 1 g/L SO_4^{2-}. Taken together, these results and those

in the current study suggest that calcite dissolution occurs sooner at lower SO_4^{2-} concentrations (50 mg/L) in the presence of 0.5 g calcite. However, a clear calcite dissolution pattern was not detected for columns containing 0.05 g calcite at either the 400 mg/L or 50 mg/L SO_4^{2-} concentration (Figures 5-12e and 5-13). The dissolution of 0.05 g calcite resulted in an increase in Ca^{2+} concentration (~35 mg/L) at 28 days, with a subsequent but smaller increase also being observed. One possible explanation for that observation is that the inhibitory effect of SO_4^{2-} increases as the Ca^{2+} and Mg^{2+} concentrations increase (Gledhill & Morse, 2006). The results presented in this chapter suggest that a >35 mg/L Ca^{2+} concentration may be needed to increase the SO_4^{2-} inhibitory effect on calcite dissolution.

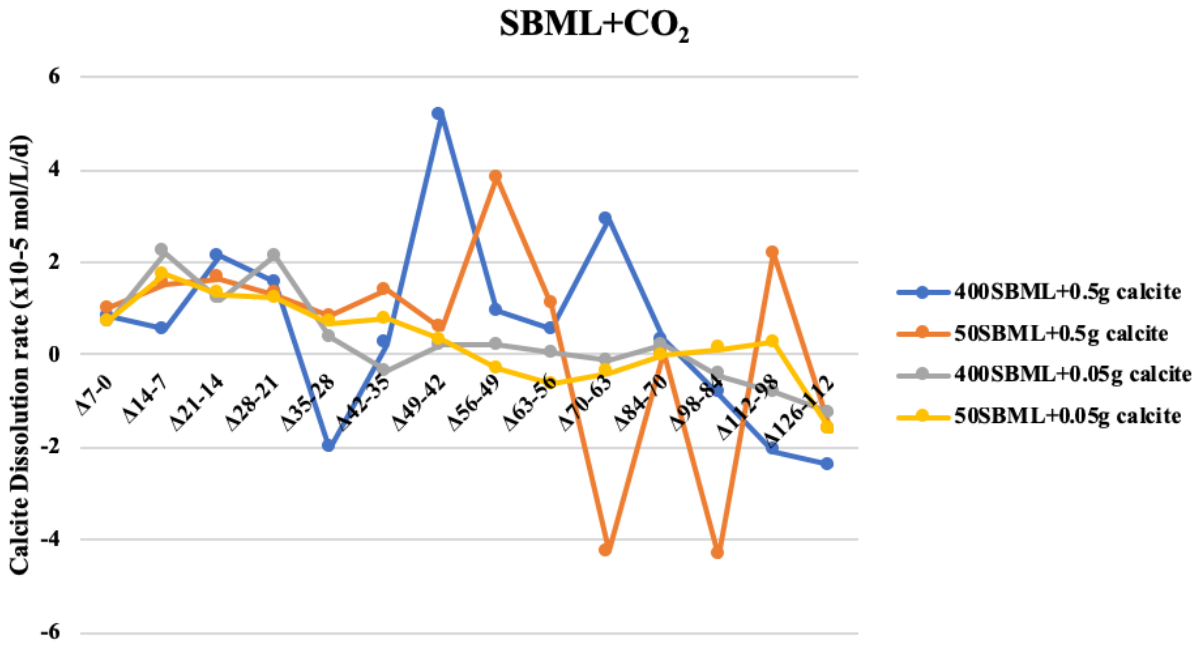

Figure 5-13 Calculated calcite dissolution rate in synthetic BML water used for the 1 L column experiments. Note: The calcite dissolution rate was calculated from the dissolved calcium concentration result under the assumption that the measured concentration reflects the dissolution event.

The experimental data presented in this section indicate that a high sulfate concentration (400 mg/L) delays calcite dissolution. Previous research studies have shown that high sulfate

concentrations (~2.7 g/L and 1 g/L SO_4^{2-}) can reduce calcite dissolution by approximately 40% and 20%, respectively (Gledhill & Morse, 2006; Sjöberg, 1978). Those two studies were conducted in water with approximately 2–4 times higher SO_4^{2-} concentrations and much higher salinity levels than those in the BML water. The calcite dissolution inhibition mechanism is thought to involve adsorption of SO_4^{2-} anions to the calcite surface, which could prevent further calcite surface reactions (Gledhill & Morse, 2006; Song et al., 2017).

5.9 Conclusion

Calcite dissolution triggered by a CO_2-mediated pH reduction was described in chapter 5a; however, a lower dissolution rate, by at least one order of magnitude, than the rates reported previously was observed. By using the PHREEQC computer simulation program, the BML-BCR mix water chemistry profile at equilibrium was calculated. Although the theoretically calculated pH values were similar to the experimental values, a significant discrepancy in Ca^{2+} ion concentration was detected between the calculated and measured values. Several studies have shown that a high SO_4^{2-} concentration can inhibit or reduce calcite dissolution (Compton & Brown, 1994; Gledhill & Morse, 2006; Sjöberg, 1978). On that basis, the inhibitory effect of SO_4^{2-} on calcite dissolution was tested in SBML water with 400 mg/L or 50 mg/L sulfate concentrations. A higher calcite dissolution rate (3.8×10^{-5} mol/L/d, Δ49-42) was observed in SBML water containing 50 mg/L sulfate than that (2.9×10^{-5} mol/L/d; Δ70-63) in SBML water containing 400 mg/L sulfate. These results suggest that a high (400 mg/L) SO_4^{2-} concentration can reduce the calcite dissolution rate in SBML water by approximately 23%.

5.10 Reference

Alkattan, M., Oelkers, E. H., Dandurand, J. L., & Schott, J. (2002). An experimental study of calcite dissolution rates at acidic conditions and 25 degrees C in the presence of NaPO3 and MgCl2. *Chem Geol, 190*(1-4), 291-302.

Buhmann, D., & Dreybrodt, W. (1987). Calcite Dissolution Kinetics in the System H2o-Co2-$CaCO_3$ with Participation of Foreign Ions. *Chem Geol, 64*(1-2), 89-102.

Compton, R. G., & Brown, C. A. (1994). The Inhibition of Calcite Dissolution Precipitation - Mg2+ Cations. *J Colloid Interface Sci, 165*(2), 445-449.

Dompierre, K. A., Lindsay, M. B. J., Cruz-Hernandez, P., & Halferdahl, G. M. (2016). Initial geochemical characteristics of fluid fine tailings in an oil sands end pit lake. *Sci Total Environ, 556*, 196-206.

Gledhill, D. K., & Morse, J. W. (2006). Calcite dissolution kinetics in Na-Ca-Mg-Cl brines. *Geochim Cosmochim Acta, 70*(23), 5802-5813.

Gutjahr, A., Dabringhaus, H., & Lacmann, R. (1996). Studies of the growth and dissolution kinetics of the CaCO3 polymorphs calcite and aragonite II. The influence of divalent cation additives on the growth and dissolution rates. *J Cryst Growth, 158*(3), 310-315.

Pokrovsky, O. S., Golubev, S. V., & Schott, J. (2005). Dissolution kinetics of calcite, dolomite and magnesite at 25 degrees C and 0 to 50 atm pCO(2). *Chem Geol, 217*(3-4), 239-255.

Poon, H. Y., Brandon, J. T., Yu, X. X., & Ulrich, A. C. (2018). Turbidity Mitigation in an Oil Sands Pit Lake through pH Reduction and Fresh Water Addition. *J Environ Eng, 144*(12).

Sjöberg, E. L. (1978). *Kinetics and mechanism of calcite dissolution in aqueous solutions at low temperatures.* (Doctoral thesis) Almqvist & Wiksell. p.92

Song, J., Zeng, Y. C., Wang, L., Duan, X. D., Puerto, M., Chapman, W. G., Biswal, S., Hirasaki, G. J. (2017). Surface complexation modeling of calcite zeta potential measurements in brines with mixed potential determining ions (Ca2+, CO32-, Mg2+, SO42-) for characterizing carbonate wettability. *J Colloid Interface Sci, 506*, 169-179.

Chapter 5 c: The effect of dolomite dissolution on CO_2-mediated turbidity reduction

5.11 Introduction

In addition to calcite dissolution, dissolution of another carbonate mineral, i.e., dolomite ($MgCa(CO_3)_2$; Equation 5-2), was hypothesized to have occurred in the BML water (Dompierre et al., 2016).

$$CaMg(CO_3)_2 + 2CO_2 \leftrightarrow Ca^{2+} + Mg^{2+} + 4HCO_3^- \quad \text{(Equation 5-2)}$$

Dompierre et al. (2016) reported XRD and pore water chemistry (i.e., dissolved Ca^{2+} and Mg^{2+} concentrations) results for BML water, and their results were suggestive of the depletion of dolomite mineral in the BML water. Thus, the objective in chapter 5c is to examine 1) the effect of dolomite dissolution on BML water turbidity reduction and 2) whether the CO_2-mediated turbidity reduction in BML water can be enhanced by adding a mixture of dolomite and calcite.

5.12 Materials and Methods

Information on the materials used and the experimental methods has been provided in section 5.2 (chapter 5a). A sample of dolomite crystal (dolomite-1; a kind gift from the geology student laboratory in the Department of Earth and Atmospheric Science, University of Alberta) was used in the experiments in this chapter. The dolomite-1 crystal was crushed and sieved to a 45–75 µm size, and the crushed dolomite-1 was characterized as described in section 5.2. A sample of bulk dolomite rock (dolomite-2) was a kind gift from Dr. Matthew Lindsay, University of Saskatchewan. The dolomite-2 sample was crushed and sieved to a 45–75 µm size, and the crushed dolomite-2 was characterized as described in section 5.2.

The crushed and sieved dolomite products were used to determine if the addition of a mixture of dolomite and calcite can enhance turbidity reduction in a 60% OSPW and 40% BCR water solution (60/40 water) when CO_2 is added. The dolomite-1 experiment was performed in

duplicate; approximately 0.5 g of carbonate mineral (dolomite-1) was tested in 60/40 water with and without CO_2 added . The dolomite-2 experiment was performed in duplicate; approximately 0.5 g of carbonate mineral (dolomite-2 and/or calcite) were tested in 60/40 water with and without CO_2 added (Table 5.8). The results were compared with the results obtained from the calcite and dolomite dissolution experiments in sections 5.3.3 (chapter 5a) and 5.13 (chapter 5c).

Table 5-8 Summary of mixed carbonate mineral (dolomite-2 and calcite) dissolution experimental setup.

Columns	Dolomite (g)	Calcite (g)
60/40-noCO_2-1	0	0
*60/40-noCO_2-2	0	0
60/40-CO_2-1	0	0
60/40-CO_2-2	0	0
100% dolomite-2-noCO_2-1	0.502	0
100% dolomite-2-noCO_2-2	0.503	0
100% dolomite-2-CO_2-1	0.501	0
100% dolomite-2-CO_2-2	0.504	0
50% dolomite-2-noCO_2-1	0.249	0.251
50% dolomite-2-noCO_2-2	0.251	0.251
50% dolomite-2-CO_2-1	0.251	0.25
50% dolomite-2-CO_2-2	0.25	0.249
25% dolomite-2-noCO_2-1	0.126	0.377
25% dolomite-2-noCO_2-2	0.125	0.376
25% dolomite-2-CO_2-1	0.127	0.377
25% dolomite-2-CO_2-2	0.127	0.376
0% dolomite-2-noCO_2-1	0	0.5
0% dolomite-2-noCO_2-2	0	0.503
0% dolomite-2-CO_2-1	0	0.499
0% dolomite-2-CO_2-2	0	0.5

* The 60/40-noCO_2-2 column was discarded after day 7 due to column leakage.

5.13 Results and Discussion

The purity of the crushed dolomite-1 sample (45–75 µm) was confirmed by XRD and SEM-EDS analyses (Figure 5-14a &d). The SEM images revealed that the majority of the crushed dolomite-1 particles were within the 45–75 µm size range (Figure 5-14b & c).

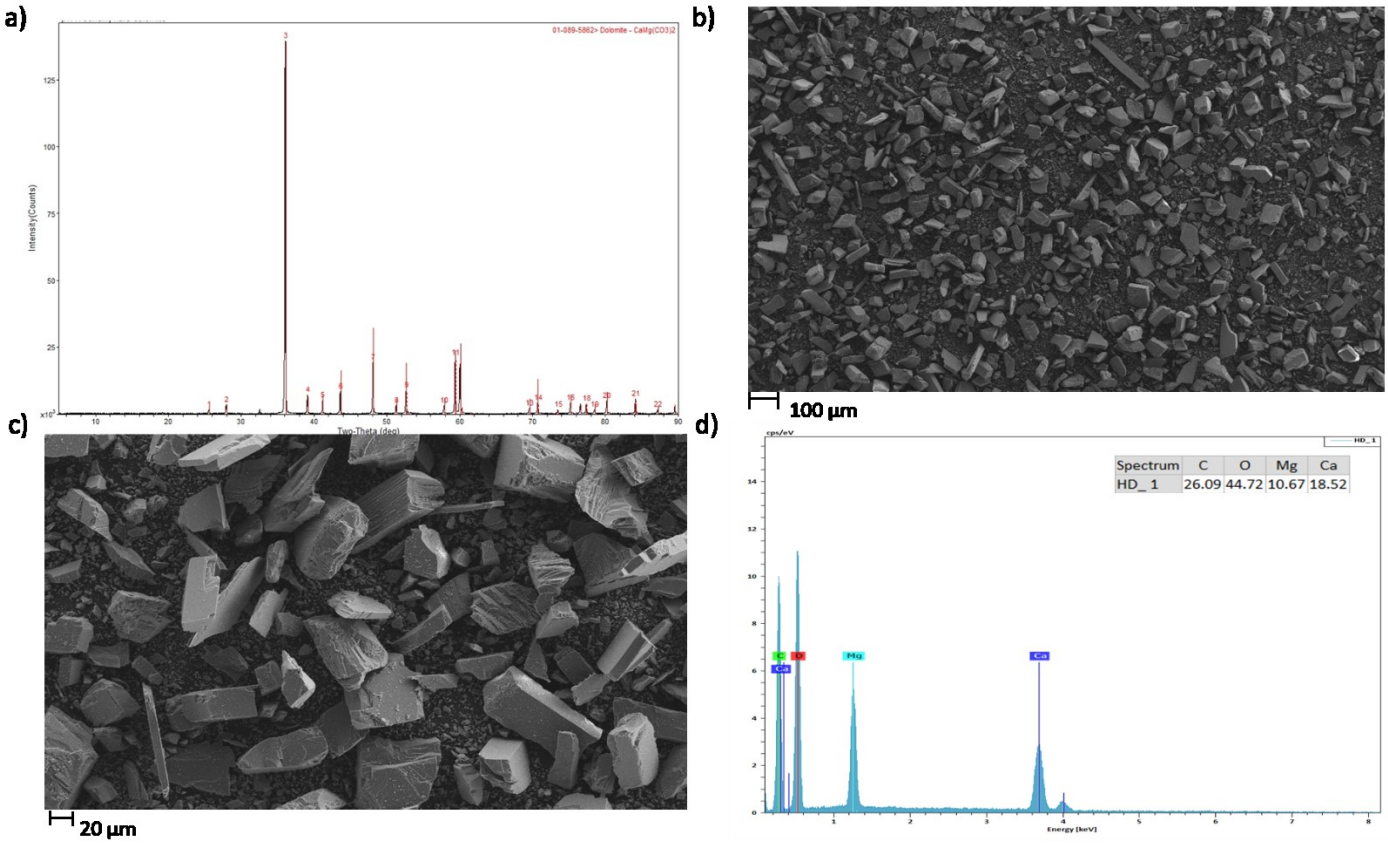

Figure 5-14 Characterization of crushed dolomite-1 crystal (45–75 µm) based on a) XRD and b-d) SEM-EDS results. Note: An enlarged version of the dolomite-1 XRD result is presented in the appendix (Figure A-6).

Crushed dolomite-1 samples were used in the 1 L column-based experiment, and various experimental parameters were monitored over a period of 70 days. Between days 0 and 14, pH reduction was observed in the 60/40-CO_2+0.5g-dolomite-1 column, whereas an increase in pH (from 6.3 to 7.1) was observed from day 28 to day 70 (Figure 5-15a). In addition, an increase in

alkalinity from 465 to 500 mg/L (as $CaCO_3$) was observed in the 60/40-CO_2+0.5g-dolomite-1 column (Figure 5-15b). These results suggest that dolomite dissolution likely occurred upon the addition of CO_2 conditions. With respect to the 60/40-noCO_2+0.5g-dolomite-1 column, only a minor change was detected in pH and alkalinity levels (Figure 5-15a & b). A 93.6% turbidity reduction was observed in 60/40-CO_2+0.5g-dolomite-1 column compared to a 90.1% turbidity reduction in the 60/40-noCO_2+0.5g-dolomite-1 column (Figure 5-15c). However, due to limited in sample size a statistical significance in turbidity for 60/40-noCO_2+0.5g-dolomite-1 column and for 60/40-CO_2+0.5g-dolomite-1 columns cannot be established (*p*-value = 0.4). Interestingly, a minor reduction in zeta potential (from −33.4 to −28.9 mV) was observed in the 60/40-CO_2+0.5g-dolomite-1 column in the initial 28 days, but an increase was observed after 28 days with the zeta potential reaching ~ −32 mV on day 70 (Figure 5-6d). Taken together these results suggested that dolomite dissolution occurred in the 60/40-CO_2+0.5g-dolomite-1 column during the first 28 days of the experimental period. Indeed, increases in both dissolved Mg^{2+} and Ca^{2+} concentrations were detected during the same period in the 60/40-CO_2+0.5g-dolomite-1 column (Figure 5-16f & g). The estimated dolomite dissolution rate between days 0 and 4 was 6.2×10^{-6} M/d, based on the assumption that the molar concentration of the dissolved Ca^{2+} and Mg^{2+} are equal to the molar concentration of the dissolved dolomite (Figure 5-16h). A sharp decline in the rate of dolomite dissolution was observed after day 14 (Figure 5-16h). The turbidity reduction observed in the 60/40-CO_2+0.5g-dolomite-1 column (93.6%, Table 5-9) after day 56 of the experiment was comparable to the turbidity reduction in the 60/40-CO_2 column without the addition of carbonate material (95.4%, Table 5-4).

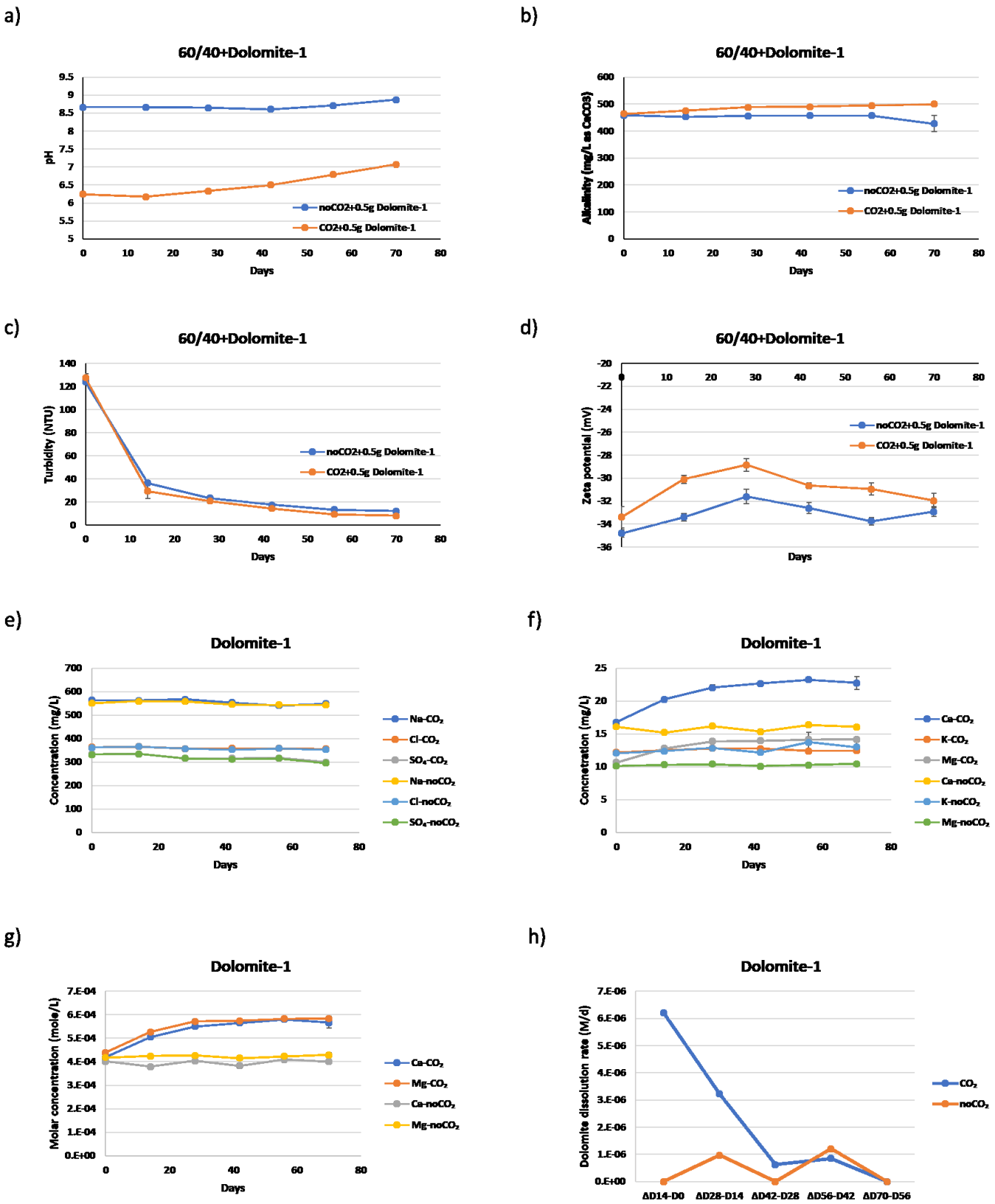

Figure 5-15 Physical and chemical results from the dolomite-1 dissolution experiment. Note: Averaged values are plotted and the error bars represe-nt the standard error.

Table 5-9 Summary of turbidity changes in the dolomite-1 dissolution experiment

	Initial (NTU)	Final (NTU) (day 56)	Percent change (%)
60/40+0.5g dolomite-1-noCO_2	124	12.3	90.1
60/40+0.5g dolomite-1+CO_2	127.5	8.2	93.6

To determine whether the turbidity reduction can be enhanced by adding a mixture of calcite and dolomite, a series of experiments were performed in which 100%, 50%, 25% and 0% dolomite-2 was supplemented with 0%, 25%, 50% and 100% calcite, respectively, to obtain a total of 0.5 g carbonate material (Table 5-8). Based on the XRD-based characterization of the crushed dolomite-2 sample, two possible minerals were identified, dolomite ($CaMg(CO_3)_2$) and ankerite ($Ca(Fe, Mg, Mn)(CO_3)_2$; Figure 5-16a); however, only Ca, Mg, C, Si and O elements were detected by the SEM-EDS analysis (Figure 5-16d). The SEM images showed that the majority of the crushed dolomite-2 particles were within the 45–75 μm size range.

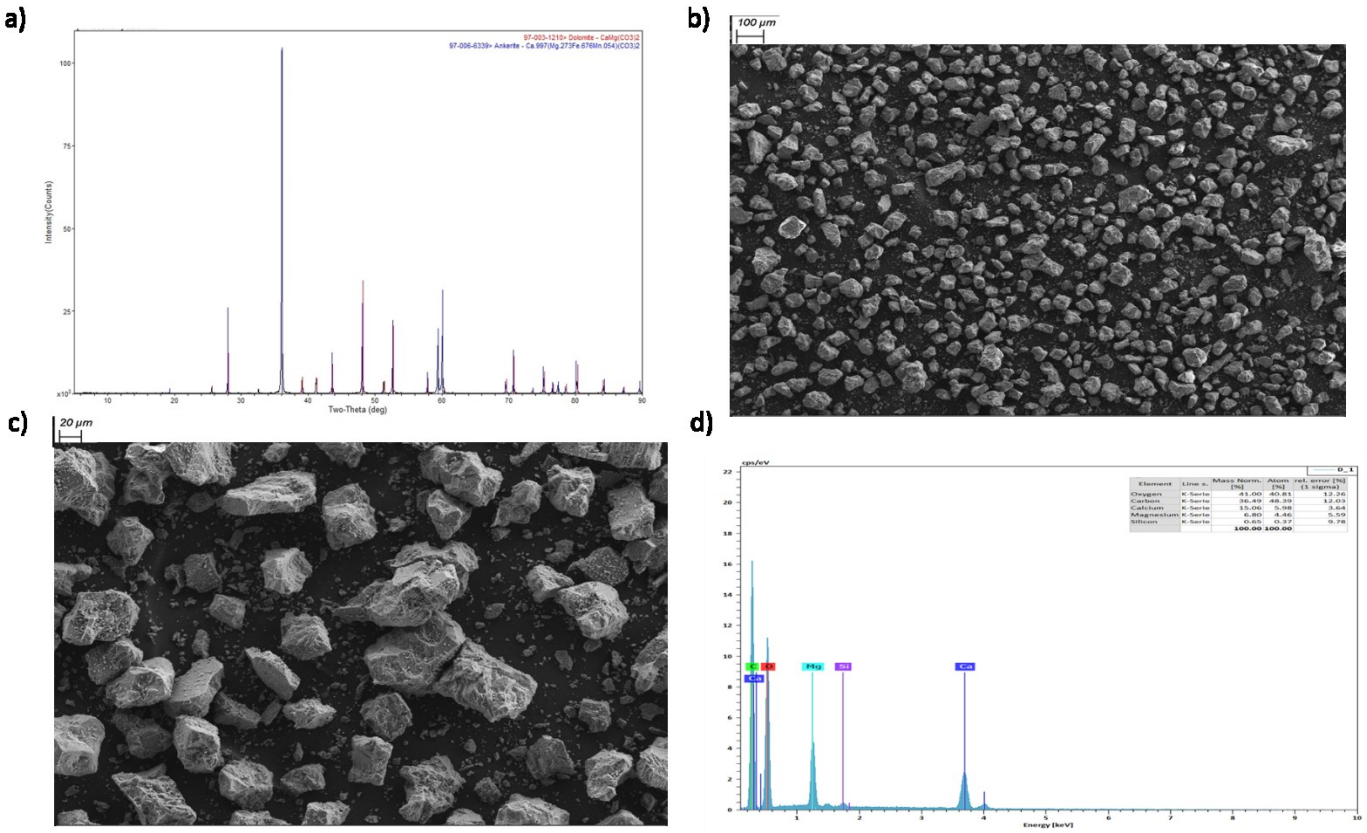

Figure 5-16 Characterization of crushed dolomite-2 (45–75 µm) based on a) XRD and b-d) SEM-EDS results. Note: An enlarged version of the dolomite-2 XRD result is presented in the appendix (Figure A-7).

As demonstrated by the stable water chemistry in the noCO_2 control columns throughout the experimental period, no carbonate mineral dissolution was apparent in those columns. Consistent pH, alkalinity, and zeta potential levels were observed in the noCO_2 control columns over the 84 day experimental period (Figure 5-17a). These observations are consistent with the report that calcite becomes supersaturated (in other words, it precipitates) when the pH of a solution rises (Zhang & Dawe, 1998). Indeed, after re-interpreting the 60/40-noCO2 column results obtained by Brandon (2016), the current results indicate oversaturation of both calcite and dolomite (Table 5-1, chapter 5a, section 5.3.1).

A decrease in pH was observed in all CO_2-treated columns regardless of the addition of calcite or dolomite (Figure 5-17b); moreover, throughout the experiment increases in pH levels were observed for all CO_2-treated columns. Carbonate mineral dissolution was likely promoted by the reducing solution pH conditions, such as those in the CO_2-treated columns (e.g., pH 6.1–6.3).

The degree of increase in solution pH appeared to follow a pattern, i.e., there was a higher degree of pH increase with a lowering of the amount of dolomite added (pH with 0% dolomite > pH with 25% dolomite > pH with 50% dolomite > pH with 100% dolomite; Figure 5-17b). While a stable alkalinity level was observed for the noCO_2 control columns, a marked alkalinity increase with a decreasing amount of dolomite was observed for all columns, except for the alkalinity level in the 50%-dolomite-2-CO_2 column (Figure 5-17d). Overall, these results were indicative of the occurrence of carbonate mineral (calcite and dolomite) dissolution. The varying degrees of increases in pH and alkalinity are likely attributed to the possibility that less dolomite was dissolved compared to the amount of calcite dissolved. Indeed, many experimental studies have reported that dolomite has approximately 10–20 times slower dissolution kinetics than calcite

(Appelo et al., 1984; Busenberg & Plummer, 1982; Chou et al., 1989; Pokrovsky & Schott, 2001).

The effect of the change in solution chemistry due to carbonate mineral dissolution was apparent in both the water turbidity and the zeta potential measurements. The turbidity reductions (89%–91%) were similar among the noCO_2 columns regardless of the presence of dolomite (Figure 5-17e and Table 5-10). The carbonate-containing columns (i.e., 100%–0%-dolomite-2-CO_2 with 0%–100% calcite) showed high percentage turbidity reductions (~98%) compared to the reductions in the 60/40-CO_2-only column (~95%; Figure 5-17e and Table 5-10). A 97% turbidity reduction was observed for the 100%-dolomite-2 column, which was lower than the reductions in the 0%-, 25%-, and 50%-dolomite columns, which had turbidity reductions of 98%, 98% and 99%, respectively (Table 5-6). Interestingly, the final turbidity measurement for the 100%-dolomite-2 column (4.4 NTU) was almost twice that for the 0%-dolomite-2 column (2.4 NTU; Table 5-10). A similar trend was observed in the results of zeta potential measurements; the less dolomite-2 present the less negative the resulting zeta potential measurement (Figure 5-17g & h). However, due to limited in sample size statistical significance in turbidity reduction between 100%– and 0%-dolomite-2-CO_2 (p-value = 0.4) cannot be established, and increase in sample size should be included in future research.

In order to verify the occurrence of dolomite and/or calcite dissolution, dissolved ion levels were measured. A stable dissolved ion concentration was observed for the noCO_2 control columns over the 98 day experimental period (Figure 5-18a and Figure A-8). Among the CO_2-treated columns, a greater increase in Ca^{2+} ion concentration was observed when the amount of calcite added was increased (Figure 5-18b). However, only the 60/40+CO_2+100%-dolomite-2 column displayed a substantial increase in Mg^{2+} concentration over the 98 day period (Figure 5-18d).

According to equation 5-2, equal Mg^{2+} and Ca^{2+} ion molar concentrations are expected when dolomite dissolution occurs. As expected, the molar concentration ratio for the Mg^{2+} and Ca^{2+} ions was close to unity for the 60/40+CO_2+100%-dolomite-2 column throughout the 98 day experimental period (Figure 5-18g). Taken together, the dissolved ion results were consistent with the pH and alkalinity measurements showing that the dissolution of dolomite occurs more slowly than that of calcite. In addition, an almost two-fold difference in final turbidity was observed for the 100%-dolomite-2-CO_2 column (4.4 NTU) compared to the ~2 NTU observed in columns containing lesser amounts of dolomite (50%, 25%, and 0%). According to Birtwell (2008), surface water turbidity between 3 to 8 NTU has a limited effect on fish predation, with no apparent effect on fish when turbidity is below 3 NTU.

To understand the stability behaviour of the suspended FFT (clay) particles under carbonate mineral dissolution conditions, the Derjaguin-Landau-Verwey-Overbeek (DLVO) theory was applied by incorporating the physical and chemical data from the mixed carbonate mineral experiment. The DLVO theory suggests an explanation of the comprehensive distribution of forces, such as repulsive and attractive forces between two particles, relating to particle separation distances (Derjaguin & Landau, 1993; Li et al., 2008; Missana & Adell, 2000). In the present study, only the electrostatic repulsion and Van der Waals forces were used to calculate the total interaction energy (Derjaguin & Landau, 1993; Li et al., 2008; Missana & Adell, 2000). A gradual decrease in the total interaction energy was observed in all columns from day 0 to day 42 (Figures 5-19 and A5), which is consistent with the observed turbidity reduction pattern (Figure 5-17e & f). Interestingly, for the carbonate mineral-containing columns, an increase in the total interaction energy was observed on day 70 (Figures 5-19 and A6). At a distance of approximately 20 nm between 2 suspended clay particles, the highest total interaction energy

was observed in all tested columns, suggesting that sufficient energy is available to bring the FFT (clay) particles close together. While similar total interaction energy levels were observed for all tested noCO_2 columns, there was a decrease in total interaction energy for the CO_2-treated columns with decreasing amounts of dolomite on day 42 (Figure 5-19e). Indeed, a statistical significant difference in energy barrier (at 20 nm) was observed between 100% dolomite-2-CO_2 and 0% dolomite-2-CO_2 columns (p-value = 0.03) on day 42 (Figure 5-19). An energy barrier value of less than 20 kT was observed for columns that received CO_2 treatment and contained carbonate minerals (dolomite and/or calcite), which indicates that FFT aggregates were likely to form, thereby enhancing settlement of FFT. These results suggest that calcite dissolution lowers the energy barrier for FFT (clay) particles to coagulate/flocculate under a reduced pH condition. However, only the electrostatic repulsion and Van der Waals forces were considered in the DLVO calculations undertaken in this study; thus, these results might not be applicable to a more dynamic condition, such as those present in the BML. Therefore, caution must be exercised when applying the DLVO theory to predict the coagulation/flocculation conditions present in the BML. Moreover, previous research results have been inconsistent, which has led to an expansion of the DLVO theory so that it can include more parameters, such as Lewis acid-base, steric and hydration interaction parameters (Benitez et al., 2007; Grasso et al., 2002).

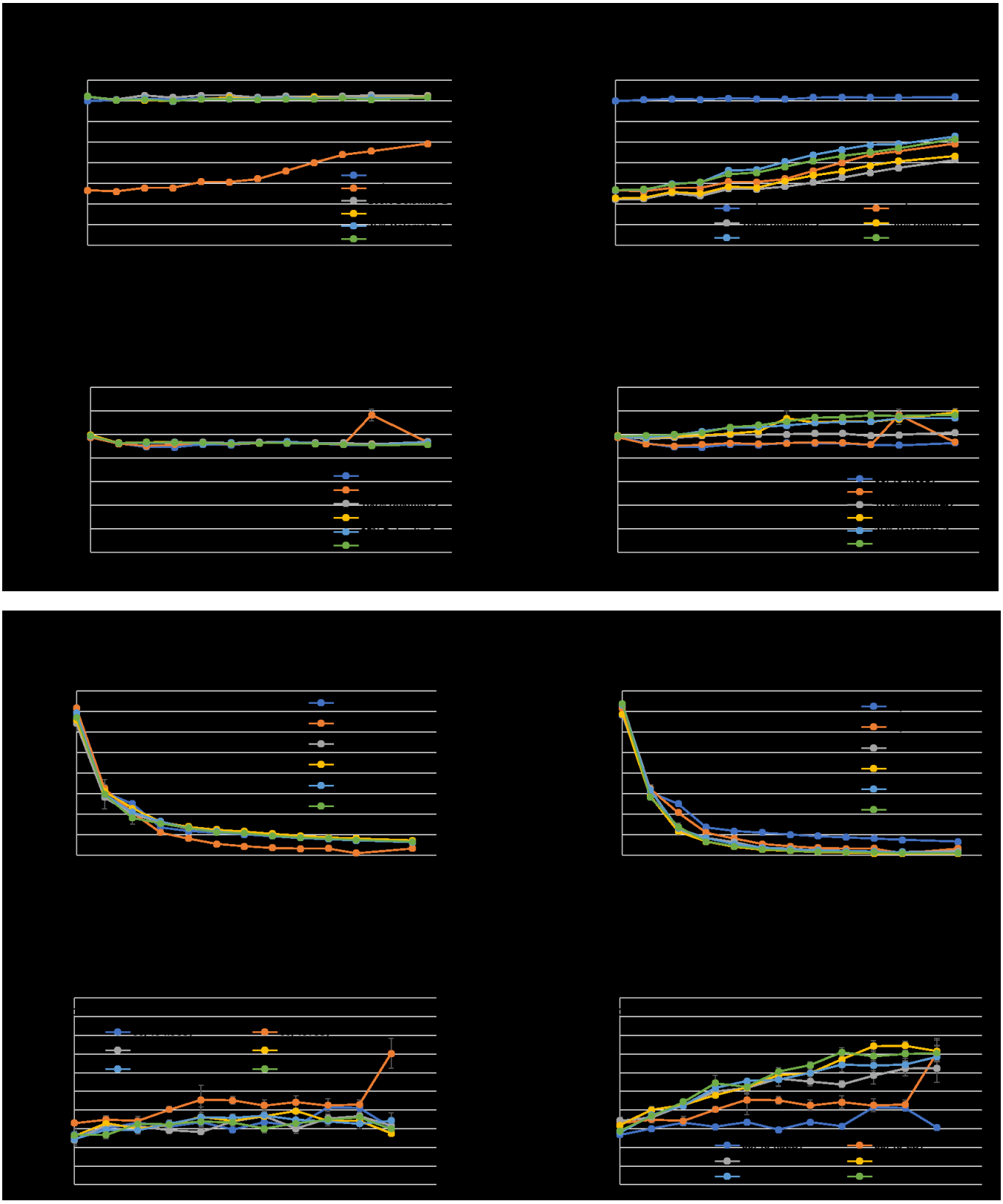

Figure 5-17 Physical and chemical measurements for the mixed carbonate mineral (dolomite and calcite) dissolution experiment. Note: Averaged values are plotted and the error bars represent the standard error.

Table 5-10 Summary of turbidity reduction percentages for the mixed carbonate mineral (dolomite and calcite) dissolution experiment.

Columns	Initial (NTU)	Final (NTU) (Day 56)	Percent change (%)
60/40-noCO_2	136.5	13.4	90.2
60/40-CO_2	143.5	7.045	95.1
100% dolomite-2-noCO_2	128.5	13.05	89.8
100% dolomite-2-CO_2	146.5	4.365	97
50% dolomite-2-noCO_2	131.5	14.6	88.9
50% dolomite-2-CO_2	137.5	2	98.6
25% dolomite-2-noCO_2	139	12.8	90.8
25% dolomite-2-CO_2	146.5	2.635	98.2
0% dolomite-2-noCO_2	134.5	13.6	89.9
0% dolomite-2-CO_2	147.5	2.395	98.4

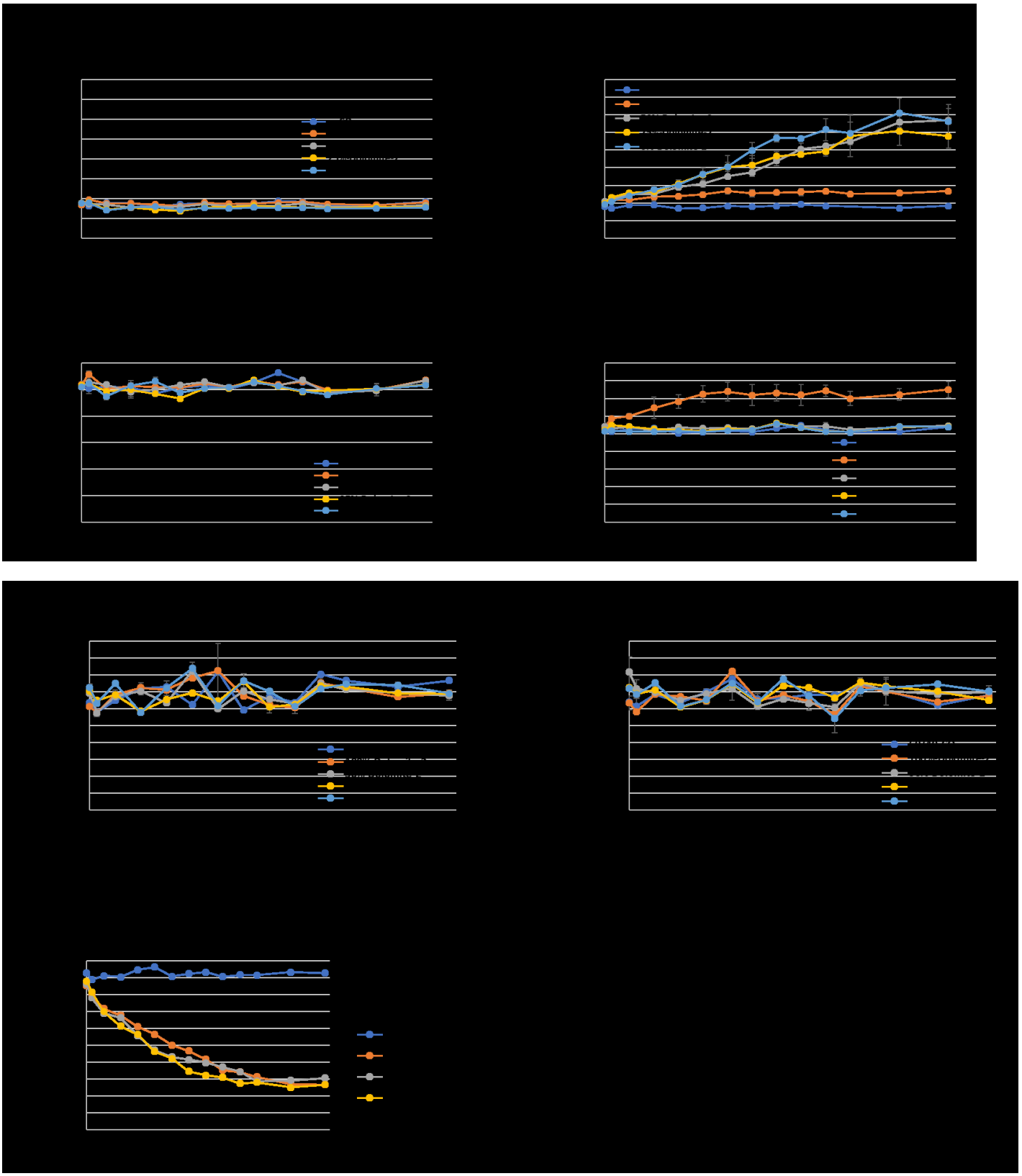

Figure 5-18 Dissolved ion concentrations in the mixed carbonate mineral (dolomite and calcite) dissolution experiment.

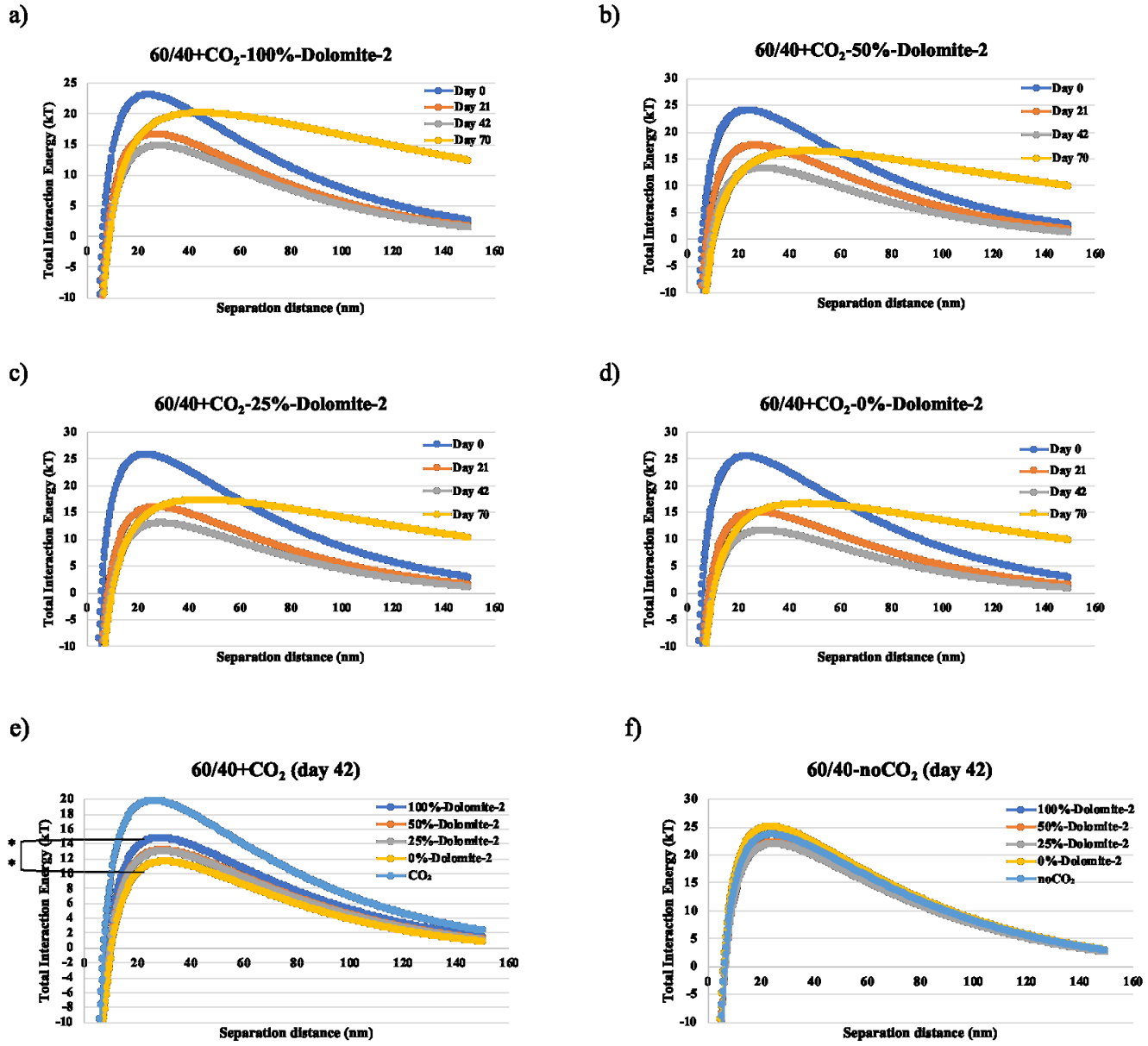

Figure 5-19 Total interaction energy as a function of interparticle distance for CO_2 treatment columns. a) 60/40+CO_2+100%-dolomite-2 column, b) 60/40+CO_2+50%-dolomite-2 column, c) 60/40+CO_2+25%-dolomite-2 column, d) 60/40+CO_2+0%-dolomite-2 column and interaction energy profiles on day 42 for e) CO_2-treated columns and f) noCO_2 columns. ** for *p*-value≤0.01.

Even though dolomite dissolution resulted in final concentrations of 0.5 mM for both Mg^{2+} and Ca^{2+} ions, a more negative zeta potential value was observed for the 60/40+CO_2-100%-Dolomite-2column compared to that for the calcite-containing (50%-, 25%-, and 0%-Dolomite-2) CO_2-treated columns. Results from DLVO modelling also showed that a high calcite concentration resulted in a lower energy barrier to interparticle interaction. This observation can be attributed to the cation exchange (CEC) property of clay. Chorom and Rengasamy (1995) showed a selective CEC preference for the cations released from illite of sodium > potassium > magnesium > calcium. Holden et al. (2012) reported a higher abundance of calcium cations than magnesium cations in clay (kaolinite-illite)-containing sediment samples from Fort McMurray (Alberta). These results suggest that kaolinite and/or illite have a higher adsorption preference for calcium cations than magnesium cations. Indeed, Udo (1978) reported that a calcium-kaolinitic clay arrangement is more thermodynamically stable than a magnesium-kaolinitic clay arrangement and that the calcium exchange for magnesium resulted in an increase in standard free energy and enthalpy changes.

Taken together, results from sections 5.3.3 and 5.3.5 showed that FFT settling can be enhanced by CO_2-mediated pH reduction and carbonate dissolution. Lowering the pH (range 5.8–6 in our experiments) by using CO_2 can reduce the negative surface charge along the edge and octahedral sheet features of a clay particle (Appelo & Postma, 2005; Liu et al., 2013). Thus, the electrostatic repulsion force between suspended clay particles is reduced (Siddique et al., 2014a), and this reduction promotes edge-to-edge and edge-to-face association between particles (Rand & Melton, 1977). On the other hand, CO_2-mediated calcite dissolution resulted in a dissolved calcium ion concentration increase, which increased solution ionic strength and reduced DDL thickness (Siddique et al., 2014a). Due to the combination of pH reduction with the Ca^{2+}

concentration increase, the energy barrier for interparticle interaction was reduced by decreasing the dominance of the electrostatic repulsive force. Under this condition, the Van de Waals attractive interaction between suspended particles is favoured (Li et al., 2008) and particle aggregates can be formed through particle collisions induced by Brownian motion (Elimelech, 1998; Rand & Melton, 1977).

5.14 Conclusion

The stability of suspended clay particles is an important parameter within industrial processes, soil chemistry assessments and environmental research. Knowledge of the particles' stability parameter can provide additional insights for enhanced water recycling from tailings ponds, tailings reclamation and inventory management in oil sands operations. Several studies have demonstrated that dissolved CO_2 plays a role in the settling or densification of oil sands tailings (Brandon, 2016; Ibanez et al., 2014; Poon et al., 2018; Siddique et al., 2014a; Zhu et al., 2011). In addition, carbonate mineral dissolution was hypothesized to be one of the mechanisms active within CO_2-mediated oil sands tailings settling or densification (Siddique et al., 2014a; Siddique et al., 2014b). Thus, the objective in chapter 5c was to examine 1) the effect of dolomite dissolution on BML water turbidity reduction and 2) whether the CO_2-mediated turbidity reduction in BML water can be further enhanced by adding a combination of dolomite and calcite. Addition of crushed dolomite crystal (dolomite-1) produced no significant improvement in turbidity reduction compared to that from CO_2 treatment alone, i.e., 93.6% and 95.4%, respectively. With the addition of a combination of carbonate minerals (calcite and dolomite-2), a slightly higher turbidity reduction was observed in CO_2-treated columns containing a relatively higher level of calcite. Furthermore, a lower total interparticle interaction energy, calculated by applying DLVO theory, was estimated for the CO_2-treated column containing calcite only. These

results suggest that CO_2-induced calcite dissolution could enhance turbidity reduction in BML water; however, the dissolution of calcite was reduced by the high sulfate concentration in the BML water. Taken together, these results are consistent with reports from previous studies showing that 1) CO_2 addition results in a surface charge reduction on clay particles through adsorption of H^+ ions, 2) carbonate mineral dissolution results in increasing the availability of divalent cations (Ca^{2+} and Mg^{2+}), 3) the increase in divalent cation concentrations results in reducing the DDL thickness of the clay particles and 4) the reduction of the DDL thickness results in reduced overall interaction energy thereby promoting coagulation/flocculation processes. Further research is needed to 1) determine the sulfate concentration that would have a minimal effect on carbonate mineral (calcite and dolomite) dissolution and 2) apply an extended DLVO theory to account for additional forces appropriate to the conditions of BML water.

5.15 Reference

Appelo, C. A. J., Beekman, H. E., & Oosterbaan, A. W. A. (1984). Hydrochemistry of springs from dolomite reefs in the southern Alps of northern Italy *IAHS Pub* (Vol. 150, pp. 125-138): IAHS Pub.

Appelo, C. A. J., & Postma, D. (2005). *Geochemistry, groundwater and pollution* (2nd ed.). Leiden ; New York: Balkema.CRC press. 683p

Benitez, E. I., Genovese, D. B., & Lozano, J. E. (2007). Effect of pH and ionic strength on apple juice turbidity: Application of the extended DLVO theory. *Food Hydrocoll, 21*(1), 100-109.

Birtwell, I. K. (2008). The validity of including turbidity criteria for aquatic resource protection in land development guidelines (Pacific and Yukon Region). In M. A. Farrell & A. Jonsson (Eds.). [Ottawa] :: Fisheries and Oceans Canada.

Brandon, J. T. (2016). *Turbidity Mitigation in an Oil Sands End Pit Lake through pH Reduction and Fresh Water Addition.* (Master's thesis), University of Alberta.130p

Busenberg, E., & Plummer, L. N. (1982). The Kinetics of Dissolution of Dolomite in Co2-H2o Systems at 1.5-Degrees-C to 65-Degrees-C and O-Atm to 1-Atm Pco2. *Am J Sci, 282*(1), 45-78.

Chorom, M., & Rengasamy, P. (1995). Dispersion and zeta potential of pure clays as related to net particle charge under varying pH, electrolyte concentration and cation type. *European J Soil Sci, 46*(4), 657-665.

Chou, L., Garrels, R. M., & Wollast, R. (1989). Comparative-Study of the Kinetics and Mechanisms of Dissolution of Carbonate Minerals. *Chem Geol, 78*(3-4), 269-282.

Derjaguin, B., & Landau, L. (1993). Theory of the Stability of Strongly Charged Lyophobic Sols and of the Adhesion of Strongly Charged-Particles in Solutions of Electrolytes. *Prog Mater Sci, 43*(1-4), 30-59.

Dompierre, K. A., Lindsay, M. B. J., Cruz-Hernandez, P., & Halferdahl, G. M. (2016). Initial geochemical characteristics of fluid fine tailings in an oil sands end pit lake. *Sci Total Environ, 556*, 196-206.

Elimelech, M. (1998). *Particle deposition and aggregation : measurement, modelling, and simulation* (Pbk. ed.). [Oxford, [England] ; Boston]: Butterworth-Heinemann.

Grasso, D., Subramaniam, K., Butkus, M., Strevett, K., & Bergendahl, J. (2002). A review of non-DLVO interactions in environmental colloidal systems. *Rev Environ Sci Bio, 1*(1), 17-38.

Holden, A. A., Mayer, K. U., & Ulrich, A. C. (2012). Evaluating methods for quantifying cation exchange in mildly calcareous sediments in Northern Alberta. *Appl Geochem, 27*(12), 2511-2523.

Ibanez, M., Wijdeveld, A., & Chassagne, C. (2014). The Role of Mono- and Divalent Ions in the Stability of Kaolinite Suspensions and Fine Tailings. *Clays and Clay Minerals, 62*(5-6), 374-385.

Li, Q., Jonas, U., Zhao, X. S., & Kapp, M. (2008). The forces at work in collodial self-assembly: a review on fundamental interactions between collodial particels. *Asia-Pac J Chem Eng, 3*(3), 255-268.

Liu, L. Y., Hu, Y., Min, F. F., Zhang, M. X., & Song, S. X. (2013). Characterizations and Stability of Colloidal Coal-Measure Kaolinite in Aqueous Suspensions: A Review. *Surf Rev Lett, 20*(1).

Missana, T., & Adell, A. (2000). On the applicability of DLVO theory to the prediction of clay colloids stability. *J Colloid Interface Sci, 230*(1), 150-156.
Pokrovsky, O. S., & Schott, J. (2001). Kinetics and mechanism of dolomite dissolution in neutral to alkaline solutions revisited. *Am J Sci, 301*(7), 597-626.
Poon, H. Y., Brandon, J. T., Yu, X. X., & Ulrich, A. C. (2018). Turbidity Mitigation in an Oil Sands Pit Lake through pH Reduction and Fresh Water Addition. *J Environ Eng, 144*(12).
Rand, B., & Melton, I. E. (1977). Particle Interactions in Aqueous Kaolinite Suspensions .1. Effect of Ph and Electrolyte Upon Mode of Particle Interaction in Homoionic Sodium Kaolinite Suspensions. *J Colloid Interface Sci, 60*(2), 308-320.
Siddique, T., Kuznetsov, P., Kuznetsova, A., Arkell, N., Young, R., Li, C., Guigard, C., Underwood, E., Foght, J. M. (2014a). Microbially-accelerated consolidation of oil sands tailings. Pathway I: changes in porewater chemistry. *Front Microbiol, 5*, 106.
Siddique, T., Kuznetsov, P., Kuznetsova, A., Li, C., Young, R., Arocena, J. M., & Foght, J. M. (2014b). Microbially-accelerated consolidation of oil sands tailings. Pathway II: solid phase biogeochemistry. *Front Microbiol, 5*, 107.
Udo, E. J. (1978). Thermodynamics of Potassium-Calcium and Magnesium-Calcium Exchange-Reactions on a Kaolinitic Soil Clay. *Soil Science Society of America Journal, 42*(4), 556-560.
Zhang, Y. P., & Dawe, R. (1998). The kinetics of calcite precipitation from a high salinity water. *Appl Geochem, 13*(2), 177-184.
Zhu, R., Liu, Q. X., Xu, Z. H., Masliyah, J. H., & Khan, A. (2011). Role of Dissolving Carbon Dioxide in Densification of Oil Sands Tailings. *Energy & Fuels, 25*(5), 2049-2057.

Chapter 6 : Summary, Engineering Significance and Recommendations for Future Work

6.1 Summary

Increasing focus is being placed upon the management of a vast inventory of oil sands process-affected water (OSPW) and fluid fine tailings (FFT) generated from the surface mining of oil sands. As the Alberta Energy Regulator has directed a 10-year (end of mine life) reclamation timeline for FFT (Directive 085), there is an increasing urgency to turn such mining wastes and associated disturbed lands into a permanent self-sustaining ecosystem. However, the slow FFT dewatering rate and the toxicity of OSPW pose significant technical challenges to the reclamation process. Water capping technology, such as that used for pit lakes (PL), has the potential to produce ecologically sustainable lakes after the closure of open pit mines (Castendyk et al., 2009). Water quality is one of the most important and challenging parameters when establishing a pit lake for FFT, as it can be influenced by geochemical, limnological, hydrological and climatic processes as well as interactions among those factors (Castendyk et al., 2009). A PL with poor water quality can pose significant ecological, environmental and public health risks (Castendyk et al., 2009). In 2012, Base Mine Lake (BML), a full-scale demonstration PL, was commissioned. However, high surface-water turbidity was observed, with the FFT in suspension being a major contributor to that surface-water turbidity. The suspension of FFT was partly due to 1) the ebullition of biogenic gases from degradation of residual organics (i.e., organic chemicals including diluent), 2) the highly stable nature of suspended FFT, namely the highly negatively charged and small size of the clay particles in the FFT and 3) the relatively high pH in the OSPW (~ pH 8). The experiments described in this thesis represent an attempt to 1) identify the impact of naphtha diluent on biogenic gas generation and release of organics from FFT, 2) test the organics removal capacity of an advanced oxidation system that may potentially be used to remove residual organics transported to the surface water of the PL

and 3) examine the mechanism associated with turbidity reduction obtained by using carbon dioxide.

6.2 Conclusions and Engineering Significance

This section provides a conclusion, engineering significance, and recommendations from the research works presented in this thesis.

6.2.1 Effect of Naphtha Diluent on Organic Transport and Microbial Dynamics in Oil Sands Tailings

While several previous studies have investigated biodegradation of organics in oil sands tailings, experiments performed for this thesis provided genetic data to support the chemical observation results and provided indirect evidence that the ebullition of biogenic gases can serve as a mechanism for organic transport from FFT to the mesocosm headspace. This study tested three different naphtha diluent concentrations (0.2%, 0.8% and 1.5% w/v) to represent low, typical and high diluent concentrations. Through functional gene and 16S rRNA sequencing analyses, various members of the sulfate reducing bacteria (SRB) community proliferated between week 0 and week 5. Over that period and within the MFT-PW-0.8% mesocosm, the Desulfobulbaceae increased by 580%, Desulfobacteraceae increased by 260%, Desulfuromonadaceae increased by 100% and Desulfomicrobiaceae increased by 505%. In the same mesocosms, the microbial community shifted to methanogens between week 5 and week 11, with a 380% increase in Methanoregulaceae and a 360% increase in Methanotrichaceae. Moreover, the relative abundance of the microbial community increased with the increase in diluent concentration. The microbial community results were corroborated by the chemical data results obtained from this mesocosm-based study; in the MFT-PW-0.8% mesocosm, both H_2S (5.5 μmol in week 5) and CH_4 (10870 μmol in week 11) were generated. The identification of members of the

Anaerolinealeaceae (*Leptolinea*, *Longilinea* and *Bellilinea*) and Synergistaceae (*Syntrophus* and *Smithella*) families in the MFT samples further suggest the presence of syntrophic relationships among the anaerobic hydrocarbon degraders.

In addition, the level of transport of benzene and toluene from the MFT to the mesocosm headspace was measured. The MFT-PW-0.8% and MFT-SPW-0.8% mesocosms showed the highest benzene and toluene release rates. The benzene release pattern (with the highest release rate of 0.15 μg/mL MFT/d between week 4 and week 6) was supported by the highest increase in H_2S (5.5 μmol) emission observed at week 6 in the MFT-PW-0.8% mesocosm. The toluene release pattern (with the highest release rate of 0.05 μg/mL MFT/d between week 11 and week 15) coincided with the highest increase in CH_4 emission (10870 μmol) at week 11 in the MFT-PW-0.8% mesocosm. These results provide further evidence that anaerobic biodegradation of residual organics present in diluent occurs within the MFT, and that biogenic gas emissions can be a mechanism by which organics, such as benzene and toluene compounds, adsorbed in the FFT be transported to the surface water of a PL.

Engineering significance and recommendations from this research:

- This study examined the effect of naphtha diluent on biogenic gas generation and endogenous microbial dynamics in MFT under an anaerobic condition. Three diluent concentrations were tested (0.2%, 0.8%, and 1.5%) to represent low, typical and high diluent concentrations. Even at the highest naphtha diluent concentration (1.5% w/v) tested, there was no detectable inhibitory (toxic) effect on the microbial communities. In fact, higher microbial activity levels were observed with the 1.5% w/v diluent concentration than with the 0.8% and 0.2% w/v diluent concentrations. This observation

could be important as an increase in diluent concentration may result from tailings pond water reuse. Such reuse may further increase microbial activities within the FFT, and when this FFT is used in future PL construction, it may contribute to increased turbidity over a prolonged period.

- The assessment of benzene and toluene (BT) transport and release from the MFT provided valuable insight into the abiotic organics transport processes from MFT to surface water.
- Similar BT release rates were observed when using the 0.8% and 1.5% diluent concentrations, and the BT release in the mesocosms would exceed that in the Alberta ambient air quality guideline. In addition, at all three diluent concentrations tested, the benzene release in the mesocosms would exceed that in the Alberta ambient air quality guideline.
- Taken together this study provides a foundation useful in the protection of public and environmental health and safety as the results advance our understanding of the mechanisms involved in chemical (organics) transport and BML surface-water turbidity.
- Based on these results, it is recommended that future research efforts be focused on benzene, toluene, ethylbenzene and xylene (BTEX) removal from tailings and/or surface water to improve public and worker health and safety because 1) benzene is a carcinogen and BTEX compounds can affect animal central nervous systems, 2) anaerobic BTEX degradation occur after the degradation of more labile organic compounds thereby increasing the likelihood for transportation of BTEX to surface water and its subsequent release and 3) benzene releases in the experimental mesocosms exceeded the Alberta ambient air quality guideline even in mesocosms with the lowest diluent concentration

(0.2%). To achieve improved public and worker health and safety through reducing BTEX exposure, anaerobic benzene biodegradation efficiency should be improved as benzene is considered recalcitrant under anaerobic conditions; moreover, dissolved BTEX compounds should be removed from surface waters (e.g., OSPW) to control BTEX exposure due to inhalation.

6.2.2 Organic Removal with an Advanced Oxidation System

This dissertation describes the first systematic study on the BTEX adsorptive and BTEX removal capacities of expanded graphite (EG) and describes an EG-based advanced oxidation system (AOS). Based on the results of a batch experiment, hydrophobicity appears to be the EG adsorption mechanism involved in BTEX compound adsorption as EG had higher adsorption preferences for *p*-xylene (37% adsorbed) and ethylbenzene (29% adsorbed) compared to that for benzene (12% adsorbed) and toluene (17% adsorbed). While the application of electricity increased the overall BTEX adsorption in the AOS (i.e., 99% *p*-xylene removal with electricity compared to 45% *p*-xylene removal without electricity), the possible occurrence of iodine-mediated oxidation and presence of its product(s) have yet to be determined. These initial results suggest that direct application of EG or development of an EG-based AOS system might not be effective in removing residual organics from OSPW.

Engineering significance and recommendation from this research are:

- This was the first study to examine the effectiveness of EG and EG-based AOS system on BTEX adsorption and removal respectively.
- The study results provide insights into possible adsorption mechanisms and show some of the possible limitations of using EG and AOS for BTEX adsorption and removal.

- The observations from this study are important not only to oil and gas wastewater applications but also to contaminated drinking water applications.
- Due to its selective nature toward xylene and the requirement for using electricity, the use of an AOS is not recommended for treating the BTEX component of OSPW. The use of adsorbent material was shown to be ineffective in removing BTEX or other organics from oil and gas wastewater; thus, future research should focus on other technologies, such as chemical oxidation.

6.2.3 A Mechanistic Study for Carbon Dioxide-mediated Turbidity Reduction

In the current literature, a few studies have investigated carbon dioxide (CO_2)-mediated tailings dewatering and consolidation, but the exact mechanisms have not been fully elucidated. Both FFT and suspended FFT were identified as sources of calcite; as a result, the effect of CO_2-mediated calcite dissolution on the turbidity of the BML surface water was examined. CO_2-mediated calcite dissolution reduced the BML surface-water turbidity level (99% reduction from an initial 224 NTU) to a greater extent than that from CO_2 treatment alone (95% reduction from an initial 199 NTU). In addition, a high sulfate concentration (~400 mg/L) reduced the calcite dissolution rate by 20%, resulting in calcite dissolution rates of 3.8×10^{-5} mol/L/d (between day 49 and day 56) and 2.9×10^{-5} mol/L/d (between day 63 and day 70) with SO_4^{2-} concentrations of 50 mg/L and 400 mg/L, respectively. The DLVO mathematical modelling process reveals the surface interactions between two colloidal particles based on the balancing of attractive and repulsive forces between particles, and a low calculated total interaction energy level indicates that conditions are favourable for colloidal particle aggregation under given solution chemistry conditions. Based on DLVO modelling results, a lower total interaction energy level was calculated for a CO_2-treated column with 0.5 g of calcite added (11.5 kT) than that for a CO_2-

treated column with 0.5 g of dolomite added (14.7 kT). The results suggest that CO_2-mediated calcite dissolution changes the chemistry of the tested water, providing improved conditions for the suspended FFT to settle.

Engineering significance and recommendation from this research:

- The results of this study provide a mechanistic context for enhanced CO_2-mediated BML surface-water turbidity reduction, namely carbonate minerals dissolution ($CaCO_3$ and $CaMg(CO_3)_2$). This is important because, in addition to chemical treatment technologies (e.g., use of alum), dissolution of natural minerals (e.g., calcite and dolomite) can be exploited to promote turbidity reduction in tailings ponds and BML. The results can provide a valuable insight into alternative methods for increasing water recycling in oil sands tailings ponds and for enhanced turbidity reduction in BML and other PL.
- The effect of a high SO_4^{2-} concentration on the microbial dynamics in oil sands tailings was examined in this (summarized in section 6.2.1) and previous studies. However, this was the first study to examine the negative impact of a high SO_4^{2-} concentration on abiotic calcite dissolution in an oil sands context. The results of this study could be the basis for further elucidation of the biogeochemical interactions within existing and future PL endeavours.
- Results from this study provided a geochemical context for previous BML field observations. Dompierre et al. (2016) observed that the pH in BML decreased with depth (average 7.4 pH), and anaerobic hydrocarbon degradation was implicated in the observed pH reduction at the FFT-water interface in BML. Based on the water chemistry data, these authors hypothesized that carbonate mineral (dolomite) dissolution had occurred, leading to the observed increase in Ca^{2+} and Mg^{2+} in the FFT pore water in BML

(Dompierre et al., 2016). Despite these field observations, the BML turbidity level has remained high (Dompierre et al., 2016; Lawrence et al., 2016).

- BML turbidity can be reduced through pH-mediated carbonate mineral dissolution in conjunction with CO_2 addition. Due to 1) the high cost associated with CO_2 addition, 2) the environmental concerns related to the dissipation of CO_2 from BML water to the atmosphere and 3) the high sulfate concentration in the OSPW, it is not economically viable to mitigate BML turbidity with CO_2 addition. Based on results from the present study, it is recommended that additional BCR water be added to BML water to further reduce the sulfate concentration in BML. Since a low pH (~ 6) was reported at the OSPW-FFT interface in BML, carbonate mineral dissolution in BML could be enhanced by reducing the dissolved sulfate concentration. As a result, the BML surface-water turbidity would be reduced through the increased abundance of divalent cations, such as Ca^{2+} and Mg^{2+}.

6.3 Avenues for Future Research

Several important avenues of further research have been identified based on the results presented in this dissertation.

6.3.1 Future Research: Extension of the Present Work

1) Holowenko et al. (2000) and Salloum et al. (2002) reported that high sulfate concentrations could inhibit methane production in MFT, observations that indicate that, by preventing SRB proliferation, methanogenesis could be minimized. Environmentally friendly SRB inhibitors, such as extracts from *Piper guineese*, could be tested. Indeed, piperine, a *P. guineese* extract, was reported to have biocidal effect on *Desulfotomaculum* spp. in ethanol, methanol, petroleum spirit and water (Oguzie et al., 2012a; Oguzie et al., 2012b). These authors showed that the

minimum concentration of piperine needed to inhibit the growth of *Desulfotomaculum* spp. in ethanol or petroleum spirit was 6.25 mg/mL (Oguzie et al., 2012b).

In addition to the conventional acetoclastic and hydrogenotrophic pathways in anaerobic methanogenesis, direct interspecies electron transfer (DIET) pathway has been hypothesized (Chen et al., 2014; Liu et al., 2015; Lovley, 2017; Rotaru et al., 2014; Tang et al., 2016; Zhang et al., 2017). Ye et al. (2018) showed that hematite (Fe_2O_3), which is the major mineral found in Bauxite tailings, can enhancing methanogenesis. These authors suggested that the extracellular polymeric substances play a major role in the DIET process (Ye et al., 2018). Based on these results, further research is needed to elucidate the DIET pathways in the BML.

2) Typically, EG is prepared through sulphuric acid intercalation followed by a thermal expansion treatment. Zhao et al. (2014) demonstrated that perchloric acid and potassium permanganate can be used in the intercalation process and that microwaves can be used for the thermal expansion process. These authors showed that EG had a high adsorption capacity for the organics rhodamine B and 4-chlorophenol. Different intercalating agents can produce EG with different physical, electrical, thermal and chemical properties (Dresselhaus & Dresselhaus, 2002). Therefore, by selecting among various intercalating agents, BTEX adsorption capacity could be improved. As a result, the sulphur-free EG, as described by Zhao et al. (2014), could be tested for use in an AOS application.

3) Chemicals, such as lime and alum, are commonly used as coagulants or flocculants in waste and drinking water treatments. Indeed, Syncrude Canada Ltd. had decided to used alum to mitigate BML surface turbidity. However, the long-term effects of alum treatment on BML turbidity and biogeochemistry are yet to be described. Recently, an alternative coagulant, based

on extracts from *Opuntia ficus-indica*, was tested for turbidity reduction in OSPW (Choudhary et al., 2019). Indeed, several plant extracts (*Moringa oleifera*, *Margaritarea dicoidea* and banana pith) can serve as biodegradable and natural coagulants (Camacho et al., 2017; Choudhary & Neogi, 2017; Kakoi et al., 2016). With renewed interest in environmentally responsible treatments, various alternative coagulants should be tested in current or future oil sands PL endeavours, and the results compared to those from conventional approaches (e.g., alum and calcium chloride).

6.4 References

Camacho, F. P., Sousa, V. S., Bergamasco, R., & Teixeira, M. R. (2017). The use of *Moringa oleifera* as a natural coagulant in surface water treatment. *Chem Eng J, 313*, 226-237.

Castendyk, D. N., Eary, L. E., & Society for Mining Metallurgy and Exploration (U.S.). (2009). *Mine pit lakes : characteristics, predictive modeling, and sustainability*. Littleton, Colo.: Society for Mining, Metallurgy & Exploration.

Chen, S. S., Rotaru, A. E., Liu, F. H., Philips, J., Woodard, T. L., Nevin, K. P., & Lovley, D. R. (2014). Carbon cloth stimulates direct interspecies electron transfer in syntrophic co-cultures. *Bioresource Technology, 173*, 82-86.

Choudhary, M., & Neogi, S. (2017). A natural coagulant protein from *Moringa oleifera*: isolation, characterization, and potential use for water treatment. *Mater Res Express, 4*(10).

Choudhary, M., Ray, M. B., & Neogi, S. (2019). Evaluation of the potential application of cactus (*Opuntia ficus-indica*) as a bio-coagulant for pre-treatment of oil sands process-affected water. *Sep Purif Technol, 209*, 714-724.

Dompierre, K. A., Lindsay, M. B. J., Cruz-Hernandez, P., & Halferdahl, G. M. (2016). Initial geochemical characteristics of fluid fine tailings in an oil sands end pit lake. *Sci Total Environ, 556*, 196-206.

Dresselhaus, M. S., & Dresselhaus, G. (2002). Intercalation compounds of graphite. *Adv Phys, 51*(1), 1-186.

Holowenko, F. M., MacKinnon, M. D., & Fedorak, P. M. (2000). Methanogens and sulfate-reducing bacteria in oil sands fine tailings waste. *Can J Microbiol, 46*(10), 927-937.

Kakoi, B., Kaluli, J. W., Ndiba, P., & Thiong'o, G. (2016). Banana pith as a natural coagulant for polluted river water. *Ecol Eng, 95*, 699-705.

Lawrence, G. A., Tedford, E. W., & Pieters, R. (2016). Suspended solids in an end pit lake: potential mixing mechanisms. *Can J Civ Eng, 43*(3), 211-217.

Liu, F. H., Rotaru, A. E., Shrestha, P. M., Malvankar, N. S., Nevin, K. P., & Lovley, D. R. (2015). Magnetite compensates for the lack of a pilin-associated c-type cytochrome in extracellular electron exchange. *Environmental Microbiology, 17*(3), 648-655.

Lovley, D. R. (2017). Syntrophy Goes Electric: Direct Interspecies Electron Transfer. *Annual Review of Microbiology, Vol 71, 71*, 643-664.

Oguzie, E. E., Adindu, C. B., Enenebeaku, C. K., Ogukwe, C. E., Chidiebere, M. A., & Oguzie, K. L. (2012a). Natural Products for Materials Protection: Mechanism of Corrosion Inhibition of Mild Steel by Acid Extracts of *Piper guineense*. *J Phys Chem C, 116*(25), 13603-13615.

Oguzie, E. E., Ogukwe, C. E., Ogbulie, J. N., Nwanebu, F. C., Adindu, C. B., Udeze, I. O., Oguzie, F. Eze, F. C. (2012b). Broad spectrum corrosion inhibition: corrosion and microbial (SRB) growth inhibiting effects of *Piper guineense* extract. *J Mater Sci, 47*(8), 3592-3601.

Rotaru, A. E., Shrestha, P. M., Liu, F., Markovaite, B., Chen, S., Nevin, K. P., & Lovley, D. R. (2014). Direct Interspecies Electron Transfer between Geobacter metallireducens and Methanosarcina barkeri. *Applied and Environmental Microbiology, 80*(15), 4599-4605.

Salloum, M. J., Dudas, M. J., & Fedorak, P. M. (2002). Microbial reduction of amended sulfate in anaerobic mature fine tailings from oil sand. *Waste Manag Res, 20*(2), 162-171.

Tang, J., Zhuang, L., Ma, J. L., Tang, Z. Y., Yu, Z., & Zhou, S. G. (2016). Secondary Mineralization of Ferrihydrite Affects Microbial Methanogenesis in Geobacter-Methanosarcina Cocultures. *Applied and Environmental Microbiology, 82*(19), 5869-5877.

Ye, J., Hu, A. D., Ren, G. P., Chen, M., Tang, J. H., Zhang, P. Y., Zhou, S. G., & He, Z. (2018). Enhancing sludge methanogenesis with improved redox activity of extracellular polymeric substances by hematite in red mud. *Water Research, 134*, 54-62.

Zhang, S., Chang, J. L., Lin, C., Pan, Y. R., Cui, K. P., Zhang, X. Y., Liang, P., & Huang, X. (2017). Enhancement of methanogenesis via direct interspecies electron transfer between Geobacteraceae and Methanosaetaceae conducted by granular activated carbon. *Bioresource Technology, 245*, 132-137.

Zhao, Q., Cheng, X. W., Wu, J., & Yu, X. J. (2014). Sulfur-free exfoliated graphite with large exfoliated volume: Preparation, characterization and its adsorption performance. *J Ind Eng Chem, 20*(6), 4028-4032.

Bibliography

Abu Laban, N., Tan, B., Dao, A., & Foght, J. (2015a). Draft Genome Sequence of Uncultivated *Desulfosporosinus sp*. Strain Tol-M, Obtained by Stable Isotope Probing Using [13C6]Toluene. *Genome Announc, 3*(1).

Abu Laban, N., Tan, B., Dao, A., & Foght, J. (2015b). Draft Genome Sequence of Uncultivated Toluene-Degrading *Desulfobulbaceae* Bacterium Tol-SR, Obtained by Stable Isotope Probing Using [13C6]Toluene. *Genome Announc, 3*(1).

Achtnich, C., Bak, F., & Conrad, R. (1995). Competition for Electron-Donors among Nitrate Reducers, Ferric Iron Reducers, Sulfate Reducers, and Methanogens in Anoxic Paddy Soil. *Biology and Fertility of Soils, 19*(1), 65-72.

Agteren, M. H., Keuning, S., & Janssen, D. B. (1998). *Handbook on Biodegradation and Biological Treatment of Hazardous Organic Compounds*. Dordrecht: Springer Netherlands.

Akuzawa, N., Hane, Y., Toyama, E., & Abe, T. (2004). Electrical conductivity change of AM-GICs by ternarization with ammonia. *J Phys Chem Solids, 65*(2-3), 191-194.

Alberta Energy Regulator. (2016a). *Directive 085: Fluid Tailings Management for Oil Sands Mining Projects*. Retrieved from http://www.aer.ca/documents/directives/Directive085.pdf.

Alberta Energy Regulator. (2016b). *In Situ* Impacts. Retrieved from https://www.aer.ca/about-aer/spotlight-on/oil-sands/in-situ-impacts

Alberts, B. (2002). *Molecular biology of the cell* (4th ed.). New York: Garland Science.

Alkattan, M., Oelkers, E. H., Dandurand, J. L., & Schott, J. (2002). An experimental study of calcite dissolution rates at acidic conditions and 25 degrees C in the presence of NaPO3 and MgCl2. *Chem Geol, 190*(1-4), 291-302.

Allen, E. W. (2008a). Process water treatment in Canada's oil sands industry: II. A review of emerging technologies. *J Environ Eng and Sci, 7*(5), 499-524.

Allen, E. W. (2008b). Process water treatment in Canada's oil sands industry: I. Target pollutants and treatment objectives. *J Environ Eng and Sci, 7*(2), 123-138.

Allouch, A., Le Calve, S., & Serra, C. A. (2013). Portable, miniature, fast and high sensitive real-time analyzers: BTEX detection. *Sensor Actuat B Chem, 182*, 446-452.

Anderson, J. W., Neff, J. M., Cox, B. A., Tatem, H. E., & Hightower, G. M. (1974). Characteristics of Dispersions and Water-Soluble Extracts of Crude and Refined Oils and Their Toxicity to Estuarine Crustaceans and Fish. *Mar Biol, 27*(1), 75-88.

Appelo, C. A. J., Beekman, H. E., & Oosterbaan, A. W. A. (1984). Hydrochemistry of springs from dolomite reefs in the southern Alps of northern Italy *IAHS Pub* (Vol. 150, pp. 125-138): IAHS Pub.

Appelo, C. A. J., & Postma, D. (2005). *Geochemistry, groundwater and pollution* (2nd ed.). Leiden ; New York: Balkema.

Arasteh, R., Masoumi, M., Rashidi, A. M., Moradi, L., Samimi, V., & Mostafavi, S. T. (2010). Adsorption of 2-nitrophenol by multi-wall carbon nanotubes from aqueous solutions. *Appl Surf Sci, 256*(14), 4447-4455.

Arkell, N., Kuznetsov, P., Kuznetsova, A., Foght, J. M., & Siddique, T. (2015). Microbial metabolism alters pore water chemistry and increases consolidation of oil sands tailings. *J Environ Qual, 44*(1), 145-153.

Ball, J. W., Nordstrom, D. K., & Geological Survey (U.S.). (1991). *User's manual for WATEQ4F, with revised thermodynamic data base and test cases for calculating speciation of major, trace, and redox elements in natural waters / by James W. Ball and Kirk Nordstrom*. Menlow Park, Calif.: U. S. Geological Survey.

Bandosz, T. J. (2006). *Activated carbon surfaces in environmental remediation Interface science and technology v. 7* (pp. 1 online resource.). Retrieved from http://www.sciencedirect.com/science/bookseries/15734285/7

Bang, J. H., Jang, Y. N., Kim, W., Song, K. S., Jeon, C. W., Chae, S. C., Lee, S-W, Park, S-J. Lee, M. G. (2011). Precipitation of calcium carbonate by carbon dioxide microbubbles. *Chem Eng J, 174*(1), 413-420.

Bansal, R. C., & Goyal, M. (2005). *Activated carbon adsorption* (pp. 1 online resource.). Retrieved from https://www.taylorfrancis.com/books/9781420028812

Benitez, E. I., Genovese, D. B., & Lozano, J. E. (2007). Effect of pH and ionic strength on apple juice turbidity: Application of the extended DLVO theory. *Food Hydrocoll, 21*(1), 100-109.

Berg, J. C. (2010). *An introduction to interfaces & colloids : the bridge to nanoscience*. World Scientific. 785p

Birtwell, I. K. (2008). The validity of including turbidity criteria for aquatic resource protection in land development guidelines (Pacific and Yukon Region). In M. A. Farrell & A. Jonsson (Eds.). [Ottawa] :: Fisheries and Oceans Canada.

Boethling, R. S., & Mackay, D. (2000). *Handbook of property estimation methods for environmental chemicals environmental and health sciences* (pp. 1 online resource.). Retrieved from https://www.taylorfrancis.com/books/9781420026283

Bolland, M. D. A., Posner, A. M., & Quirk, J. P. (1980). Ph-Independent and Ph-Dependent Surface-Charges on Kaolinite. *Clays and Clay Minerals, 28*(6), 412-418.

Bordenave, S., Kostenko, V., Dutkoski, M., Grigoryan, A., Martinuzzi, R. J., & Voordouw, G. (2010). Relation between the activity of anaerobic microbial populations in oil sands tailings ponds and the sedimentation of tailings. *Chemosphere, 81*(5), 663-668.

Brandon, J. T. (2016). *Turbidity Mitigation in an Oil Sands End Pit Lake through pH Reduction and Fresh Water Addition.* (Master's thesis), University of Alberta. (130p)

Brown, T. L. (2006). *Chemistry : the central science* (10th ed.). Upper Saddle River, NJ: Pearson Prentice Hall.

Buhmann, D., & Dreybrodt, W. (1987). Calcite Dissolution Kinetics in the System H2o-Co2-Caco3 with Participation of Foreign Ions. *Chem Geol, 64*(1-2), 89-102.

Burkus, Z., Wheler, J., & Pletcher, S. (2014). *GHG Emissions from Oil Sands Tailings Ponds: Overview and Modelling Based on Fermentable Substrates*. Retrieved from Edmonton:

Burland, S. M., & Edwards, E. A. (1999). Anaerobic benzene biodegradation linked to nitrate reduction. *Appl Environ Microbiol, 65*(2), 529-533.

Busenberg, E., & Plummer, L. N. (1982). The Kinetics of Dissolution of Dolomite in Co2-H2o Systems at 1.5-Degrees-C to 65-Degrees-C and O-Atm to 1-Atm Pco2. *Am J Sci, 282*(1), 45-78.

Camacho, F. P., Sousa, V. S., Bergamasco, R., & Teixeira, M. R. (2017). The use of *Moringa oleifera* as a natural coagulant in surface water treatment. *Chem Eng J, 313*, 226-237.

Canadian Association of Petroleum Producers. (2018). *2018 CAPP Crude Oil Forecast, Markets & Transportation*. Retrieved from https://www.capp.ca/publications-and-statistics/publications/320294

Canadian Centre for Occupational Health and Safety. Chemical Profiles - Benzene. Retrieved January 9, 2019, from Canadian Centre for Occupational Health and Safety https://www.ccohs.ca/oshanswers/chemicals/chem_profiles/benzene.html

Castendyk, D. N., Eary, L. E., & Society for Mining Metallurgy and Exploration (U.S.). (2009). *Mine pit lakes : characteristics, predictive modeling, and sustainability*. Littleton, Colo.: Society for Mining, Metallurgy & Exploration.

Çeçen, F., & Aktaş, Ö. (2012). *Activated carbon for water and wastewater treatment integration of adsorption and biological treatment* (pp. 1 online resource (xxviii, 388 p.)). Retrieved from https://ebookcentral.proquest.com/lib/ualberta/detail.action?docID=822729

Chakraborty, R., O'Connor, S. M., Chan, E., & Coates, J. D. (2005). Anaerobic degradation of benzene, toluene, ethylbenzene, and xylene compounds by *Dechloromonas* strain RCB. *Appl Environ Microbiol, 71*(12), 8649-8655.

Chen. (2015). Modeling of Experimental Adsorption Isotherm Data. *Information, 6*(1), 14-22.

Chen, M., Walshe, G., Fru, E. C., Ciborowski, J. J. H., & Weisener, C. G. (2013). Microcosm assessment of the biogeochemical development of sulfur and oxygen in oil sands fluid fine tailings. *Appl Geochem, 37*, 1-11.

Chen, S. S., Rotaru, A. E., Liu, F. H., Philips, J., Woodard, T. L., Nevin, K. P., & Lovley, D. R. (2014). Carbon cloth stimulates direct interspecies electron transfer in syntrophic co-cultures. *Bioresource Technology, 173*, 82-86.

Chi Fru, E., Chen, M., Walshe, G., Penner, T., & Weisener, C. (2013). Bioreactor studies predict whole microbial population dynamics in oil sands tailings ponds. *Appl Microbiol Biotechnol, 97*(7), 3215-3224.

Chou, L., Garrels, R. M., & Wollast, R. (1989). Comparative-Study of the Kinetics and Mechanisms of Dissolution of Carbonate Minerals. *Chem Geol, 78*(3-4), 269-282.

Chorom, M., & Rengasamy, P. (1995). Dispersion and zeta potential of pure clays as related to net particle charge under varying pH, electrolyte concentration and cation type. *European J Soil Sci, 46*(4), 657-665.

Choudhary, M., & Neogi, S. (2017). A natural coagulant protein from *Moringa oleifera*: isolation, characterization, and potential use for water treatment. *Mater Res Express, 4*(10).

Cumulative Environmental Management Association. (2012). *End pit lakes guidance document* (pp. 1 online resource (434 p.)). Retrieved from http://www.deslibris.ca/ID/234915

Daifullah, A. A. M., & Girgis, B. S. (2003). Impact of surface characteristics of activated carbon on adsorption of BTEX. *Colloid Surface A, 214*(1-3), 181-193.

Davies-Colley, R. J., & Smith, D. G. (2001). Turbidity, suspended sediment, and water clarity: A review. *J Am Water Resour Assoc, 37*(5), 1085-1101.

Derjaguin, B., & Landau, L. (1993). Theory of the Stability of Strongly Charged Lyophobic Sols and of the Adhesion of Strongly Charged-Particles in Solutions of Electrolytes. *Prog Mater Sci, 43*(1-4), 30-59.

Dhillon, A., Lever, M., Lloyd, K. G., Albert, D. B., Sogin, M. L., & Teske, A. (2005). Methanogen diversity evidenced by molecular characterization of methyl coenzyme M reductase A (*mcr*A) genes in hydrothermal sediments of the Guaymas Basin. *Appl Environ Microbiol, 71*(8), 4592-4601.

Dompierre, K. A., Barbour, S. L., North, R. L., Carey, S. K., & Lindsay, M. B. J. (2017). Chemical mass transport between fluid fine tailings and the overlying water cover of an oil sands end pit lake. *Water Resour Res, 53*(6), 4725-4740.

Dompierre, K. A., Lindsay, M. B. J., Cruz-Hernandez, P., & Halferdahl, G. M. (2016). Initial geochemical characteristics of fluid fine tailings in an oil sands end pit lake. *Sci Total Environ, 556*, 196-206.
Dresselhaus, M. S., & Dresselhaus, G. (2002). Intercalation compounds of graphite. *Adv Phys, 51*(1), 1-186.
Durmusoglu, E., Taspinar, F., & Karademir, A. (2010). Health risk assessment of BTEX emissions in the landfill environment. *J Hazard Mater, 176*(1-3), 870-877.
Eckert, W. F., Masliyah, J. H., Gray, M. R., & Fedorak, P. M. (1996). Prediction of sedimentation and consolidation of fine tails. *AIChE J, 42*(4), 960-972.
Elimelech, M. (1998). *Particle deposition and aggregation : measurement, modelling, and simulation* (Pbk. ed.). [Oxford, [England] ; Boston]: Butterworth-Heinemann.
Ermler, U., Grabarse, W., Shima, S., Goubeaud, M., & Thauer, R. K. (1997). Crystal structure of methyl coenzyme M reductase: The key enzyme of biological methane formation. *Science, 278*(5342), 1457-1462.
Fedorak, P. M., Coy, D. L., Salloum, M. J., & Dudas, M. J. (2002). Methanogenic potential of tailings samples from oil sands extraction plants. *Can J Microbiol, 48*(1), 21-33.
Fedorak, P. M., Coy, D. L., Dudas, M. J., Simpson, M. J., Renneberg, A. J., & MacKinnon, M. D. (2003). Microbially-mediated fugitive gas production from oil sands tailings and increased tailings densification rates. *J Environ Eng and Sci, 2*(3), 199-211.
Foght, J. M., Gieg, L. M., & Siddique, T. (2017). The microbiology of oil sands tailings: past, present, future. *FEMS Microbiol Ecol, 93*(5).
Folarin, Y., An, D., Caffrey, S., Soh, J., Sensen, C. W., Voordouw, J.,Jack, T., Voordouw, G. (2013). Contribution of make-up water to the microbial community in an oilfield from which oil is produced by produced water re-injection. *Int Biodeter Biodegr, 81*, 44-50.
Gallup, D. L., Isacoff, E. G., & Smith, D. N. (1996). Use of Ambersorb(R) carbonaceous adsorbent for removal of BTEX compounds from oil-field produced water. *Environmental Progress, 15*(3), 197-203.
Gee, K. F., Poon, H. Y., Hashisho, Z., & Ulrich, A. C. (2017). Effect of naphtha diluent on greenhouse gases and reduced sulfur compounds emissions from oil sands tailings. *Sci Total Environ, 598*, 916-924.
Gledhill, D. K., & Morse, J. W. (2006). Calcite dissolution kinetics in Na-Ca-Mg-Cl brines. *Geochim Cosmochim Acta, 70*(23), 5802-5813.
Government of Alberta. (2015). *Lower Athabasca Region : tailings management framework for the mineable Athabasca oil sands*.
Government of Alberta, (2016). Oil Sands: Facts and Statistics. Retrieved from https://open.alberta.ca/publications/oil-sands-facts-and-stats
Government of Alberta. (2018). *Environmental Quality Guidelines for Alberta Surface Waters*. Edmonton, Alberta Retrieved from https://open.alberta.ca/dataset/5298aadb-f5cc-4160-8620-ad139bb985d8/resource/38ed9bb1-233f-4e28-b344-808670b20dae/download/environmentalqualitysurfacewaters-mar28-2018.pdf.
Grasso, D., Subramaniam, K., Butkus, M., Strevett, K., & Bergendahl, J. (2002). A review of non-DLVO interactions in environmental colloidal systems. *Rev Environ Sci Bio, 1*(1), 17-38.
Gregory, R. S., & Levings, C. D. (1998). Turbidity reduces predation on migrating juvenile Pacific salmon. *Transactions of the American Fisheries Society, 127*(2), 275-285.

Grein, F., Ramos, A. R., Venceslau, S. S., & Pereira, I. A. C. (2013). Unifying concepts in anaerobic respiration: Insights from dissimilatory sulfur metabolism. *BBA Bioenergetics, 1827*(2), 145-160.

Guo, J. H., Peng, Y. Z., Ni, B. J., Han, X. Y., Fan, L., & Yuan, Z. G. (2015). Dissecting microbial community structure and methane-producing pathways of a full-scale anaerobic reactor digesting activated sludge from wastewater treatment by metagenomic sequencing. *Microb Cell Fact, 14*.

Gutjahr, A., Dabringhaus, H., & Lacmann, R. (1996). Studies of the growth and dissolution kinetics of the CaCO3 polymorphs calcite and aragonite II. The influence of divalent cation additives on the growth and dissolution rates. *J Cryst Growth, 158*(3), 310-315.

Gutmann, V. (1991). Fundamental Considerations About Liquid Water. *Pure Appl Chem, 63*(12), 1715-1724.

Hansen, B. R., & Davies, S. R. H. (1994). Review of Potential Technologies for the Removal of Dissolved Components from Produced Water. *Chem Eng Res Des, 72*(A2), 176-188.

Headley, J. V., Goudey, S., Birkholz, D., Linton, L. R., & Dickson, L. C. (2001). Toxicity Screening of Benzene, Toluene, Ethylbenzene and Xylene (BTEX) Hydrocarbons in Groundwater at Sour-Gas Plants. *Can Water Resour J, 26*(3), 345-358.

Hemond, H. F., & Fechner-Levy, E. J. (2015). *Chemical fate and transport in the environment* (Third edition. ed.).

Hogg, R., Healy, T. W., & Fuerstenau, D. W. (1966). Mutual Coagulation of Colloidal Dispersions. *Trans Faraday Soc, 62*(522p), 1638.

Holden, A. A., Mayer, K. U., & Ulrich, A. C. (2012). Evaluating methods for quantifying cation exchange in mildly calcareous sediments in Northern Alberta. *Appl Geochem, 27*(12), 2511-2523.

Holowenko, F. M., MacKinnon, M. D., & Fedorak, P. M. (2000). Methanogens and sulfate-reducing bacteria in oil sands fine tailings waste. *Can J Microbiol, 46*(10), 927-937.

Hsieh, C. T., & Teng, H. S. (2000). Influence of mesopore volume and adsorbate size on adsorption capacities of activated carbons in aqueous solutions. *Carbon, 38*(6), 863-869.

Hubert, C. R. J., Oldenburg, T. B. P., Fustic, M., Gray, N. D., Larter, S. R., Penn, K., Rowan, A.K., Seshadri, R., Sherry, A., Swainsbury, R., Voordouw, G., Voordouw, J.K., Head, I. M. (2012). Massive dominance of *Epsilonproteobacteria* in formation waters from a Canadian oil sands reservoir containing severely biodegraded oil. *Environ Microbiol, 14*(2), 387-404.

Humphries, M. (2008). *North American Oil Sands history of development, prospects for the future* (pp. 31 p.). Retrieved from http://fas.org/sgp/crs/misc/RL34258.pdf

Hunter, R. J. (2001). *Foundations of colloid science* (2nd ed.). Oxford ; New York: Oxford University Press.

Hurley, D. L. (2017). *Wind waves and internal waves in Base Mine Lake.* (Master's thesis) University of British Columbia. Retrieved from https://open.library.ubc.ca/collections/ubctheses/24/items/1.0351993

Ibanez, J. G. (2007). *Environmental chemistry : fundamentals*. 1st Ed. New York: Springer. 334p

Ibanez, M., Wijdeveld, A., & Chassagne, C. (2014). The Role of Mono- and Divalent Ions in the Stability of Kaolinite Suspensions and Fine Tailings. *Clays and Clay Minerals, 62*(5-6), 374-385.

Inagaki, M., Toyoda, M., Iwashita, N., Nishi, Y., & Konno, H. J. C. l. (2001). Exfoliated graphite for spilled heavy oil recovery. Carbon Letters *2*(1), 1-8.

Inagaki, M., Toyoda, M., Iwashita, N., Nishi, Y., Konno, H., Fujita, A., & Kihara, T. J. T. (2002). Sorption, recovery and recycle of spilled heavy oils using carbon materials. Spill Sci Technol Bull. *2002*(201), 16-25.

Jeeravipoolvarn, S., Scott, J. D., & Chalaturnyk, R. J. (2009). 10 m standpipe tests on oil sands tailings: long-term experimental results and prediction. *Can Geotech J, 46*(8), 875-888.

Kakoi, B., Kaluli, J. W., Ndiba, P., & Thiong'o, G. (2016). Banana pith as a natural coagulant for polluted river water. *Ecol Eng, 95*, 699-705.

Kaminsky, H. A. W., Etsell, T. H., Ivey, D. G., & Omotoso, O. (2009). Distribution of Clay Minerals in the Process Streams Produced by the Extraction of Bitumen from Athabasca Oil Sands. *Can J Chem Eng, 87*(1), 85-93.

Kang, F. Y., Zheng, Y. P., Zhao, H., Wang, H. N., Wang, L. N., Shen, W. C., & Inagaki, M. (2003). Sorption of heavy oils and biomedical liquids into exfoliated graphite - Research in China. *New Carbon Mater, 18*(3), 161-173.

Kleinsteuber, S., Schleinitz, K. M., Breitfeld, J., Harms, H., Richnow, H. H., & Vogt, C. (2008). Molecular characterization of bacterial communities mineralizing benzene under sulfate-reducing conditions. *FEMS Microbiol Ecol, 66*(1), 143-157.

Kumar, K. V., & Sivanesan, S. (2005). Comparison of linear and non-linear method in estimating the sorption isotherm parameters for safranin onto activated carbon. *J Hazard Mater, 123*(1-3), 288-292.

Kunapuli, U., Lueders, T., & Meckenstock, R. U. (2007). The use of stable isotope probing to identify key iron-reducing microorganisms involved in anaerobic benzene degradation. *Isme Journal, 1*(7), 643-653.

Lan, G. H., Li, Z. T., Zhang, H., Zou, C. J., Qiao, D. R., & Cao, Y. (2011). Relationship of microbial diversity from recycled injection water and high-temperature petroleum reservoirs analyzed by polymerase chain reaction denaturing gradient gel electrophoresis (PCR-DGGE). *Afr J Biotechnol, 10*(53), 11004-11010.

Langmuir, D. (1997). *Aqueous environmental geochemistry*. Upper Saddle River, N.J.: Prentice Hall.

Lawrence, G. A., Tedford, E. W., & Pieters, R. (2016). Suspended solids in an end pit lake: potential mixing mechanisms. *Can J Civ Eng, 43*(3), 211-217.

Li, H., Ai, M. Q., Han, S. Q., Guo, Y. L., Li, N. N., Shi, R. J., Zeng, X., Leng, S., Zhao, J., Liu, X., Zhang, Y. (2012). Microbial diversity and functionally distinct groups in produced water from the Daqing Oilfield, China. *Petrol Sci, 9*(4), 469-484.

Li, Q., Jonas, U., Zhao, X. S., & Kapp, M. (2008). The forces at work in collodial self-assembly: a review on fundamental interactions between collodial particels. *Asia-Pac J Chem Eng, 3*(3), 255-268.

Liu, F. H., Rotaru, A. E., Shrestha, P. M., Malvankar, N. S., Nevin, K. P., & Lovley, D. R. (2015). Magnetite compensates for the lack of a pilin-associated c-type cytochrome in extracellular electron exchange. *Environmental Microbiology, 17*(3), 648-655.

Liu, L. Y., Hu, Y., Min, F. F., Zhang, M. X., & Song, S. X. (2013). Characterizations and Stability of Colloidal Coal-Measure Kaolinite in Aqueous Suspensions: A Review. *Surf Rev Lett, 20*(1).

Lovley, D. R., Holmes, D. E., & Nevin, K. P. (2004). Dissimilatory Fe(III) and Mn(IV) reduction. *Adv microb Physiol, Vol. 49, 49*, 219-286.

Lovley, D. R. (2017). Syntrophy Goes Electric: Direct Interspecies Electron Transfer. *Annual Review of Microbiology, Vol 71, 71*, 643-664.

Mackinnon, M., & Boerger, H. (1991). *Assessment Of A Wet Landscape Option For Disposal Of Fine Tails Sludge From Oil Sands Processing*. Annual Technical Meeting. Petroleum Society of Canada.
Mahdavi, H. (2014). *The application of algae for the removal of metals and naphthenic acids from oil sands tailings pond water.* (Doctoral thesis), University of Alberta. Retrieved from http://hdl.handle.net/10402/era.39068
Masliyah, J. H., & Bhattacharjee, S. (2006). *Electrokinetic and colloid transport phenomena*. Hoboken, N.J.: Wiley-Interscience.
Metcalf & Eddy, Tchobanoglous, G., Stensel, H. D., Tsuchihashi, R., Burton, F. L., Abu-Orf, M., Bowden, G., & Pfrang, W. (2014). *Wastewater engineering : treatment and resource recovery* (Fifth edition / ed.).
Mikula, R., Munoz, V., Lam, W., & Payette, C. (1993). *Structure in oil sands fine tailings.* Paper presented at the Proceedings of the Fine Tailings Fundamentals Symposium, Oil Sands our Petroleum Future, Edmonton, AB.
Missana, T., & Adell, A. (2000). On the applicability of DLVO theory to the prediction of clay colloids stability. *J Colloid Interface Sci, 230*(1), 150-156.
Morel, A., & Loisel, H. (1998). Apparent optical properties of oceanic water: dependence on the molecular scattering contribution. *Applied Optics, 37*(21), 4765-4776.
Morse, J. W., Arvidson, R. S., & Luttge, A. (2007). Calcium carbonate formation and dissolution. *Chemical Reviews, 107*(2), 342-381.
Moustafa, A. M., McPhedran, K. N., Moreira, J., & Gamal El-Din, M. (2014). Investigation of mono/competitive adsorption of environmentally relevant ionized weak acids on graphite: impact of molecular properties and thermodynamics. *Environ Sci Technol, 48*(24), 14472-14480.
Muller, A. L., Kjeldsen, K. U., Rattei, T., Pester, M., & Loy, A. (2015). Phylogenetic and environmental diversity of DsrAB-type dissimilatory (bi)sulfite reductases. *ISME J, 9*(5), 1152-1165.
Mullineaux, R. D., & Raley, J. H. (1963). High Temperature Reactions of Iodine with Hydrocarbons .2. Aromatization. *J Am Chem Soc, 85*(20), 3178-&.
Ogumi, Z., Ohashi, S., & Takehara, Z. (1985). Application of the Spe Method to Organic Electrochemistry .6. Oxidation of Cyclohexanol to Cyclohexanone on Pt-Spe in the Presence of Iodine and Iodide. *Electrochimica Acta, 30*(1), 121-124.
Oguzie, E. E., Adindu, C. B., Enenebeaku, C. K., Ogukwe, C. E., Chidiebere, M. A., & Oguzie, K. L. (2012a). Natural Products for Materials Protection: Mechanism of Corrosion Inhibition of Mild Steel by Acid Extracts of *Piper guineense*. *J Phys Chem C, 116*(25), 13603-13615.
Oguzie, E. E., Ogukwe, C. E., Ogbulie, J. N., Nwanebu, F. C., Adindu, C. B., Udeze, I. O., Oguzie, F. Eze, F. C. (2012b). Broad spectrum corrosion inhibition: corrosion and microbial (SRB) growth inhibiting effects of *Piper guineense* extract. *J Mater Sci, 47*(8), 3592-3601.
Ohshima, H. (2012). *Electrical phenomena at interfaces and biointerfaces fundamentals and applications in nano-, bio-, and environmental sciences* (pp. 1 online resource (xviii, 850 p.)). Retrieved from https://ebookcentral.proquest.com/lib/ualberta/detail.action?docID=818455
OSTC. (2012). *Technical Guide for Fluid Fine Tailings Management*. Retrieved from http://www.cosia.ca/uploads/documents/id7/TechGuideFluidTailingsMgmt_Aug2012.pdf

Parkhurst, D. L., & Appelo, C. A. J. (2013). *Description of input and examples for PHREEQC version 3—A Computer Program for Speciation, Batch-reaction, One-dimensional Transport, and Inverse Geochemical Calculations.* Denver, Colo.: U.S. Department of the Interior, U.S. Geological Survey.

Penner, T. J., & Foght, J. M. (2010). Mature fine tailings from oil sands processing harbour diverse methanogenic communities. *Can J Microbiol, 56*(6), 459-470.

Plummer, L. N., Wigley, T. M. L., & Parkhurst, D. L. (1978). The kinetics of calcite dissolution in CO 2 -water systems at 5 degrees to 60 degrees C and 0.0 to 1.0 atm CO 2. *278*(2), 179-216.

Pokrovsky, O. S., & Schott, J. (2001). Kinetics and mechanism of dolomite dissolution in neutral to alkaline solutions revisited. *Am J Sci, 301*(7), 597-626.

Pokrovsky, O. S., Golubev, S. V., & Schott, J. (2005). Dissolution kinetics of calcite, dolomite and magnesite at 25 degrees C and 0 to 50 atm pCO(2). *Chem Geol, 217*(3-4), 239-255.

Poon, H. Y., Brandon, J. T., Yu, X. X., & Ulrich, A. C. (2018). Turbidity Mitigation in an Oil Sands Pit Lake through pH Reduction and Fresh Water Addition. *J Environ Eng, 144*(12). 10.1061/(Asce)Ee.1943-7870.0001472

Qin, J. Y., Moustafa, A., Harms, H., El-Din, M. G., & Wick, L. Y. (2015). The power of power: Electrokinetic control of PAH interactions with exfoliated graphite. *J Hazard Mater, 288*, 25-33.

Raley, J. H., Bittner, C. W., & Mullineaux, R. D. (1963). High Temperature Reactions of Iodine with Hydrocarbons .1. Dehydrogenation. *J Am Chem Soc, 85*(20), 3174.

Ramos-Padron, E., Bordenave, S., Lin, S., Bhaskar, I. M., Dong, X., Sensen, C. W., Fournier, J., Voordouw, G., Gieg, L. M. (2011). Carbon and sulfur cycling by microbial communities in a gypsum-treated oil sands tailings pond. *Environ Sci Technol, 45*(2), 439-446.

Rand, B., & Melton, I. E. (1977). Particle Interactions in Aqueous Kaolinite Suspensions .1. Effect of Ph and Electrolyte Upon Mode of Particle Interaction in Homoionic Sodium Kaolinite Suspensions. *J Colloid Interface Sci, 60*(2), 308-320.

Revil, A., Hermitte, D., Spangenberg, E., & Cocheme, J. J. (2002). Electrical properties of zeolitized volcaniclastic materials. *J Geophys Res - Solid Earth, 107*(B8).

Revil, A., Pezard, P. A., & Glover, P. W. J. (1999). Streaming potential in porous media 1. Theory of the zeta potential. *J Geophys Res - Solid Earth, 104*(B9), 20021-20031.

Rickard, D., & Sjoberg, E. L. (1983). Mixed Kinetic Control of Calcite Dissolution Rates. *Am J Sci, 283*(8), 815-830.

Risacher, F. F., Morris, P. K., Arriaga, D., Goad, C., Nelson, T. C., Slater, G. F., & Warren, L. A. (2018). The interplay of methane and ammonia as key oxygen consuming constituents in early stage development of Base Mine Lake, the first demonstration oil sands pit lake. *Appl Geochem, 93*, 49-59.

Rooney-Varga, J. N., Anderson, R. T., Fraga, J. L., Ringelberg, D., & Lovley, D. R. (1999). Microbial communities associated with anaerobic benzene degradation in a petroleum-contaminated aquifer. *Appl Environ Microbiol, 65*(7), 3056-3063.

Rosenberg, E., DeLong, E. F., Lory, S., Stackebrandt, E., & Thompson, F. L. (2014). *The prokaryotes : Other major lineages of bacteria and the archaea* (pp. 1 online resource). Retrieved from http://link.springer.com/10.1007/978-3-642-38954-2

Rotaru, A. E., Shrestha, P. M., Liu, F., Markovaite, B., Chen, S., Nevin, K. P., & Lovley, D. R. (2014). Direct Interspecies Electron Transfer between Geobacter metallireducens and Methanosarcina barkeri. *Applied and Environmental Microbiology, 80*(15), 4599-4605.

Saeed, T., Al-mutairi, M., Ali, L. N., Al-obaid, T., & Beg, M. U. (1998). The Effect of Temperature on the Composition and Relative Toxicity of the Water-Soluble Fraction of Kuwait Crude Oil (Export) in the Seawater. *Int J Environ An Chem, 72*(4), 275-287.

Saidi-Mehrabad, A., He, Z., Tamas, I., Sharp, C. E., Brady, A. L., Rochman, F. F., Bodrossy, L., Abell, G.C.J., Penner, T., Dong, X., Dunfield, P. F. (2013). Methanotrophic bacteria in oilsands tailings ponds of northern Alberta. *ISME J, 7*(5), 908-921.

Salloum, M. J., Dudas, M. J., & Fedorak, P. M. (2002). Microbial reduction of amended sulfate in anaerobic mature fine tailings from oil sand. *Waste Manag Res, 20*(2), 162-171.

Santillano, D., Boetius, A., & Ramette, A. (2010). Improved dsrA-Based Terminal Restriction Fragment Length Polymorphism Analysis of Sulfate-Reducing Bacteria. *Appl Environ Microbiol, 76*(15), 5308-5311.

Sawyer, C. N., McCarty, P. L., Parkin, G. F., & Sawyer, C. N. (1994). *Chemistry for environmental engineering* (4th ed.). New York: McGraw-Hill.

Sawyer, C. N., McCarty, P. L., & Parkin, G. F. (2003). *Chemistry for environmental engineering and science* (5th ed.). Boston: McGraw-Hill.

Scarlett, A. G., West, C. E., Jones, D., Galloway, T. S., & Rowland, S. J. (2012). Predicted toxicity of naphthenic acids present in oil sands process-affected waters to a range of environmental and human endpoints. *Sci Total Environ, 425*, 119-127.

Schiffer, A., Parey, K., Warkentin, E., Diederichs, K., Huber, H., Stetter, K. O., Kroneck, P.M., Ermler, U. (2008). Structure of the dissimilatory sulfite reductase from the hyperthermophilic archaeon *Archaeoglobus fulgidus*. *J Mol Biol, 379*(5), 1063-1074.

Septhum, C., Rattanaphani, S., Bremner, J. B., & Rattanaphani, V. (2007). An adsorption study of A1(III) ions onto chitosan. *J Hazard Mater, 148*(1-2), 185-191.

Shahimin, M. F. M., & Siddique, T. (2017). Sequential biodegradation of complex naphtha hydrocarbons under methanogenic conditions in two different oil sands tailings. *Environ Pollut, 221*, 398-406.

Shen, W. C., Wen, S. Z., Cao, N. Z., Zheng, L., Zhou, W., Liu, Y. J., & Gu, J. L. (1999). Expanded graphite - A new kind of biomedical material. *Carbon, 37*(2), 356-358.

Siddique, T., Fedorak, P. M., & Foght, J. M. (2006). Biodegradation of short-chain n-alkanes in oil sands tailings under methanogenic conditions. *Environ Sci Technol, 40*(17), 5459-5464.

Siddique, T., Fedorak, P. M., MacKinnon, M. D., & Foght, J. M. (2007). Metabolism of BTEX and naphtha compounds to methane in oil sands tailings. *Environ Sci Technol, 41*(7), 2350-2356.

Siddique, T., Penner, T., Semple, K., & Foght, J. M. (2011). Anaerobic biodegradation of longer-chain n-alkanes coupled to methane production in oil sands tailings. *Environ Sci Technol, 45*(13), 5892-5899.

Siddique, T., Penner, T., Klassen, J., Nesbo, C., & Foght, J. M. (2012). Microbial communities involved in methane production from hydrocarbons in oil sands tailings. *Environ Sci Technol, 46*(17), 9802-9810.

Siddique, T., Kuznetsov, P., Kuznetsova, A., Arkell, N., Young, R., Li, C., Guigard, S., Underwood, E., Foght, J. M. (2014). Microbially-accelerated consolidation of oil sands tailings. Pathway I: changes in porewater chemistry. *Front Microbiol, 5*, 106.

Siriwardane, R. V., Shen, M.-S., Fisher, E. P., & Poston, J. A. (2001). Adsorption of CO_2 on Molecular Sieves and Activated Carbon. *Energy & Fuels, 15*(2), 279-284.

Sjoberg, E. L. (1976). Fundamental Equation for Calcite Dissolution Kinetics. *Geochim Cosmochim Acta, 40*(4), 441-447.
Sjöberg, E. L. (1978). *Kinetics and mechanism of calcite dissolution in aqueous solutions at low temperatures.* Almqvist & Wiksell.
Sjoberg, E. L., & Rickard, D. (1983). The Influence of Experimental-Design on the Rate of Calcite Dissolution. *Geochim Cosmochim Acta, 47*(12), 2281-2285.
Slaugh, L. H., Raley, J. H., & Mullineaux, R. D. (1963). High Temperature Reactions of Iodine with Hydrocarbons .3. Rearrangement of Aliphatic Free Radicals. *J Am Chem Soc, 85*(20), 3180-&.
Small, C. C., Ulrich, A. C., & Hashisho, Z. (2012). Adsorption of Acid Extractable Oil Sands Tailings Organics onto Raw and Activated Oil Sands Coke. *J Environ Eng, 138*(8), 833-840.
Small, C. C., Cho, S., Hashisho, Z., & Ulrich, A. C. (2015). Emissions from oil sands tailings ponds: Review of tailings pond parameters and emission estimates. *J Petrol Sci Eng, 127*, 490-501.
Song, J., Zeng, Y. C., Wang, L., Duan, X. D., Puerto, M., Chapman, W. G., Biswal, S., Hirasaki, G. J. (2017). Surface complexation modeling of calcite zeta potential measurements in brines with mixed potential determining ions (Ca2+, CO32-, Mg2+, SO42-) for characterizing carbonate wettability. *J Colloid Interface Sci, 506*, 169-179.
Springer, E., Sachs, M. S., Woese, C. R., & Boone, D. R. (1995). Partial gene sequences for the A subunit of methyl-coenzyme M reductase (*mcr*I) as a phylogenetic tool for the family *Methanosarcinaceae*. *Int J Syst Bacteriol, 45*(3), 554-559.
Stasik, S., Loick, N., Knoller, K., Weisener, C., & Wendt-Potthoff, K. (2014). Understanding biogeochemical gradients of sulfur, iron and carbon in an oil sands tailings pond. *Chem Geol, 382*, 44-53.
Stasik, S., & Wendt-Potthoff, K. (2014). Interaction of microbial sulphate reduction and methanogenesis in oil sands tailings ponds. *Chemosphere, 103*, 59-66.
Steger, D., Wentrup, C., Braunegger, C., Deevong, P., Hofer, M., Richter, A., Baranyi, C., Pester, M., Wagner, M., Loy, A. (2011). Microorganisms with Novel Dissimilatory (Bi)Sulfite Reductase Genes Are Widespread and Part of the Core Microbiota in Low-Sulfate Peatlands. *Appl Environ Microbiol, 77*(4), 1231-1242.
Straalen, N. M. v., & Roelofs, D. (2012). *An introduction to ecological genomics* (2nd ed.). Oxford ; New York: Oxford University Press.
Suthersan, S. S. (1997). *Remediation engineering : design concepts*. Boca Raton, Fl.: CRC-Lewis Publishers.
Tanford, C. (1979). Interfacial Free-Energy and the Hydrophobic Effect. *Proceedings of the National Academy of Sciences of the United States of America, 76*(9), 4175-4176.
Tang, J., Zhuang, L., Ma, J. L., Tang, Z. Y., Yu, Z., & Zhou, S. G. (2016). Secondary Mineralization of Ferrihydrite Affects Microbial Methanogenesis in Geobacter-Methanosarcina Cocultures. *Applied and Environmental Microbiology, 82*(19), 5869-5877.
Tang, K., Baskaran, V., & Nemati, M. (2009). Bacteria of the sulphur cycle: An overview of microbiology, biokinetics and their role in petroleum and mining industries. *Biochem Eng J, 44*(1), 73-94.

Tang, Y. Q., Li, Y., Zhao, J. Y., Chi, C. Q., Huang, L. X., Dong, H. P., & Wu, X. L. (2012). Microbial communities in long-term, water-flooded petroleum reservoirs with different *in situ* temperatures in the Huabei Oilfield, China. *PLoS One, 7*(3), e33535.

Toyoda, M., & Inagaki, M. (2000). Heavy oil sorption using exfoliated graphite - New application of exfoliated graphite to protect heavy oil pollution. *Carbon, 38*(2), 199-210.

Tundisi, J. G., & Tundisi, T. M. (2012). *Limnology* (pp. 1 online resource (xxii, 864 p.)). Retrieved from http://search.ebscohost.com/login.aspx?direct=true&scope=site&db=nlebk&db=nlabk&AN=437330

Udo, E. J. (1978). Thermodynamics of Potassium-Calcium and Magnesium-Calcium Exchange-Reactions on a Kaolinitic Soil Clay. *Soil Science Society of America Journal, 42*(4), 556-560.

Ulrich, A. C., & Edwards, E. A. (2003). Physiological and molecular characterization of anaerobic benzene-degrading mixed cultures. *Environ Microbiol, 5*(2), 92-102.

Venditti, R., Xuan, X. C., & Li, D. Q. (2006). Experimental characterization of the temperature dependence of zeta potential and its effect on electroosmotic flow velocity in microchannels. *Microfluid Nanofluid, 2*(6), 493-499.

Verwey, E. J. W. (1947). Theory of the Stability of Lyophobic Colloids. *J Phys Colloid Chem, 51*(3), 631-636.

Voordouw, G. (2013). Interaction of oil sands tailings particles with polymers and microbial cells: First steps toward reclamation to soil. *Biopolymers, 99*(4), 257-262.

Wagner, M., Roger, A. J., Flax, J. L., Brusseau, G. A., & Stahl, D. A. (1998). Phylogeny of dissimilatory sulfite reductases supports an early origin of sulfate respiration. *J Bacteriol, 180*(11), 2975-2982.

Weelink, S. A. B., van Eekert, M. H. A., & Stams, A. J. M. (2010). Degradation of BTEX by anaerobic bacteria: physiology and application. *Rev Environ Sci Bio, 9*(4), 359-385.

Westcott, F., & Watson, L. (2005). End pit lakes technical guidance document: Report. Cumulative Environmental Management Association. 51p. Report.

Ye, J., Hu, A. D., Ren, G. P., Chen, M., Tang, J. H., Zhang, P. Y., Zhou, S. G., & He, Z. (2018). Enhancing sludge methanogenesis with improved redox activity of extracellular polymeric substances by hematite in red mud. *Water Research, 134*, 54-62.

Zavarzin, G. A. (2010). *Microbial cycles* (Vol. 1): Academic Press. Encyclopedia of Ecology. pp. 2335-2341.

Zbik, M. S., Smart, R. S. C., & Morris, G. E. (2008). Kaolinite flocculation structure. *J Colloid Interface Sci, 328*(1), 73-80.

Zhang, S., Chang, J. L., Lin, C., Pan, Y. R., Cui, K. P., Zhang, X. Y., Liang, P., & Huang, X. (2017). Enhancement of methanogenesis via direct interspecies electron transfer between Geobacteraceae and Methanosaetaceae conducted by granular activated carbon. *Bioresource Technology, 245*, 132-137.

Zhang, Y. P., & Dawe, R. (1998). The kinetics of calcite precipitation from a high salinity water. *Appl Geochem, 13*(2), 177-184.

Zhao, Q., Cheng, X. W., Wu, J., & Yu, X. J. (2014). Sulfur-free exfoliated graphite with large exfoliated volume: Preparation, characterization and its adsorption performance. *J Ind Eng Chem, 20*(6), 4028-4032.

Zhu, R., Liu, Q. X., Xu, Z. H., Masliyah, J. H., & Khan, A. (2011). Role of Dissolving Carbon Dioxide in Densification of Oil Sands Tailings. *Energy & Fuels, 25*(5), 2049-2057.

Zinder, S. H. (1993). Physiological Ecology of Methanogens. In J. G. Ferry (Ed.), *Methanogenesis: Ecology, Physiology, Biochemistry & Genetics* (pp. 128-206). Boston, MA: Springer US.

Appendix: Additional Results

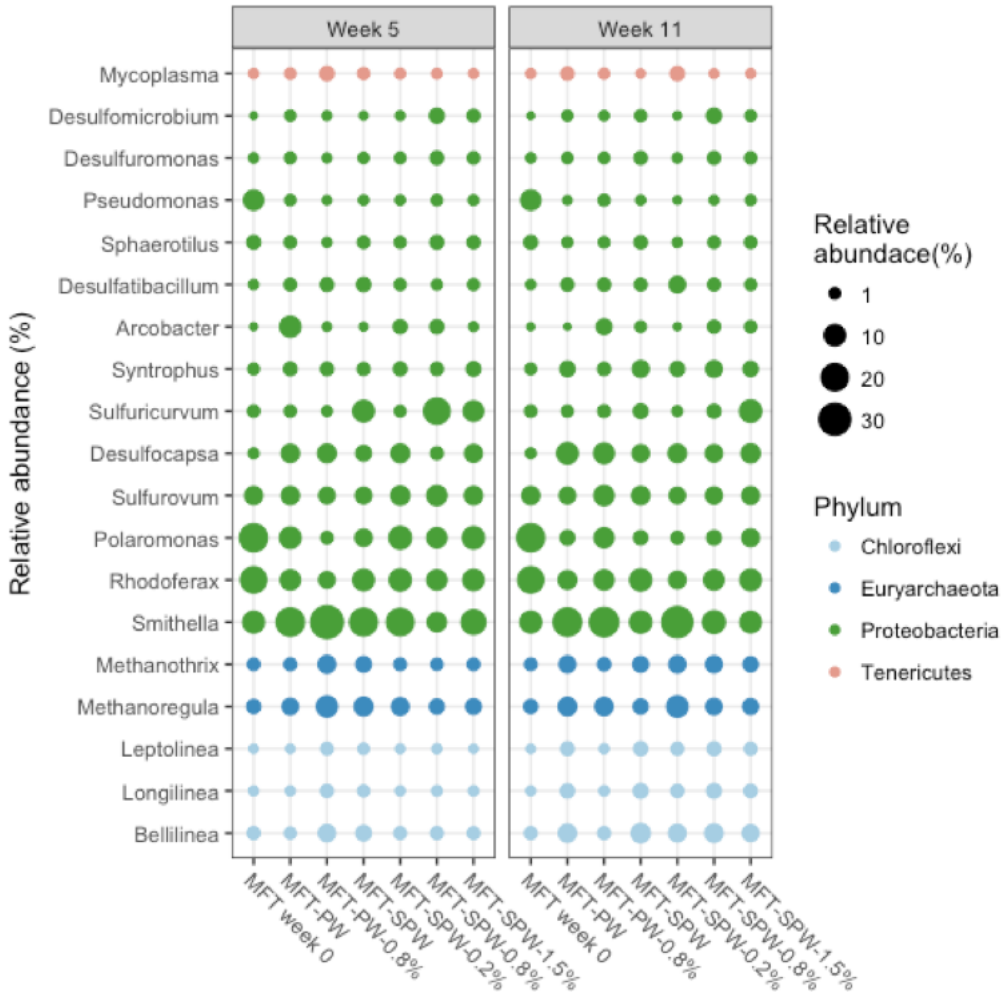

Figure A- 1 16S Microbial community analysis. The relative abundance (%) of microbial communities within the mesocosms were plotted at genus levels

Table A - 1 Relative abundance of selected sulfate-reducing bacteria and methanogens from 16S analysis. Table modified from Gee et al. (2017).

		Desulfobulbaceae ($x10^{-2}$)	Desulfobacteraceae ($x10^{-2}$)	Desulfuromonadaceae ($x10^{-2}$)	Desulfomicrobiaceae ($x10^{-2}$)	H_2S (μmol)	Methanoregulaceae ($x10^{-2}$)	Methanotrichaceae ($x10^{-2}$)	CH_4 (μmol)
	MFT week 0	1.74	0.993	1.35	0.125	0.0	2.70	1.58	0
Week 5	MFT-PW	7.37	2.45	1.40	0.920	1.8	4.92	1.74	220
	MFT-PW-0.8%	1.01	2.61	1.41	0.632	4.4	6.69	2.03	940
	MFT-SPW	6.33	2.64	2.20	1.33	4.1	3.74	3.90	0
	MFT-SPW-0.2%	6.87	4.96	0.679	0.221	5.4	10.8	5.07	152
	MFT-SPW-0.8%	6.25	2.86	2.03	3.44	11.2	5.12	4.82	2665
	MFT-SPW-1.5%	8.19	2.25	1.68	1.09	14.8	4.38	3.35	1028
Week 11	MFT-PW	11	2.73	1.13	0.919	4.9	7.15	4.85	970
	MFT-PW-0.8%	7.15	2.66	0.585	0.439	5.0	10.3	5.65	10870
	MFT-SPW	4.25	2.97	1.11	0.277	5.1	7.27	3.73	454
	MFT-SPW-0.2%	7.87	1.91	1.43	0.4.59	14.0	6.00	1.61	918
	MFT-SPW-0.8%	2.69	1.37	2.41	3.27	22.5	3.57	1.39	13945
	MFT-SPW-1.5%	7.02	2.08	1.77	1.80	17.5	4.11	1.65	17292

Table A - 2 A compilation of diluent composition used by Syncrude, Suncor and Shell Albian oil sands operators. Modified from Foght et al. (2017)

Operator	Diluent used	General composition
Syncrude	heavy naphtha	5% C_5-C_8 and 86% C_9-C_{16} aliphatics; 3-4% BTEX
Suncor	light sour naphtha	60% C_5-C_8 and 20% C_9-C_{16} aliphatics; 5-10% BTEX
Shell Albian	paraffinic	95% C_5-C_8 (balance presumably BTEX)

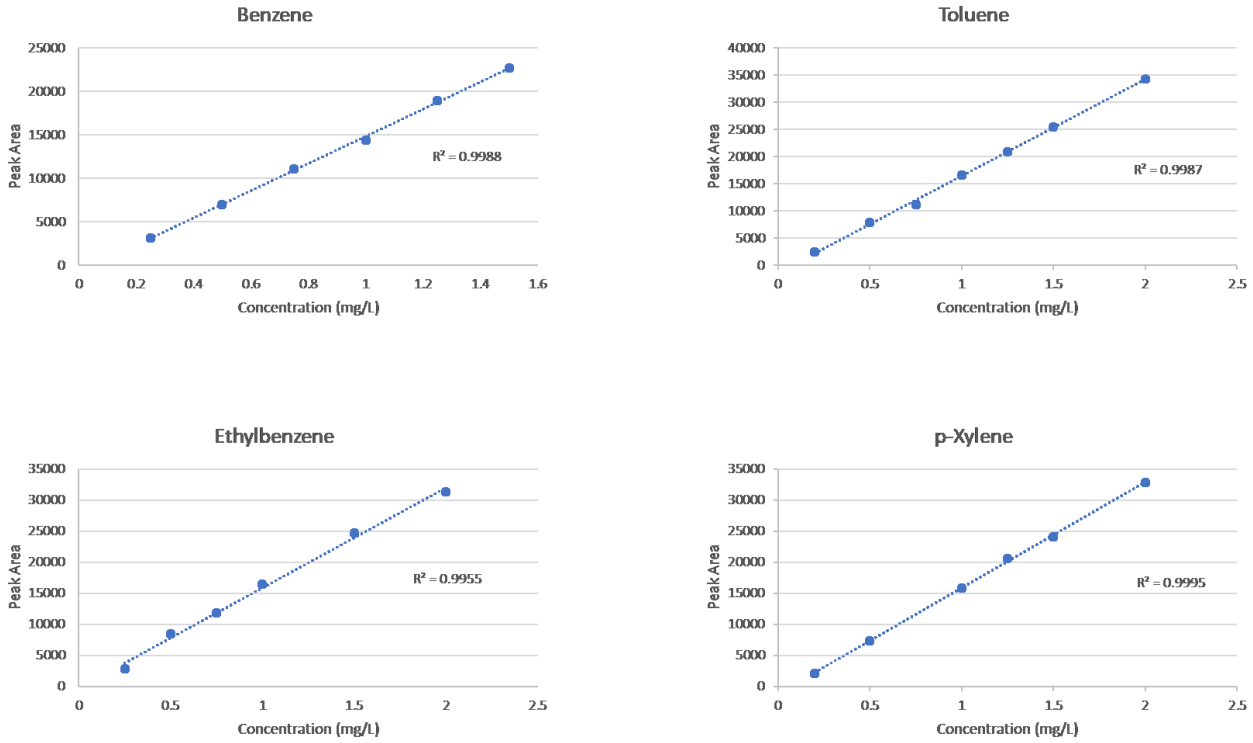

Figure A- 2 Purge & Trap GC Calibration Result.

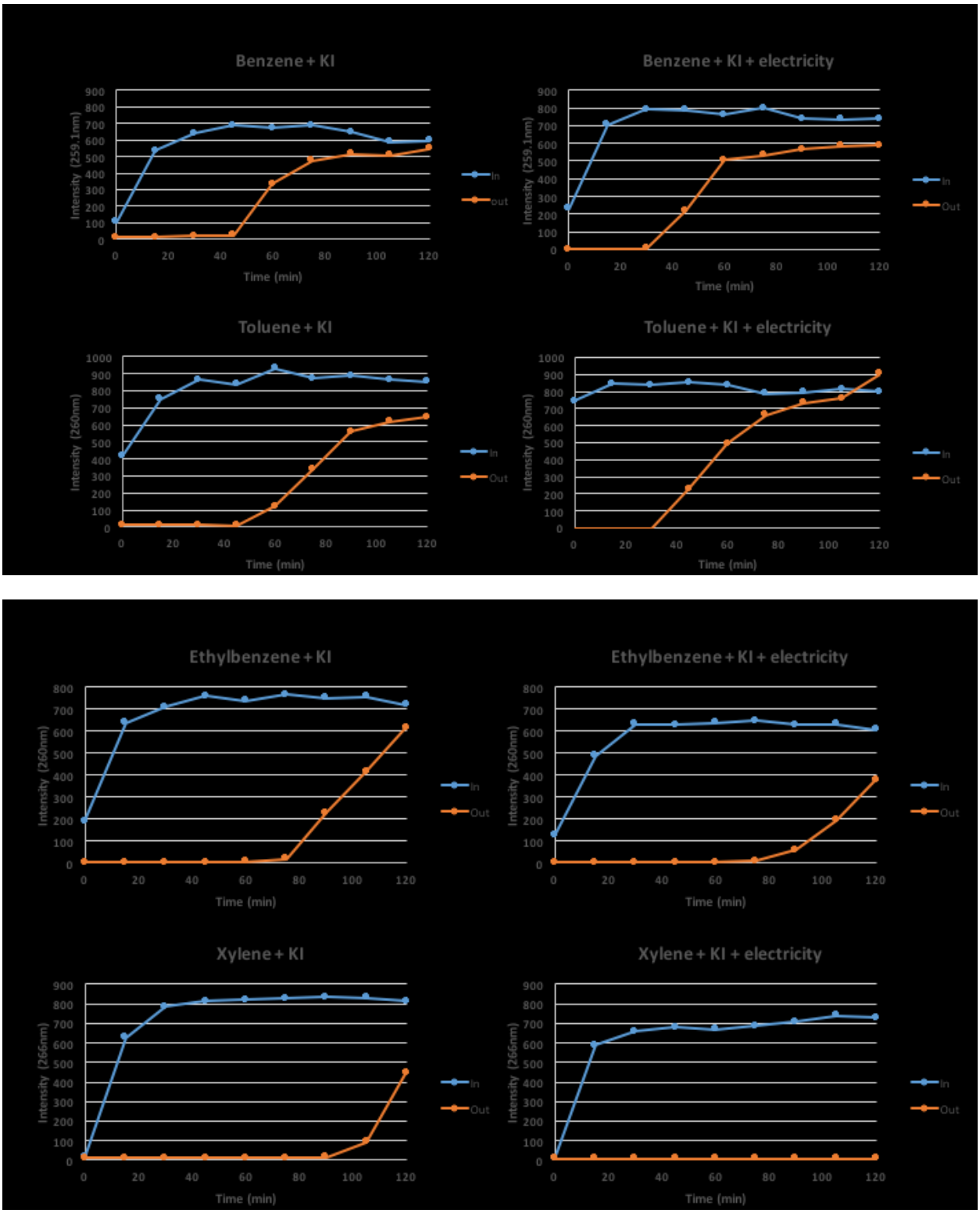

Figure A- 3 Fluorescence spectrophotography results for the AOS experiment at 4 mL/min flowrate. Both influent and effluent aqueous samples were measured and the measured intensity was shown here. Data obtained from 1 experimental trial.

Table A - 3 Total inorganic carbon (TIC) analysis results from the AOS effluent.

TIC (mg/L)									
	Blank	Benzene	Benzene +electricity	Toluene	Toluene +electricity	Ethylb enzene	Ethylbenzene +electricity	*p*-Xylene	*p*-Xylene +electricity
10 m L/min	0.06-0.19	0.34-0.60	0.2-0.29	0.24-0.32	0.19-0.28	0.24-0.34	0.2-0.26	0.13-0.18	0.15-0.17
4 mL/ min	0.04-0.15	0.18-0.24	0.16-0.25	0.13-0.19	0.18-0.22	0.11-0.21	0.16-0.22	0.18-0.24	0.25-0.36

Table A - 4 List of parameters for DLVO calculation

Parameters	Values
Permittivity of solution	7.08×10^{-10} F/m
Radius	7.5×10^{-7} m
Hamaker constant (clay-water-clay)	2×10^{-20} J
Temperature	294.65 K
Characteristic wavelength	1×10^{-7} m

Table A - 5 Recipes for making synthetic BML (SBML) water

400 mg/L SBML		50 mg/L SBML	
Chemical	g measured	Chemical	g measured
$NaHCO_3$	11.233	$NaHCO_3$	11.233
Na_2SO_4	5.915	NaCl	7.12
NaCl	5.847	KCl	0.191
KCl	0.191	$MgSO_4$-$7H_2O$	0.356
$MgCl_2$-$6H_2O$	1.003	$CaCl_2$-$2H_2O$	0.512
$CaCl_2$-$2H_2O$	0.88	$MgCl_2$-$6H_2O$	0.626
NH_4Cl	0.042	$CaSO_4$-$2H_2O$	0.431
NaF	0.042	NH4Cl	0.042
$BaCl_2$-$2H_2O$	0.007	NaF	0.042
$Na_2B_4O_7$-$10H_2O$	0.171	$BaCl_2$-$2H_2O$	0.007
LiCl	0.01	$NaBO_7$-$10H_2O$	0.171
$NaNO_3$	0.048	LiCl	0.01
$SrCl_2$-$6H_2O$	0.019	$NaNO_3$	0.05
		$SrCl_2$-$6H_2O$	0.022

Table A - 6

50SBML	p-value	400SBML	p-value
Day 36 & 63	0.095	Day 42 & 84	0.04
Day 91 & 63	0.02	Day 126 & 84	0.3

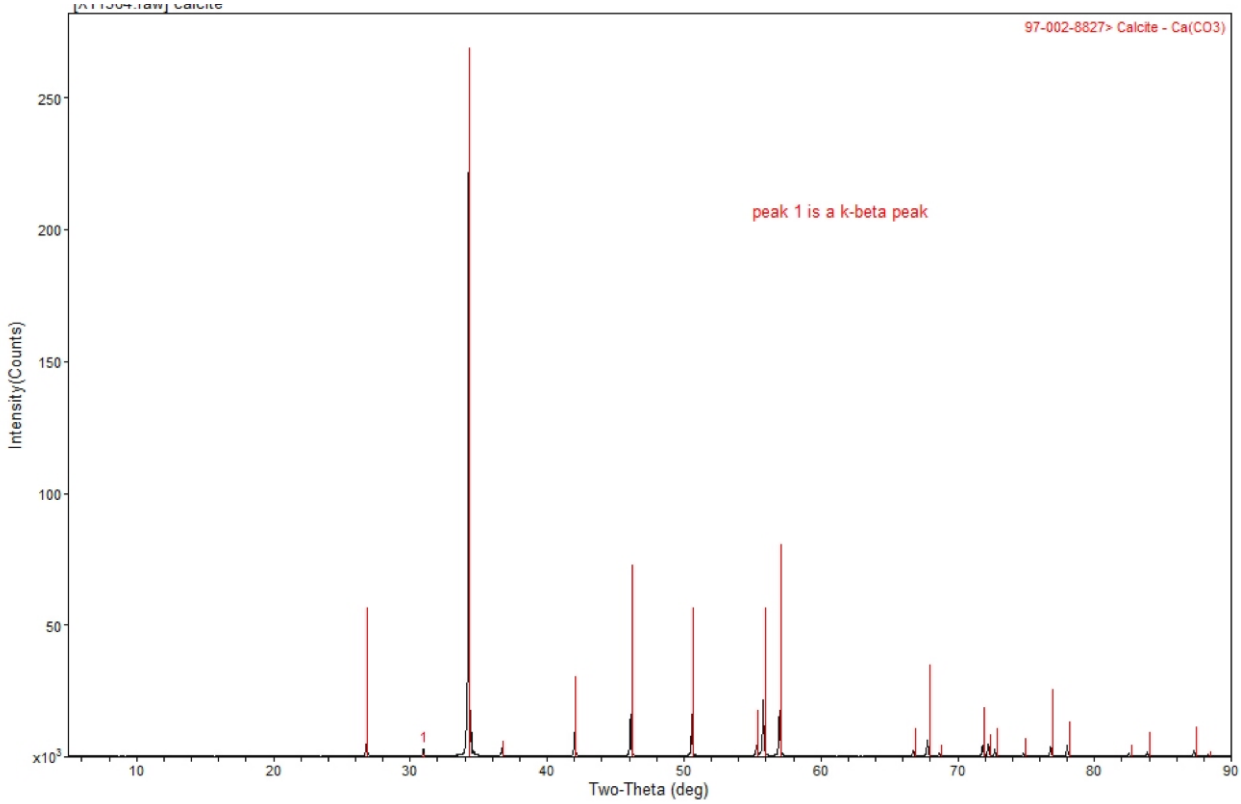

Figure A- 4 X-ray powder diffraction results for Iceland spar.

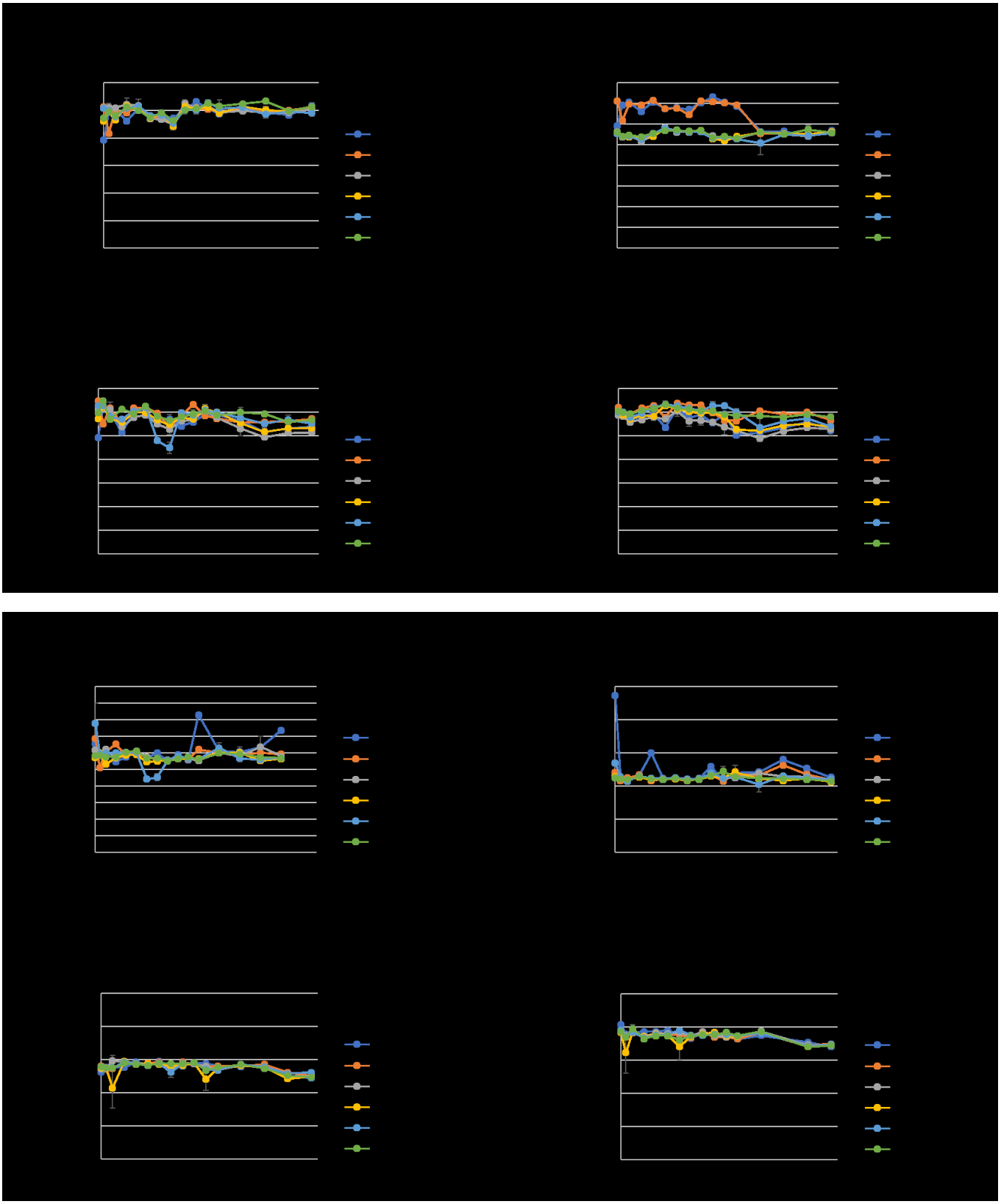

Figure A- 5 Dissolved ion concentrations in the synthetic BML water used for the calcite dissolution experiment.

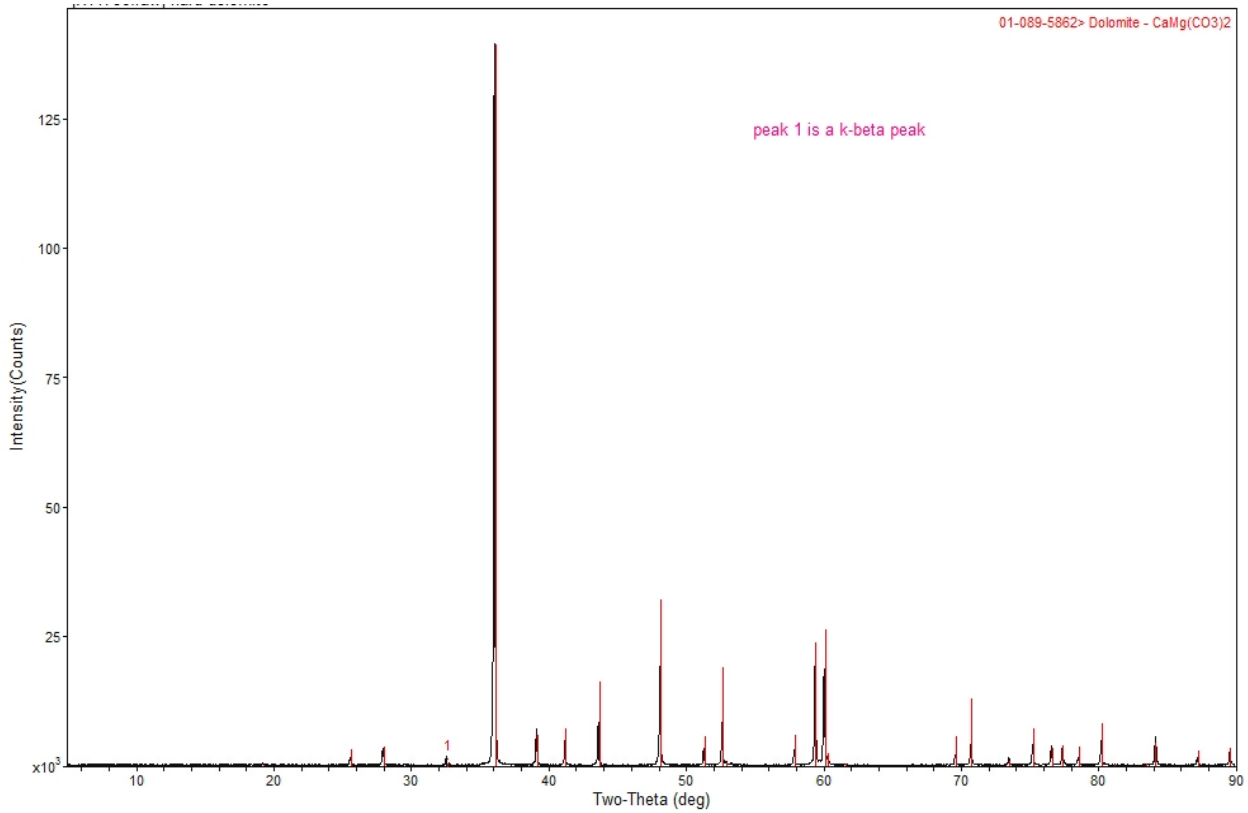

Figure A- 6 X-ray powder diffraction results for Dolomite-1.

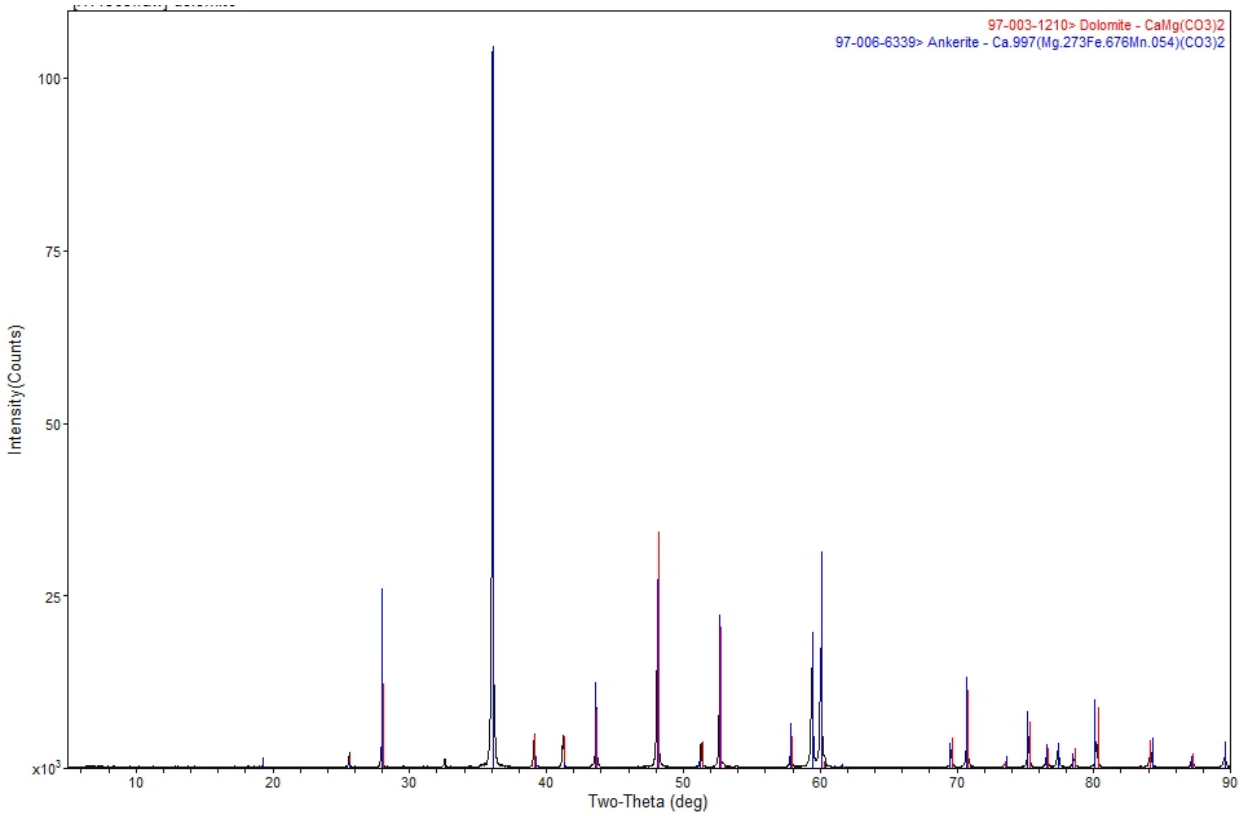

Figure A- 7 X-ray powder diffraction results for Dolomite-2.

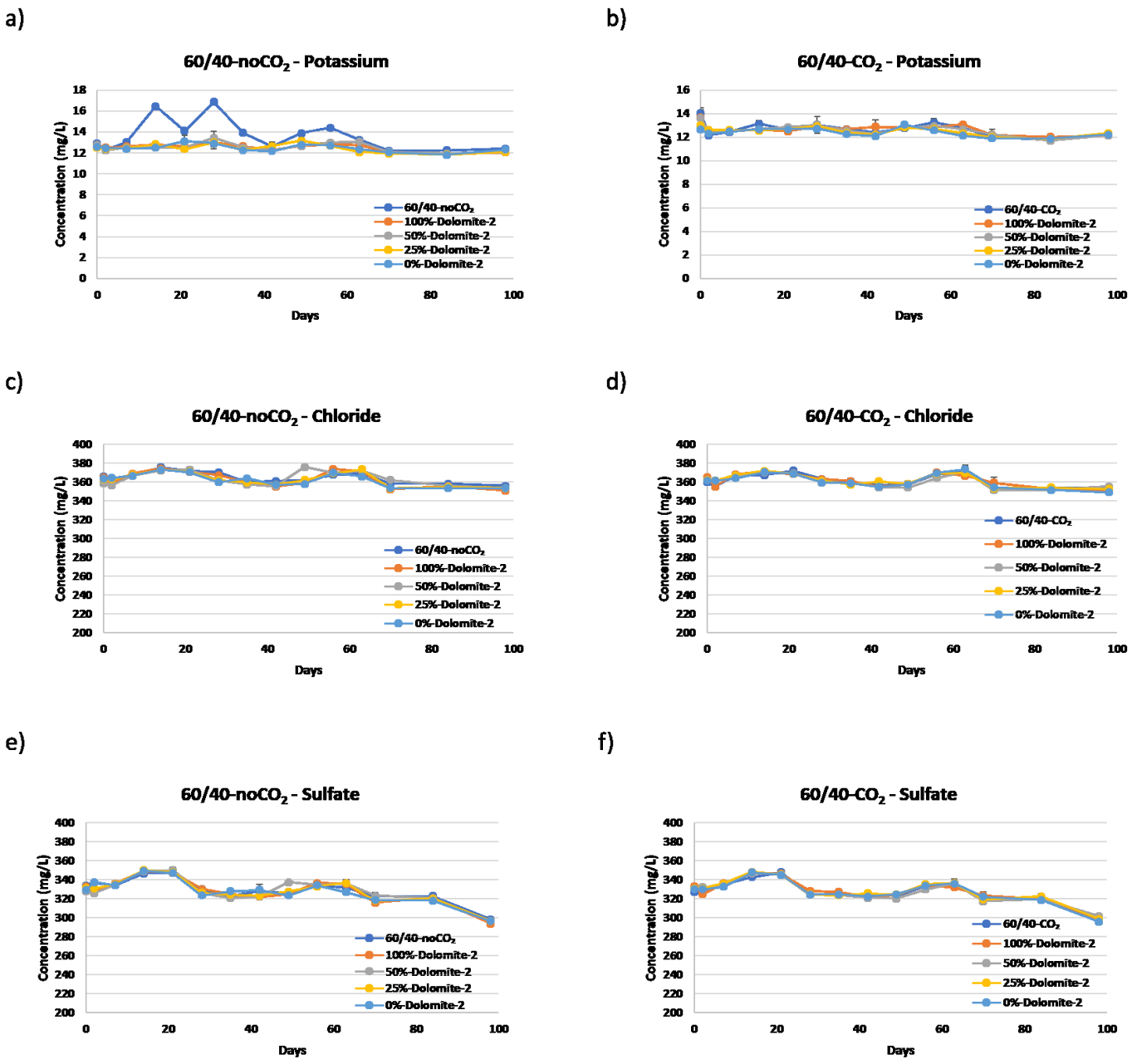

Figure A- 8 Dissolved ion concentrations in the waters used in the mixed carbonate dissolution experiment.

The following is an sample calculation for the total interaction energy for 0% dolomite-2-CO_2 at day 42 and with 26 nm particle separation distance.

To calculate the active forces (Φ_A):

$$\Phi_A = -\frac{Aa}{12S_0} = -\frac{(2\times10^{-20}\text{J})(7.5\times10^{-7}\text{m})}{12(26\times10^{-9}\text{m})} = -4.8\times10^{-20}$$

To convert to thermal energy unit:

$$= \frac{(-4.8\times10^{-20}\text{J})}{(294.65\text{K})(1.38\times10^{-23}\,\text{J/K})} = -1.18\times10^{1}$$

To calculate the Debye length (K^{-1}):

$$\kappa^{-1} = \sqrt{\frac{\varepsilon k_B T}{2IeF'}} = \sqrt{\frac{1.85\times10^{-16}}{2I}} = \sqrt{\frac{1.85\times10^{-16}}{2(0.033)}} = 5.3\times10^{-8}$$

To calculate the repulsive force (Φ_R):

$$\Phi_R = \frac{\varepsilon a\psi^2}{2} ln[1+\exp(-kS_0)]$$

$$= \frac{(7.08\times10^{-10}\,\text{C}^2/\text{J*m})(7.5\times10^{-7}\text{m})(-0.0272\text{V})^2}{2} ln\big[1 + exp\big(-(1.88\times10^{7}\text{m})(26\times10^{-9}\text{m})\big)\big] = 9.32\times10^{-20}$$

To convert to thermal energy unit:

$$= \frac{(-9.32\times10^{-20}\text{J})}{(294.65\text{K})(1.38\times10^{-23}\,\text{J/K})} = 2.31\times10^{1}$$

To calculate the net interaction energy (Φ_{net}):

$$\Phi_{net} = \Phi_A + \Phi_R = (-1.18 \times 10^1) + (2.31 \times 10^1) = 11.28$$

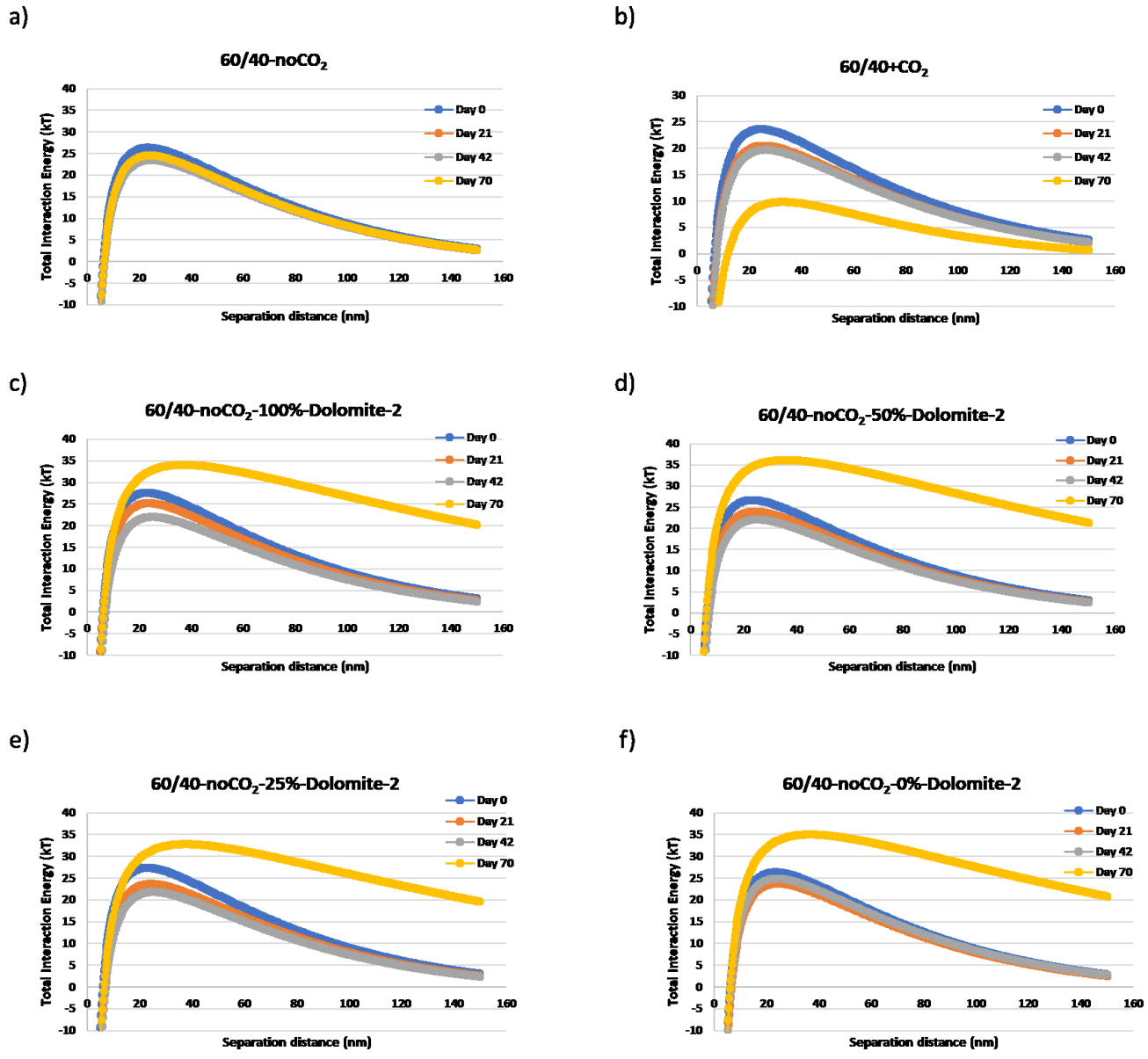

Figure A- 9 Total interaction energy as a function of interparticle distance for the noCO2 treatment columns